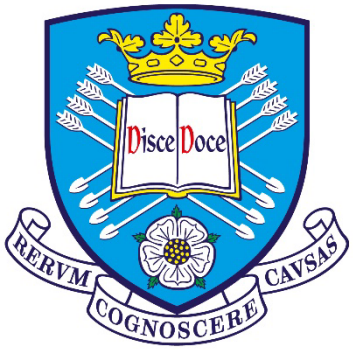

The University Of Sheffield.

Fat, fibroblasts, and fibrosis: how deposits of adipose tissue ameliorate dermal scarring

Samuel Higginbotham

A thesis submitted in partial fulfilment of the requirements for the degree of Doctor of Philosophy

The University of Sheffield

Faculty of Engineering

Department of Materials Science and Engineering

June 2022

Abstract

Hypertrophic dermal scarring is a debilitating condition for which there is no effective treatment. Autologous fat grafting is a rapidly developing technique able to regenerate scar tissue. Hypertrophic scarring is a result of dysregulated extracellular matrix deposition from an increased myofibroblast presence. Following fat grafting, scar tissue contains a lower population of myofibroblasts and a remodelled extracellular matrix. Adipose tissue used in fat grafting is often processed to form different clinical formulations before grafting. It has been suggested that a population of stromal cells contained within adipose tissue can inhibit fibroblast to myofibroblast differentiation. However, there has been no *in vitro* demonstration that clinically relevant formulations of adipose tissue can inhibit myofibroblast differentiation.

Here it is shown that paracrine factors, secreted from forms of adipose tissue used in a clinical setting, can inhibit, and reverse the differentiation of myofibroblasts *in vitro*. The clinical formulations of adipose tissue chosen for this work were; lipoaspirate, Nanofat-like adipose tissue, stromal vascular fraction-gel, and adipose derived stem/stromal cells. Cell culture medium conditioned with paracrine factors from these formulations was able to prevent expression of myofibroblast markers in TGF-β1 treated fibroblasts. Additionally, when applied to differentiated myofibroblasts, adipose tissue-derived conditioned medium lowered the expression of α-SMA.

These results are the first to demonstrate that factors released from different formulations of adipose tissue can inhibit and reverse myofibroblast differentiation in an *in vitro* model simulating the onset of scarring. This knowledge gives an insight into the clinical use of autologous fat grafting and suggests a mechanism for how fat grating treatments can remodel the extracellular matrix found in scar tissue. The data presents clear evidence that fat grafting can lower the myofibroblast population in hypertrophic scars and prevent new myofibroblasts from differentiating. This allows for a decrease in extracellular matrix tension and a lowering of scar morbidity.

Acknowledgements

I would like to thank Dr Vanessa Hearnden for her guidance and assistance at every stage of this research project. For providing me this opportunity alongside the advice and encouragement needed to finish this Ph.D., I am immensely grateful. I would also like to thank Dr Nicola Green and Prof Daniel Lambert for support, advice on experimental design, and feedback throughout various stages of my project and their support during Vanessa's maternity leave. Dr Victoria Workman deserves special thanks for many things including her patience, encouragement, and teaching over the past four years. Alongside her supervisory role she has been a good friend and made those long days of slicing up fat for 12 hours bearable. Together these people made a great supervisory team that supported me in every way possible.

Special thanks must be given to Ms Vanessa Singleton and Ms Brenka McCabe. Their support and maintenance of the laboratories I used during this time was essential. I'm sure some of my requests were incredibly annoying, yet both were always patient and accommodating.

I would like to thank Ms. Victoria Giblin, the Sheffield Hospital Directorate of Plastic, Reconstructive Hand and Burns Surgery, and the patient volunteers for providing the adipose tissue without which, this research would not have been possible. I am grateful to The University of Sheffield's Flow Cytometry Core Service for the use of their equipment. Additionally, I would like to thank the EPSRC, TCES, and The University of Sheffield's Learned Society for the funding of and during this project. I would like to thank BioRender for the use of their figure design software.

My colleagues in the Hearnden research group, Kroto, and the Dental School deserve thanks for their comradery, feedback, and the times when you fed my cells. Special acknowledgement should go to Dr George Bullock, Dr Bethany Ollington, Dr Ashley Gains, Mr Krit Rattanawonsakul, and Ms Rachel Furmidge.

My teammates from the University of Sheffield Ultimate Frisbee Club and SMOG have always kept my spirits up over the last 4 years. I am proud of the tournaments we have attended and won over this time period and cannot wait to compete at the Club World Championships this July.

I am grateful to the friendship provided by Thomas Entwistle, I believe the mutual venting over runs or football matches has been essential for both of us.

For the love, care, and support they have provided for me my entire life, my parents deserve special thanks. I appreciate all the work and effort it took to raise and provide for me during my childhood. I will never forget the love I am shown by you and the rest of my family.

Finally, I need to thank my partner Alice Rigby for just about everything. Your unwavering support and belief in me over the past four years has been essential in the completion of this work and the submission of this thesis. Your patience and encouragement have kept me going throughout the tough times of this project and your engagement with my work has speaks to me of how much you care. I am inspired by you every day.

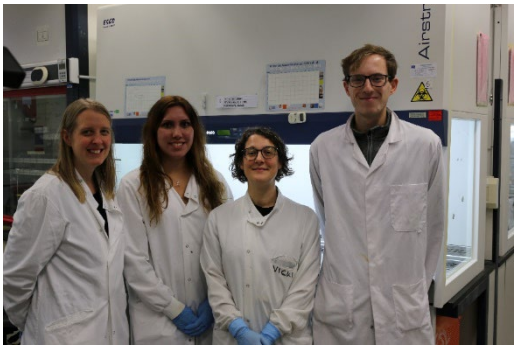

0.1 Introduction

Autologous fat grafting has been shown to be capable of regenerating hypertrophic scars (Klinger *et al.,* 2008; Rigotti *et al.,* 2007). A wide range of clinical trials have demonstrated an improvement in scar phenotype following autologous fat grafts (van Dongen *et al.,* 2021; Gentile *et al.,* 2017; Klinger *et al.,* 2013). Furthermore, formulations of adipose tissue have been developed to enhance the therapeutic benefits of this treatment (Yao *et al.,* 2017; van Dongen *et al.,* 2016; Tonnard *et al.,* 2013). Despite this promising research, there is a scarcity of high quality, *in vitro,* research investigating why adipose tissue grafting has such an effect.

Hypertrophic scars are formed of excessive extracellular matrix production as a result of dysregulated myofibroblast differentiation (Jenkins *et al.,* 2004; Desmoulire *et al.,* 1995). These cells express high quantities of extracellular matrix components and have a lowered expression of matrix metalloproteinases compared to undifferentiated fibroblasts (Johnston & Gillis, 2017). Thus, preventing the differentiation of fibroblasts to myofibroblasts is often a key aim of anti-fibrotic therapies (So *et al.,* 2011). There is evidence of decreased myofibroblast presence in scars following autologous fat grafting (Wang *et al.,* 2019; Uysal *et al.,* 2014) and evidence to suggest components of adipose tissue can inhibit myofibroblast differentiation (Hoerst *et al.,* 2019). However, there has been no *in vitro* demonstration that formulations of adipose tissue used clinically can inhibit or reverse this differentiation. As such, this thesis aims to:

1. Investigate whether paracrine factors from clinically relevant forms of adipose tissue can inhibit the differentiation of fibroblasts.

2. Examine whether paracrine factors from clinically relevant forms of adipose tissue can reverse the differentiation of myofibroblasts.

3. Identify the cellular components of adipose tissue responsible for any effect paracrine factors from clinically relevant forms of adipose tissue may have on myofibroblast differentiation.

4. Elucidate the underlying mechanisms behind any effect paracrine factors from clinically relevant forms of adipose tissue may have on myofibroblast differentiation.

This thesis begins with a literature review outlining the components of adipose tissue, how fibrosis occurs, the development of regenerative autologous fat grafting, and research investigating why fat grafting has regenerative abilities.

Following this, the 1st experimental chapter characterises the clinical formulations of adipose tissue used during this research. The methods used to generate these formulations are defined and

confocal microscopy and flow cytometry are used to understand the components that make up these formulations. Resazurin and LDH assays are used to investigate how processing these formulations affects metabolic activity and cell lysis. Finally, the congruence of these formulations with the literature are tested by examining whether cell concentration changes as processing occurs, via DNA quantification.

The 2nd experimental chapter examines if secreted factors from these adipose tissue formulations can inhibit myofibroblast differentiation. Secreted factors from adipose tissue were extracted by adding the formulations characterised in the preceding chapter to cell culture medium for 72 hours. Inhibition was assessed by western blotting, qPCR and immunocytochemistry of the expression of myofibroblast markers. Following this, the secreted factors from adipose tissue are analysed to identify target molecules that may be responsible for an inhibitory effect on myofibroblast differentiation. Hepatocyte growth factor is identified as a target molecule and its ability to inhibit myofibroblast differentiation is examined via western blotting and immunocytochemistry.

The final experimental chapter investigates whether secreted factors from these adipose tissue formulations can reverse myofibroblast differentiation. This is assessed using the same methods as the previous chapter however, examination of Ki-67 expression and lipid production is used to elucidate the mechanism behind myofibroblast de-differentiation. The thesis ends by testing whether secreted factors from these adipose tissue formulations can reverse the myofibroblast phenotype of fibroblasts isolated from scar tissue.

0.2 Outputs

Publications

-Workman V, Penuelas A, Higginbotham S, Roman S, Giblin V, MacNeil S, Green N, Hearnden V (2020). There's more to fat than stem cells, characterising fat graft materials to understand the regenerative properties of adipose tissues. TERMIS European Chapter Meeting 2020 Manchester, UK. eCM Meeting Abstracts 2020, Collection 1: 158.

Oral presentations

-18th Annual IFATS meeting 2021 (Florida, USA), "Investigating the effect of factors secreted from adipose tissue on myofibroblast differentiation"

-BioMedEng21 conference (Sheffield, UK), "Inhibition of canonical myofibroblast differentiation via factors secreted from fat"

-White Rose Biomaterials and Tissue Engineering Group annual meeting 2020 (Online) "Can myofibroblast differentiation be reversed with secreted factors from adipose tissue?"

-White Rose Biomaterials and Tissue Engineering Group annual meeting 2019 (York, UK) "The inhibitory effect of fat on myofibroblast differentiation"

Poster presentations

-White Rose Biomaterials and Tissue Engineering Group annual meeting 2021 (Sheffield, UK) "Investigating how secreted factors from adipose tissue alter myofibroblast phenotype" – **Best flash presentation**

-TERMIS 6th world conference 2021 (Online) poster presentation "There's more to fat than stem cells; characterising fat graft materials to understand the regenerative properties of adipose tissues"

-Tissue and Cell Engineering Society conference 2021 (Online) poster presentation "Investigating how secreted factors from adipose tissue alter myofibroblast and scar phenotype"

-Tissue and Cell Engineering Society and the UK Society for Biomaterials joint conference 2019 (Nottingham, UK) poster presentation "Assessing the paracrine effects of fat on dermal fibrosis.

0.3 Table of contents

0.4 List of abbreviations

ADSC – Adipose derived stromal cell

ANOVA – Analysis of variance

BMP – Bone morphogenic protein

BSA – Bovine serum albumin

CAL – Cell assisted lipotransfer

CTFG – Connective tissue growth factor

DAMP – Damage associated molecular pattern

DAPI – 4',6-diamindino-2-phenylindole

D-MEM – Dulbecco's modified Eagles medium

DMSO – Dimethyl sulfoxide

ECM – Extracellular matrix

EGF – Epidermal growth factor

ELISA – Enzyme-linked immunosorbent assay

EV – Extracellular vesicles

FCBS – Flow cytometry buffer solution

FCS – Foetal calf serum

FGF – Fibroblast growth factor

FITC – Fluorescein isothiocyanate

FMO – Fluorescence minus one

HA – Hyaluronan

HBSS – Hank's balanced salt solution

HGF – Hepatocyte growth factor

HIF – Hypoxia inducible factor

IFATS – International federation for adipose therapeutics and science

IL – Interleukin

IMS – Industrial methylated spirit

LDH – Lactate dehydrogenase

MAPK – Mitogen associated protein kinase

MMP – Matrix metalloproteinase

MSC – Mesenchymal stem cell

PBS – Phosphate buffered saline

PDGF – Platelet derived growth factor

PFA – Paraformaldehyde

PGE_2 – Prostaglandin E2

PPAR – Peroxisome proliferator-activated receptor

REC – Research ethics committee

RIPA – Radioimmunoprecipitation assay

SDS – Sodium dodecyl sulphate

SMA – Smooth muscle actin

SVF – Stromal vascular fraction

TBS – Tris-buffered saline

TGF-β – Transforming growth factor-β

TIMP – Tissue inhibitor of metalloproteinase

TNF – Tumour necrosis factor

VEGF – Vascular endothelial growth factor

0.5 List of figures

Chapter 1: Literature review

Chapter 2: Materials and methods

Chapter 3: Characterisation of adipose tissue formulations

Chapter 4: Investigating the ability of factors from adipose tissue to inhibit a myofibroblast phenotype

Chapter 5: Investigating the ability of factors from adipose tissue to reverse a myofibroblast phenotype

0.6 List of tables

Chapter 1: Literature review

Chapter 2: Materials and methods

Chapter 4: Investigating the ability of factors from adipose tissue to inhibit a myofibroblast phenotype

0.7 List of equations

Chapter 2: Materials and methods

Chapter 1: Literature review

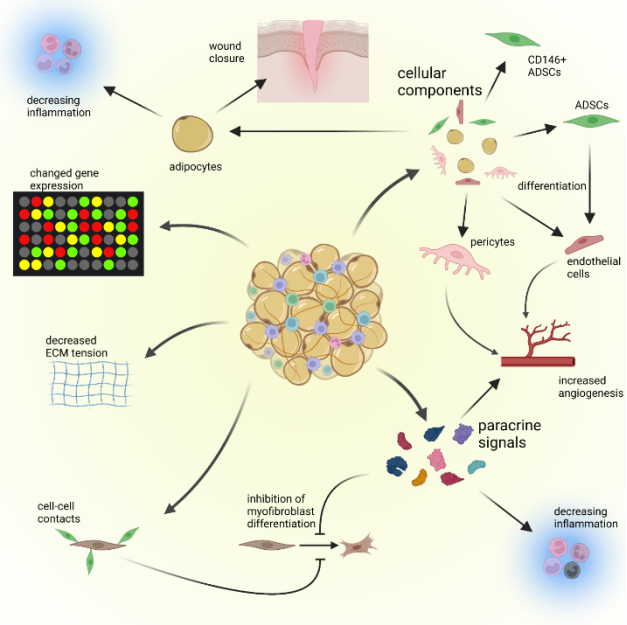

1.0 Introduction

This chapter focuses on reviewing the literature surrounding autologous fat grafting and its use in scar regeneration. The chapter begins by establishing the components of adipose tissue and moves onto an overview of wound healing and current fibrosis treatment strategies. The development of regenerative autologous fat grafting and the use of different clinical formulations is documented. Furthermore, clinical trials on autologous fat grafting as a hypertrophic scar treatment are reviewed. The evidence and mechanisms behind the regenerative ability of autologous fat grafting are compared. A concluding section focusses on evidence that fat grafting can inhibit fibroblast to myofibroblast differentiation and demonstrates the gap in the literature this thesis attempts to address. Finally, the aims and objectives of this research are stated.

1.1 Adipose tissue and its components

Adipose tissue is a heterogenous collection of different cellular populations capable of a broad range of functions (Zhang *et al.,* 1994, 2017; Shabalina *et al.,* 2013; Cushman, 1970). It is a connective tissue found in deposits around the body and is mainly found as either subcutaneous or visceral adipose tissue (Lee *et al.,* 2013). Subcutaneous adipose tissue exists underneath the skin whereas visceral adipose tissue is located around various organs (figure 1.1). The main locations of subcutaneous adipose tissue are in the abdominal region and the gluteal region with visceral adipose tissue being located mainly above the stomach, below the intestine, and around the heart (reviewed in Bjørndal *et al.,* 2011).

It was originally thought that the only functions of adipose tissue were to store triglycerides for metabolism and to act as a layer of insulation (Kershaw & Flier, 2004). However, it has been realised that adipose tissue plays an important role in endocrine signalling across the body and secretes cytokines termed adipokines. Leptin was the first adipokine discovered in 1994 (Zhang *et al.,* 1994) and others such as adiponectin (Maeda *et al.,* 1996; Scherer *et al.,* 1995), resistin (Steppan *et al.,* 2001), and tumour necrosis factor alpha (TNF-α; Fain *et al.,* 2004) have been shown to play a vital role in energy homeostasis and immune response (reviewed in Kershaw & Flier, 2004; Lago *et al.,* 2007). This secretory profile makes adipose tissue a key endocrine regulator.

Adipose tissue itself exists in three forms, white, brown (Seale *et al.,* 2008), and beige (Wu *et al.,* 2012). White adipose tissue is primarily involved in the storage of energy in the form of triglycerides, with adipocytes in white adipose tissue containing large lipid vesicles containing triglycerides (Cushman, 1970). Due to the anhydrous and highly reduced state of triglycerides, they make incredibly efficient energy storage molecules which are oxidised to glycerol and NADPH to be used in respiration (Bjørndal *et al.,* 2011). White adipose tissue also secretes a large amount of leptin (Zhang *et al.,* 1994) and adiponectin (Maeda *et al.,* 1996; Scherer *et al.,* 1995). Brown adipose tissue on the other hand is responsible for converting fatty acids into heat (Shabalina *et al.,* 2013) and is found in small deposits mainly around the neck (Bjørndal *et al.,* 2011). Beige adipose tissue contains a mixture of white and brown adipocytes, combining both functions (Wu *et al.,* 2012).

Adipose tissue is implicated in inflammatory signalling. Adipose tissue itself contains immune cells such as macrophages but also secretes a variety of cytokines that regulate inflammation such as TNF-α (Fain *et al.,* 2004) and interleukin (IL)-10 (Zhang *et al.,* 2017).

A variety of different cellular populations make up adipose tissue with cells ranging from adipocytes (S, W. Cushman, 1970; Alexander, 2016) to pericytes (Pierantozzi *et al.,* 2015) and adipose derived stromal cells (Zuk *et al.,* 2001). This wide variety of different cells is perhaps the

reason for adipose tissues varied secretory profile. Outlined in the sections below are the main cellular components of adipose tissue.

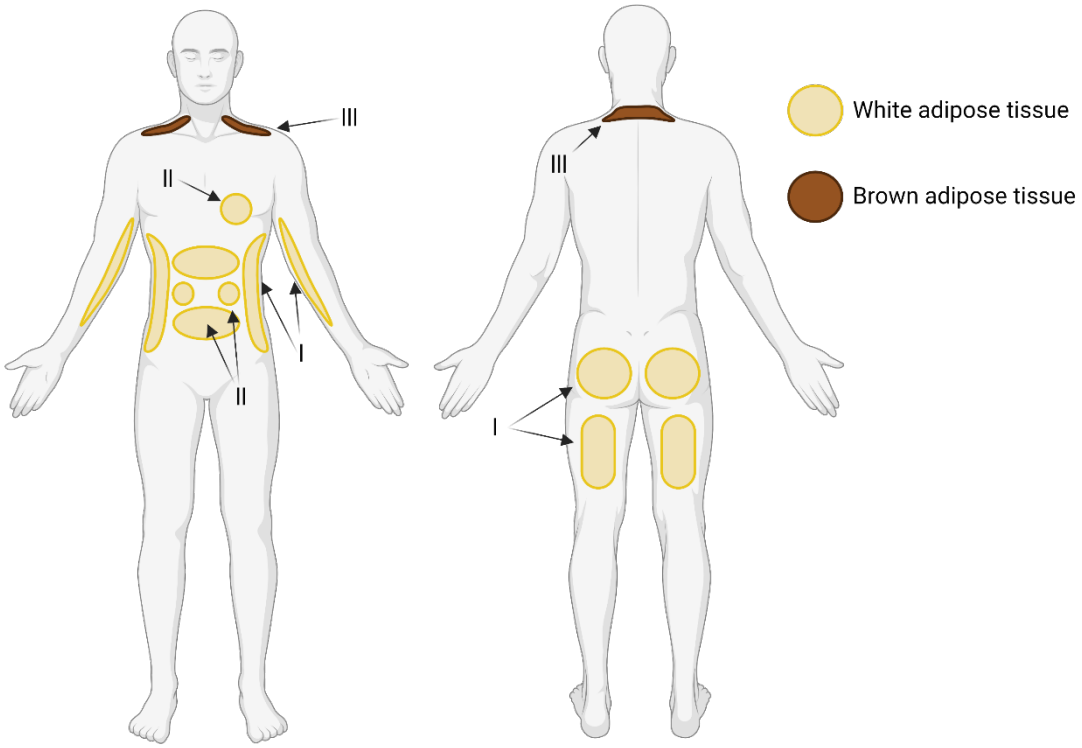

Figure 1.1. Locations of adipose tissue deposits throughout the body. The main deposits of white adipose tissue are stored (I) subcutaneously and (II) around the body's internal organs. The main store of brown adipose tissue is (III) around the neck. Figure created with Biorender.com, based on Bjørndal *et al.,* (2011).

1.1.1 Adipocytes

Adipocytes make up the vast majority of the volume of adipose tissue (Alexander, 2016). Adipocytes themselves contain large volumes of lipid. This collection of lipid is the reason why adipose tissue is such an effective energy store. Adipocytes in white adipose tissue contain few mitochondria but large lipid vesicles (Cushman, 1970) whereas brown adipose tissue contains smaller lipid vesicles but more mitochondria (Cinti, 2009). The fatty acids in brown adipocytes are used to generate a proton gradient that is released in a futile manner from the mitochondria by uncoupling protein 1 (Heaton *et al.,* 1978). While providing heat, this process appears to be essential for maintaining metabolic health, with uncoupling protein 1 appearing to protect from diabetes and obesity (Cederberg *et al.,* 2001). While the cell lineage of white adipocytes is still unclear it has been determined that brown and white adipocytes come from distinct cell lineages (Seale *et al.,* 2008).

Despite the large lipid vacuole and function as energy storage, adipocytes are very active in endocrine signalling with important adipokines such as adiponectin and leptin being secreted exclusively by adipocytes (Maeda *et al.,* 1996; Scherer *et al.,* 1995). These cells are more than capable of affecting their surrounding environment (Bell *et al.,* 2008; Plikus *et al.,* 2017; Shook *et al.,* 2020). The plasma membrane of adipocytes contains caveolae (Cushman 1970), invaginations formed by caveolin proteins, which are responsible for the intake of lipids, vesicles, and other extracellular signals (Pilch *et al.,* 2011).

Adipose tissue is a heterogeneous and dynamic tissue. Adipocyte turnover in adipose tissue is roughly 8 % a year and the makeup of adipose tissue can vary significantly between individuals (Parlee *et al.,* 2014). Adipose tissue in obese humans is different to adipose tissue found in “lean” individuals which is a result in changes to the adipocytes found in the adipose tissue (Fuster *et al.,* 2016). As calorific intake increases, the number and size of adipocytes increases dramatically (Salans *et al.,* 1973), leading to weight gain. This increase in adipocyte size and number leads to adipocyte dysfunction resulting in increased inflammatory signalling, decreased capillarisation, altered adipokine secretion, and tissue dysfunction (Fuster *et al.,* 2016). This change in obese adipose tissue highlights the heterogenous nature of the tissue between individuals as adipocyte number and size can vary massively between individuals (Salans *et al.,* 1973).

While making up the majority of the volume of adipose tissue, adipocytes only account for about 15 % of the cellular number in adipose tissue (Eto *et al.,* 2009). The remaining cell population in adipose tissue is grouped together in a population referred to as the Stromal Vascular Fraction (SVF).

1.1.2 The SVF

The stromal vascular fraction was first described in 1964 (Rodbell, 1964). Adipose tissue from rats was digested via collagenase treatment and centrifuged. This produced a three-layered sample with adipocytes and lipid isolated at the top, with liquid underneath, and a pellet of cells at the bottom. This pellet was found to contain populations of stromal and vascular cells and as such has been termed the Stromal Vascular Fraction. The SVF has been found to contain a wide variety of cells (figure 1.2) including endothelial cells (Koh *et al.,* 2011), pericytes (Vezzani *et al.,* 2018), smooth muscle cells (Yoshimura *et al.,* 2006), hematopoietic stem and immune cells (Fuster *et al.,* 2016; Han *et al.,* 2010; Wu *et al.,* 2007; Weisberg *et al.,* 2003), fibroblasts (Yoshimura *et al.,* 2006), and pre-adipocytes (Carraro *et al.,* 1991; Rodeheffer *et al.,* 2008). Portions of extracellular matrix (ECM) have also been found to be present in the SVF (van Dongen *et al.,* 2019). Finally, a population of multipotent stromal cells, capable of adipogenic, chondrogenic, and osteogenic differentiation was discovered in 2001 (Zuk *et al.,* 2001) and termed adipose derived stromal cells (ADSC).

These cells generated excitement in the tissue engineering community as this population was an easily isolatable, large population of multipotent cells (Gimble & Guilak, 2003). The regenerative properties of adipose tissue are often attributed to ADSCs (Rehman *et al.,* 2004; Spiekman *et al.,* 2014; Kruger *et al.,* 2018; Zhao *et al.,* 2018; Borrelli, *et al.,* 2020) however this is far from the case, with the SVF also able to aide tissue regeneration (Pallua, *et al.,* 2014b; Domergue *et al.,* 2016; van Dongen *et al.,* 2016; Chae *et al.,* 2017; Gentile *et al.,* 2017). The SVF is able to spontaneously assemble into capillary networks *in vivo* as a result of the endothelial and pericytic cells present (Koh *et al.,* 2011). Additionally, the SVF has other pro-angiogenic properties (Pallua, *et al.,* 2014b; Chae *et al.,* 2017; Vezzani *et al.,* 2018). Immune cells are found in the SVF and contained within are populations of T-cells (Wu *et al.,* 2007), macrophages (Fuster *et al.,* 2016) and dendritic cells (Bertola *et al.,* 2012). Finally, the SVF has been found to contain pre-adipocyte cells (Carraro *et al.,* 1991; Rodeheffer *et al.,* 2008). These cells are often found attached to adipocytes and are responsible for replacing these cells upon adipocyte apoptosis *in vivo* (Rigamonti *et al.,* 2011). It is becoming clear that following the first few days of grafting, a significant portion of the adipocyte population is lost (Kølle *et al.,* 2013; Torio-Padron *et al.,* 2011). These cells still play an important role in the regenerative properties of adipose tissue and it is also likely that these pre-adipocytes in the SVF play a role in replacing the adipocyte population (Rigamonti *et al.,* 2011).

Together, these populations comprise a heterogeneous fraction of adipose tissue that is becoming increasingly important in tissue regeneration (Pallua, *et al.,* 2014b; Domergue *et al.,* 2016; van Dongen *et al.,* 2016; Chae *et al.,* 2017; Gentile *et al.,* 2017). Below, the function of some of the key cells in the SVF will be outlined further.

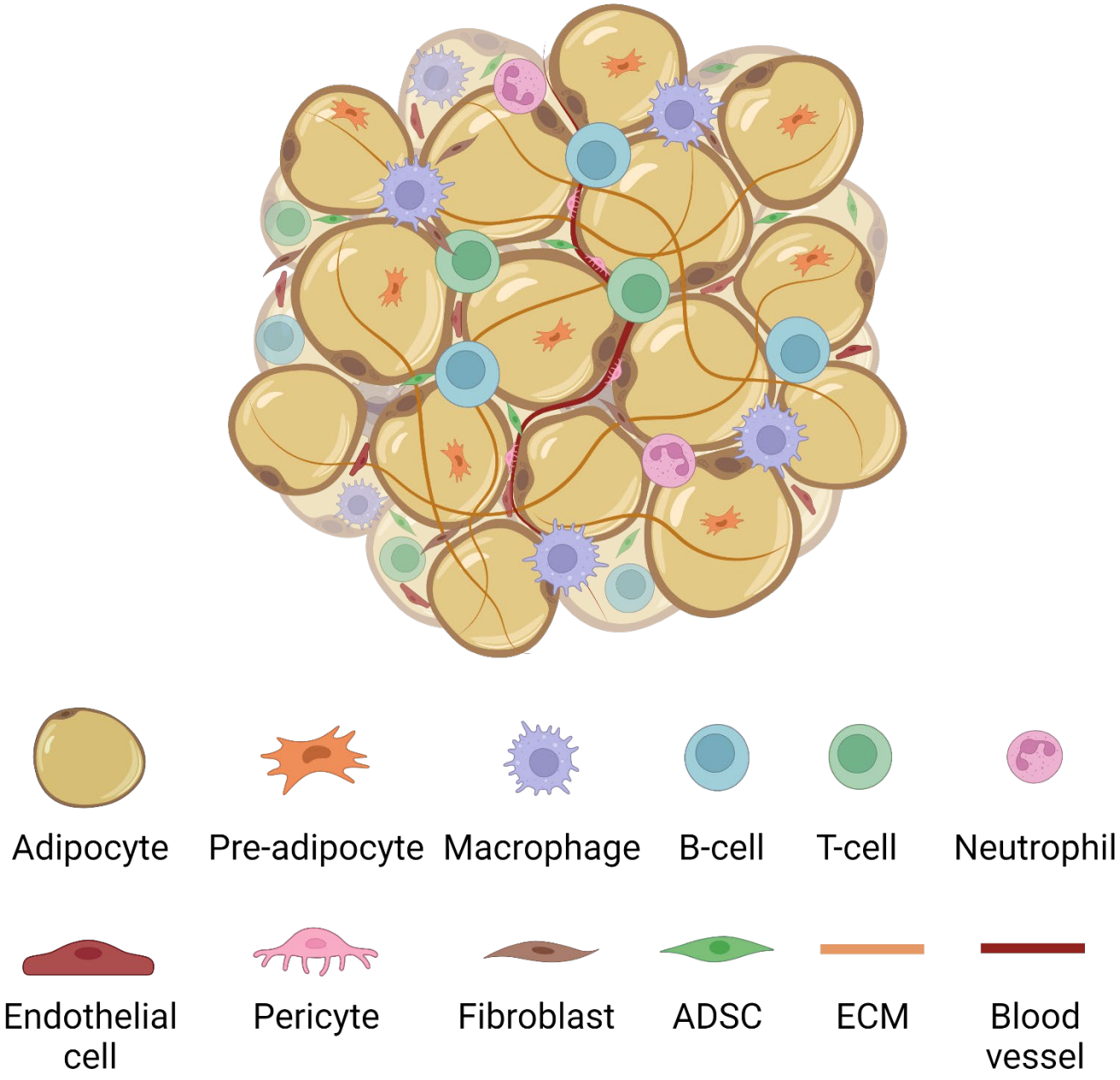

Figure 1.2. The components of adipose tissue. Adipose tissue is composed of tightly packed adipocytes with blood vessels, ECM and SVF filling the spaces between adipocytes. The SVF is composed of immune cells, endothelial cells, fibroblasts and ADSCs. Figure created with Biorender.com.

Table 1.1. Proportions of cellular populations in adipose tissue. The percentage of different cell types found in adipose tissue. Numbers calculated from Eto *et al.* (2009).

	Cell type	**Percentage of adipose tissue (by number)**
	Adipocytes	14.6 %
SVF cells	Fibroblasts, smooth muscle cells + others	46.1 %
	White blood cells	9.4 %
	ADSCs	24.4 %
	Endothelial cells	4.7 %

1.1.2.1 Endothelial cells and angiogenesis

Endothelial cells are mesodermal in origin (Slukvin & Kumar, 2018) and play a vital role in cellular homeostasis. These cells form a vascular network which is responsible for the transport of oxygen and endocrine factors around the body. Endothelial cells form in monolayer vessels that form the body's vascular network. This monolayer acts as a semi-permeable barrier which allows for the release of oxygen along with paracrine and endocrine signalling, whilst preventing coagulants from acting on blood cells (Sumpio *et al.,* 2002).

Angiogenesis is an important process in the body. Oxygen can diffuse roughly 150 µm from capillaries and thus cells more than 150 µm from a blood supply will suffer from a lack of oxygen (Olive *et al.* 1992). During wounding, capillary networks are damaged and cells at the wound site suffer from hypoxia (Xing *et al.,* 2011). Thus, damaged vessels require regrowth. This occurs via a process termed angiogenesis. Cells in hypoxic conditions begin secretion of hypoxia inducible factor (HIF; Xing *et al.,* 2011) and vascular endothelial growth factor (VEGF; Shweiki *et al.,* 1992). Endothelial "tip cells" with a high number of VEGF receptors then migrate by movement of filopodia towards high concentrations of VEGF. Proliferation of endothelial cells behind the tip cell then causes the "growth" of new blood vessels towards the site of low oxygen and relieves the cells of their hypoxic conditions (Gerhardt *et al.,* 2003; Ruhrberg *et al.,* 2002). When concentrations of VEGF normalise, ECM and basement membrane is deposited and pericytes bind to stabilise the newly grown blood vessels (Chiaverina *et al.,* 2019). This is the "sprouting" form of angiogenesis, wherein new blood vessels are grown outwards from existing capillary networks. The second type of angiogenesis is intussusceptive growth of vessels between other blood vessels (Djonov *et al.,* 2002). However, it is sprouting angiogenesis that occurs around wounds (Guerra *et al.,* 2021).

Relieving hypoxic conditions is an important part of wound healing (Lindegren *et al.,* 2019; Xing *et al.,* 2011; Olive *et al.,* 1992) and endothelial cells in the SVF have been shown to aide in this (Koh *et al.,* 2011; Shepherd *et al.,* 2004; Rehman *et al.,* 2004). Endothelial cells in the SVF have been shown to integrate into newly formed blood vessels and begin proliferation a day after implantation (Shepherd *et al.,* 2004). Furthermore, endothelial cells from injected SVF are capable of reassembling damaged vasculature. ADSCs from the SVF can also play a role in promoting angiogenesis with ADSCs implanted into hypoxic conditions producing VEGF and another angiogenic factor; hepatocyte growth factor (HGF; Koh *et al.,* 2011). Additionally, it has been shown that ADSCs from the SVF can differentiate into endothelial cells (Cao *et al.,* 2005).

1.1.2.2 Pericytes

Pericytes were first identified as contractile cells at endothelial junctions (reviewed in Sims, 1986). It is now understood however, that pericytes adhere to invaginations in the endothelial basement membrane. These cells form "peg and socket" junctions at short distances (20 nm) from the endothelial cell lining in capillaries (Caruso *et al.,* 2009). As such, pericytes form an important relationship with endothelial cells and are regulators of angiogenesis. Pericytes tend to bind and wrap around several endothelial cells towards the end of capillary structures (Sugihara *et al.,* 2020), encourage endothelial cell proliferation in angiogenesis and stabilise blood vessel structure (Carmeliet & Jain, 2011).

The relationship between pericytes and endothelial cells is essential for humans. The contraction of pericytes at capillary junctions appears to play a vital role in maintaining vessel structure with the removal of these cells leading to blood leakage in micro vessels (Bjarnegård *et al.,* 2004). Furthermore, pericytes secrete pro-angiogenic factors, including VEGF, a factor essential for vessel growth (Darland *et al.,* 2003).

ADSCs have been observed to differentiate into pericytes (Mannino *et al.,* 2020; Katz *et al.,* 2005) or take on a pericyte phenotype. These ADSCs secrete pro-angiogenic factors (Traktuev *et al.,* 2008), lead to increased vessel length, and have been shown to localise around vascular networks (Amos *et al.,* 2008).

1.1.2.3 Immune cells in the SVF

The stromal vascular fraction has been shown to have immunomodulatory properties. This is in some part due to the factors secreted by ADSCs in the SVF (Choi *et al.,* 2019; Zhu *et al.,* 2018; Kruger *et al.,* 2018; Zhao *et al.,* 2018). However, it is also due to the immune cells found in adipose tissue and the SVF (Guo *et al.,* 2016). The SVF has been found to contain macrophages (Bornstein *et al.,* 2000; Villena *et al.,* 2001; Martinez-Santibañez *et al.,* 2014), dendritic cells, both T and B lymphocytes, and natural killer cells (Wetzels *et al.,* 2018). These cells play a role in protecting adipose tissue from infection however they can be somewhat dysregulated in metabolic diseases. In obese adipose tissue, more macrophages are present and there is constant, low-level inflammation in the tissue from these immune cells (Hotamisligil *et al.,* 1993; Weisberg *et al.,* 2003).

Dendritic cells were discovered in the lymph nodes of mice and been shown to have a key role in antigen presentation (Steinman & Witmer, 1978). These cells take up antigens (Rosales & Uribe-Querol, 2017) and travel to the lymph nodes. Dendrites then present the antigens to native T-cells which causes them to become activated (Engleman *et al.,* 1981; Doyle and Strominger, 1987).

These T lymphocytes (T-cells) are activated into either T_H1 or T_H2 cells (Romagnani, 1999). T_H2 cells secrete pro-inflammatory interferon-γ, promoting macrophage activity (Viallard *et al.,* 1999; Yang *et al.,* 1999) and release IL-2, which stimulates cytotoxic T-cells (Rollings *et al.,* 2018). T-cells are distinguished from T_H1 or T_H2 cells by the marker CD8 and release cytotoxic molecules from their granules to kill pathogens (Gotcha *et al.,* 1996). T_H2 on the other hand, present the processed antigen from the dendritic cell to B lymphocytes (B-cells) causing them to produce antibodies or act as memory B cells, preventing future infection (Andersson & Melcherst, 1981).

Macrophages are thought to make up 20 % of the cells in the SVF (Morris *et al.,* 2015), although macrophage number is lower in brown adipose tissue (Villena *et al.,* 2001). They are important in the phagocytosis of pathogens and lysed cells (Rosales & Uribe-Querol, 2017). However, they play a vital role in inflammatory signalling and fibrosis (Witherel *et al.,* 2019) and are a major cell responsible for the foreign body response and biomaterial rejection (Anderson *et al.,* 2008). Macrophages were thought to be derived from monocytes however it is now considered that macrophages are present at birth and are derived from the embryonic yolk sac (Waqas *et al.,* 2017). Monocytes from the blood can differentiate into macrophages though and are thought to boost macrophages numbers (Scott *et al.,* 2016).

Macrophages can exhibit multiple phenotypes. Initially thought of as M1 “classically activated” macrophages that were considered pro-inflammatory and M2 “alternatively activated”, considered anti-inflammatory. It is now realised that macrophage activation is more of a plastic spectrum with many more phenotypes recognised (reviewed in Witherel *et al.,* 2019). This fact will be addressed later, however, in this section, for the sake of simplicity, macrophages will be referred to as M1-like or M2-like. The majority of macrophages in the SVF exhibit an M2-like phenotype and are considered important not just in the inflammatory response but also vascular regulation (Morris *et al.,* 2015). Despite this, both M1-like and M2-like macrophages have been implicated as acting in a pro-fibrotic manner. M1-like macrophages have been shown to produce VEGF and have been shown to reduce fibroblast migration (Bank *et al.,* 2017; Dondossola *et al.,* 2017) however, they also secrete the pro-inflammatory cytokine IL-6 and have caused increased myofibroblast differentiation (Ma *et al.,* 2012). Furthermore, M1-like macrophages secrete IL-1β, also leading to fibrosis (Zhang *et al.,* 1993). M2-like macrophages on the other hand, have also been linked to increased fibrosis with production of resistin-like molecule-α causing increased collagen production (Knipper *et al.,* 2015). Additionally, macrophages have been shown to be capable of myofibroblast differentiation (Knipper *et al.,* 2015). It is clear these cells play a role in fibrosis.

1.1.2.4 Adipose derived stromal cells

It had been previously noted that within the isolated SVF there were populations of progenitor cells (Rodbell, 1964). It was demonstrated in 2001 that these progenitor cells were a population of mesenchymal stem cell (MSC) like cells found within the SVF. These cells, termed adipose derived stromal cells, were found to have the capacity to differentiate into cells of adipogenic, chondrogenic, osteogenic, and myogenic lineages (Zuk *et al.,* 2001). In addition to this, ADSCs have also shown endothelial (Cao *et al.,* 2005) and neurogenic differentiation potential (Ning *et al.,* 2006).

This discovery caused great excitement in the tissue engineering field as these cells showed the ability to differentiate into cells that could restore cartilage (Barlian *et al.,* 2018), bone (Hashemibeni *et al.,* 2016), and neurons (Wu *et al.,* 2021) yet overcome some of the traditional problems of stem cells such as cell yield, sourcing, and the invasiveness of isolation. ADSCs can be isolated in high numbers from lipoaspirate from liposuction (Zuk *et al.,* 2001). Liposuction itself is a minimally invasive procedure (reviewed in Bellini *et al.,* 2017a) and the lipoaspirate is a waste product and thus there are less ethical issues behind the source of the cells. As ADSCs are isolated from the waste product of liposuction, autologous ADSCs can be used, eliminating the risk of rejection from the body. Additionally, after several passages in culture ADSCs have been shown to lose histocompatibility proteins and no longer illicit an immune response (McIntosh *et al.,* 2006) thus leaving open the possibility of allogenic ADSC transplantation.

There are multiple terms used in the literature for ADSCs, including names such as adipose derived stem/stromal cell (Angmalisang *et al.,* 2018; Uysal *et al.,* 2014; Raposio *et al.,* 2014), processed lipoaspirate cells (Zuk *et al.,* 2001), and adipose derived mesenchymal stem cell (Sherman *et al.,* 2019; Desai *et al.,* 2014). The accepted term from the society IFATS (International Federation for Adipose Therapeutics and Science; formally the International Fat Applied Technology Society) is “Adipose Derived Stem Cell” (Bourin *et al.,* 2013). The term “adipose derived stromal cell” will be used throughout this thesis. This is because while ADSCs do have the capacity for multilineage differentiation that stem cells do, there is debate over whether the telomeres of these cells are preserved and thus whether they are fully “stem-like” (Izadpanah *et al.,* 2006; Estes *et al.,* 2006; Katz *et al.,* 2005). The IFATS does accept this reasoning and referring to ADSCs as “stromal” as opposed to “stem” is accepted (Bourin *et al.,* 2013).

Adipose tissue is of mesodermal origin and develops in the embryo around a similar time to fibroblasts (Berry *et al.,* 2013). As such, ADSCs are mesenchymal and share similar CD markers with MSCs. Both ADSCs and MSCs are positive for CD90 and CD105 (Mildmay-White & Khan, 2017; Bourin

et al., 2013; Huang *et al.,* 2013; Dominici *et al.,* 2006; Gimble & Guilak, 2003). There is variation among the markers found on ADSCs however, with some reports suggesting ADSCs are positive for markers CD146 (Huang *et al.,* 2013; Gimble & Guilak, 2003) and CD34 (Mildmay-White & Khan, 2017; Bourin *et al.,* 2013; Gronthos *et al.,* 2001), while others have found ADSCs to be negative for such surface proteins (Mildmay-White & Khan, 2017; Huang *et al.,* 2013; Pachón-Peña *et al.,* 2011; Zuk *et al.,* 2002). The markers present on ADSCs can also vary with time (Mitchell *et al.,* 2006). It has been noted that ADSCs appear to be heterogenous throughout the body with large sub-populations of ADSCs from the same individual expressing different surface proteins (Borrelli *et al.,* 2020a; Borrelli *et al.,* 2020b). Given the heterogenous nature of ADSC markers, it has been agreed that ADSCs can be defined as such if expressing at least two of a list of CD markers known to be expressed by ADSCs and show a capacity for adipogenic, chondrogenic, and osteogenic differentiation (Bourin *et al.,* 2013).

ADSCs are often viewed as the major cell responsible for the regenerative properties of adipose tissue (Borrelli, Patel, Blackshear, *et al.,* 2020; Kruger *et al.,* 2018; Zhao *et al.,* 2018; Spiekman *et al.,* 2014; Rehman *et al.,* 2004). This is partly because of the differentiation capacity discussed above, however, ADSCs also secrete a wide range of regenerative factors such as hepatocyte growth factor (HGF), VEGF, and fibroblast growth factors (FGFs; Moon *et al.,* 2012). Furthermore, ADSCs can influence their surrounding environment via the release of these paracrine factors and signals (Crewe *et al.,* 2018; Spiekman *et al.,* 2014; Moon *et al.,* 2012). It is also through their secretory profile that ADSCs are seen as a key tool in tissue engineering.

1.1.3 The extracellular matrix

The final key constituent of adipose tissue is the extracellular matrix. The ECM is a 3D connective tissue found between epithelial and endothelial tissues (figure 1.3, Frantz, Stewart and Weaver, 2010). This structure acts as a scaffold which cells are able to bind to and migrate along (Donaldson *et al.,* 1982). Alongside this, the ECM supports other cellular functions and can influence these actions via mechanotransduction (Humphrey *et al.,* 2014) and the release of growth factors (Folkman *et al.,* 1988; Lin *et al.,* 2011). As such, dysfunction or dysregulation of the ECM can result in many different diseases (reviewed in Sonbol, 2018).

The ECM is composed of roughly 300 different proteins, the majority of which are fibrous proteins such as collagens, fibronectin, and elastin, alongside proteoglycans (Hynes & Naba, 2012). There are 28 different collagen proteins found in mammals and roughly 30 % of the total protein weight in animals is collagen. The majority of collagen in the ECM comes in the form of collagen type I, III, and IV (Gordon & Hahn, 2010). Collagen type IV is used to form the basement membrane, a

barrier between epithelial cells and the ECM (Pöschl *et al.,* 2004) whereas the majority of collagen fibres in the ECM are collagen type l, and lll (Gordon & Hahn, 2010). These fibres are the main "structure" of the ECM, provide strength and stiffness to the tissue, and allow for cell migration (Donaldson *et al.,* 1982). Collagen binds to cells via integrin proteins on cell membranes, this causes clustering of integrin receptors and the formation of focal adhesion complexes (Schwartz, 2010).

Collagen fibres are composed of heterotrimers of collagen α1 and α2 helices which are crosslinked by lysyl oxidase (Marturano *et al.,* 2013; Pauling & Corey, 1951). Compared to other fibrous proteins in the ECM, collagen has a relatively short half-life, with turnover ranging from between 40 to 180 days dependent on the tissue (Gineyts *et al.,* 2000). As such, collagen homeostasis is being constantly maintained by fibroblasts. Fibroblasts secrete most components of the ECM such as collagen, elastin, and fibronectin (Mariggio *et al.,* 2009; Adachi *et al.,* 1998; Sephel & Davidson, 1986) but also secrete matrix metalloproteinases (MMPs; Bauer *et al.,* 1975; Tandara & Mustoe, 2011). These proteins degrade collagen and relieve tension in the ECM. Tissue inhibitor of metalloproteinases (TIMPs) inhibit MMPs (Bauer *et al.,* 1975). This results in a dynamic balance in the ECM with collagen and TIMP production counterbalanced by MMPs leading to ECM homeostasis.

While collagen is the most abundant component, other fibrous proteins make up the ECM. Elastin is an important molecule that provides the ECM with its elasticity. Tropoelastin is secreted and assembles into elastin fibres via lysyl oxidase crosslinking (Sato *et al.,* 2007). These fibres bind with ECM components such as collagen and stretch during periods of increased tension and rebound once relieved (Frantz *et al.,* 2010). Proteoglycans contain highly anionic glycosaminoglycans structures which maintains the hydration of the ECM (Souza-Fernandes *et al.,* 2006) and allow for the sequestering and storage of growth factors (Frantz *et al.,* 2010; Folkman *et al.,* 1988). Fibronectin is another fibrous protein that binds to cells via integrins. When bound, tension across fibronectin increases and more binding sites are revealed on fibronectin which allows for the self-assembly of fibronectin fibres (Zhong *et al.,* 1998).

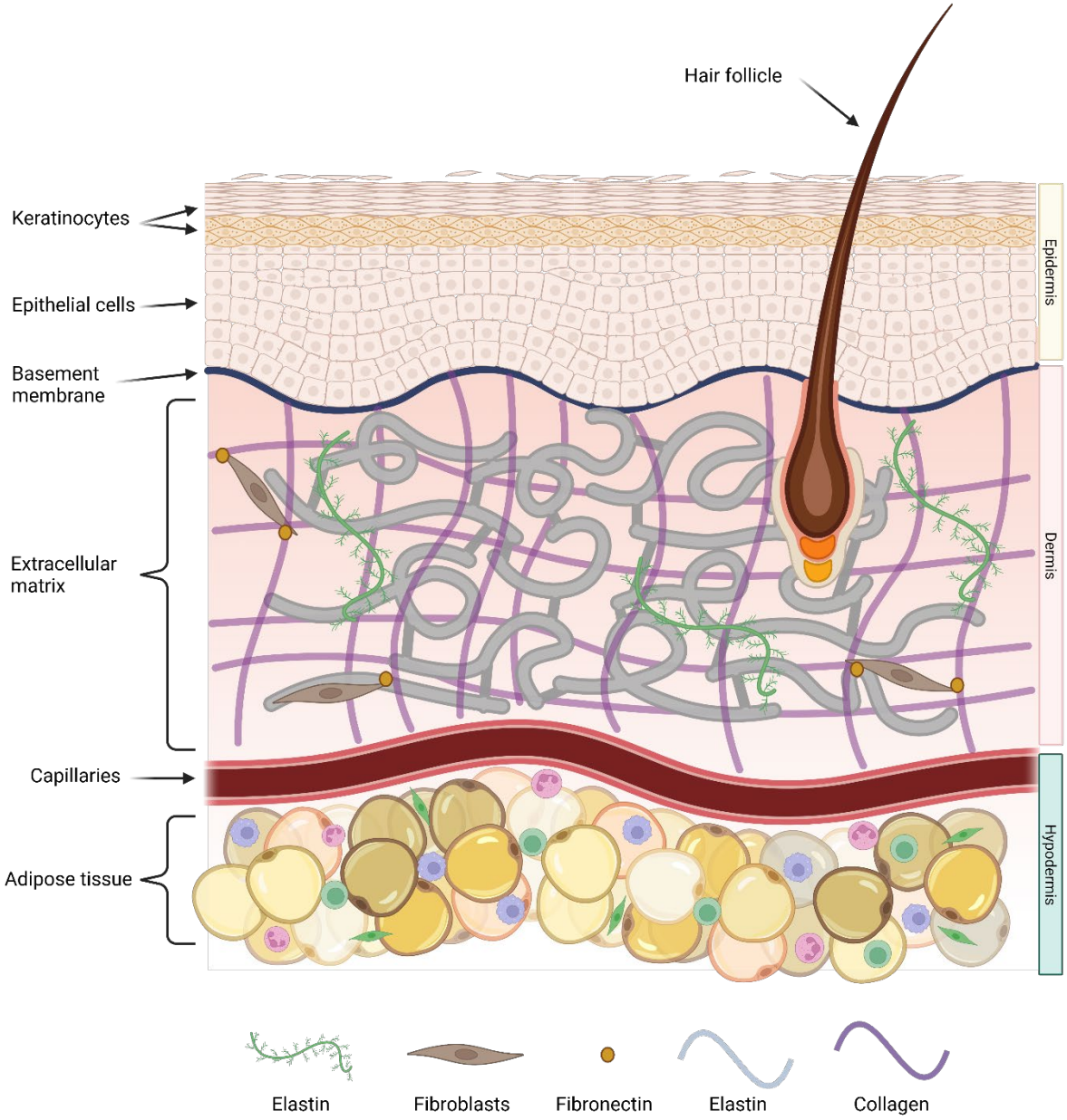

Figure 1.3. The structure of skin and the ECM. One of the main locations of the ECM is in connective tissue underneath the skin in the dermis. The skin is composed of layers of keratinocytes above epithelial cells in the epidermis. Collagen IV forms a basement membrane separating the dermis from the epidermis. Elastin, collagen, fibroblasts, and elastin form the dermis alongside blood vessels and adipose tissue in the hypodermis. Figure created with Biorender.com.

Fibronectins and integrins allow for tension in the ECM to influence and affect cell signalling. Integrins are a family of transmembrane receptors that bind to the ECM. These receptors are composed of an α and β subunit and are grouped into four main classes based on the different subunits involved in their formation (reviewed in Humphries *et al.,* 2006). The cytoplasmic domain of integrins binds to the actin cytoskeleton of the cell while the ligand binding sites bind to fibronectin (Schwartz, 2010). These fibronectin proteins bind collagen fibres and form a focal adhesion complex. When tension across the ECM is increased and collagen fibres contract, integrins along the cell membrane bundle, causing more binding of fibronectins to integrins and leads to cell signalling via mechanotransduction (figure 1.4). This can activate Rho and mitogen activated protein kinase (MAPK) signalling within the cell and alters the structure of the actin cytoskeleton (Humphrey *et al.,* 2014).

The ECM acts as a dynamic store of growth factors and proteins. The anionic glycoproteins sequester growth factors (Folkman *et al.,* 1988) and fibronectin contains binding sites for the storage of growth factors such as VEGF, HGF, and platelet derived growth factor BB (PDGF- Rahman *et al.,* 2005; Wijelath *et al.,* 2006; Lin *et al.,* 2011). While the ECM acts as a reservoir of growth factors, contraction of the ECM is also capable of activating latent forms of growth factors that exist in the ECM (Wipff *et al.,* 2007; Allen *et al.,* 2012).

Taken together, the components of the ECM facilitate many cellular functions in the surrounding tissues (Donaldson *et al.,* 1982; Lin *et al.,* 2011; Humphrey, *et al.,* 2014). Dysregulation of the ECM can lead to disease, and this is what occurs during fibrosis.

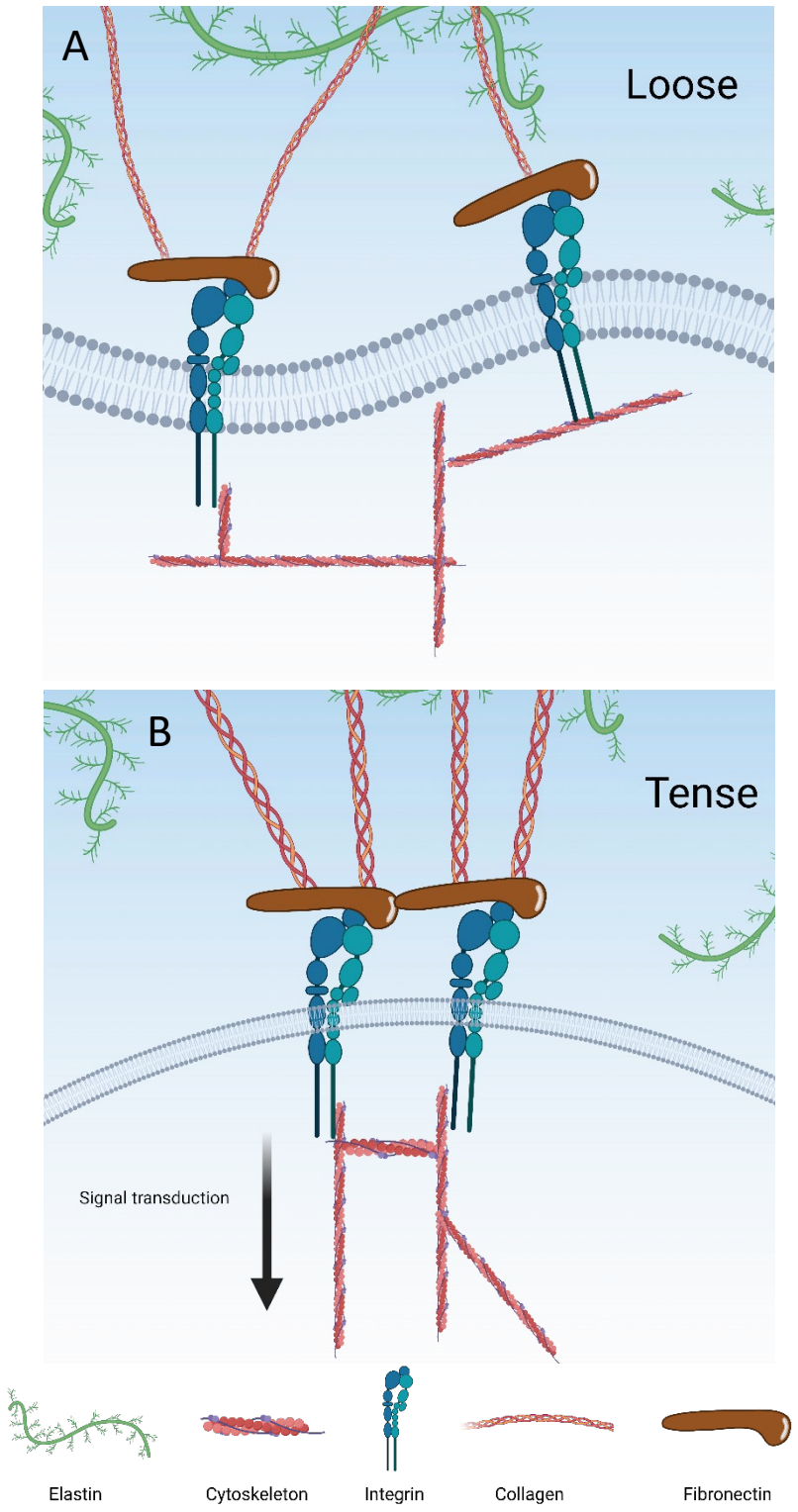

Figure 1.4. Integrin mechanotransduction. Collagen binds to fibronectin, which in turn binds to integrins across the cell membrane. When the ECM goes from a relaxed state **(A)** to one through which tension is applied **(B)** integrin proteins cluster, applying force along the cells cytoskeleton and activating Rho and MAPK signalling. This demonstrates how forces from the ECM can affect cell signalling. Figure created with Biorender.com.

1.2 Fibroblasts and fibrosis

1.2.1 Wound healing

Fibrosis is a result of excessive deposition of ECM because of dysregulated wound healing (Linares *et al.,* 1972; Craig *et al.,* 1975). Reparative wound healing is composed of four main phases: haemostasis, inflammatory, proliferative, and remodelling (figure 1.5; Singer, 2022). Immediately after a wound occurs, epithelial and endothelial cells are damaged, blood vessels are broken, and the body is exposed to foreign elements such as pathogens. The wound is sealed, and haemostasis restored by the formation of a fibrin clot. Fibrinogen in blood plasma is converted to fibrin and forms a clot around the wound which fibronectin binds to, allowing for more ECM components to bind to the clot (Makogonenko *et al.,* 2002).

Following the initial sealing of the wound, the inflammatory phase begins where damage associated molecular patterns (DAMP) released by damaged and lysed cells cause activation of toll-like receptors in innate immune cells (Maung *et al.,* 2005). This leads to inflammatory signalling and the release of pro-inflammatory signals such as TNF-α, IL-1, -6, and -8 (Lateef *et al.,* 2019; Chen *et al.,* 2013). This causes migration of immune cells such as leukocytes, neutrophils and M2-like macrophages to the wound where the proliferative phase begins (Lateef *et al.,* 2019).

In the proliferative phase, VEGF is secreted, angiogenesis occurs, and new blood vessels begin to form (Lateef *et al.,* 2019; Asahara *et al.,* 1999). Additionally, macrophages secrete factors that lead to the migration of fibroblasts to the wound (Chen *et al.,* 2019). Granulation tissue composed of ECM, fibroblasts, and immune cells begin to form and replace the initial fibrin clot while fibroblasts secrete ECM components and align collagen around the wound (Narayanan *et al.,* 1989). Furthermore, transforming growth factor-β (TGF-β) 1 is released from platelets and macrophages, causing differentiation of the fibroblasts to myofibroblasts (Chen *et al.,* 2019; Desmouliere *et al.,* 1993; Assoian *et al.,* 1983). Myofibroblasts cause contraction of the underlying wound tissue and bring the edges of the wound closer together, allowing for quicker re-epithelisation (Putra *et al.,* 2020). Finally, the wound undergoes a remodelling phase where MMPs are secreted to remodel the ECM surrounding the wound and immune cells and myofibroblasts undergo apoptosis to halt the wound healing process (Lee *et al.,* 2020; Linge *et al.,* 2005).

This reparative healing leaves behind a scar at the initial site of wounding. This scar tissue is characterised by the presence of type l collagen in parallel bundles. These parallel fibres are weaker than native collagen in the ECM (Rawlins *et al.,* 2006; van Zuijlen *et al.,* 2003). Furthermore, elastin around the wound is often repaired improperly, meaning that scar tissue is less flexible than native

tissue as well (Wagenseil & Mecham, 2007). This means dermal scar tissue is weak and inelastic, which if located at important functional areas can impair limb function (van Baar *et al.,* 2006).

Regenerative wound healing with no scar formation is found during embryonic development (Whitby & Ferguson, 1991). Wounds during this time leave no scar and undergo a slightly altered wound healing pathway with less IL-6 (Liechty *et al.,* 2000) release and more TGF-β3 present as opposed to TGF-β1 (Shah *et al.,* 1995).

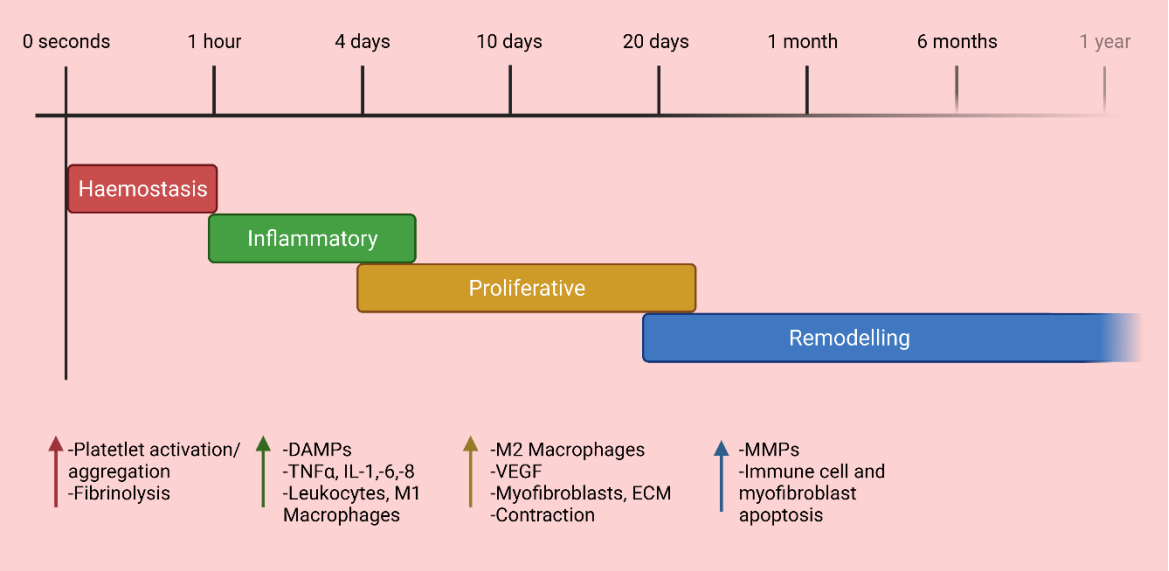

Figure 1.5. The timescale of wound healing. The four phases of wound healing occur across varying timescales and there are periods of overlapping signalling. The initial stages of haemostasis occur over hours whereas the remodelling phase can be maintained for months. Figure created with Biorender.com.

1.2.2 Fibroblasts in fibrosis

As mentioned in the above section, fibroblasts play a key role in wound healing by the production of ECM components and causing contraction of the epithelial layer around the wound (Putra *et al.,* 2020; Mariggio *et al.,* 2009). Fibroblasts are mesenchymal cells that are found in all connective tissues and the ECM (Driskell *et al.,* 2013). There is no definitive marker for fibroblasts. Vimentin and COL1A1 can be used (Tarbit *et al.,* 2019; Florin *et al.,* 2004) however, these are present in endothelial (Mork *et al.,* 1990) and chondrocyte cells as well (Florin *et al.,* 2004). Fibroblasts promote tensional homeostasis in the ECM. When placed in collagen matrixes, fibroblasts bind to the fibres via integrin receptors and generate tension across the matrix. While the tension across the matrix can be externally increased and decreased, once the force affecting the matrix is removed, the original tension across the matrix will be restored by fibroblasts. These cells can also organise the deposition of collagen. Fibroblasts bind to the collagen, contract, and then release the fibres (Humphrey *et al.,* 2014). Through repeated cycles of this contraction fibroblasts can control the alignment of the ECM. Fibroblasts are derived from heterogenous sub-populations across the body and dermal fibroblasts are derived from two different lineages with papillary fibroblasts in the upper dermis and reticular fibroblasts residing in the lower dermis. It is these reticular fibroblasts that are responsible for synthesising the majority of the ECM during wound healing (Driskell *et al.,* 2013).

During wound healing, fibroblasts are differentiated into myofibroblasts by a variety of different factors and pathways (figure 1.6; discussed later in section 1.2.3). Myofibroblasts were found in granulation tissue around wounds in 1971. It was noted that, unlike fibroblasts, the cells contained bundles of smooth muscles fibres across the cell (Gabbiani & Ryan, 1971). These bundles are alpha smooth muscle actin (α-SMA) fibres and are characteristic of the myofibroblast (Desmouliere *et al.,* 1993). These fibres cause the myofibroblast cell to contract and due to the integrin connections myofibroblasts have with collagen fibres in the matrix, contraction of the myofibroblasts causes increased contraction and tension exerted across the ECM in the granulation tissue (Hinz *et al.,* 2001). Additionally, myofibroblasts secrete more collagen compared to fibroblasts and have increased expression of TIMPs (Johnston & Gillis, 2017), meaning the balance of ECM production to degradation shifts in favour of ECM production.

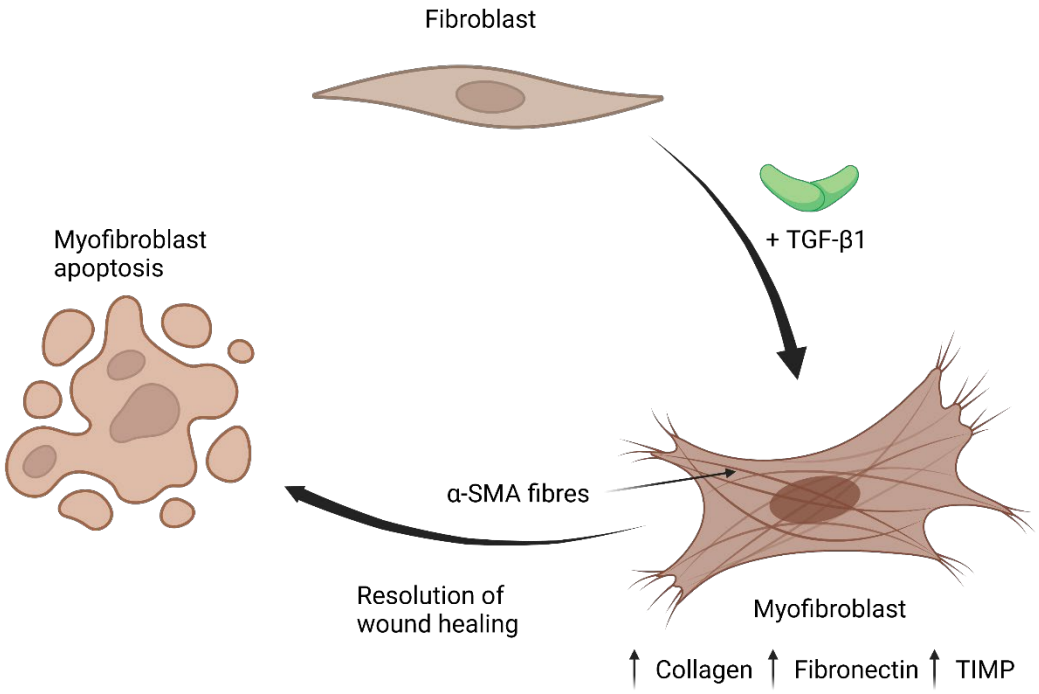

Figure 1.6. Myofibroblast activation. Fibroblast differentiation to myofibroblasts occurs during wound healing by TGF-β1 released into the ECM. This differentiation is characterised by an increase in collagen, fibronectin, and TIMP expression alongside the formation of α-SMA stress fibres across the myofibroblast. This causes contraction across the cell and by extension, the ECM. Upon the cessation of wound healing, myofibroblasts undergo apoptosis. Figure created with Biorender.com.

This increase in ECM production is an important factor in wound healing and following the cessation of this process myofibroblasts undergo apoptosis and leave behind a scar (Desmoulire *et al.,* 1995). However, this process can become dysregulated and hypertrophic scarring can occur. Hypertrophic scars are characterised by excessive collagen deposition and increased contraction (Tuan & Nichter, 1998). In hypertrophic scars collagen fibres are also increasingly aligned compared to native scars (Verhaegen *et al.,* 2009). This combination of increased contraction and thicker tissue results in painful and inelastic scars.

Scarring in organs, such as the lung, replaces the native tissue and reduces function. Dermal scarring results in painful and inelastic scars, reducing limb function if scarring occurs at joints, and are cosmetically undesirable, significantly effecting patients' mental health (van Baar *et al.,* 2006; Choi *et al.,* 2013; Hoogewerf *et al.,* 2014; Singer, 2022). These scars are a result of deep or chronic wounds causing overexpression of inflammatory signals. Receptors for inflammatory markers TNF-α and IL-1β are found to be overexpressed in scars alongside the myofibroblast activator TGF-β1 (Salgado *et al.,* 2012). This results in scars having increased fibroblasts and myofibroblasts present in the tissue (figure 1.7; Nedelec *et al.,* 2001). Furthermore, the macrophage populations in fibrotic lungs are found to be altered, perhaps leading to increased inflammatory activation (Wipff *et al.,* 2007). This increase in myofibroblast activation is coupled with a decrease in myofibroblast apoptosis (Linge *et al.,* 2005) and leads to increased contraction in the scar (figure 1.7). This generates a positive feedback loop as increased contraction in the ECM causes latent TGF-β1 sequestered in the ECM to be released (Wipff *et al.,* 2007), causing more myofibroblast activation and increased contraction. Thus, myofibroblast activation is at the centre of hypertrophic scar formation.

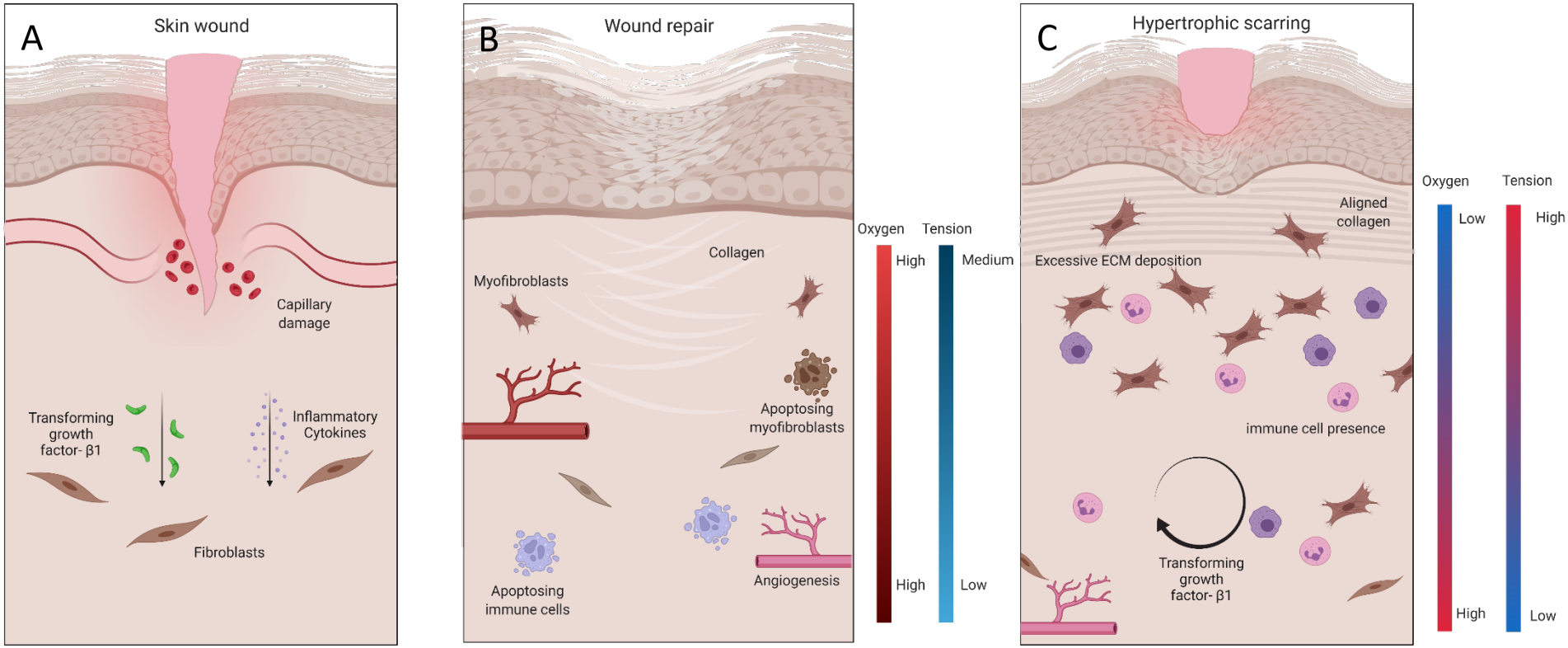

Figure 1.7. The hypertrophic environment. Upon the initial injury **(A)**, skin and capillaries are damaged, and a fibrin clot forms. Inflammatory signalling occurs attracting fibroblasts and causing the formation of granulation tissue. Following normal wound healing **(B)**, angiogenesis occurs to relieve the hypoxic environment, collagen is produced to cause contraction of the wound and following this myofibroblasts undergo apoptosis. In hypertrophic scarring **(C)**, less angiogenesis occurs, and a positive feedback loop occurs wherein, chronic inflammation leads to persistent myofibroblast presence. This leads to excessive ECM production, increasing tension across the tissue and releasing more latent TGF-β1, causing more myofibroblast activation. Figure created with Biorender.com.

1.2.3 Canonical and non-canonical myofibroblast activation

Fibroblasts can be differentiated to myofibroblasts via a number of different signalling pathways and stimuli (Midgley *et al.,* 2013; Akhmetshina *et al.,* 2012; Wipff *et al.,* 2007; Grotendorst & Duncan, 2005). However, the principle signalling factor in fibrosis is TGF-β1 which activates the SMAD signalling pathway and drives "canonical" differentiation (Evans *et al.,* 2003; Desmouliere *et al.,* 1993).

1.2.3.1 The TGF-β superfamily

The TGF-β superfamily are a group of growth factors that are essential for an assortment of cellular functions (reviewed in Morikawa *et al.,* 2016). There are three isoforms found in mammals (TGF-β1,2, and 3) which share high levels of homology (Derynck *et al.,* 1988). TGF-β proteins exert their signalling effects via TGF receptors. These are homodimer kinase receptors and are referred to as TGF receptors type l and ll. The type ll receptor is always active however, the type l receptor remains inactive until bound by a ligand (Heldin & Moustakas, 2016).

TGF-β1 is secreted by numerous cell types in an inactivate form termed the large latent complex (Wipff *et al.,* 2007). TGF-β1 exists in this form and is stored in the ECM as this latent form by fibronectin (figure 1.8; Miyazono *et al.,* 1991). This complex can be cleaved by proteases (Abe *et al.,* 1998; Lyons *et al.,* 1988) or increased ECM matrix contraction (Wipff *et al.,* 2007) allowing the active form of TGF-β1 into the surrounding ECM to bind to TGF receptors in nearby cells.

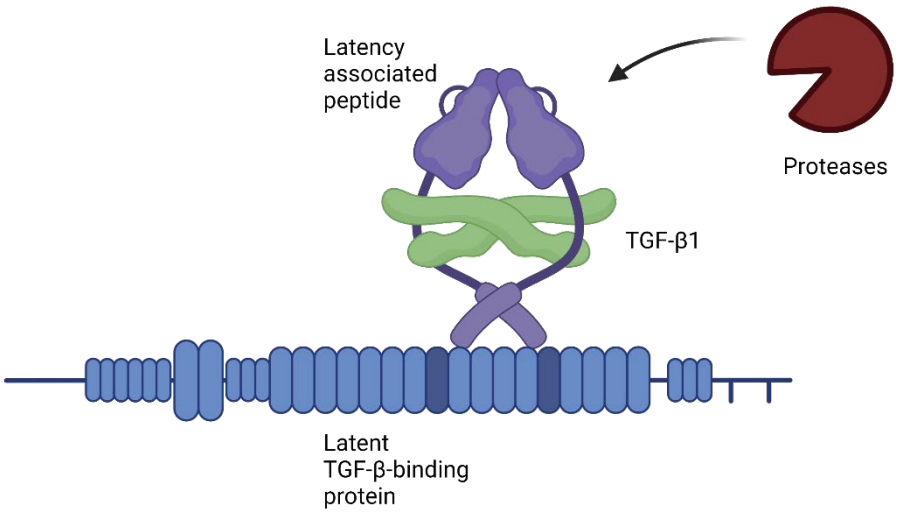

Figure 1.8. The large latent complex. TGF-β1 exists as the large latent complex in the ECM. TGF-β1 can be removed from this complex and activated via enzyme cleavage or ECM contraction. Figure created with BioRender.com.

1.2.3.2 SMAD signalling

Following TGF-β1 binding to the TGF receptors, heterodimerisation of the type l and ll receptors occurs, causing the phosphorylation of the SMAD2/3 complex (Derynck *et al.,* 1988; Assoian *et al.,* 1983). Phosphorylation of SMAD2/3 allows for binding of SMAD4 which allows the complex to translocate into the nucleus (Meng *et al.,* 2012). From there, the SMAD2/3/4 complex alters gene expression of the cell directly and indirectly (Morikawa *et al.,* 2016). This pathway can be regulated by several key molecules (figure 1.9). Both SMAD6 and SMAD7 inhibit this pathway, and the overexpression of SMAD7 can suppress fibrotic pathology (Li *et al.,* 2002; Imamura *et al.,* 1997).

This pathway is one of the ways through which TGF-β1 in the ECM can effect change on the surrounding cells. TGF-β1 has been shown to cause expression of α-SMA and differentiation of fibroblasts to myofibroblasts through this pathway (Desmouliere *et al.,* 1993; Hinz *et al.,* 2001). Gene expression is altered in fibroblasts by this SMAD signalling and appears to promote the expression of connective tissue growth factor (CTFG; Tsai *et al.,* 2018). CTGF acts downstream of SMAD signalling and is induced by TGF-β1 dependent SMAD signalling and both cytokines are found in elevated concentrations in scar tissue (Chen *et al.,* 2000). CTGF is responsible for ECM remodelling by fibroblasts and appears to cause myofibroblast differentiation as applying CTGF alone to fibroblasts leads to myofibroblast induction, independent of TGF-β1 (Tsai *et al.,* 2018; Grotendorst & Duncan, 2005). To summarise, TGF-β1 signalling induces a SMAD signalling cascade that increases expression of CTFG, causing myofibroblast differentiation.

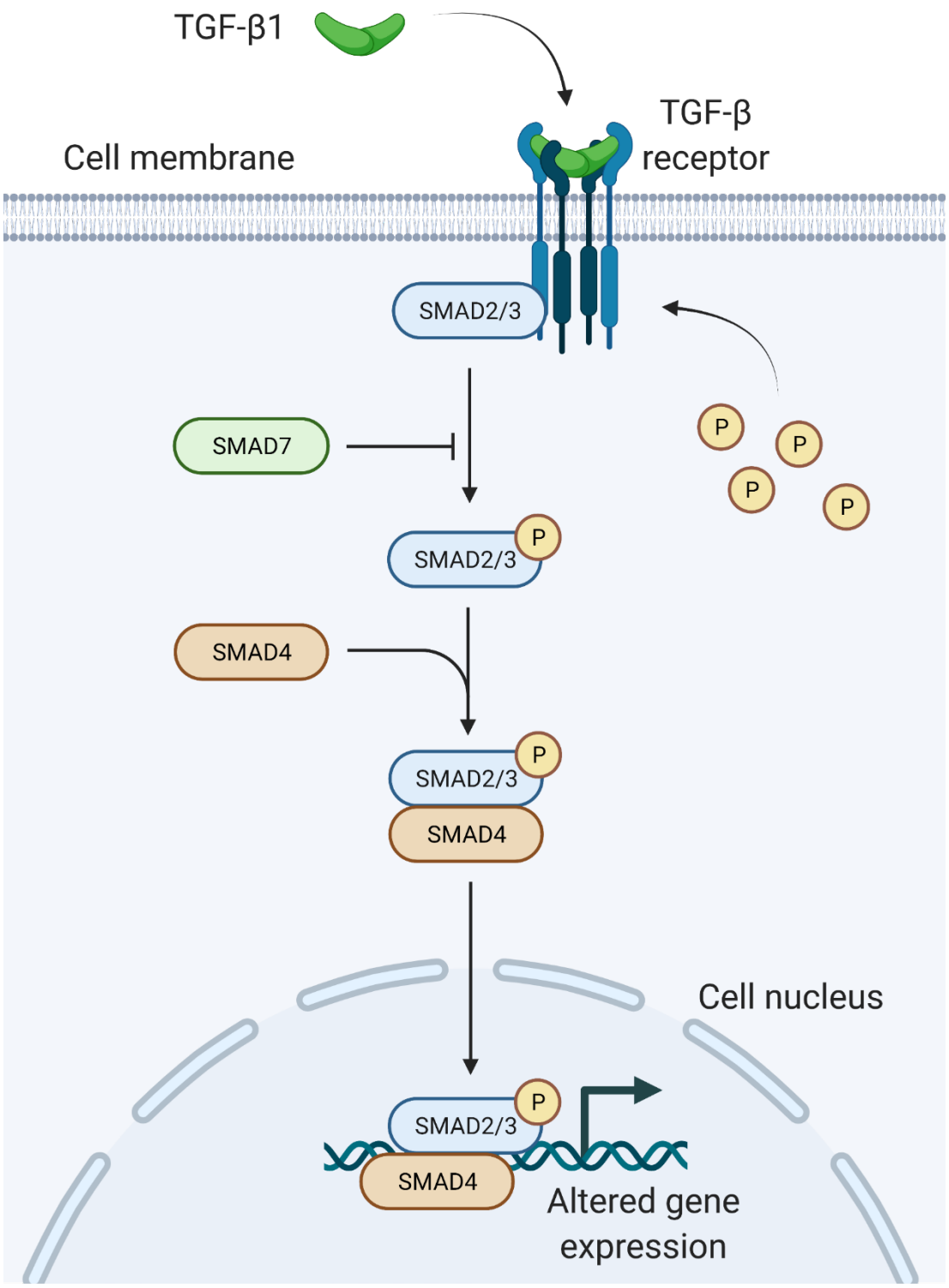

Figure 1.9. Canonical myofibroblast activation. Differentiation of fibroblasts to myofibroblasts occurs by signalling in the SMAD pathway. Binding of TGF-β1 to the TGFβR causes phosphorylation of the SMAD2/3 complex. This allows for binding of SMAD4 and translocation into the cell nucleus and altering gene expression. Figure created with Biorender.com.

1.2.3.3 Non-canonical myofibroblast activation

The other two main pathways through which myofibroblast activation occurs are the non-canonical Wnt/β-Catenin and Hyaluronan (HA)/ERK signalling pathways (Midgley *et al.,* 2013; Akhmetshina *et al.,* 2012). In native tissue, DKK-1 is present and inhibits the binding of Wnt protein to the frizzled transmembrane protein (figure 1.10). If the levels of DKK-1 are reduced, then Wnt binds to the frizzled receptor which localises with LRP5/6 (reviewed in greater detail in MacDonald & He, 2012). A multiprotein complex in the cytoplasm called the "destruction complex" binds β-catenin and leads to its degradation. Wnt binding prevents the degradation of β-catenin and allows for β-catenin translocation into the nucleus (Aberle *et al.,* 1997). β-catenin then induces gene expression of ECM producing genes (Hamburg-Shields *et al.,* 2015) and increases the expression of TGF-β1 leading to myofibroblast activation via the above canonical pathway (Akhmetshina *et al.,* 2012). There appears to be crosstalk between the two signalling pathways as in scar tissue both TGF-β1 and β-catenin accumulate and TGF-β1 reduces the amount of extracellular DKK-1 present (Sun *et al.,* 2015; Akhmetshina *et al.,* 2012), showing perhaps a positive feedback loop resulting in fibrosis.

Another signalling pathway inducing myofibroblast differentiation is ERK signalling. Hyaluronan (HA) is present in the ECM surrounding cells in healthy native tissue. HA binds to CD44 on fibroblast membranes and forms a layer around the fibroblast (Meran *et al.,* 2013). This HA layer causes CD44 to cluster on the plasma membrane and allows for co-localisation with the EGF receptor. This allows for the receptor to be phosphorylated (figure 1.11) and causes downstream phosphorylation of the ERK1/2 (Midgley *et al.,* 2013). Depending on the speed at which ERK is phosphorylated, gene expression is altered to promote either proliferation (> 30 minutes), or myofibroblast differentiation (< 5 minutes) in fibroblasts (Midgley *et al.,* 2013). It appears that in scar tissue, there is increased HA around fibroblasts. Myofibroblasts secrete less hyaluronidase, the enzyme involved in HA digestion and is another way in which dysregulation of normal function causes a positive feedback loop leading to increased myofibroblast differentiation and fibrosis (Jenkins *et al.,* 2004). It is through dysregulation of these signalling pathways and excessive myofibroblast activation through which dermal fibrosis and hypertrophic scarring occurs.

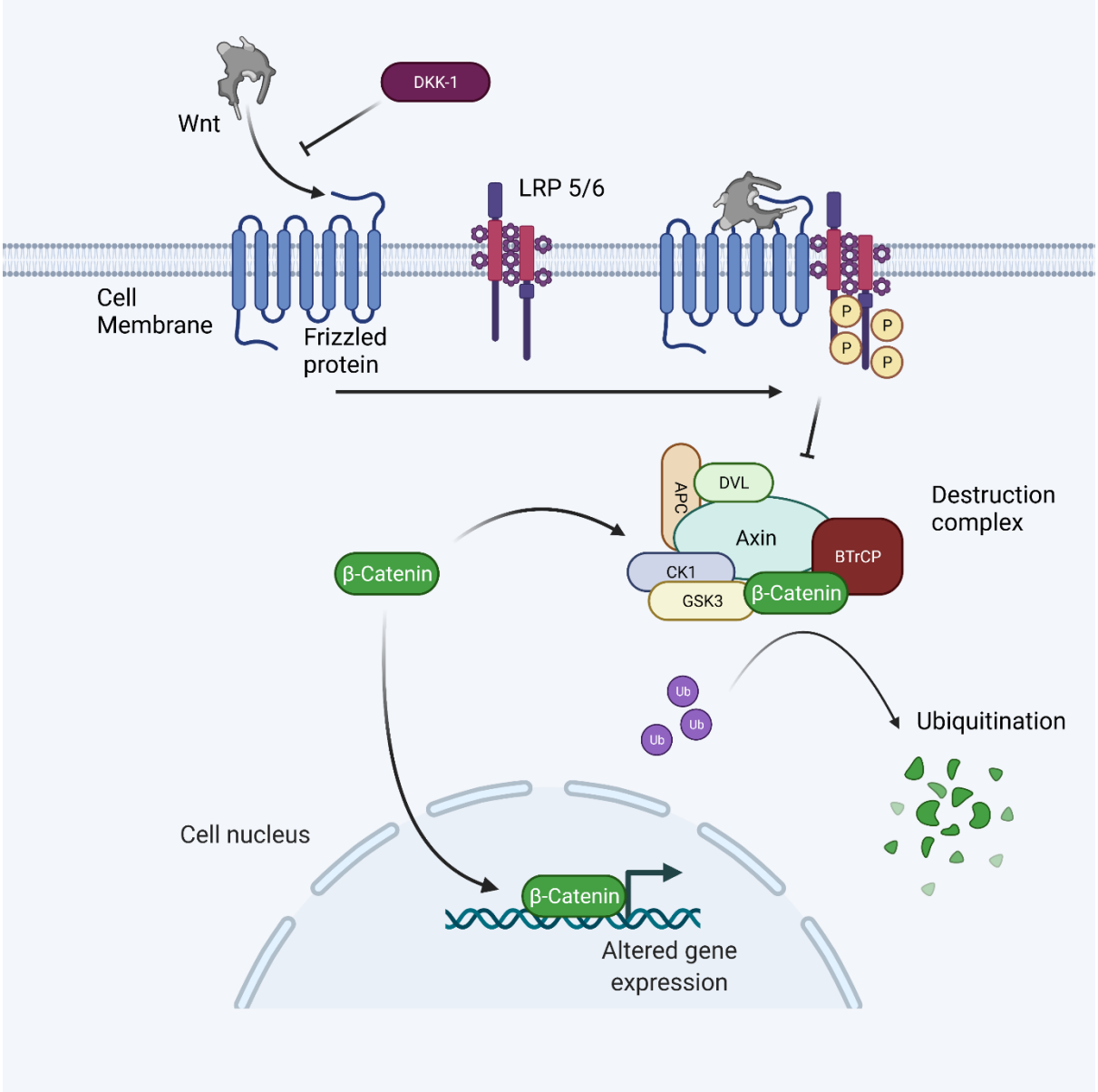

Figure 1.10. The Wnt signalling pathway. β-Catenin alters gene expression in fibroblasts and causes differentiation to myofibroblasts. However, this protein is degraded by ubiquitination via the destruction complex. Signalling from the frizzled protein and LRP5/6 as a result of Wnt binding inhibits this ubiquitination and allows for β-catenin translocation. Wnt binding is inhibited by DKK-1 however molecules such as TGF-β1 can decrease levels of DKK-1. Figure created with Biorender.com.

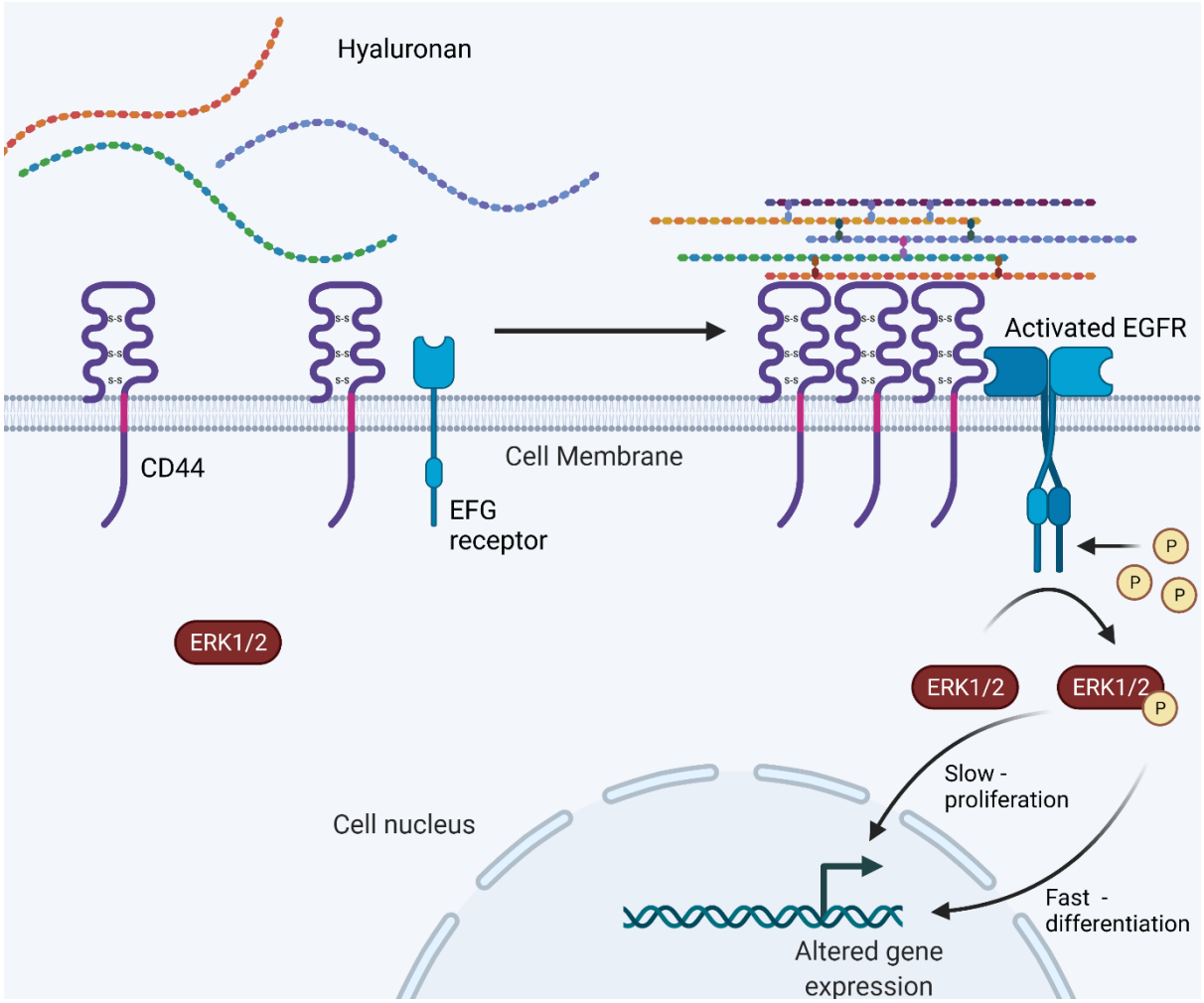

Figure 1.11. ERK 1/2 myofibroblast differentiation. Hyaluronan accumulation causes CD44 clustering at the cell membrane surface. This leads to activation of the EGF receptor. This causes phosphorylation of the ERK 1/2. This results in altered gene expression and myofibroblast differentiation. Hyaluronan production is elevated by myofibroblasts and thus Hyaluronan levels are increased in fibrotic environments. Figure created with Biorender.com.

1.2.4 Risk factors in developing fibrosis

It has been reported that roughly 35 % of people who receive a surgical skin wound will develop a hypertrophic scar (Delavary *et al.,* 2012). Individuals who receive a significant traumatic injury (such as a high degree of dermal burning; van Baar *et al.,* 2006) or are exposed to a chronic injury or inflammation (such as radiotherapy; Rigotti *et al.,* 2007) are at risk of developing dermal fibrosis and hypertrophic scarring. However, other than the type of injury, it is still not fully understood why some develop hypertrophic scars and others don't. A genetic element has not been found to influence hypertrophic scarring as levels of circulating TGF-β1 or single nucleotide polymorphisms in the TGF-β1 signalling pathways did not increase scarring susceptibility (Bayat *et al.,* 2003).

Most risk factors associated with an increased susceptibility to hypertrophic scarring appear to link back to increasing or decreasing inflammatory signals. Bacterial presence in burn wounds has been associated with hypertrophic scarring (Baker *et al.,* 2007). Bacterial presence triggers the toll like receptors in the innate immune system (as in the wound healing response) potentially over activating the inflammatory response. Furthermore, bacterial infections delay epithelialisation, leading to hypertrophic scarring (Singer & Mcclain, 2002). Those with allergies also seem more predisposed to hypertrophic scarring (Smith *et al.,* 1987). Allergic reactions are symptoms of an over-active immune response and increased mast cell inflammatory signalling (Amin, 2012). Mast cells also synthesise collagen however, hypertrophic scar tissue was not found to have increased mast cell presence (Niessen *et al.,* 2004), so this association is not fully understood.

On the other hand, factors that decrease inflammatory signalling appear to reduce the risk of hypertrophic scarring (Lee *et al.,* 2013; Ko *et al.,* 2012; Sørensen, 2012). Smoking is strongly associated with pulmonary fibrosis (Andersson *et al.,* 2021) but ironically decreases macrophage-based inflammation (Sørensen, 2012) and collagen synthesis. This means it is associated with decreasing the risk of hypertrophic scarring (Knuutinen *et al.,* 2002). Statins decrease inflammatory cytokine production and have been weakly associated with decreased hypertrophic scarring (Ko *et al.,* 2012) and chemotherapy reduces immune cell activation and collagen synthesis, meaning it too appears to protect from fibrosis (Lee *et al.,* 2013).

Age is negatively associated with developing fibrosis (Delavary *et al.,* 2012). This is once again believed to be due to a dampened inflammatory response associated with aging (Enoch & Price, 2004). However, collagen deposition is altered during aging and deposition of type l collagen appears to be more random (Enoch & Price, 2004), perhaps providing protection from fibrosis.

As stated in the above section, increased ECM tension causes release of latent TGF-β1 (Wipff *et al.,* 2007) and thus it is unsurprising that skin exposed to a stretching force is more at risk of developing hypertrophic scars (Quatresooz *et al.,* 2006).

There is little evidence to support that gender plays a role in susceptibility to hypertrophic scarring (Kim *et al.,* 2012). Gender is a risk factor in other forms of fibrosis with women almost three times as likely to develop systemic sclerosis as men. The rate of incidence is highest in premenopausal women and high levels of estrogen are considered to be responsible (Steen *et al.,* 1997). Treating fibroblasts with estrodial does promote fibrosis and the deposition of ECM (Aida-Yasuoka *et al.,* 2013) but there is counter evidence that it offers a protective effect (Avouac *et al.,* 2020) and promotes the degradation of SMAD3 (Ito *et al.,* 2010). Interfering with the SMAD pathway is a key target for current anti-fibrotic therapies (Miller *et al.,* 2006; Liguori *et al.,* 2008; So *et al.,* 2011; Meng *et al.,* 2012).

1.2.5 Current treatments for hypertrophic scarring

Treatment options and therapies are available for fibrosis and hypertrophic/keloid scars (Shockley, 2011; Leventhal *et al.,* 2006; Kuo *et al.,* 2004; Berman & Bieley, 1996) however, no treatment is currently completely effective. There are surgical interventions such as scar excision/revision where the scar tissue is removed, and re-epithelialisation is then allowed to occur. This treatment can be effective but is invasive and there is a high rate of scar recurrence (Leventhal *et al.,* 2006; Berman & Bieley, 1996). In all surgical interventions, attempts are made to relieve skin tension given it is a major risk factor in scar formation (Wipff *et al.,* 2007; Quatresooz *et al.,* 2006). Techniques such as Z-plastys, where the scar is remodelled to align with the skin to reduce tension across the area, are more effective and lead to less recurrence (Shockley, 2011). Newer, dermabrasion techniques use diamond wire to remove the scar layer however, scars are often made worse by this technique (Poulos *et al.,* 2003).

Traditionally, silicone gel or pressure dressing have been recommended and used to treat large areas of scar tissue (Mustoe *et al.,* 2002). Pressure dressings are thought to reduce collagen deposition (Kelly, 2004) and stimulate MMP production (Renò *et al.,* 2002) and silicone gel sheets are theorised to keep the scar area hydrated (Berman *et al.,* 2007). Though both are accepted treatments for scars there is little evidence to support a positive effect. Likewise, extract from onions was thought to be anti-inflammatory and traditionally considered to have anti-scarring abilities (Dorsch *et al.,* 1990) however, later research has shown onion extract to be of little therapeutic value (Jackson & Shelton, 1999).

Laser treatment and cryotherapy treatments of scars is a promising treatment option that is showing some success (Kuo *et al.,* 2004). Laser selection is important as while erbium:yttrium-aluminium-garnet lasers were theorised to inhibit the release of TGF-β1 (Nowak *et al.,* 2000), they were found to have no effect on scars and even caused burns on patients (Leclère & Mordon, 2010). The use of 585 nm wavelengths lasers though has been shown to reduce TGF-β1 expression and remodel collagen in scar tissue (Kuo *et al.,* 2004). The use of cryogenic agents on scar tissues has also shown some promise (Har-Shai *et al.,* 2008) however, more research is required into the treatment.

There are some therapeutic agents that are currently used to treat hypertrophic scars with mixed results. As mentioned before, onion extract is used however this is likely ineffective (Jackson & Shelton, 1999). Vitamin-E is suggested to aide hypertrophic scar appearance yet there is little evidence of its effectiveness (Baumann *et al.,* 1999). The injection of corticosteroids is commonly used on scars and is thought to reduce the effect of TGF-β1 on fibroblasts (Miller *et al.,* 2006) and decrease inflammation (Pérez *et al.,* 2001).

There have been many treatments designed to inhibit or alter TGF-β1 signalling in scarring such as the use of mannose-6-phosphate (ClinicalTrials.gov 2009) or Metelimumab (Denton *et al.,* 2007). However, these treatments have failed to prove effective. The most famous example is Avotermin. Ferguson et al. had noted that TGF-β3 was found in regenerative wound healing as opposed to TGF-β1 (Ferguson & O'Kane, 2004) and thus developed a treatment to administer recombinant TGF-β3 (So *et al.,* 2011). This treatment initially proved effective however failed to show any effect at stage lll clinical trials (McKee, 2011). This helps to highlight that there is no current effective treatment of fibrotic scars and that research into fibrosis therapeutic techniques is needed.

1.3 Fat grafting in tissue regeneration

1.3.1 The Coleman technique

Subcutaneous grafting of adipose tissue has been shown to regenerate dermal scars (Klinger *et al.,* 2008; Rigotti *et al.,* 2007). To understand how the use of autologous fat grafting in regenerative medicine has developed, it is important to understand the close relationship it has with aesthetic and reconstructive surgery. Advances in the field have sometimes been as a result of techniques established by surgeons to enhance the use of fat in aesthetic surgery (Tonnard *et al.,* 2013; Yoshimura *et al.,* 2008; Coleman, 2006). Therapies using adipose tissue in a regenerative capacity have arisen as a result of observations by surgeons that fat transplants rejuvenated the surrounding skin (Mojallal *et al.,* 2009; Coleman, 2006). This is highlighted by the fact that the first uses of fat tissue in surgery date back to the early 1900s, however it is only in the past 15 years that adipose tissue has been manipulated to illicit a regenerative response.

The first graft of adipose tissue was carried out in 1893 (Bellini *et al.,* 2017b) and in the early 20th century adipose tissue has been used as filler material underneath scars or wrinkles to reduce the signs of ageing (Bellini *et al.,* 2017b). Adipose tissue was an effective filling material and was a good option due to its abundance in the body and its autologous nature. However, adipose tissue has to be removed by invasive surgery and thus these techniques did not become more commonly used until the development of liposuction in the 1970s (Illouz, 1983). Liposuction uses a cannula with suction applied to it to collect large amounts of adipose tissue in a relatively non-invasive manner which can be carried out under local anaesthetic (Bellini *et al.,* 2017a). This technique is now a commonly used procedure with 400,000 people undergoing liposuction every year in the U.S. alone (Deleon *et al.,* 2021).

Despite the increasing occurrence of adipose grafting, operational procedures varied from surgeon to surgeon, with little record kept of the effectiveness of treatments. This ensured the field did not significantly progress until the work of Coleman. Coleman noted the tendency of other surgeons to work with inconsistent techniques or report the techniques they had used incorrectly (Coleman, 1995, 2006). Furthermore, it was a common occurrence for adipose tissue to be re-absorbed following grafting (Kølle *et al.,* 2013; Khouri *et al.,* 2012). To minimise this re-absorption, Coleman created a standardised protocol for autologous fat grafting (Coleman, 2006). The 'Coleman technique' is the basis for fat grafting to this day (Kølle *et al.,* 2013).

Coleman developed a protocol to extract adipose tissue that would break the macrostructure into smaller 'parcels' to inject back into the body while not causing significant damage to the cells in the adipose tissue. A 10 ml syringe was connected to the liposuction machine

and the plunger retracted to generate negative pressure (Coleman, 2002). He suggested syringes larger than 10 ml would create too much negative pressure and damage the tissue. Furthermore, a blunt cannula was then used to reinject the lipoaspirate back into the body as a sharp needled cannula led to the destruction of the adipose cells (Bellini *et al.,* 2017a). Coleman believed a 17-gauge cannula was the most useful size for reinjection of the adipose tissue parcels (Coleman, 2006). Contemporary histological analysis and cell counting demonstrated that this form of aspirating adipose tissue indeed did not negatively affect the yield or the macrostructure of adipose tissue (von Heimburg *et al.,* 2004; Jauffret *et al.,* 2001). Admittedly, these images are grainy and black and white however, more up to date electron microscopy (Eto *et al.,* 2009) and immunofluorescence staining (Matsumoto *et al.,* 2006) have supported these original findings. Unfortunately, in these two more recent papers, there is limited detail in the methods as to how the tissue was extracted. The authors don't state the exact methods of adipose tissue aspiration and in the case of Matsumoto et al., the method of re-insertion is not specified. Despite this, there is ample evidence when combined with Jauffret *et al.,* and von Heimburg *et al.,* to suggest that lipoaspiration and especially lipoaspiration carried out using the Coleman technique does not damage adipose tissue significantly.

In addition to maintaining the cellular integrity of the adipose tissue, Coleman also centrifuged the lipoaspirate to remove oil from the tissue. Others describe this as a wash step (Sesé *et al.,* 2020; Tonnard *et al.,* 2013), however Coleman emphasises that this is incorrect as washing the adipose tissue may lead to damage to the tissue (Coleman, 1998).

1.3.2 Adipose tissue resorption

Despite Coleman's refining of various aspects of fat grafting, there remained problems with the long-term viability of these grafts. The fat tissue itself was often observed to be reabsorbed by the body with up to as much as 85 % of the graft volume being lost a few months after insertion (Kølle *et al.,* 2013; Khouri *et al.,* 2012). This led to unpredictable surgical outcomes which Coleman did try to address with his grafting technique (Coleman, 1995). Coleman believed that inserting adipose tissue as the cannula was withdrawn and layering the lipoaspirate led to better resorption outcomes and advocated for more consistent photographic evidence to better assess resorption (Coleman, 1995, 2006).

Nevertheless, resorption remains an issue with grafting techniques (Herly *et al.,* 2017). This is historically seen as a result of adipocyte death due to inadequate tissue oxygenation and vascular support post transplantation (Karacaoglu *et al.,* 2005). Given that adipocytes provide the main structural volume of adipose tissue, if these cells are resorbed then most of the volume of an adipose tissue graft is also resorbed (Eto *et al.,* 2009). In 2001 it was discovered that a subpopulation

of MSCs could be isolated from lipoaspirate, and that they could differentiate into multiple different cell lineages including adipocytes (Zuk *et al.,* 2001). These cells are now what we know as ADSCs, and their discovery led to advances and excitement in the adipose grafting community. These ADSC were found to secrete angiogenic factors and were capable of endothelial differentiation, improving neovascularisation *in vivo* (Cao *et al.,* 2005; Rehman *et al.,* 2004). It was theorised that the neovascular properties of these ADSCs could be used to assist the survival of adipocytes upon grafting. A technique known as "cell-assisted lipotransfer" (CAL) was developed whereby lipoaspirate was removed from patients and half of the lipoaspirate was used to isolate ADSCs (figure 1.12). These ADSCs were then added to the remaining half of lipoaspirate that was then injected as the graft tissue. This technique led to decreased resorption of adipose tissue grafts and in animal studies the ADSCs transplanted as part of the CAL were found to undergo endothelial differentiation and become incorporated into the existing vascular networks (Matsumoto *et al.,* 2006). Furthermore, CAL was shown to be effective at reducing resorption of adipose tissue during autologous fat grafting (Yoshimura *et al.,* 2008). The effectiveness of this technique was demonstrated by a triple-blind, placebo-controlled trial of CAL that found that grafts using CAL retained a higher volume of adipose tissue over 121 days compared to traditional lipoaspirate grafting (Kølle *et al.,* 2013). Though it is worth mentioning that the authors of this trial altered the original CAL technique from Matsumoto et al. for this trial. Kølle et al. isolated ADSCs two weeks before the main grafting operation and expanded the ADSC population. This allowed them to add ADSCs at a significantly higher level than would otherwise be possible in CAL. However, given that the elective nature of most fat grafting operations this is not an unreasonable modification to the technique and while it weakens the results in relation to CAL in Yoshimura *et al.,* it demonstrates the effectiveness of this modified technique and the power of ADSCs.

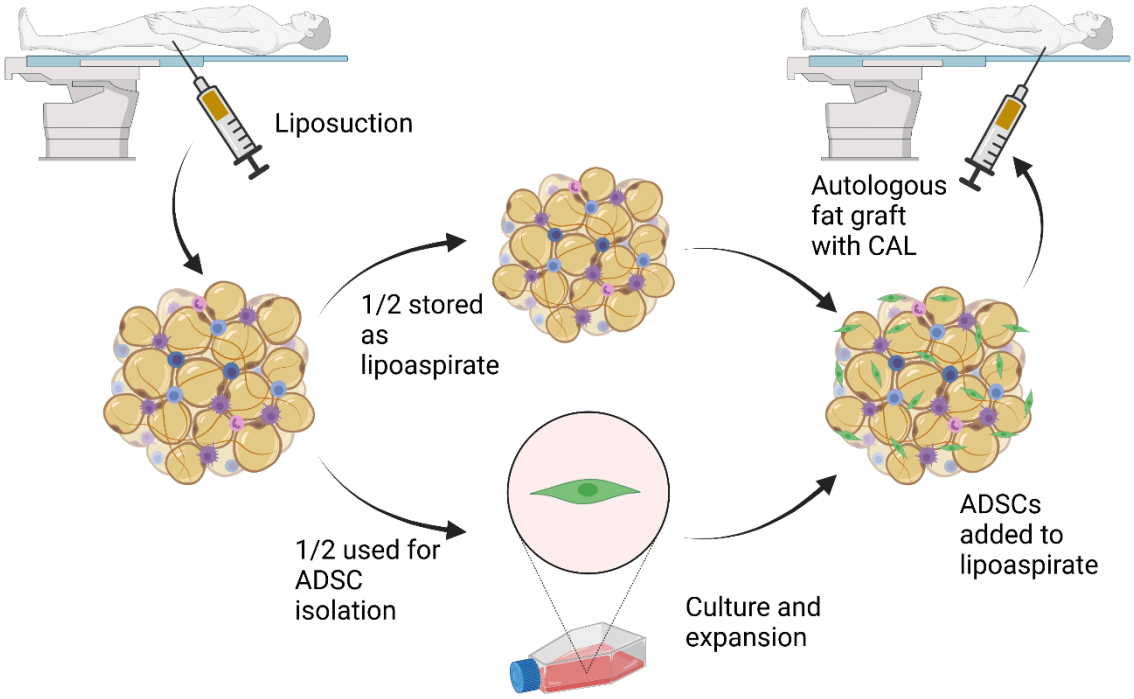

Figure 1.12. Cell-assisted lipotransfer. Resorption of adipose tissue is decreased when ADSCs are used to augment adipose grafts. CAL is carried out by removing adipose tissue and separating the tissue in half. One half is used to isolate ADSCs. These ADSC are then used to augment unaltered adipose tissue that is grafted back into the patient at the intended grafting site. Figure created with Biorender.com.

1.3.3 Adipose tissue in skin regeneration

It had been previously noted by Coleman that along with the effective filling of depressed hand scars, adipose tissue grafts had a regenerative impact on the skin, refreshing it and often improving the scar (Coleman, 2002). Along with these observations, the discovery of the ADSC subpopulation and the effect they had on the local microenvironment prompted Rigotti et al. (2007) to assess the regenerative potential of adipose tissue. The authors took lipoaspirate and injected it underneath fibrotic lesions caused by radiotherapy and evaluated skin morbidity pre- and post-operatively using the LENT-SOMA scale (Routledge *et al.,* 2003). Rigotti et al. found an improvement in all but one patient with skin found to be more hydrated with less collagen present, and increased amounts of vasculature (Rigotti *et al.,* 2007). It should also be noted, the authors did not carry out the Coleman technique. They noted that their adipocytes appeared damaged and did have high rates of resorption. The treatment was shown to be effective on the vast majority of patients (12) however, the trial only contained 13 individuals.

This work was then supported by results from Klinger at al. who injected lipoaspirate underneath facial burns (Klinger *et al.,* 2008). This was a small series of case studies with all three patients' burns healing after treatment. The vasculature and ECM of the burn area improved and the skin regained elasticity (figure 1.13). The authors of both these papers hypothesised that it is the ADSC population of the adipose tissue that is responsible for the regenerative affect observed (Klinger *et al.,* 2008; Rigotti *et al.,* 2007). It should also be noted that both studies only treated patients with very severe injuries. This perhaps overstates the effectiveness of any treatment, as any improvement would be more noticeable. Furthermore, due to the severity of the cases, no placebo controls were used although histological images were taken to support their observations. Finally, both studies used a small number of patients. The work of these two groups were effective at demonstrating the potential of regenerative autologous fat grafting however future studies would require controls and much larger numbers of participants.

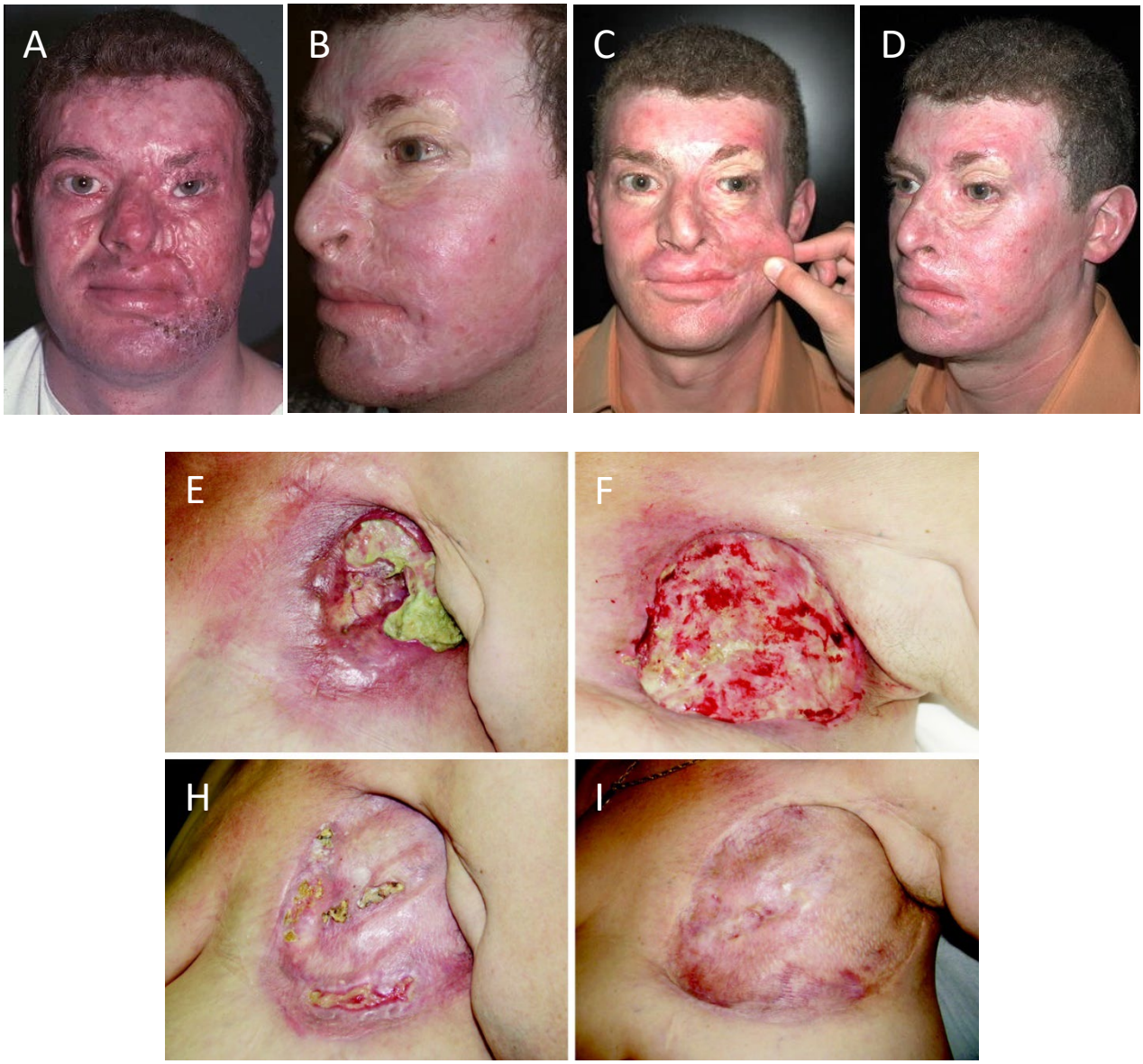

Figure 1.13. The regenerative ability of adipose grafting. (A-D) Images of a case study from Klinger *et al.,* (2008) showing a scar **(A)** 5-years after injury and **(B)** 8-years following injury. Two autologous fat grafts, 3 months apart, lead to a regeneration of the tissue **(C-D)** 3 months following treatment. Images used under Copyright Clearance Centre Rights licence 5307821059173. **(E-I)** Images of patient from a clinical trial by Rigotti *et al.,* (2007). Images show an ulcer following **(E)** radiotherapy, **(F)** autologous fat graft, **(H)** skin graft, **(I)** three more autologous fat grafts. Images used under Copyright Clearance Centre Rights licence 5307821458215.

1.3.4 Isolating the SVF

1.3.4.1 Nanofat

This work led to increased investigation into the regenerative ability of adipose tissue on scars (Jaspers *et al.,* 2017; Byrne *et al.,* 2016; Maione *et al.,* 2014; Gentile *et al.,* 2014; Pallua *et al.,* 2014b; Klinger *et al.,* 2013). These studies often posited that ADSCs and the cells in the SVF were the main components of adipose tissue responsible for the regenerative affects seen (Jaspers *et al.,* 2017; Carstens *et al.,* 2017; Byrne *et al.,* 2016; Uysal *et al.,* 2014; Pallua *et al.,* 2014b). The SVF could be isolated enzymatically via treatment from collagenase enzyme and the cellular yield is high (5 $x10^5$ cells/gram of lipoaspirate; Carstens *et al.,* 2015). Regulatory bodies, including the American Food and Drug Administration consider that using enzymatic agents upon cells is more than "minimal manipulation" and thus places strict regulatory measures on enzymatic-SVF (U.S. Department of Health and Human Services Food and Drug Administration *et al.,* 2020, page 14). As a result of this many techniques to process adipose tissue in a non-enzymatic manner have been developed (van Dongen *et al.,* 2019; Yao *et al.,* 2017; Mashiko *et al.,* 2017; lo Furno *et al.,* 2017; Bianchi *et al.,* 2013; Tonnard *et al.,* 2013).

Nanofat is an adipose formulation developed by Tonnard et al. in 2013. Initially the technique was developed to allow adipose tissue to be inserted into more delicate areas using smaller cannulas (27-gauge) than the bulky structure of lipoaspirate would allow (Tonnard *et al.,* 2013). By passing the lipoaspirate between two syringes with a Luer-Lock connector (figure 1.14), this solution is filtered, and the shear force applied to the adipose tissue causes a liquid paste to form. This paste could be injected with a smaller cannula. Live-dead staining identified that the adipocytes in the lipoaspirate had been lysed and this led to the conversion of the adipose tissue into a liquid form. The authors noted a "rejuvenation" of skin treated with injections of Nanofat and believed that cells in the SVF were key to this effect.

Since this initial paper Nanofat has gone on to be used to treat and heal damaged skin and scars effectively in case studies and small clinical trials (Uyulmaz *et al.,* 2018; Gentile *et al.,* 2017; Kemaloğlu, 2016). Tonnard and others (Sesé *et al.,* 2019; lo Furno *et al.,* 2017; Tonnard *et al.,* 2013) have suggested that high volumes of secreted factors such as VEGF, HFG, and platelet-derived growth factor (PDGF) play a role in this, alongside factors from the lysed adipocytes promoting an inflammatory response. Nanofat is a good potential therapeutic due to the easily injectable nature of the formulation. Tonnard insists that due to the lack of adipocytes contained within, Nanofat is not a filling material (Tonnard *et al.,* 2020) and shouldn't be used as such. In the 2013 paper, the authors claim that there are no adipocytes in the Nanofat (Tonnard *et al.,* 2013) and in their

live/dead imaging this certainly appears to be the case. However, in other work characterising Nanofat there does appear to be a small number of adipocytes remaining (Sesé *et al.,* 2019; lo Furno *et al.,* 2017). The number remaining does seem to be very small and likely insignificant, but it should be noted that Nanofat is not devoid of adipocytes as Tonnard et al. claim.

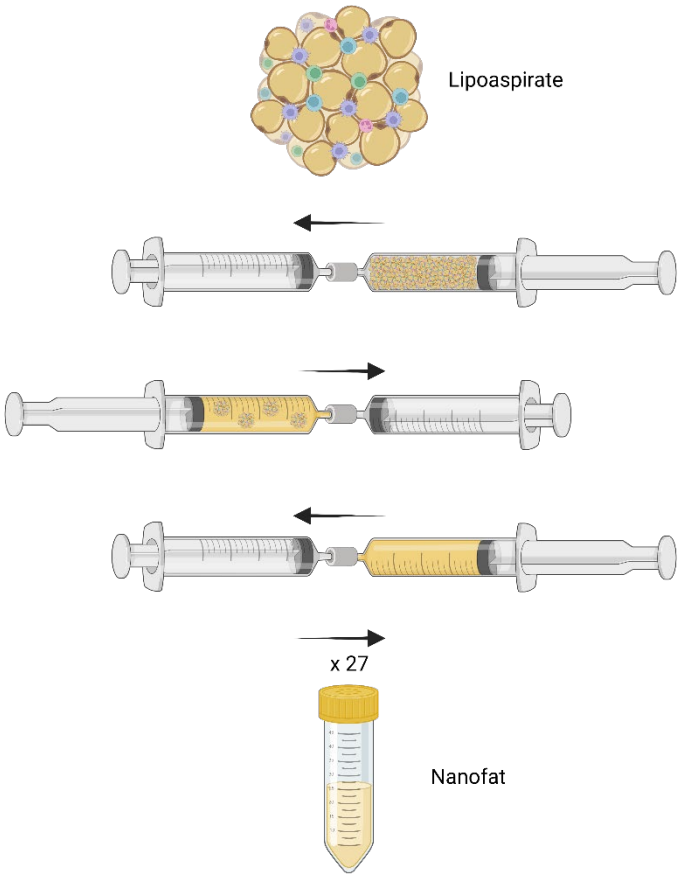

Figure 1.14. Nanofat generation. Nanofat is generated by passing adipose tissue between syringes 30 times. A pass is defined as transferring adipose tissue from one syringe to the other. This fragments the adipose tissue and causes lysis of the adipocyte population in the adipose tissue and leads to a paste forming. Figure created with Biorender.com.

There has been relatively little work to characterise the Nanofat formulation. Osinga et al. (2015) investigated the effect that Nanofat generation had on cell viability and found there was no decrease in viability when adipose tissue was converted to Nanofat. More recent work on the other hand has demonstrated that increasing shear force on adipose tissue when making Nanofat does lower cell viability (Qiu *et al.,* 2021; Chen *et al.,* 2020) and decrease cell yield. As adipocytes make up only a small portion of adipose tissue's cellular population their lysis is unlikely to give the appearance of a significant decrease in cell number when cell counts are performed from confocal images, such as in the work by Osinga *et al.,* for a more accurate measure of cell number, cells should be counted via DNA quantification. The group also found no decrease in adipocyte number which disagrees with other literature (Sesé *et al.,* 2019; lo Furno *et al.,* 2017; Tonnard *et al.,* 2013). This is possibly a result of Osinga et al. counting adipocytes by eye using confocal images stained with BODIPY, where it is difficult to establish whether stained lipid is an adipocyte or a lipid vesicle released by a lysed adipocyte.

Originally, Tonnard et al. (2013) believed that conversion of lipoaspirate to Nanofat reduced the volume of adipose tissue by 90 % and isolated roughly 20,000 SVF cells for every ml of lipoaspirate started with. A more recent study has shown that Nanofat formation only reduces the volume of lipoaspirate by 15 % and contains 6.6 x10^6 SVF cells (Sesé *et al.,* 2019). This is in part due to developments in the Nanofat technique (the authors of Sesé et al. (2019) collaborated with Tonnard to develop specific filters for Nanofat grafting that will likely result in less tissue loss). Also, cell number was quantified in a more accurate manner (DNA quantification as opposed to microscopically counting cells).

In an attempt to maximise the number of ADSCs in Nanofat, lo Furno et al. removed the filtration step to make what they termed "Nanofat 2.0". They agree that the regenerative effects of adipose tissue and Nanofat likely derive from the SVF alongside factors secreted from lysed adipocytes. Nanofat 2.0 was found to contain more cells than Tonnard's Nanofat and the cells that were isolated proliferated faster (lo Furno *et al.,* 2017). The authors unfortunately do not provide a number of cells per gram (or ml) of adipose tissue and while staining for a variety of ADSC markers, they do not give a percentage of cells expressing all these markers. This makes it difficult to directly compare the data generated for Nanofat 2.0 to work done by Tonnard and Sesé and limits this works impact on the field. As such there are few research groups using this formulation.

The effectiveness of Nanofat has been demonstrated clinically in small scale case studies (Kemaloğlu, 2016) and larger scale trials (Uyulmaz *et al.,* 2018; Gentile *et al.,* 2017). Modifications to the Nanofat technique have been trialled and methods to increase the number of SVF cells in the

Nanofat yielded better clinical results (Gentile *et al.,* 2017). This trial used histological evaluation of the scars post treatment alongside patient and clinician scoring, however contained no placebo control. Another trial also demonstrated that Nanofat treatment reduced scarring; however, this was only assessed by patient and clinician score, and again with no placebo control (Uyulmaz *et al.,* 2018). The flaws in these trials indicate that larger scale, controlled trials are needed to investigate the impact Nanofat has on scar tissue but there is enough initial evidence to suggest it is a promising treatment.

1.3.5 Alternative methods of mechanically isolating the SVF

One of the benefits of mechanically emulsifying adipose tissue into Nanofat was that by removing the adipocyte population, the concentration of SVF cells and ADSCs was increased in this formulation (Sesé *et al.,* 2019). In an attempt to concentrate the SVF population in adipose tissue other forms of mechanical emulsification of adipose tissue have been developed (van Dongen *et al.,* 2019; Yao *et al.,* 2017; Mashiko *et al.,* 2017; Bianchi *et al.,* 2013). Lipogems® is a device to emulsify lipoaspirate by placing the adipose tissue in a sealed container with ball bearings and shaking the container (Bianchi *et al.,* 2013). Histological images of this Lipogem® generated adipose tissue show a fragmentation of the macrostructure of lipoaspirate. However, the tissue was less fragmented than Nanofat (Sesé *et al.,* 2019). Furthermore, the percentage of ADSCs in the tissue was increased relative to unprocessed lipoaspirate but no total values were given and thus it is impossible to compare the cellular yield to other techniques (Bianchi *et al.,* 2013). Lipogem® generated adipose tissue has shown some positive regenerative effect in clinical trials (Lonardi *et al.,* 2019; Barfod & Blønd, 2019) however, there is little research in relation to Lipogems® and scarring.

Another method of adipose tissue emulsification is using sharp blades (Mashiko *et al.,* 2017). Adipose tissue was placed in a container with spinning blades that broke apart the tissue and lysed the adipocytes, making a formulation the authors termed “squeezed fat”. The authors of this study made an emulsified fat similar to Tonnard et al. (2013) to compare their formulation to. Squeezed fat was more fragmented in comparison to unprocessed lipoaspirate however appeared to have more structure than Nanofat. The cellular yield was about 320,000 cells per gram of lipoaspirate and was higher than in the Nanofat they generated (130,000). However, the cellular yield was still less than half of that recorded by Sesé et al. (2019) in their Nanofat.

By disrupting the fat and lysing adipocytes Tonnard et al. had been able to concentrate the number of SVF cells in their adipose formulations. This was improved upon further by the development of formulations often termed “SVF-gels” (Sesé *et al.,* 2020; Wang *et al.,* 2019; Yao *et al.,* 2017; van Dongen *et al.,* 2016). These gels are formulations of adipose tissue that have been

emulsified and fragmented (often to make Nanofat) and the resulting solution is centrifuged (figure 1.15). This processing of the adipose tissue generates an oil phase that can be removed, leaving only SVF cells in a paste/ gel that can be injected underneath the skin in small 27-gauge needles (Yang *et al.,* 2021; Wang *et al.,* 2019).

Histological examination of this SVF-gel reveals a heavily disaggregated formulation with little structure remaining. The formulation mostly contains clusters of SVF cells (Sesé *et al.,* 2020). The yield per gram or ml of the formulation is also considerably higher than Nanofat or aspirated adipose tissue with yields ranging from 30 $x10^7$ cells/g (Sesé *et al.,* 2020) to 4 $x10^5$ cells/ml (Yang *et al.,* 2021; Yao *et al.,* 2017). SVF-gel has been shown to increase the rate of healing in wound models (Wang *et al.,* 2019; Yao *et al.,* 2017) and regenerate hypertrophic scars (Yang *et al.,* 2021). These gels have also been shown to heal wounds more quickly than collagenase isolated SVF cells, implying that the ECM components left in the gel aide regeneration (Wang *et al.,* 2019). However, this study didn't add an equal number of cells between SVF and SVF-gel treated conditions and so this may be a result of more SVF cells being added in the SVF gel. This gel seems effective in regenerating and rejuvenating skin (Yang *et al.,* 2021; Wang *et al.,* 2019; Yao *et al.,* 2017). However, there are few comparisons between the effectiveness of SVF-gel and other adipose tissues such as Nanofat and lipoaspirate. Even in studies comparing the formulations, there is no controlled comparison between patients (Yang *et al.,* 2021). As such, further characterisation as to the effectiveness of these formulations compared to each other is required and is something this work hopes to address.

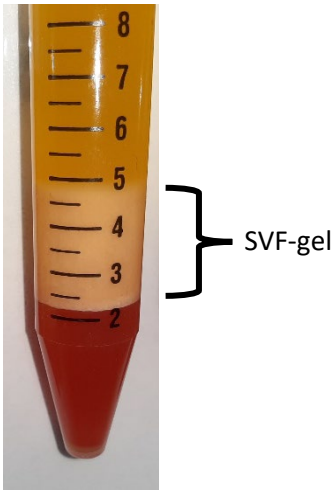

Figure 1.15. SVF-gel. Nanofat and other emulsified fat formulations can be centrifuged to remove the lipid oil from the SVF and ECM (highlighted segment).

1.3.6 Clinical trials of autologous fat grafting

Klinger *et al.,* (2008) and Rigotti *et al.,* (2007) represent the first uses of autologous fat grafting to alleviate the symptoms of hypertrophic scarring. Since this time, there has been an increase in the reported use of autologous fat grafting as a clinical treatment (Brown *et al.,* 2020; Gal *et al.,* 2017; Jaspers *et al.,* 2017; Juhl *et al.,* 2016; Byrne *et al.,* 2016; Maione *et al.,* 2014; Pallua *et al.,* 2014a; Klinger *et al.,* 2013; Azzam *et al.,* 2013; Sardesai & Moore, 2007). Overall, it is reported that grafting lipoaspirate underneath fibrotic scars does improve the scar tissue with an increase in elasticity (Jaspers *et al.,* 2017), a decrease in hardness (Maione *et al.,* 2014; Klinger *et al.,* 2013), and decreased pain (Sardesai & Moore, 2007). Most studies use the POSAS system to assess the improvement of scar tissue (Brown *et al.,* 2020; Jaspers *et al.,* 2017; Juhl, Karlsson, & Damsgaard, 2016; Byrne *et al.,* 2016; Maione *et al.,* 2014; Pallua *et al.,* 2014a; Klinger *et al.,* 2013; Sardesai & Moore, 2007). This system objectively measures the vascularity, pigmentation, and pliability of scars using simple non-invasive measurements. Additionally, it subjectively assesses the pain in the patients from their point of view (Lenzi *et al.,* 2019). The Vancouver Scar Scale can also be used (Gal *et al.,* 2017) and contains the objective measures POSAS does (as POSAS is based upon the Vancouver Scar Scale) however, it does not include the patient's opinion (Baryza & Baryza, 1995).

A concern in the reporting of these data is often a lack of a control (Byrne *et al.,* 2016; Maione *et al.,* 2014; Pallua *et al.,* 2014a; Sardesai & Moore, 2007). The most common control is the injection of saline under a separate section of the scar and comparing that to the section of scar tissue treated with adipose tissue (Brown *et al.,* 2020; Jaspers *et al.,* 2017; Klinger *et al.,* 2013). However, many reported data sets do not have this control (Byrne *et al.,* 2016; Maione *et al.,* 2014; Pallua *et al.,* 2014a; Sardesai & Moore, 2007) lowering the impact of the work. The use of this control in future is of critical importance given recent data that while autologous grafting of lipoaspirate does improve the POSAS score in treated scars, there was no difference to scars receiving a subcutaneous injection of saline (Brown *et al.,* 2020). This work by Brown et al. was a randomised, double blinded, placebo-controlled trial, which many reports of autologous fat grafting healing scars are not (Byrne *et al.,* 2016; Maione *et al.,* 2014; Pallua *et al.,* 2014a; Sardesai & Moore, 2007) and thus is fairly robust data. The only criticism of this trial would be the relatively small number of patients treated (17, Brown *et al.,* 2020). The number of patients in most case studies or trials is between 20-80 (Jaspers *et al.,* 2017; Maione *et al.,* 2014; Pallua *et al.,* 2014a). There are examples with fewer than this (8; Gal, Ramirez and Maguina, 2017) and the largest patient number identified for this thesis is 694 (Klinger *et al.,* 2013). In future, patient number must increase to improve the standard of data.

Another issue with data on autologous fat grafting is selectivity of reporting. In a recent meta-analysis of autologous fat grafting studies (Walocko *et al.,* 2018), a report indicating that autologous fat grafting made no improvement to scar quality (Gal *et al.,* 2017) wasn't included despite meeting the inclusion criteria, in my opinion. A possible explanation as to why it was not included was that only a minimal volume of lipoaspirate was added underneath scars (5ml; Gal, Ramirez and Maguina, 2017) and thus Walocko et al. didn't consider the data useful. There are also examples of studies stating methods of quantifying scar improvement that were carried out but the results are then not reported in the respective study (Malik *et al.,* 2019; Gentile *et al.,* 2017).

There are studies using injected ADSC in humans to treat various conditions (Hurd *et al.,* 2020; Jones *et al.,* 2018; Fodor & Paulseth, 2016), however, to my knowledge there has been no study carried out investigating injecting ADSCs to treat human scar tissue (although the effect of factors secreted from ADSCs has been investigated (Zhou *et al.,* 2016)). This is likely because of the difficulties of using ADSCs in humans mentioned earlier and because Nanofat and SVF techniques concentrate the number of SVF and ADSC cells (Sesé *et al.,* 2019, 2020) and are thus an acceptable substitute to use. Nanofat has been demonstrated to be effective at lowering POSAS scores in trials (Rageh *et al.,* 2021; Uyulmaz *et al.,* 2018; Bhooshan *et al.,* 2018; Gentile *et al.,* 2017). It should be noted that treating more established scars (> 5 years) with Nanofat led to more effective outcomes in one report (Bhooshan *et al.,* 2018).

There have been reports of complications following fat grafting treatments (Rageh *et al.,* 2021; Shen *et al.,* 2016). Furthermore, SVF cells release factors that could aide in the growth of cancers and tumours raising the question of the safety of autologous fat grafting. Large scale trials have been carried out and found that autologous fat grafting is safe in an oncological setting (Hanson *et al.,* 2020) and the risk of complications has been found to be exceedingly low (Hurd *et al.,* 2020; Krastev *et al.,* 2018).

SVF injections under scars have also been shown to improve quality (Lee *et al.,* 2018; Gentile *et al.,* 2014), improve functionality (Carstens *et al.,* 2017), and elasticity (Carstens *et al.,* 2015). It should be noted though, that there is variation in these SVF treatments with mechanical isolation from Nanofat (Bhooshan *et al.,* 2018; Gentile *et al.,* 2017), centrifugation (Lee *et al.,* 2018), and enzymatic isolation (Carstens *et al.,* 2017; Gentile *et al.,* 2014). A recent study by Van Dongen et al. (2021) is a well-designed, double-blind, placebo-controlled trial examining the impact of mechanically isolated SVF on scar. The key finding from this trial was that while an initial improvement (6 months post-operation) was seen in SVF treated scars, following the 12-month check-up there was no difference compared to saline control. This questions the findings of other

studies that did not follow up at least 12 months following treatment (Jaspers *et al.,* 2017; Juhl *et al.,* 2016; Maione *et al.,* 2014).

Overall, there is good initial evidence that autologous grafting of lipoaspirate, Nanofat and SVF improves the quality of scars (Bhooshan *et al.,* 2018; Carstens *et al.,* 2017; Klinger *et al.,* 2013). However, questions raised by more rigorous trials (van Dongen *et al.,* 2021; Brown *et al.,* 2020) highlight the need for more high-level testing and investigations into the mechanisms behind adipose tissues regenerative impact on scar tissue.

1.4 The mechanisms behind adipose tissue scar amelioration

1.4.1 Increased angiogenesis

Following dermal injury, the vasculature surrounding the wound is often damaged, leading to a decreased oxygen supply around the wound. This often leads to the wound environment becoming hypoxic and triggering the release of HIF-1α (Xing *et al.,* 2011), leading to a change in gene expression in the surrounding tissue (Lindegren *et al.,* 2019). Scars have been shown to contain increased levels of HIF-1α (Distler *et al.,* 2007). HIF-1α release is important in regular wound healing as it causes secretion of VEGF-1 in the surrounding cells (Lin *et al.,* 2004), leading to blood vessel repair. However, it also encourages CTFG expression which, as previously described in section 1.1.2.1, leads to myofibroblast differentiation (Tsai *et al.,* 2018; Grotendorst & Duncan, 2005). Furthermore, prolonged exposure to HIF-1α has been shown to increase TGF-β1 production and increase expression of collagen and fibronectin genes (Distler *et al.,* 2007). Finally, in radiation induced scars, hypoxia induced genes and CTFG expression is dysregulated (Lindegren *et al.,* 2019), making it clear that hypoxia exacerbates fibrosis.

In clinical trials and case studies, following autologous fat grafting with adipose tissue, Nanofat, or the SVF, there is often a reported increase in vascularisation around and in the scar tissue (Lee *et al.,* 2018; Bhooshan *et al.,* 2018; Gentile *et al.,* 2017; Sultan *et al.,* 2012; Rigotti *et al.,* 2007). One of the main hypotheses as to why adipose tissue increases this vascularity is the SVF contains among it pro-angiogenic cells. Inside the SVF there are endothelial cells that form the lining of blood vessels (Eto *et al.,* 2009), alongside ADSCs that can differentiate into endothelial cells (Cao *et al.,* 2005). These cells from the SVF have been injected into animal models and have been found to be incorporated into the new blood vessels that have been formed (Koh *et al.,* 2011). Additionally, the SVF also contains pericytes which are an essential cell in angiogenesis. These cells secrete VEGF (Darland *et al.,* 2003), encourage the proliferation and growth of endothelial cells and new vessels (Carmeliet & Jain, 2011), and maintain the integrity of these vessels by binding at vessel junctions (Sims, 1986).

Adipose tissue can also stimulate angiogenesis and help relieve hypoxia in a paracrine fashion. Lipoaspirate has been found to secrete pro-angiogenic factors such as VEGF, PDGF-BB, and insulin-like growth factor-1 (Choi *et al.,* 2019; Grasys *et al.,* 2016). Grasys *et al.* had previously found that the SVF secretes these same growth factors and speculated that the SVF is responsible for the production of most of these secretory growth factors from adipose tissue (Pallua, *et al.,* 2014b). It should be noted however, that they did not directly compare the concentration of these growth factors released from lipoaspirate to just the SVF, so these conclusions need further testing. In

addition to this, grafted adipose tissue has also been shown to change the gene expression profile of irradiated tissue (Lindegren *et al.,* 2019). The group found that hypoxic genes were upregulated following radiation damage however, adipose tissue grafting removed this up-regulation. The mode of action through which adipose tissue had this effect was not identified. Despite this, the *in vivo* and *in vitro* literature has clearly demonstrated that adipose tissue can promote angiogenesis and relieve hypoxia.

ADSCs have also been shown to play a role in relieving hypoxia and secrete paracrine signals that promote angiogenesis (Rehman *et al.,* 2004). Cell culture media conditioned with paracrine factors from ADSCs has been used to increase the expression of ephrin-B2, a marker of blood vessel formation (Angmalisang *et al.,* 2018). Alongside this, extracellular vesicles collected from ADSCs promoted the formation of new blood vessels in mice models (Mou *et al.,* 2019). Although, the contents of these extracellular vesicles were not examined, so the factors responsible can only be hypothesised.

It has been observed that there is a sub-population of pro-angiogenic ADSC that are CD34+/CD146+ (Borrelli, *et al.,* 2020; Deleon *et al.,* 2021). These ADSCs were found to secrete significantly more pro-angiogenic factors than other ADSCs and promote vessel formation in animals to a greater degree than CD146- ADSCs (Borrelli, *et al.,* 2020). Furthermore, this sub-population was shown to restore vascularity in an animal burn model at an increased rate compared to CD146- ADSCs (Deleon *et al.,* 2021).

A final mechanism through which adipose tissue has been observed to increase angiogenesis is by promoting the differentiation of monocytes to M2-like macrophages (Dong *et al.,* 2013). When treated with ADSC extracellular vesicles, more M2-like macrophages were found to be present in the recipient tissue (Yi *et al.,* 2021) and these macrophages have been shown to secrete pro-angiogenic cytokines such as VEGF (Dong *et al.,* 2013).

1.4.2 Modulating the immune system

Fibrosis is often caused by chronic inflammation or over expression of pro-inflammatory cytokines (Borthwick *et al.,* 2013). Grafting of adipose tissue into animal models has been shown to decrease the levels of pro-inflammatory cytokines such as TNF-α, cyclooxygenase-2 and nitic oxide synthase (Huang *et al.,* 2015). Furthermore, animal models using grafted ADSCs have led to; increased levels of IL-10 (Zhang *et al.,* 2017), inhibition of IL-6, IL-1β, and TNF-α production (Kotani *et al.,* 2017), reduced immune cell recruitment, and was shown to limit collagen deposition following wounding (Zhang *et al.,* 2017). It should be noted however, that Zhang et al. carried out their experiments in diabetic mice and while there will be dysregulated inflammation in these mice the

inflammatory context will not be identical to hypertrophic scarring. In Kotani *et al.,* following bleomycin treatment, more mice survived when ADSCs were injected. The authors attributed this increased survival to lowered inflammation as a result of the ADSC injection. They also showed increased macrophage apoptosis but unfortunately did not investigate whether this effect was applied to all macrophages evenly or was in favour of a particular macrophage phenotype (Kotani *et al.,* 2017).

There is evidence that ADSCs illicit this anti-inflammatory response in a paracrine fashion, with ADSC conditioned media and ADSC derived extracellular vesicles being capable of reducing inflammation in both obese mice (Zhao *et al.,* 2018), and humans (Kruger *et al.,* 2018). Once again, an obese model is not a perfect replica of a fibrotic model however, there is constant inflammation found in obese tissue (Fuster *et al.,* 2016). Both groups found that IL-10 was increased in tissue following either conditioned media- or extracellular vesicle-treatment and M2-like macrophages were present in increased number (Kruger *et al.,* 2018; Zhao *et al.,* 2018). Although once again, Zhao et al. did not investigate the contents of the ADSC derived extracellular vesicles, so it can only be speculated that ADSC-derived extracellular vesicles are the source of this IL-10 increase.

The traditional M1-like, classically activated, or M2-like, alternatively activated, model of macrophage activation is a simplistic view of macrophage activation. It is now understood that a spectrum of activation states exists with IL-10 leading to activation of a M2c, anti-inflammatory phenotype (Witherel *et al.,* 2019). It is my belief that factors from ADSCs and adipose tissue are leading to this form of macrophage polarisation via IL-10 release.

ADSCs are not the only cellular population in adipose tissue that reduce inflammation. Transplanted SVF leads to less M1-like macrophage presence in wounds (Choi *et al.,* 2019), reduced IL-6 and TNF-α production (Zhu *et al.,* 2018), and more IL-10 expression in murine models (Choi *et al.,* 2019). Additionally, direct comparisons between the SVF and ADSC using equal numbers of cells demonstrate the SVF has a greater anti-inflammatory affect (Choi *et al.,* 2019; Bowles *et al.,* 2017). In addition to any paracrine signalling from the grafted SVF, there will also be a population of immune cells in the SVF (Eto *et al.,* 2009) that may contribute to this, especially as the SVF has been found to contain a significant population of M2-like macrophages (Guo *et al.,* 2016).

1.4.3 Restoring correct tissue environment

Adipocytes also play a role in the immunomodulatory ability of adipose tissue. SVF isolated from mice with the adiponectin gene knocked out contains more M1-like macrophages and increased inflammatory cytokines. On the other hand, treatment with adiponectin led to adipose tissue with more M2-like macrophages present (Ohashi *et al.,* 2010). Given the production of

adiponectin by adipocytes (Scherer *et al.,* 1995; Maeda *et al.,* 1996), it is likely that adipocytes also play a role in an anti-inflammatory action from adipose tissue.

Adipocytes themselves play an important role in wound healing and help to regulate the process. The removal of adipocytes from the dermis leads to decreased inflammation at the outset of the wound healing response and decreased contraction around the wound site, delaying wound healing (Shook *et al.,* 2020). Furthermore, adipocytes repopulate the dermis following wounding of the skin. If this re-population is inhibited then a failure of wound closure and chronic inflammation is observed in mice models (Schmidt & Horsley, 2013). Additionally, there are reports of myofibroblasts surrounding hair follicles differentiating to adipocytes around wounds (Plikus *et al.,* 2017; Guerrero-Juarez *et al.,* 2019). Taken together, these reports show that adipocytes play a role in ordinary wound healing and via lipolysis can exert changes on the wound microenvironment (Shook *et al.,* 2020). It is possible that a mechanism behind adipose tissue-dependent scar regeneration is the restoration of the adipocyte population in the dermis and a restoration of adipocyte-based signalling normally exhibited in the wound microenvironment (Schmidt & Horsley, 2013).

This poses the question of why SVF-based treatments such as Nanofat and SVG-gel are also effective at scar regeneration as they contain few adipocytes (Sesé *et al.,* 2020; Tonnard *et al.,* 2013). However, adipocyte progenitors are found in the SVF (Carraro *et al.,* 1991; Rodeheffer *et al.,* 2008) and ADSCs are capable of adipocyte differentiation (Zuk *et al.,* 2001). In fact, isolated ADSCs differentiated via adipogenic differentiation media were implanted into mice scarring models and showed comparable healing to Coleman fat grafting (Chen *et al.,* 2017). There were limitations to this, the main one being that in cells treated with differentiation media, differentiated adipocytes were not sorted from undifferentiated ADSCs and while there was a large adipocyte presence it cannot be ensured that all ADSCs will have differentiated. Thus, as opposed to seeing the effect of only differentiated adipocytes on scarring, the group might have been observing adipocytes and ADSCs. Despite this, the work shows the importance of adipocytes in ordinary wound healing and further demonstrates how the SVF may be impacting on scarring.

A clinical trial has observed that an injection of only saline, as opposed to adipose tissue, underneath scars can also lead to improved scar quality (Brown *et al.,* 2020). This highlights perhaps that disrupting underlying scar tissue and “resetting” the wound microenvironment may help regenerate scar tissue. This is likely because in scars the ECM is under increased tension (Meyer & Mcgrouther, 1991) which can lead to a feedback loop wherein the tension releases TGF-β1 from the latent TGF-β1 complex (Wipff *et al.,* 2007), causing myofibroblast differentiation and increasing ECM

tension and so on. The injection of adipose tissue (or anything) may reset ECM tension. Additionally, the healthy ECM of the injected adipose tissue or SVF may lower the tension in the surrounding microenvironment. The ECM of adipose tissue has been demonstrated to increase the rate of wound healing and generate healthy ECM (Zhou *et al.,* 2019) and hydrogels composed of adipose tissue ECM have been used to deliver growth factors that aide wound regeneration (van Dongen *et al.,* 2019).

Autologous fat grafting may also lead to inhibition of myofibroblast differentiation via increasing the number of cells present in the dermis. When plated at a low density, fibroblasts spontaneously differentiate into myofibroblasts (Masurtt *et al.,* 1996). However, when seeded at a high density with cells surrounding them differentiation is inhibited (Petridou *et al.,* 1999). This inhibition is likely a result of the high number of cells surrounding the fibroblasts binding the N-cadherin proteins on the outer membrane of the fibroblasts, which has been shown to inhibit myofibroblast differentiation (Michalik *et al.,* 2011). Mesenchymal stem cells (Ishimine *et al.,* 2013) and ADSCs possess N-cadherin (Ritter *et al.,* 2015). By implanting a large population of cells into the dermis and ECM, autologous fat grafting may provide a large cell population that binds fibroblast N-cadherin and inhibits myofibroblast differentiation.

1.4.4 Inhibition of myofibroblast differentiation

A final mechanism through which adipose tissue might regenerate scars is by preventing the differentiation of fibroblasts to myofibroblasts (Ma *et al.,* 2020; Spiekman *et al.,* 2014; Uysal *et al.,* 2014). This would lower ECM production, relieve tension in the wound microenvironment and prevent more scar tissue from being produced.

Following autologous fat grafting, there has been an observed decrease in TGF-β1 levels around the site of the graft (Sultan *et al.,* 2012). Alongside this, injecting ADSCs following the induction of fibrosis lowered the levels of secretory TGF-β1 present in the surrounding tissue (Lee *et al.,* 2014). By decreasing the levels of TGF-β1 in the wound microenvironment, it is likely there will be less myofibroblast activation and thus decreased ECM production. This is supported by data showing that paracrine factors in ADSC-derived conditioned media lowered TGF-β1 and CTGF in a pulmonary fibrosis model. In turn there was decreased collagen gene expression in the lung tissue implying that less myofibroblast activation was occurring (Rathinasabapathy *et al.,* 2016).

Alongside reducing factors that cause myofibroblast differentiation such as TGF-β1 and CTGF, paracrine factors released by adipose tissue can also inhibit the various pathways (such as the SMAD pathway) that lead to differentiation (Ma *et al.,* 2020; Spiekman *et al.,* 2014; Uysal *et al.,* 2014). FGF proteins are a family of proteins that are antagonists to TGF-β1 induced myofibroblast

differentiation (Mattey *et al.,* 1997). In a wound model, fibroblasts (most likely myofibroblasts in this context) treated with FGF displayed increased apoptosis and decreased collagen production, leading to less contraction in the wound (Akasaka *et al.,* 2007).

FGF-2 has been observed to inhibit collagen production and myofibroblast differentiation in pulmonary fibrosis (Koo *et al.,* 2018) and decrease markers of myofibroblast differentiation in cardiac fibroblasts (Liguori *et al.,* 2018). FGF-1, -9, and -18 have also been demonstrated to lower myofibroblast differentiation markers in a fibrotic model (Joannes *et al.,* 2016). There is evidence that FGF inhibits myofibroblast differentiation through the ERK signalling pathway (Koo *et al.,* 2018) and the SMAD pathway (Liguori *et al.,* 2018), especially via reducing SMAD2 phosphorylation (Ramos *et al.,* 2010).

Adipose tissue secretes FGFs (Mydlo *et al.,* 1998) and ADSCs also produce basic-FGF when implanted into wounds (Uysal *et al.,* 2014). When implanted underneath wounds in rats, ADSCs decreased contraction and myofibroblast presence around the wound which the authors attributed to FGF-dependent inhibition of differentiation (Uysal *et al.,* 2014). This is plausible and reasonable but as I have described multiple times in this section ADSCs secrete a plethora of growth factors (Pallua, *et al.,* 2014b). The authors should have removed or eliminated FGF signalling and investigated whether ADSCs were still capable of myofibroblast inhibition to strengthen their hypothesis (Uysal *et al.,* 2014). Nevertheless, FGF is clearly capable of inhibiting myofibroblast differentiation (Liguori *et al.,* 2018; Koo *et al.,* 2018; Joannes *et al.,* 2016). Furthermore, ADSCs that have been differentiated to myofibroblasts via TGF-β1 have been reversed back to ADSCs via treatment with FGF (Desai *et al.,* 2014). Altogether, the production of FGF by adipose tissue appears to play a role in inhibiting myofibroblast differentiation in wounds.

Another molecule implicated in inhibiting myofibroblast differentiation is HGF. HGF has been consistently shown to inhibit myofibroblast differentiation (Dai & Liu, 2004; Rahman *et al.,* 2005; Yang *et al.,* 2003, 2005). Adipocytes produce HGF that has been shown to interact with the surrounding microenvironment (Bell *et al.,* 2008) and HGF released from adipose tissue ECM can alleviate radiation induced fibrosis (Chinnapaka *et al.,* 2021).

ADSCs have also been shown to secrete HGF (Ma *et al.,* 2020) and following injection of ADSCs at the site of irradiation, HGF production is increased alongside a decrease in expression of pro-fibrotic molecules such as TGF-β1 and CTFG (Ejaz *et al.,* 2019). The authors hypothesised that HGF was the responsible factor however, it was not until Ma et al. used an HGF antibody to remove the anti-fibrotic effect of HGF in ADSC-derived conditioned medium that this could be confirmed (Ma *et al.,* 2020). The decrease in collagen expression and production following ADSC injection and

conditioned media treatment implies that ADSC-derived HGF is inhibiting fibroblast to myofibroblast differentiation in fibrosis.

This work highlights not just the anti-fibrotic effect of HGF but is suggestive of the paracrine abilities of ADSCs to inhibit myofibroblast differentiation. Investigation has shown that conditioned media derived from ADSCs is able to decrease markers of myofibroblast differentiation (Deng *et al.,* 2018; Spiekman *et al.,* 2014).

In vivo work has demonstrated that factors secreted from adipose tissue can decrease the markers of myofibroblast differentiation (Ma *et al.,* 2020; Ejaz *et al.,* 2019; Koo *et al.,* 2018; Uysal *et al.,* 2014). There remains limited *in vitro* evidence, however, that this is specifically a result of paracrine factors inhibiting myofibroblast differentiation signalling. Furthermore, the few papers investigating this have only looked at ADSC-secreted factors (Liguori *et al.,* 2018; Deng *et al.,* 2018; Spiekman *et al.,* 2014) and not whole adipose tissue or the SVF. Given that these tissues are injected and grafted underneath scars (Gentile *et al.,* 2017; Klinger *et al.,* 2013; Tonnard *et al.,* 2013) it appears to be an oversight that ability of these formulations to inhibit myofibroblast differentiation has not been established *in vitro*.

Spiekman et al. (2014) were the first to demonstrate that media conditioned with ADSC-derived growth factors could inhibit myofibroblast differentiation *in vitro*. The group incubated ADSCs in cell culture medium and then collected the medium now "conditioned" with the growth factors and paracrine molecules secreted from the ADSCs. This ADSC-derived conditioned medium was then applied to fibroblasts alongside TGF-β1. α-SMA and collagen production in the fibroblasts was significantly decreased alongside the contractile ability of the fibroblasts compared to TGF-β1 treated fibroblasts. The factors within this ADSC conditioned medium were not examined however, and a mechanism for this myofibroblast inhibition was not established (Spiekman *et al.,* 2014). The same authors investigated whether FGF was the molecule responsible and while recombinant FGF was able to inhibit myofibroblast differentiation in vitro, ADSC conditioned medium couldn't (Liguori *et al.,* 2018). The group suggested the concentration of recombinant FGF they added was significantly higher than that in the conditioned medium however the authors didn't measure cytokine levels in their conditioned medium, so it is impossible to confirm this. It also appears odd that in one report from the same group, ADSC conditioned medium was able to inhibit myofibroblast differentiation (Spiekman *et al.,* 2014) and was unable to in another (Liguori *et al.,* 2018). An explanation for this may be growth factor concentration in the conditioned medium. The group collected conditioned medium from ADSCs when they were "90 % confluent". This is not an objective measure of cell number and may have led to reproducibility issues related to the

concentration of growth factors in their conditioned medium. Alternatively, in Spiekman et al. dermal fibroblasts are used and in Liguori et al. cardiac fibroblasts are used. There may be differences in how factors secreted by ADSCs interact with TGF-β1 signalling in these fibroblasts from different locations. Finally, ADSC age may be a factor with a report of young ADSCs (4-month-old mice-derived) protecting from fibrosis better than old ADSCs (22-month-old mice-derived; Tashiro *et al.,* 2015). ADSCs used in Spiekman et al. and Liguori et al. may have been derived from patients of different ages.

Additionally, while demonstrating myofibroblast differentiation inhibition *in vitro* is useful, scars treated with autologous fat grafts are often years old (Gentile *et al.,* 2017; Jaspers *et al.,* 2017; Carstens *et al.,* 2017; Klinger *et al.,* 2008). Thus, it is likely myofibroblasts will also be present and the ability of factors from adipose tissue to reverse myofibroblast differentiation would be key to scar regeneration. Spiekman et al. did apply ADSC-derived conditioned medium to already differentiated myofibroblasts derived from keloid scars but found there was little reversal of myofibroblast differentiation (Spiekman *et al.,* 2014). There was success however when ADSCs were co-cultured with scar derived myofibroblasts as the paracrine signals released by the ADSCs was able to lower α-SMA production and reverse the myofibroblast phenotype in vitro (Deng *et al.,* 2018). This work will be discussed in more detail in section 5.3 however, I don't believe this work conclusively proves ADSC-derived factors can reverse myofibroblast differentiation as the scar myofibroblasts are cultured in serum which has been demonstrated to have a similar effect on myofibroblasts (Kato *et al.,* 2020; Hecker *et al.,* 2011).

This section highlights a gap in the current literature whereby a mechanism for adipose tissue-based inhibition of myofibroblast differentiation *in vitro* has not been established (Spiekman *et al.,* 2014). As well as this, the ability of factors from adipose tissue to reverse myofibroblast differentiation has not been confirmed. Finally, all the literature investigating adipose tissue-based myofibroblast inhibition *in vitro* has been focussed on factors secreted by ADSCs (Liguori *et al.,* 2018; Deng *et al.,* 2018; Spiekman *et al.,* 2014). There has been a lack of investigation of the *in vitro* effects of paracrine factors released by other formulations of clinically relevant adipose tissue.

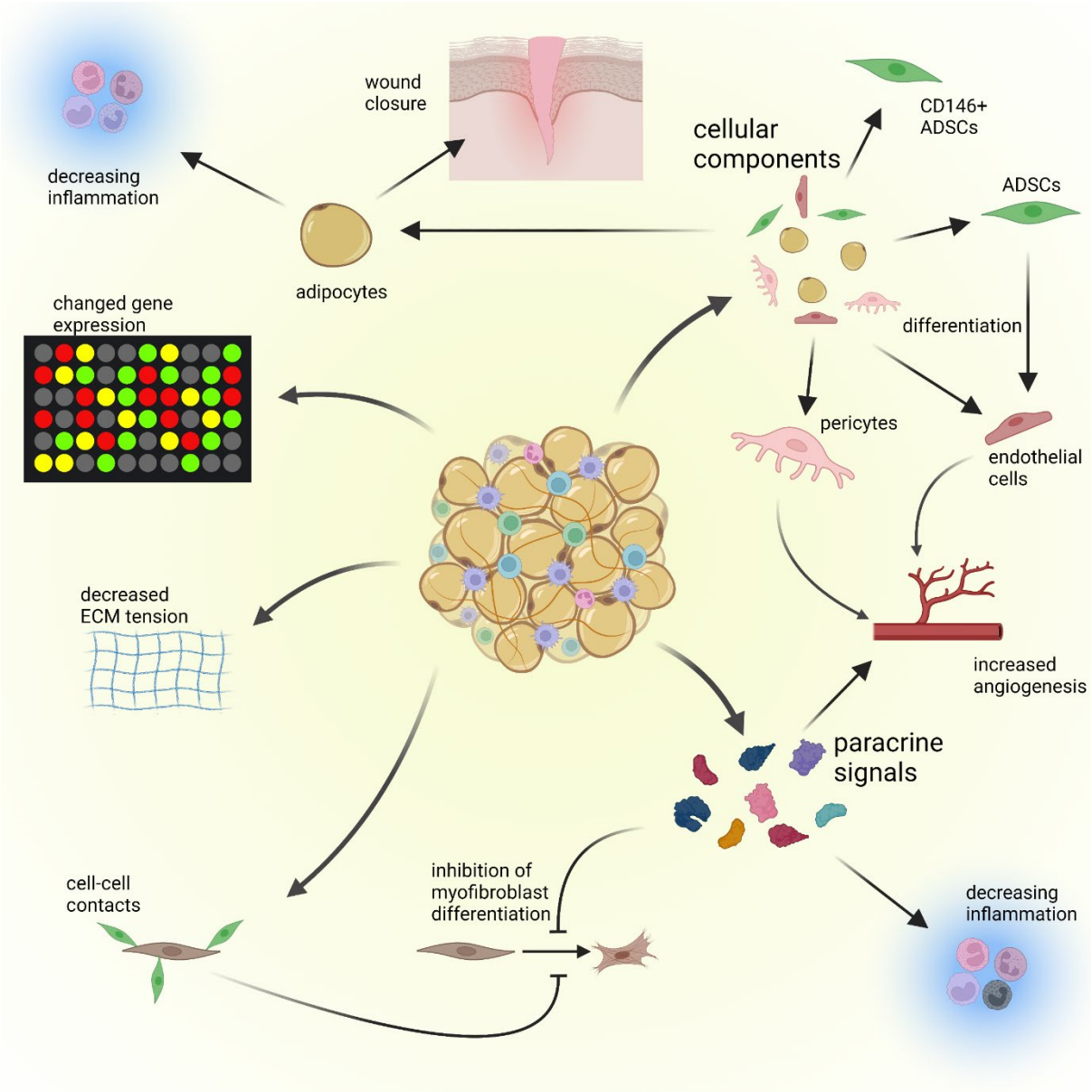

Figure 1.16. Methods of scar regeneration via adipose tissue grafting. The section above charts the *in vitro* mechanisms and hypothesises behind adipose tissue's regenerative effect in hypertrophic scars. Data has suggested that adipocytes supplied by the graft lead to lowered inflammation and increased wound closure. While ADSCs can differentiate into endothelial cells and become incorporated into new blood vessels and CD146+ ADSCs are pro-angiogenic. Pericytes found in adipose tissue also lead to increased angiogenesis. Adipose tissue grafting changes the gene expression in the surrounding tissue and relieves hypoxia. Paracrine signals released from adipose tissue has also led to decreased inflammation and increased angiogenesis. These paracrine signals have also been implicated in the inhibition of myofibroblast differentiation. This mechanism is investigated *in vitro* in this thesis.

1.5 Aims and Objectives

Given the data presented by the literature in the section above, I hypothesise that paracrine factors released by formulations of adipose tissue clinically grafted under scars can inhibit and reverse the differentiation of fibroblasts to myofibroblasts. I theorise that this occurs via the TGF-β1 canonical pathway. There is *in vivo* work implying this occurs however, there is little *in vitro* analysis to confirm this.

As such, in this thesis I aim to address these gaps in the literature. My objectives for this work are as follows.

1. Investigate whether paracrine factors from clinically relevant forms of adipose tissue can inhibit the differentiation of fibroblasts.

2. Examine whether paracrine factors from clinically relevant forms of adipose tissue can reverse the differentiation of myofibroblasts.

3. Identify the cellular components of adipose tissue responsible for any effect paracrine factors from clinically relevant forms of adipose tissue may have on myofibroblast differentiation.

4. Elucidate the underlying mechanisms behind any effect paracrine factors from clinically relevant forms of adipose tissue may have on myofibroblast differentiation.

This work will be carried out by generating various formulations of adipose tissue based upon those used clinically (Yao *et al.,* 2017; Tonnard *et al.,* 2013). The paracrine factors secreted by these formulations will be added simultaneously to fibroblasts alongside TGF-β1. Markers of myofibroblast differentiation will then be examined and used to judge whether paracrine factors from adipose tissue can inhibit myofibroblast differentiation. The molecules released from these formulations will be characterised and used to elucidate the mechanisms behind any adipose tissue-dependent myofibroblast inhibition. Fibroblasts will be differentiated to myofibroblasts with TGF-β1 and paracrine factors from adipose tissue added following differentiation. Myofibroblast markers will be measured to examine whether myofibroblast differentiation has been reversed following treatment with paracrine factors from adipose tissue. Finally, myofibroblasts from scar tissue will be treated with these paracrine factors to determine whether adipose tissue can reverse the myofibroblast phenotype of scar fibroblasts.

Chapter 2: Materials and Methods

2.1 Materials

2.1.1 Transforming growth factor-beta 1

Recombinant human transforming growth factor-beta (TGF-β) 1 was supplied by Peprotech (London, UK). The protein was derived from human embryonic kidney-293 immortalised cells and arrived lyophilised. The powder was reconstituted in 10 mM, pH 3 citric acid monohydrate (Merck, Gillingham, UK) in phosphate buffered saline (PBS; Thermo Fisher Scientific, Loughborough, UK) to a concentration of 0.1 mg/ml. This solution was then diluted in PBS containing 15 mM bovine serum albumin (BSA; Merck) to give a final concentration of 10 ng/µl TGF-β1. This was stored at -20 ^{o}C until use.

2.1.2 Foretinib

The molecule foretinib was purchased from Cambridge Bioscience (Cambridge, UK) and arrived lyophilised. Foretinib was initially resuspended into aliquots of 1 mg/ml in dimethyl sulfoxide (DMSO; Merck) and stored at -80 °C. Upon use, the foretinib solution was diluted further in DMSO into aliquots of 0.1 mg/ml (160 µM) and was diluted to a final working concentration in cell culture medium. Final working concentration will be described in the relevant experimental sections. Foretinib inhibits kinase enzymes such as the C-Met receptor and its structure is shown in figure 2.1.

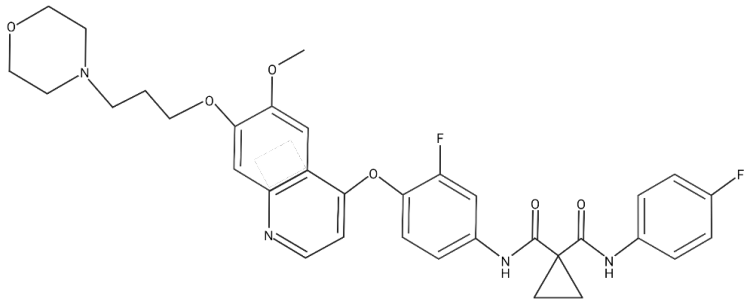

Figure 2.1. IUPAC structure of Foretinib molecule. Molecular formula, $C_{34}H_{34}F_2N_4O_6$, molecular weight, 632.7 kDa.

2.1.3 Hepatocyte growth factor

Recombinant human hepatocyte growth factor (HGF) was supplied by Peprotech. The protein was derived from human embryonic kidney-293 immortalised cells and arrived lyophilised. The powder was reconstituted in 10 mM, pH 3 citric acid monohydrate in PBS to a concentration of 1 µg/ml. This was stored at -20 ^{o}C until use. When needed, this solution was then diluted in PBS containing 15 mM BSA to give a final working concentration of 40 ng/ml.

2.1.4 Solutions used

2.1.4.1 Cell culture solutions

Table 2.1. Components in 1 L of Hank's balanced salt solution (HBSS). Supplied by Thermo Fisher Scientific.

Component	Final concentration (mg/L)
$CaCl_2$	140
$MgCl_2$-$6H_2O$	100
$MgSO_4$-$7H_2O$	100
KCl	400
KH_2PO_4	60
$NaHCO_3$	350
NaCl	8000
Na_2HPO_4	48
D-enantiomer glucose	1000
Phenol red	10

Table 2.2. Components of 10 % D-MEM. Penicillin and Streptomycin were purchased combined (5ml), all components were filter sterilised before purchase through a 0.2 µm filter.

Component	Volume (ml)	Final concentration	Supplier
Dulbecco's-modified eagle medium (D-MEM)	439	4500 mg/L – glucose, sodium pyruvate, sodium bicarbonate	Merck
Foetal calf serum (FCS)	50	-	PAN Biotech (Wimborne, UK)
L-enantiomer glutamine	5	200 mM	Merck
Penicillin	5	10000 units/ml	Merck
Streptomycin		10 mg/ml	Merck
Amphotericin B solution	1	250 µg/ml	Merck

Table 2.3. Components of MesenPRO RS™ medium. Penicillin and Streptomycin were purchased and combined (5ml), all components were filter sterilised before purchase through a 0.2 µm filter.

Component	Volume (ml)	Final concentration	Supplier
MesenPRO RS™ basal medium	479	-	Thermo Fisher Scientific
MesenPRO RS™ growth supplement	10	-	Thermo Fisher Scientific
L-enantiomer glutamine	5	200 mM	Merck
Penicillin	5	10000 units/ml	Merck
Streptomycin		10 mg/ml	Merck
Amphotericin B Solution	1	250 µg/ml	Merck

Table 2.4. Adipogenic differentiation medium.

Component	Volume (ml)	Final concentration	Supplier
Dexamethasone	2	20 µg/ml	Merck
3-Isobutyl-1-methylxanthine (in absolute ethanol)	1.1	0.5 mM	Merck
Insulin (in 0.01 HCl)	1	10 µg/ml	Merck
Indomethacin	1	100 µM	Merck
MesenPRO RS™ basal medium	94	-	Thermo Fisher Scientific
L-enantiomer glutamine	1	200 µM	Merck

2.1.4.2 Reverse transcription master solution

Table 2.5. Reagents and corresponding volumes in reverse transcription master solution.

Component	Volume (µL)	
	With MultiScribe™ enzyme	Without MultiScribe™ enzyme
10X RT buffer	2.0	2.0
25X dNTP mix (100 mM)	0.8	0.8
10X RT random primers	2.0	2.0
MultiScribe™ reverse transcriptase enzyme	1.0	-
Nuclease-free H2O	3.2	4.2
Total per reaction	10.0	10.0

2.1.4.3 Quantitative polymerase chain reaction master solution

Table 2.6. Reagents and corresponding volumes in quantitative polymerase chain reaction master solution.

Component	Volume (µl)
2X SYBR green Lo Rox mix (PCR Biosystems, London, UK)	5
Forward primer (10 µM)	0.5
Reverse primer (10 µM)	0.5
RNase free water	3.5
cDNA	0.5

2.1.4.4 Primers used in quantitative polymerase chain reaction

The nucleotide sequence for the forward and reverse primers for the cDNA targets can be found in table 2.6 and were diluted in RNase free water (Qiagen, Manchester, UK) to 10 µM for use. All primers were supplied by Merck.

Table 2.7. Primers used in quantitative polymerase chain reaction.

Primer	Forward	Reverse
RNU6-1	5'- CTCGCTTCGGCAGCACA - 3'	5' - AACGTTCACGAATTTGCGT - 3'
α-SMA	5' - GAAGAAGAGGACAGCACTG - 3'	5' - TCCCATTCCCACCATCAA - 3'
COL1A1	5' - GTGGCCATCCAGCTGACC - 3'	5' - AGTGGTAGGTGATGTTCTGGGAG - 3'
FN1-EDA	5' - TGGAACCCAGTCCACAGCTATT - 3'	5' - GTCTTCTCCTTGGGGGTCACC - 3'

2.1.4.5 Protein lysis buffer

Protein lysis buffer was made up in batches of 10 ml and aliquoted into 1 ml aliquots and stored at -20 °C until use.

Table 2.8. Components of protein lysis buffer.

Reagent	Final concentration	Supplier
Radioimmunoprecipitation buffer (RIPA buffer)	999 µl/ml	Universal Biologics (Cambridge, UK)
Complete mini protease inhibitor cocktail	1 tablet/ 10 ml	Merck
Benzonuclease nuclease enzyme	1 µl/ml	Merck

Table 2.9. Enzyme concentrations in one tablet of Complete Mini Protease Inhibitor Cocktail. Information supplied by Merck.

Protease	Enzyme concentration (mg/ml)
Pancreas extract	20
Thermolysin	0.5
Chymotrypsin	2
Trypsin	20
Papain	330

2.1.4.6 Tris buffered saline

Tris buffered saline (TBS) was made up to 1 L with deionised water. Hydrochloric acid (1M) was used in combination with a SevenMulti™ pH meter (Mettler Toledo, Leicester, UK) to adjust the acidity of the solution to pH 7.6, this usually took 45 ml of acid (table 2.9). Tween 20 was added at a concentration of 1 ml/L to make 0.1 % TBS Tween 20 wash solution used for western blotting.

Table 2.10. Components of 0.1 % TBS Tween 20.

Component	Final concentration
Tris(hydroxymethyl)aminomethane (VWR chemicals, Lutterworth, UK)	6.05 (g/L)
Sodium chloride (VWR chemicals)	8.76 (g/L)
Hydrochloric acid (1 M; Merck)	45 (ml/L)
Deionised water	954 (ml/L)
Tween 20 (Merck)	1 (ml/L)

2.1.4.7 Semi-dry transfer solution

Table 2.11. Components of semi-dry transfer solution.

Component	Mass/volume
Tris(hydroxymethyl)aminomethane	5.8 (g/L)
Glycine (Merck)	2.9 (g/L)
Sodium dodecyl sulphate (1.9 M; VWR chemicals)	3.6 (ml/L)
Methanol (absolute; Thermo Fisher)	200 (ml/L)
Deionised water	800 (ml/L)

2.1.5 Antibodies and stains used

2.1.5.1 Fluorescent stains used

Table 2.12. Fluorescent stains used to label adipose tissue. All supplied by Affymatrix, Thermo Fisher Scientific.

Dye/Stain	Dilution	Solubilised in	Excitation λ (nm)	Laser used	Supplier
4,4-difluoro-5-(2-Thienyl)-4-Bora-3a,4a-diaza-s-indacene-3-dodecanoic acid (BODIPY	5 µM	Methanol (absolute)	543	HeNe1 (543 nm)	Thermo Fisher Scientific
MemBrite fix 640/660	1:1000	HBSS	633	HeNe2 (633 nm)	Thermo Fisher Scientific
4',6-diamindino-2-phenylindole (DAPI)	1:1000	DMSO	405	Argon 2 (458 nm)	Merck

2.1.5.2 Flow cytometry antibodies used

Table 2.13. Antibodies used for flow-cytometry. All supplied by Affymatrix, Thermo Fisher Scientific.

Antibody	Conjugated fluorophore	Filter (nm)	Excitation λ (nm)
Anti-CD31	APC eFluor® 780	Red 780	633
Anti-CD34	PE	Blue 575	488
Anti-CD45	eFluor® 450	Violet 450	405
Anti-CD73	PE-Cy7	Blue 780	488
Anti-CD90	PerCP eFluor® 710	Blue 695	488
Anti-CD105	APC	Red 660	633
Anti-CD146	FITC	Blue 530	488

2.1.5.3 Fluorescent antibodies used

All fluorescent antibodies used were diluted in 1 % (w/v) BSA in PBS and stored at –20 °C until use.

Table 2.14. Fluorescent antibodies used.

Antibody	Species	Dilution	Blocking protein	Supplier	Excitation λ (nm)	Laser used
Ki-67	Rabbit	1:1000	BSA	Abcam (Cambridge, UK)	-	-
α-SMA	Mouse	1:1000	BSA	Abcam	-	-
Anti-rabbit Alexa Fluor® 647 conjugated	Donkey	1:1000	BSA	Abcam	651	HeNe2 (633 nm)
Anti-mouse Alexa Fluor® 555 conjugated	Goat	1:1000	BSA	Abcam	555	HeNe1 (543 nm)
α-SMA-fluorescein isothiocyanate conjugated	Mouse	1:500	BSA	Merck	488	LED, 488 nm filter used

2.1.5.4 Western blotting antibodies used

Antibodies used in western blotting were diluted in either 5 % (w/v) BSA in PBS or 5 % (w/v) dry milk powder (Generon, Slough, UK) dissolved in PBS, depending on the manufacturer's instructions.

Table 2.15. Antibodies used for western blotting.

Antibody	Species	Size (kDA)	Dilution	Blocking protein	Supplier
Anti-α-SMA	Rabbit	42 kDa	1:10000	Dry milk powder	Abcam
Anti-GAPDH	Mouse	37 kDa	1:5000	Dry milk powder	Proteintech, (Manchester, UK)
Anti-β-actin	Mouse	42 kDa	1:10000	BSA	Merck
Anti-mouse, horseradish peroxidase conjugated	Horse	N/A	1:3000	BSA	Cell Signaling Technology (London, UK)
Anti-rabbit, horseradish peroxidase conjugated	Goat	N/A	1:3000	BSA	Abcam

2.2 Adipose tissue processing methods

All work on adipose tissue was carried out in a class II biological safety cabinet (Walker, Glossop, UK) under laminar flow. Adipose tissue was kept in a sterile environment by cleaning all surfaces in the safety cabinet with a solution of 70 % (v/v) industrial methylated spirit (IMS; Thermo Fisher Scientific) and deionised water with paper towels. All materials entering the safety cabinet were cleaned in a similar manner. Unless otherwise specified, all centrifugation steps were carried out in a universal classic 320/320 R centrifuge (Hettich Zentrifugen, Surrey, UK). Prior to use, adipose tissue was stored at room temperature in a locked cabinet, any materials isolated from adipose were collected within 24 hours of receiving the sample. All incubation steps were carried out at 37 °C in a hydrated, 5 % CO_2 atmosphere Sanyo (Sheffield, UK) humidified incubator.

2.2.1 Ethical approval for the use of human tissue

Human adipose tissue and skin was collected, processed, and handled following a protocol approved by the NHS research ethics committee (REC) reference 15/YH/1077 from September 2018 to July 2021, and REC reference 21/NE/0115 from July 2021 onwards. This allowed the collection of adipose tissue and skin under informed consent from patients. Adipose tissue samples were typically taken from leftover adipose tissue removed for fat grafting in abdominoplasty, breast mastectomy, and gender reassignment operations. However, this list is not exhaustive and leftover adipose tissue from any routine procedure in which adipose tissue would normally be discarded could be used. Excess adipose tissue was not taken from the patients, only tissue that was taken out by the surgeon and subsequently unused was given for use. Operations were carried out by the Sheffield Hospital Directorate of Plastic, Reconstructive Hand and Burns Surgery at the Royal Hallamshire Hospital in Sheffield, UK. Consent was taken by researchers who have completed consent training under the 2004 Human Tissue Act. Only the minimal necessary information for audit was collected such as: patient name, hospital ID number and date of procedure. The only additional information that could be known about patients was whether any skin attached to the adipose tissue contained a scar, assessed by a clinician. Once tissue arrived at the laboratory, it was logged and assigned a random three number code and access to person-identifiable information was on a need-to-know basis. Unprocessed tissue was disposed of via incineration after 7 days.

2.2.2 Generation of minced adipose tissue and lipoaspirate from adipose tissue

Human adipose tissue was received either as whole, solid adipose tissue with skin attached or as the liquid product of liposuction (figure 2.2A-B). Solid adipose tissue was then minced with a scalpel removing large blood vessels and connective tissue until the adipose tissue took on an almost

liquid consistency (figure 2.2C). Before use, adipose tissue would be washed in a similar manner to the Coleman technique (Coleman, 1998). The adipose tissue was washed in 10 ml Luer-Lock ended syringes (B. Braun, Sheffield, UK). The plunger was removed from the barrel of the syringe and a syringe cap (B. Braun) placed on the end. The now empty barrel of the syringe was filled with 5 ml of adipose tissue and 5 ml of PBS. To secure the plunger end of the syringe, the plastic end of the plunger was removed and placed in the end of the syringe barrel. Adipose tissue was then left to settle in the syringe for 10 minutes to allow the PBS to flow through the syringe. Following this, syringes were centrifuged for 3 minutes at 1200 *xg* (figure 2.3). The rubber stopper was removed from the syringe and the liquid discarded. This process removed any blood and anaesthetic drugs used in surgery. For the purposes of this work, adipose tissue taken from solid, whole, tissue and processed by mincing with a scalpel was termed “minced adipose tissue”. If adipose tissue was taken from the liquid tissue product of liposuction and washed, it was termed “lipoaspirate”. These two forms of tissue were the starting points of processing to further formulations. The difference between the two forms of adipose tissue was that minced adipose tissue came from solid excess tissue and lipoaspirate was generated from the liquid waste product of liposuction. Further forms of processed adipose tissue would be generated from either minced adipose tissue or lipoaspirate.

2.2.3 Processing adipose tissue into emulsified fat

Minced adipose tissue or lipoaspirate was processed into a formulation termed “emulsified fat”. This formulation was designed to be similar to “Nanofat” described by Tonnard *et al.,* (2013) where the adipocytes are lysed and the larger macro-structure of adipose tissue is disrupted. Minced adipose tissue or lipoaspirate was placed in a 20 cc syringe (BD Biosciences, Wokingham, Berkshire) and connected to a second, identical, syringe with a 3.2 mm female-female Luer lock (Thermo Fischer Scientific). Adipose tissue was then passed to the opposing syringe 30 times by applying force on the syringe plunger. One “pass” was defined as adipose tissue being transferred from one syringe to the other. Forcing the adipose tissue through the Luer-Lock applied shear force to the adipose tissue leading to a breakdown of its macro-structure and converting the adipose tissue into a paste-like formulation (figure 2.2D). The opposing syringe was removed, and the emulsified liquid was passed into a separate 30 ml centrifuge tube for use as emulsified fat.

2.2.4 Generating lipocondensate from emulsified fat

Emulsified fat could be further processed into a formulation termed “lipocondensate”, this is similar to other “SVF-gel” formulations in the literature where the stromal vascular fraction (SVF) of adipose tissue is isolated (Wang *et al.,* 2019). A 500 µm filter (PluriSelect, Cambridge, UK) was placed

atop a 50 ml centrifuge tube (Sarstedt) and emulsified fat was slowly poured into the filter. Forceps were then swirled around the filter to aide liquid transfer through the filter and remove any remaining clumps of matrix and fibrous tissue in the emulsified fat. This filtrate was then poured into a 10 cc syringe with the plunger of the syringe removed and a cap placed on the syringe end. The plastic end of the plunger was removed and placed in the end of the syringe barrel to secure the contents of the syringe. This filtrate was then centrifuged in the syringe at 2000 *xg* for 3 minutes. This procedure generated a multilayer solution with the central layer being referred to as "lipocondensate" (figure 2.2F). To begin with, the filtrate did not consistently separate (mentioned later in chapter 3, results section 3.2.4). If lipocondensate did not form, it would be placed in a 4 °C fridge to condense and was then warmed at room temperature until liquid and then re-centrifuged. Once an emulsion had formed, lipid oil was removed from above the lipocondensate using a Pasteur pipette and the red liquid layer below the lipocondensate was allowed to drain from the syringe.

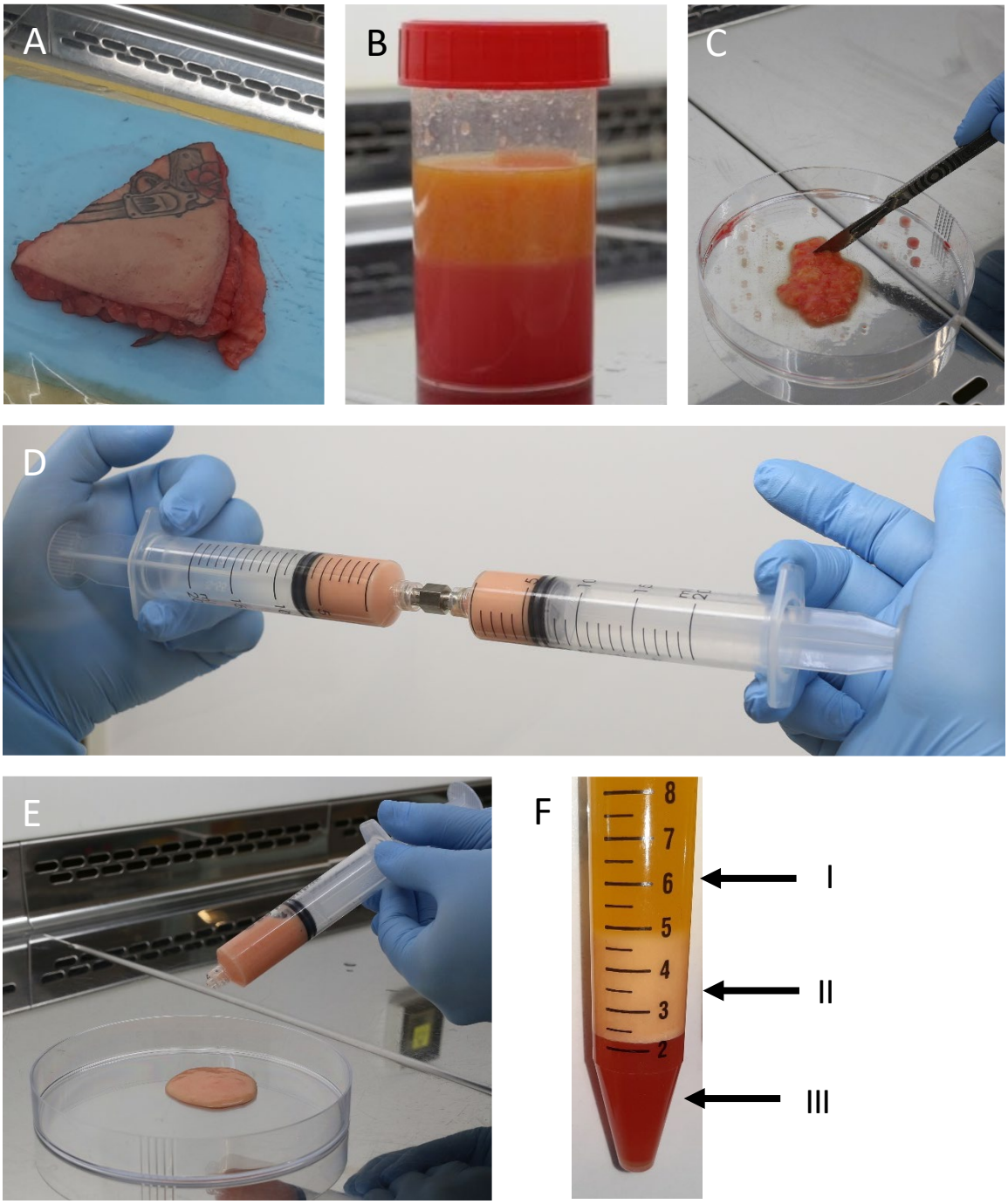

Figure 2.2. Stages of adipose tissue processing. (A-B) Adipose tissue was received as either whole tissue with skin attached (A) or as semi-liquid lipoaspirate (orange layer; B). **(C)** To make minced adipose tissue, whole adipose tissue was minced with a scalpel and connective tissue and blood vessels removed until the consistency shown above was reached**. (D-E)** Emulsified fat. **(F)** Emulsified fat was then taken, filtered and centrifuged to form lipocondensate. Centrifugation led to the formation of a three-phase solution with lipid on top (I), waste liquid below (III) and lipocondensate in between (II).

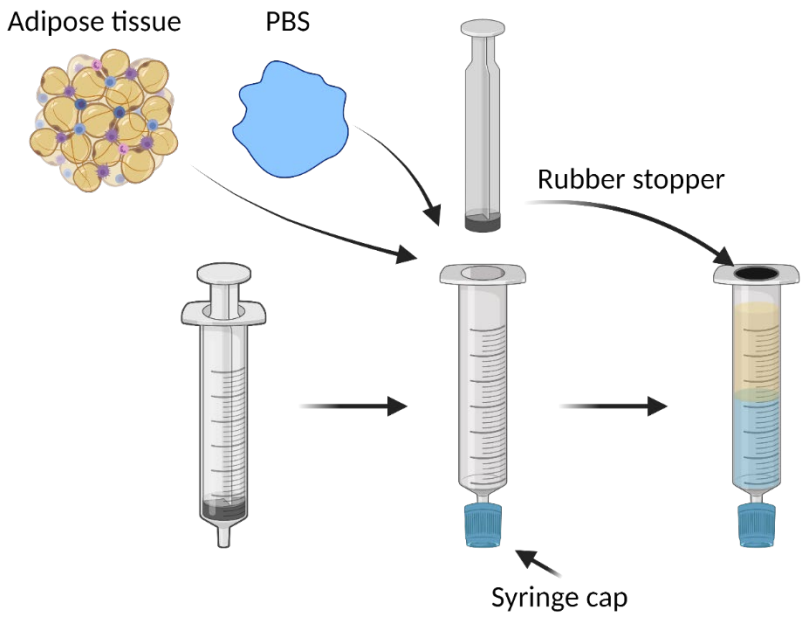

Figure 2.3. Schematic of how anaesthetic was removed using PBS.

2.3 Cell culture methods

2.3.1 Primary cell isolation

All cell culture work was carried out in a class II biological safety cabinet under laminar flow. When not in use (and at all incubation steps unless otherwise stated), cells were incubated at 37 °C in a hydrated, 5 % CO_2 atmosphere humidified incubator. Cells were kept in a sterile environment by cleaning all surfaces in the safety cabinet with a solution of 70 % (v/v) IMS and deionised water with paper towels. All materials entering the safety cabinet were cleaned in a similar manner. Unless otherwise specified, all centrifugation steps were carried out in a universal classic 320/320 R centrifuge.

2.3.1.1 Adipose derived stromal cell isolation

ADSC could be isolated either from solid adipose tissue or lipoaspirate. Before use, anaesthetic was removed as described in section 2.2.2. If solid tissue was used, 10 cm^3 of adipose tissue was taken and was minced as described in section 2.2.2. If lipoaspirate was used, 10 ml of lipoaspirate was taken for use. This adipose tissue was then added to an equal volume of a sterile mixture of 0.1 % (w/v) collagenase 1 (Merck), 0.1 % (w/v) BSA, and 5 ml of a combined mixture of 10000 units/ml penicillin and 10 mg/ml streptomycin in HBSS (table 2.1). This solution was incubated at 37 °C for 40 minutes, being inverted 10 times every 10 minutes.

Following this, the adipose tissue mixture was centrifuged at 257 *xg* for 8 minutes. This formed a layered solution with four phases (figure 2.4). The lipid oil, red liquid, and adipose tissue

layers were removed using a Pasteur pipette, while avoiding disturbing the underlying pellet containing the ADSCs. The pellet was washed, and collagenase neutralised by the addition of 10 ml of MesenPRO RS™ medium and re-centrifuged at 2645 *xg* for 8 minutes. The supernatant was poured away and the cell pellet resuspended as before in MesenPRO RS™ Medium, the resulting solution was transferred to a T75 cell culture flask (Sarstedt). After 24 hours the medium was replaced, and the flask washed with 5 ml of PBS.

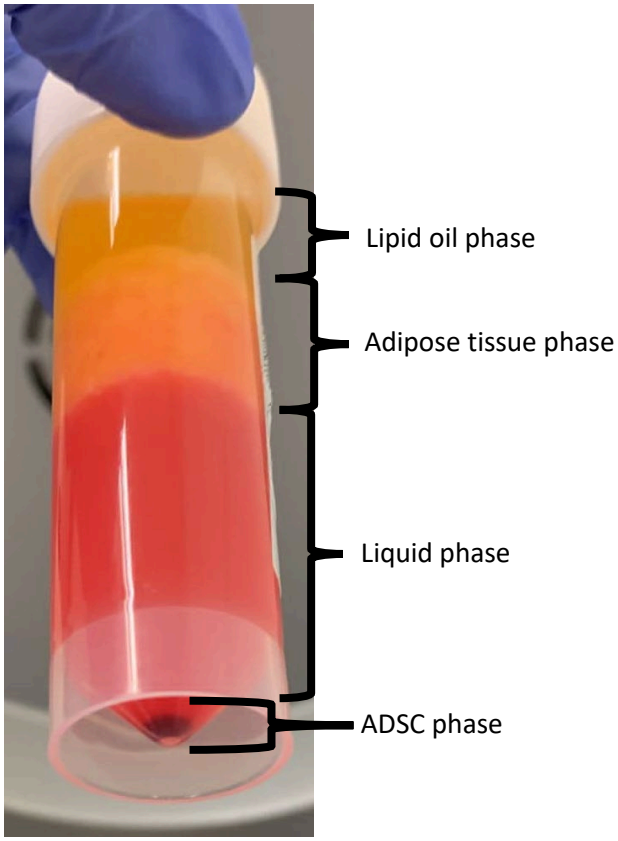

Figure 2.4. ADSC isolation. Following treatment with collagenase and centrifugation, ADSCs can be isolated from the pellet formed.

2.3.1.2 Human dermal fibroblast isolation

Skin was removed from adipose tissue using a Braithwaite knife (Swann Morton, Sheffield, UK). A 25 mm^2 piece was cut from the main section and subsequently sliced into 0.5 mm^2 pieces. These were incubated in 10 ml of 0.1 % w/v Difco trypsin (BD biosciences) for 18 hours in a 4 ^oC fridge. The skin in Difco trypsin was transferred to a Petri dish (Thermo Fisher Scientific) and the epidermal layer removed by gentle pulling with forceps, and subsequently discarded. The remaining dermis was scraped to remove keratinocytes which were not subsequently used by me. Following this step, the pieces of dermis were placed in a fresh Petri dish and a 10 ml mixture of collagenase 1 (0.05 % w/v) and 20 % v/v FCS in D-MEM was added and incubated at 37°C for 24 hours.

Collagenase/skin mixture was transferred to a 30 ml centrifuge tube (SLS select, Nottingham, UK) and centrifuged at 608 *xg* for 10 minutes. Supernatant was removed and the pellet resuspended in 10 % D-MEM and transferred to a T25 cell culture flask (VWR International) and incubated at 37 ^oC for 24 hours. Finally, culture medium was changed, and the flask washed with PBS.

2.3.1.3 Human scar fibroblast isolation

To isolate scar fibroblasts, a section of skin containing scar tissue was required. Scar tissue was identified by clinical staff before the tissue was sent to me. Scar tissue would be identified by a pale, wrinkled area of skin, often in lines indicating where the skin had been punctured. The scar, or a 25 mm^2 piece of scar (whichever was smaller) was cut from the main section of skin, with care being taken to only slice away scar tissue so as to not isolate dermal fibroblasts. From this point, scar fibroblasts were isolated from skin in an identical manner to dermal fibroblasts as described in section 2.3.1.2.

2.3.1.4 Maintenance of primary cell cultures

Fibroblasts and scar fibroblasts were maintained in a solution of 10 % D-MEM (see table 2.2). Fibroblasts and scar fibroblasts were cultured once a month in 10 % D-MEM containing no antimicrobial agents (penicillin, streptomycin, and amphotericin B solution) and observed to ensure that good sterile technique was being maintained and that cultures did not contain latent microbial infections.

Adipose derived stromal cells were cultured in MesenPRO RS^{TM} medium (Thermo Fisher Scientific). This is a medium specifically designed for mesenchymal cell culture and contains a low concentration (2 %) of supplemented serum so as to avoid spontaneous differentiation of mesenchymal stromal cells such as ADSCs in routine culture (see table 2.3).

ADSC were cultured once a month in MesenPRO RS™ medium containing no antimicrobial agents (penicillin, streptomycin, and amphotericin B solution) and observed to ensure that good sterile technique was being maintained and that cultures did not contain latent microbial infections. Cells were tested monthly for mycoplasma to ensure there was no contamination.

Serum supplements for cell culture medium are known to contain TGF-β1 (Danielpour *et al.,* 1989). As a purpose of this work was measuring the effect of TGF-β1 on fibroblasts, all experimental work was carried out in cell culture medium without serum. In these cases, the serum was replaced with additional D-MEM or MesenPRO RS™ basal medium. This work also wanted to study the concentration of growth factors and proteins released from adipose tissue. To achieve this, adipose tissue was cultured in MesenPRO RS™ basal medium, with no serum or supplements added. During culture, growth factors from the adipose tissue would be released into the medium. This medium was removed, stored (discussed later), and termed "conditioned medium". Serum free MesenPRO was used so that any proteins normally found in the serum would not artificially increase the concentration of proteins found in the adipose conditioned medium. When carrying out experiments containing both (scar) fibroblast culture and adipose tissue conditioned medium, then (scar) fibroblasts would be cultured in serum free MesenPRO RS™ basal medium (Serum free MesenPRO) for consistency before the addition of adipose tissue conditioned medium.

Once made into solutions, all cell culture medium was stored at 4 °C until use and warmed to 37 °C in a water bath before contacting cells to avoid temperature shock.

2.3.2 Passaging of primary cell cultures

ADSC and (scar) fibroblasts were fed twice a week in their respective cell culture medium. Upon cells reaching 90 % confluency they were sub-cultured. To do this, cell culture media was removed, and the surface of the cell flask was washed by the addition and removal of 5 ml of PBS. To detach cells from the tissue culture plastic, 5 ml of 0.5 g/L trypsin – 0.2 g/L EDTA in HBSS was warmed to 37 °C and applied to the cells. This solution was left in contact with the cells for 10 minutes in a humidified 37 °C, 5 % CO_2 incubator and was observed under a light microscope to check for full detachment of cells. Following this, the appropriate media was added at a 1:1 ratio to the trypsin-EDTA-cell solution so that the serum would neutralise the trypsin-EDTA. The resulting solution was centrifuged at 152 *xg* for 5 minutes to pellet the cells. The supernatant was removed, and the cell pellet resuspended in MesenPRO RS™ medium or 10 % D-MEM depending on cell type. At this stage, cells could be counted using a glass hemocytometer (see section 2.3.3). The number of times a cell culture encountered trypsin was tracked as the "passage number". ADSC were not used past passage number 6 and fibroblasts were not used past passage number 7. This was due to an

observed decrease in growth rate and dampened response to chemical stimulants such as TGFβ-1 that is associated with cellular senescence.

2.3.3 Counting of total cell number

Following detachment from cell culture plastic via trypsin-EDTA, the total cell number could be calculated. A glass hemocytometer (Hawksley, Lancing, UK) was prepared by cleaning the device and a glass coverslip with 70 % IMS in deionised water solution and being left to dry. Moisture was applied to the hemocytometer by breathing on it and the coverslip placed directly on top. Newtonian refraction rings on the coverslip demonstrated it had adhered to the hemocytometer. After cells had been pelleted and re-suspended in appropriate cell culture medium, a micropipette was used to disturb the cell solution to ensure that cells were equally distributed and had not sunk to the bottom of the vessel. Next, 50 µl of cell solution was taken and placed between the hemocytometer counting chamber and the glass coverslip (figure 2.5A). Cells were placed in the counting chamber by placing a drop of the cell suspension at the edge of the coverslip and allowing capillary action to take the liquid underneath the coverslip and into the counting chamber. Using an AE 2000 inverted light microscope (Motic, Barcelona, Spain) the counting chambers were viewed at x 10 magnification and the cells counted (figure 2.5B). Cells were counted under the following rules:

a) Cells were counted from at least 2 of the 9 large, numbered squares in each of the two hemocytometer chambers. If the number of cells varied dramatically between squares (< or > than 10) then additional squares were counted, in the order shown in figure 2.5B, lowest to highest.

b) Cells were discounted if they were sitting on the left or bottom border of the square (see red lines and circles) and counted if they lay on the right, or top border (green circles).

c) If a square contained an artefact or debris that was not a cell, then that square and the corresponding square in the other chamber would not be counted and another square used instead.

d) Cell pellets were initially resuspended in enough cell culture medium to give between 40-100 cells per square. If there were not 40 cells in a square then the cells in solution would be re-pelleted by centrifugation and resuspended in a smaller volume of cell culture medium to concentrate cells. This was to get a more accurate cell count because if only a small number of cells were counted, when scaled up in equation 2.1, then each counted cell would contribute to a much larger percentage of the total cell count. This could have led to the count being significantly altered by random chance.

e) If it was apparent that there were more than 100 cells per square, then the cell solution was diluted and re-counted for the sake of expediency. The volume of cell culture medium required

to get this dilution was typically 1 ml of 10 % D-MEM for fibroblasts and 5 ml of MesenPRO RS™ medium for ADSC.

f) To calculate the total number of cells/ml, the following equation would be used.

Total cells = Average cells per square x 10^4 x dilution factor (ml of cell culture medium)

Equation 2.1. Calculation of total cells in culture.

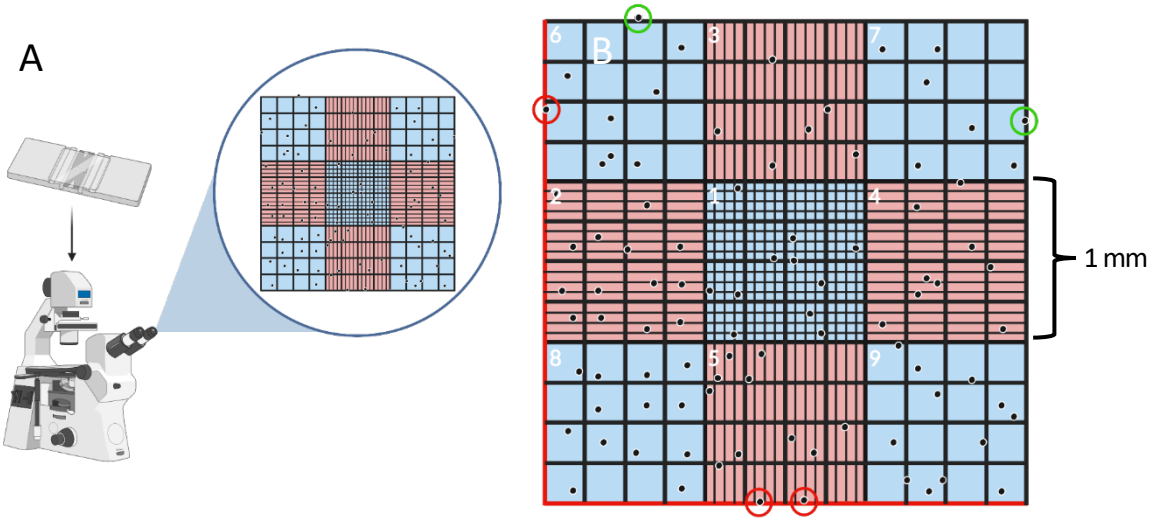

Figure 2.5. Cell counting methodology. (A) Cells were placed in a hemocytometer and viewed at x10 magnification using an inverted light microscope. **(B)** Schematic view of cell counting chamber. Black dots represent cells.

2.3.4 Cryogenic preservation and resurrection

For long term storage, cells were removed from the flask as described in section 2.3.2 however after centrifugation, the total cell number was counted. These cells were then centrifuged again and resuspended in freezing media (10 % DMSO and 90 % FCS) at a concentration of $1x10^6$ cells/ml. Following resuspension, the solution was aliquoted into cryovials (Sarstedt) with $1x10^6$ cells per vial. Cells were then frozen by placing in a controlled rate freezing container ("Mr Frosty", Thermo Fisher Scientific) in a -80 °C freezer for at least 24 hours. After this, they were transferred to a liquid nitrogen dewar at -196 °C until needed.

To resurrect these cells, a cryovial was removed from liquid nitrogen and warmed in a 37 °C water bath for one minute. After the cell suspension had melted, the solution was transferred to a T75 cell culture flask containing warm cell culture medium. To ensure all cells were extracted, each vial was washed with an additional 1 ml of cell culture medium. After 24 hours the medium in the cell flask was changed and cells were then cultured as described in section 2.3.1.4.

2.3.5 Generation of adipose tissue conditioned medium

To extract paracrine factors from adipose tissue, processed formulations of adipose tissue were added to serum free MesenPRO for 72 hours in a 37 °C, 5 % humidified CO_2 incubator to allow growth factors and proteins to migrate from the adipose tissue and into the medium. This was termed "conditioned medium". Conditioned medium was generated from minced adipose tissue, lipoaspirate, emulsified fat, lipocondensate, ADSC, and free floating lipid removed from the adipose tissue during the previous stages of processing (section 2.2.4). The formulations: minced adipose tissue, lipoaspirate, and emulsified fat were added to medium at a concentration of 0.1 g/ml of serum free MesenPRO. Lipocondensate and lipid were added at a concentration of 0.05 g/ml of serum free MesenPRO. This change of concentration was because early observations of the processing steps outlined in section 2.2.4 were that 1 gram of adipose tissue led to roughly 0.5 grams of lipocondensate and 0.5 grams of lipid being produced. The mass of adipose tissue used to produce adipose tissue conditioned medium was measured using a 125A balance (Precisa, Edinburgh, UK) in a 30 ml centrifuge tube. The weight of the empty container was recorded and subtracted from the weight measured when adipose tissue was added to the container to calculate mass of adipose tissue used. MesenPRO RS™ medium was conditioned using 4500 ADSCs/mm^2 on cell culture plastic for 24 hours. After 24 hours, MesenPRO RS™ medium was removed and replaced with serum free MesenPRO to remove any serum from the ADSC.

After 72 hours, all media was removed from its vessel and was centrifuged at 2645 *xg* for 8 minutes. Any remaining and floating adipose tissue was removed with forceps and disposed of. The remaining medium was then filtered through a 100 µm filter (PluriSelect), aliquoted into 1- and 3-ml aliquots to avoid multiple freeze thawing cycles and stored until use at -80 °C.

2.4 *In vitro* experimental methods

2.4.1 Assays used to characterise adipose tissue

2.4.1.1 Adipogenic differentiation

ADSCs were seeded at 10,000 cells per well in a 12 well plate in MesenPRO RS™ medium for 24 hours. Following this, the medium was removed and cells were cultured in serum free MesenPRO for 24 hours. This medium was then removed and ADSCs were treated with adipogenic differentiation medium (table 2.4) for 14 days with the medium being replaced every 3 days.

After 14 days, medium was removed and cells were fixed in 3.7 % Paraformaldehyde (PFA; Merck) for 15 minutes.

2.4.1.2 Oil red O assay

Oil red O working solution was made up fresh by adding 100 % isopropanol (Thermo Fisher Scientific) to oil red O powder (Merck) to a final concentration of 5 mg/ml. This solution was filtered through Whatman no. 1 filter paper (Thermo Fisher Scientific). Fixed cells were washed three times with PBS and treated with 60 % isopropanol for 15 minutes following which cells were washed three times in PBS and 1 ml of oil red O solution was added to each well. Cells were covered in oil red O for 20 minutes after which, the solution was removed and wells washed 5 times in PBS. Cells were then imaged at x10 magnification by an AE 2000 inverted light microscope.

Lipid vesicles were counted on Fiji software (Schindelin *et al.,* 2012) by increasing the red saturation in the colour threshold tool. The saturation on images was thresholded so that only that the red staining was visible. The image was then made binary and the dark lipid droplets were counted.

Staining could then be quantified by adding 100 % isopropanol to wells for 5 minutes to remove the stain from cells. The absorbance of this solution was then measured at 492 nm on an ELx800 photospectrometer (BioTek, Stockport, UK).

2.4.1.3 Quantification of cell death from processing

To examine the effect the processing steps (outlined in section 2.2) had upon the cells contained within the adipose tissue, assays were carried out to measure cell lysis and cell metabolic activity.

A Pierce™ lactate dehydrogenase assay was chosen to measure adipose cell lysis post processing. This assay measures cell lysis by quantifying the amount of lactate dehydrogenase (LDH) released by a cellular population. Lactate dehydrogenase is the enzyme responsible for catalysing the conversion of lactate to pyruvate and the reduction of NAD^+ to NADH in the glycolysis stage of respiration and thus is found in the cytosol of most cells. When cells are lysed and the cell membrane breaks down, lactate dehydrogenase is released (figure 2.6A). When mixed with a reaction mix provided in the Pierce™ lactate dehydrogenase cytotoxicity assay kit (Thermo Fisher Scientific), the lactate dehydrogenase converts NAD^+ found in the reaction mix to NADH. The reaction mix also contains tetrazolium salt and the enzyme diaphorase which, when combined with NADH, forms formazan. Formazan forms a dark red colour and the solutions absorption at 680 nm can then be measured as a way of semi-quantifying cell death.

All reagents used were provided in a Pierce™ lactate dehydrogenase cytotoxicity assay kit, reagents were made up as per manufacturer's instructions. 0.1 g of processed adipose tissue

(minced adipose tissue, lipoaspirate, emulsified fat, and lipocondensate) was added to 900 µl of serum free MesenPRO in a 12-well plate. Samples were left in a 37 °C, 5 % CO_2 humidified incubator for one hour to allow LDH to move into the medium from any lysed cells. Subsequently, 50 µl of medium was removed from each well and added to 50 µl of LDH reaction mixture containing NAD^+, tetrazolium salt and diaphorase in a 96-well plate in triplicate. The kit also came with a positive control reagent containing lactate dehydrogenase, 50 µl of the positive control was also added to the 96 well-plate in triplicate and 50µl of serum free MesenPRO was used as a blank sample in the same well-plate. 50 µl of LDH reaction mixture added was added to the positive control and blank wells. This well plate was then left covered for 30 minutes at room temperature after which, 50 µl of "stop solution" was added to each well to halt the conversion of NAD^+ to NADH. The well plate was then placed in a ELx800 photospectrometer and absorbance at 680 nm was recorded. This value was then normalised to a positive control as outlined in equation 2.2.

$$\frac{(Absorbance\ at\ 680\ nm - Blank\ absorbance\ value\ at\ 680\ nm)}{Positive\ control\ absorbance} = Relative\ cell\ lysis$$

Equation 2.2 Equation used to calculate the relative cell lysis of adipose tissue post processing.

2.4.1.4 Assessment of adipose tissue metabolic activity post processing

To measure cell metabolic activity, an assay using 7-hydroxy-3*H*-phenoxazin-3-one-10-oxide (resazurin dye) was carried out. Resazurin is a non-toxic dye that is reduced to resorufin by NADH. Resorufin fluoresces when excited by light at 571 nm and as $NADH/H^+$ is oxidised by cells that are respiring, the conversion of resazurin to resorufin can be used to measure cell metabolic activity (figure 2.6B).

Processed adipose tissue (0.1 g) was added to 900 µl of filter sterilised 0.1 mM resazurin dye in serum free MesenPRO in a 12-well plate. Adipose tissue in resazurin was then incubated in a 37 °C, 5 % CO_2 humidified incubator for 4 hours. Subsequently, 50 µl of this solution was removed and added to a 96-well plate. Fluorescence was measured at 570 nm/590 nm on an ELx800 photospectrometer and readings from 50 µl of 0.1 mM resazurin in untreated cell culture medium was subtracted. Following this, fluorescence values were normalised to a control reading, specified in the individual experiment (equation 2.3).

$$\frac{(Fluorescence\ at\ 570/590\ nm\ -\ Fluorescence\ of\ blank\ resazurin\ at\ 570/590\ nm)}{Fluorescence\ at\ 570/590\ nm\ of\ control\ sample} = Relative\ cell\ metabolic\ activity$$

Equation 2.3 Equation used to calculate the relative cell metabolic activity of adipose tissue post processing.

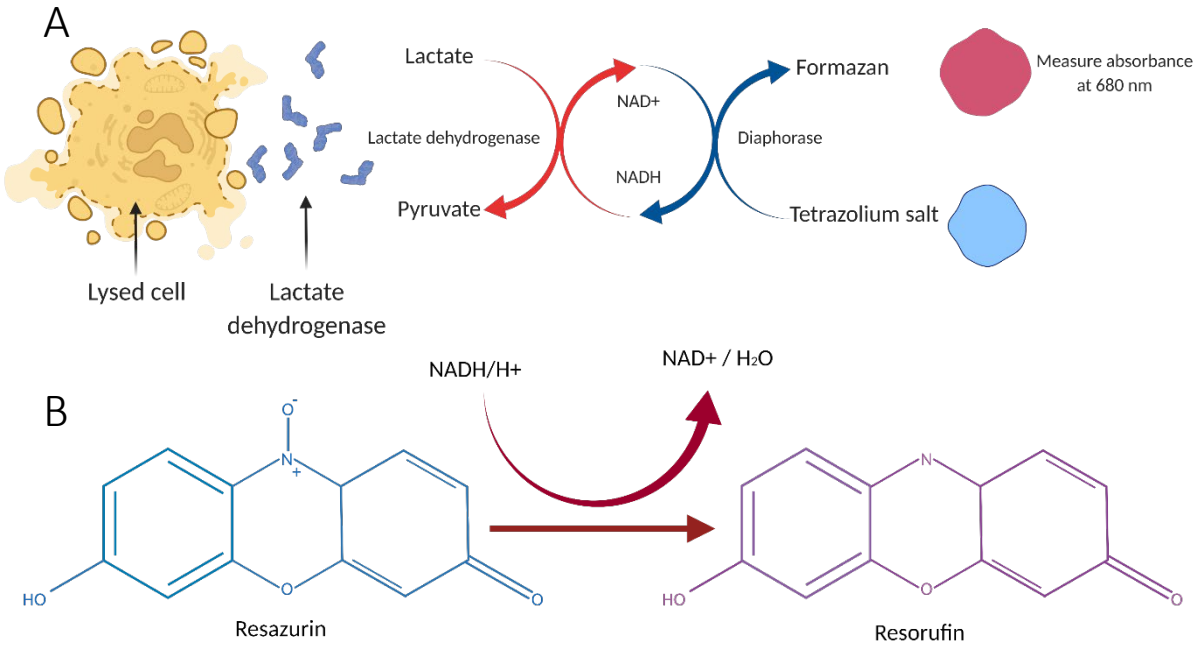

Figure 2.6. Assays used to measure cell lysis and metabolic activity. (A) The conversion of pyruvate to lactate due to the release of lactate dehydrogenase was used to measure cell lysis. **(B)** Resazurin is reduced to resorufin by the conversion of NADH to NAD^+, a by-product of respiration and a sign of healthy cell metabolism.

2.4.1.5. DNA extraction and quantification

To extract DNA, a Macherey-Nagel NucleoSpin DNA lipid tissue kit (Thermo Fisher Scientific) was used. DNA was extracted from minced adipose tissue, lipoaspirate, emulsified fat, and lipocondensate (0.05 ± 0.007 grams of tissue). All centrifugation steps were carried out in a Hawk 15/05 centrifuge at 11,000 *xg* for 30 seconds. Before extraction, adipose tissue was placed on a cell strainer (10 µm, PluriSelect) and washed several times with PBS to ensure that any DNA from cells that had ruptured before extraction was removed. Following this wash, the adipose tissue sample was placed in a NuceloSpin bead tube and 100 µl of BE buffer added. The adipose tissue was then disrupted and lysed by the addition of 40 µl of LT buffer and 10 µl of proteinase K followed by 20 minutes of agitation on a Vortex Genie 2 (Scientific industries, St. Neots) bead holder. After agitation, samples were centrifuged and 600 µl of LT mixture was added to the adipose mixture and the samples were re-centrifuged. The resulting solution was then added to a NucleoSpin DNA lipid tissue binding column, where DNA released from adipose tissue agitation was bound to a membrane in the column. The tubes were then centrifuged, and the membrane was washed by adding 500 µl of BW mixture and centrifuging followed by the addition of 500 µl B5 mixture and a centrifugation step.

The membrane was then dried with another centrifugation step and DNA was eluted from the column by the addition of 100 µl of BE buffer and a final centrifugation.

DNA was quantified using a Quant-iT™ PicoGreen® kit (Thermo Fisher Scientific). DNA collected from adipose tissue was added to PicoGreen® DS DNA reagent (diluted 1:200 in TE buffer) at a 1:1 ratio. This solution was added to a 96 well plate and incubated in the dark at room temperature for 5 minutes and fluorescence at 520 nm was measured using a ELx800 photospectrometer. Fluorescence values were compared to a standard curve generated using supplied lambda DNA standards (table 2.16). Lambda DNA standard was diluted with TE buffer and then added to PicoGreen® DS DNA reagent. Cell number was calculated by using a value of 6 pg as the amount of DNA per cell. If the fluorescence of the solution was higher than any sample in the standard curve, the solution would be diluted in TE buffer and fluorescence re-examined. DNA samples were collected and quantified by Dr. Victoria Workman and data was used with her permission.

Table 2.16. Concentration of DNA standard used to generate standard curve.

Standard	TE Buffer (µl)	Volume of DNA standard (2µg/ml) (µl)	PicoGreen® DS DNA reagent (µl)	Final DNA concentration (ng/ml)
A	0	1000	1000	1000
B	900	100	1000	100
C	975	25	1000	25
D	990	10	1000	10
E	750	250 (standard D)	1000	2.5
F	600	400 (standard E)	1000	1
G	750	250 (standard F)	1000	0.25
H	900	100 (standard G)	1000	0.025
I	1000	0	1000	0

2.4.2 Fluorescent staining of adipose tissue

To characterise the effect processing had on the macrostructure of adipose tissue, a MemBrite™ fix 640/660 cell surface staining kit (Cambridge Bioscience), BODIPY and DAPI stains were used to label adipose tissue. Different formulations of adipose tissue (minced adipose tissue, lipoaspirate, emulsified fat, and lipocondensate) were generated and 1 mg of each formulation was placed in separate Eppendorf tubes (Thermo Fisher Scientific). Membrite pre-stain buffer (Cambridge Bioscience) was diluted 1:1000 in HBSS and was added to cover adipose tissue and incubated at 37 °C for 5 minutes. MemBrite™ dye solution was diluted 1:1000 in HBSS. Pre-stain buffer was removed from fat and MemBrite™ dye solution was added to Eppendorfs and incubated with adipose tissue for 5 minutes at 37 °C. Following this, adipose tissue was stained by adding 5 µM BODIPY 558/568 and 1 µg/mL DAPI and incubating for 30 minutes at room temperature. After staining, the dyes were removed and the adipose tissue samples were washed by adding and removing PBS three times, were fixed by the addition of 3.7 % PFA, and kept at 4 °C until use.

Prior to imaging, PFA was removed from the Eppendorfs and samples were washed three times in PBS. Adipose tissue was then removed from the Eppendorfs and were encapsulated by placing samples in wells of an 8-well µ-slide (Ibidi, Glasgow, UK) and adding 1 % (w/v) agarose (Thermo Fisher Scientific) to ensure samples were not mobile while imaging occurred. Tissue samples were imaged using a Zeiss LSM 880 AiryScan confocal microscope using Zen Black 2014 software (Zeiss, Cambridge, UK). Images were taken at a x10 magnification using a UV laser (405nm) to image DAPI and two separate VIS lasers at 633 nm and 543 nm were used to image MemBrite and BODIPY respectively. Images were taken using Z-stacking and 50 images across a depth of 50 µm were taken of samples. Images were generated on Zen Blue 2014 software (Zeiss). Maximal projections were generated by combining all images of the Z-stack into one image. Orthogonal projections were generated using the “orthogonal projection” function.

2.4.3 Flow Cytometry analysis of ADSC

ADSC were allowed to grow to 90 % confluency and were separated from cell culture plastic as described in section 2.3.2. After resuspension the ADSCs were counted and a total of $10x10^6$ cells were removed and centrifuged at 600 x*g* for 5 minutes. Cells were washed twice in 1 % (w/v) BSA in PBS then resuspended in 1 µl of flow cytometry buffer solution (FCBS; Thermo Fisher Scientific) and left in an incubator at 37 °C for 30 minutes. FCBS is a solution containing various salts and is used dilute antibodies and preserve them at the correct pH. Following this, cells were washed twice in FCBS and resuspended in a solution of 20 % (v/v) human Fc receptor binding inhibitor (Thermo Fisher Scientific), 80 % (v/v) FCBS and incubated in a 4 °C fridge for 20 minutes to prevent non-specific binding of antibody Fc regions. Afterwards, cells were pelleted by centrifugation at 600 *xg*, resuspended in FCBS and aliquoted into Eppendorfs with $5x10^5$ ADSC per sample.

Fluorescent flow cytometry antibodies were then added to ADSCs in various combinations described in table 2.17. Antibody solutions were made up by diluting antibodies 1:20 in FCBS. These antibody solutions were then added to ADSC solutions at a 1:1 ratio and were incubated in the dark. The isotype control used was an antibody to mouse IgG1 K (Thermo Fisher Scientific). Cells were pelleted a final time at 600 *xg* and then fixed by adding 0.5 ml of 4 % PFA. Flow cytometry samples could be stored in this manner for a week in a 4°C fridge. Samples were then analysed on a LSRII Flow Cytometer using compensation beads and fluorescence minus one (FMO) controls to set voltage gates. Data was then analysed using Flowing Software (Turku Bioscience Centre, Turku, Finland).

Table 2.17. Antibody combinations used in flow cytometry analysis. FVD is a fixable viability dye (Thermo Fischer Scientific)

Sample	Antibody (µL)							FCBS volume (µL)
	CD31	CD34	CD45	CD73	CD105	CD90	CD146	
ADSC sample (with FVD)	5	5	5	5	5	5	5	15
ADSC sample (without FVD)	5	5	5	5	5	5	5	15
Isotype control	Isotype control Mouse IgG1 K							45
Fluorescence minus one (FMO) control CD31	x	5	5	5	5	5	5	45
FMO control CD 34	5	x	5	5	5	5	5	45
FMO control CD 45	5	5	x	5	5	5	5	45
FMO control CD 73	5	5	5	x	5	5	5	45
FMO control CD 105	5	5	5	5	x	5	5	45
FMO control CD 90	5	5	5	5	5	x	5	45
FMO control CD146	5	5	5	5	5	5	x	45

2.4.4 Extraction and quantification of fibroblast mRNA

2.4.4.1 RNA extraction

Cells were seeded in 6-well plates at a density of 35,000 cells per well in 10 % D-MEM. After 24 hours, 10 % D-MEM was removed and replaced with serum free MesenPro for 24 hours to remove FCS from the fibroblasts. Serum free medium was then removed and replaced with serum free MesenPro containing 5 ng/ml of recombinant TGF-β1 and incubated for 72 hours. This medium was then removed, and fibroblasts were washed with PBS.

RNA was then extracted from the fibroblasts seeded in each well using the RNeasy® Plus Mini kit, (Qiagen) as per the manufacturer's instructions. Fibroblasts were lysed one well at a time by the addition of 350 µl of lysis buffer containing 10 µl/ml β-mercaptoethanol (Merck) and scraping with an 18 cm flexible cell scraper (Thermo Fisher). The lysate was transferred to a gDNA elimination spin column. The lysate was stored on ice until all lysate samples had been collected. Following this all columns were centrifuged at 8,000 *xg* for 30 seconds in a Hawk 15/05 centrifuge. An equal volume of 70 % ethanol was then added to the flow-through. This solution was then transferred to a RNeasy spin column where the RNA bound to the column mesh via ionic interaction. The solution was then centrifuged at 8,000 *xg* for 30 seconds to remove the ethanol. Columns were washed with buffers RW1 and RPE (each followed by 30 seconds centrifugation at 8,000 *xg*). To elute the RNA from the column, 50 µl of RNase free water was added to the spin column and centrifuged at 13,000 *xg* for one minute. The filtrate from the previous step was then re-added to the spin column and centrifugation repeated to maximise the concentration of extracted RNA from the column. A Nanodrop 1000 (Thermo Fisher Scientific) was used to quantify RNA and the ratio of absorbance at 260 nm to absorbance at 280 nm was used to estimate the purity of extracted RNA. Samples with a 260:280 ratio of approximately 2 and an absorbance profile with a single peak were deemed pure.

2.4.4.2 Generation of cDNA

Transformation of mRNA to cDNA was carried out using a High Capacity RT PCR kit (Thermo Fisher Scientific). Reverse transcriptase reagent mixture was made as per manufacturer's instructions (see table 2.5) and 10 µl of this mixture was added to an equal volume of 10 ng/µl RNA. Reverse transcription was carried out on the RNA-reagent mixture in a Thermal Cycler Prime (Techne, Staffordshire, UK) using the protocol in table 2.18. For each cDNA sample generated, a duplicate mixture was made, and a reverse transcription reaction carried out without the addition of the reverse transcription enzyme. This sample acted as a control to ensure there was no genomic DNA contamination in the sample.

Table 2.18. Protocol used for reverse transcription PCR.

Step	Temperature (°C)	Time (minutes)
Denaturation	25	10
Annealing	37	120
Extension	85	5
Hold	4	∞

2.4.4.3 Quantification of cDNA

SYBR green quantitative polymerase chain reaction on the cDNA generated from the reverse transcription was then used to quantify gene expression of myofibroblast markers (α-SMA, COL1A1, FN1-EDA splice variant). Reagent mixtures were made containing RNase free water, x2 SYBR green Lo Rox mix, and forward and reverse primers for each myofibroblast marker (table 2.6). The nucleotide sequence for the forward and reverse primers for the cDNA targets can be found in table 2.7. Primers were diluted in RNase free water to 10 µM for use. To the different mixtures, 5 ng of cDNA was added and a qPCR reaction was carried out using a Rotor Gene Q qPCR machine, measuring fluorescence at 520 nm after excitation at 480 nm during each cycle (table 2.19). The cycle at which 0.04 fluorescence units was reached was recorded to generate a Ct value which related back to the abundance of cDNA before amplification. Using the recorded Ct values, the $2^{-\Delta\Delta CT}$ method was used to calculate the relative gene expression of genes characteristic of a myofibroblast phenotype compared to the house keeping gene RNU6-1 (Livak & Schmittgen, 2001; equation 2.4). A melt step was added following the final extension stage and reviewed visually. A single fluorescent peak demonstrated there was only one amplification product in each reaction.

$$2^{-\Delta\Delta Ct} = 2^{-(\Delta C_{t(test)} - \Delta C_{t(control)})}$$

$$\Delta C_t = \Delta C_{t\,(target)} - \Delta C_{t\,(reference\ gene:\ RNU6-1)}$$

Equation 2.4. $2^{\wedge-(\Delta\Delta\ Ct)}$ calculation. Equation used to calculate relative gene expression using CT values from qPCR.

Table 2.19. Protocol used for SYBR green qPCR.

Step	Temperature (°C)	Time	
Initial denaturation	95	10 minutes	
Denaturation	95	10 seconds	Repeat x40
Annealing	60	15 seconds	
Extension	75	20 seconds (fluorescence values acquired at this step)	
Melt	Increase from 75 to 95	90 second wait to begin, 5 second wait between each 1 °C increase in temperature	
Hold	4	∞	

2.4.5 Protein analysis of α-SMA

2.4.5.1 Extraction and quantification of fibroblast protein via western blotting

HDF were seeded in 6 well plates (Starlab, Hamburg, Germany) at 35,000 cells per well in 10 % D-MEM. After 24 hours, 10 % D-MEM was removed and replaced with serum free MesenPRO for 24 hours to remove FCS from the fibroblasts. Serum free media was then removed and replaced with serum free MesenPRO containing 5 ng/ml of recombinant TGF-β1 and incubated for 72 hours. This medium was then removed, and fibroblasts were washed by adding and then removing PBS to each well with an electronic pipette. A micropipette was then used to remove any small, remaining volumes of fluid in the wells.

Fibroblasts were lysed one well at a time by the addition of 200 µl of protein lysis buffer (see table 2.8) to wells. The base of the each well was scraped in a circular manner for 30 seconds with an 18 cm cell scraper to aide lysis. The lysate was collected with a micropipette and stored in an Eppendorf on ice for 30 minutes. Following this incubation period, the lysate was centrifuged at 10,000 *xg* in a Hawk 15/05 centrifuge for 10 minutes at 4 ^{o}C. The protein solution was extracted, taking care not to disturb the pellet of cell debris that had formed during centrifugation, and placed in a fresh Eppendorf and stored at -20 °C.

2.4.5.2 Protein quantification

Total protein concentration of lysates was quantified using a Pierce^{TM} BCA assay (Thermo Fisher), as per the manufacturer's instructions. In a 96 well plate (Greiner BioOne, KremsmÜnsten, Germany) 25 µl of protein sample was added to 200 µl of a 50:1 mixture of working reagent (50 units reagent A: 1 unit reagent B). The well plate was covered with Parafilm^{TM} (Thermo Fisher Scientific) and left to incubate at 37 °C for 30 minutes. Following this, absorbance was measured at 562 nm on an Infinite M200 photospectrometer. Unknown protein concentrations were quantified by comparing to a standard curve generated by making solutions of a known protein concentration using BSA as the protein and RIPA buffer as the diluent (see table 2.20 and figure 2.7). Once a standard curve was generated, the gradient of the trendline was then used in the equation 2.5. A fresh standard curve was generated every time a BCA assay was carried out.

Table 2.20. Protein volumes used in standard curve generation.

Vial	Volume of Diluent (µL)	Volume of Protein (µl)	Final BSA Concentration (µg/mL)
A	0	300 (From BSA stock)	2000
B	125	375 (Stock)	1500
C	325	325 (Stock)	1000
D	175	175 (From vial B)	750
E	325	325 (From vial C)	500
F	325	325 (From vial E)	250
G	325	325 (From vial F)	125
H	400	100 (From vial G)	25
I (Blank)	400	0	0

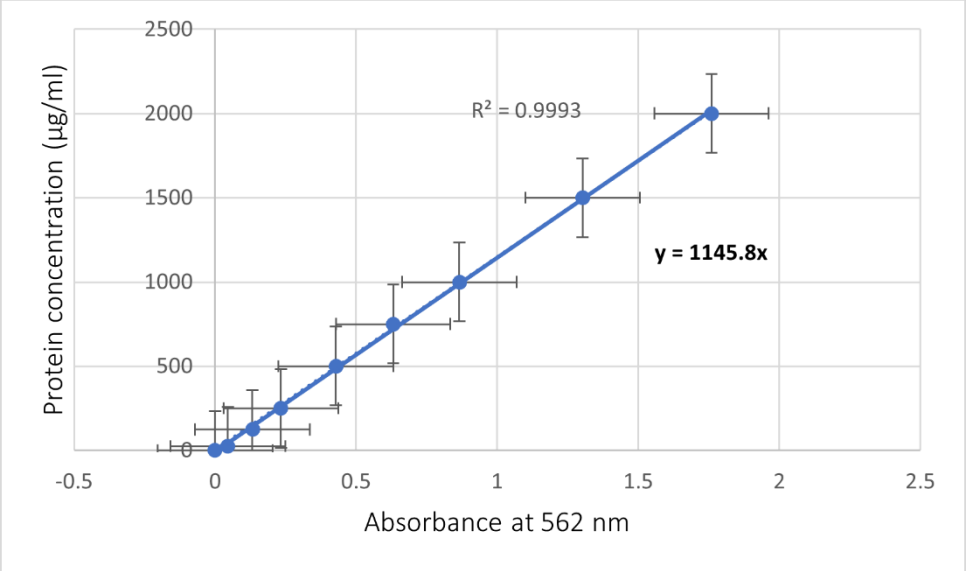

Figure 2.7. Example of BCA standard curve. Example of a standard curve generated by measuring absorbance of protein samples made up at the concentrations in table 2.18. Error bars = standard error.

$$Y = mx$$

$$Y = 1145.8\ x\ 1.746$$

$$Y = 2000\ \ \mu g/ml$$

Y = Protein concentration (µg/ml) m = gradient of trendline x = Absorbance at 562 nm

Equation 2.5. Equation used to calculate protein concentration using a BCA standard curve.

2.4.5.3 Gel electrophoresis

Following quantification, gel electrophoresis was carried out on protein lysate. Protein lysate was diluted in molecular grade water to the concentration of the lowest sample in each biological repeat to ensure an equal volume of protein would be added to each well of the gel. This protein mixture then had 5 µl of 5X Protein Loading Buffer (Thermo Fisher) added and was heated at 95 °C on a hot block (Thermo Fisher Scientific) for 3 minutes. This mixture was then added to wells of a pre-cast 4-20 % Mini-PROTEAN TGX polyacrylamide gels (Bio-Rad, Watford, UK). On average, 5-20 µg of protein lysate was added to wells. A Primestep prestained broad range protein ladder (BioLegend, London, UK) was added in one well of each gel (3 µl) so as to measure the size of any protein bands detected at later stages. Sodium dodecyl sulphate (SDS) solution (1 % v/v, in deionised water; VWR chemicals) was added to a gel tank with the acrylamide gel. Recycled SDS solution was used to fill the tank however, the solution between the gel cassette was always freshly made using deionised water as a diluent (figure 2.8A). An electric current set at 200 V was passed through the gel cassette for roughly 30 minutes, pulling the protein down the gel. This was halted when the loading dye had reached the bottom of the gel.

After electrophoresis, the protein inside the gel was transferred over to a nitrocellulose membrane. The gel was placed in between a 0.2 µm thickness nitrocellulose membrane and filter paper (both Bio-Rad) as in figure 2.8B. Both the membrane and paper were pre-wet with semi-dry transfer buffer (see table 2.10). The transfer stack was then placed in a Trans Blot Turbo and a 20 V, 2 A current run through the stack for 20 minutes. This current pulled the negatively charged protein out of the gel and onto the membrane, which bound the protein due to hydrophobic interactions between the membrane and protein.

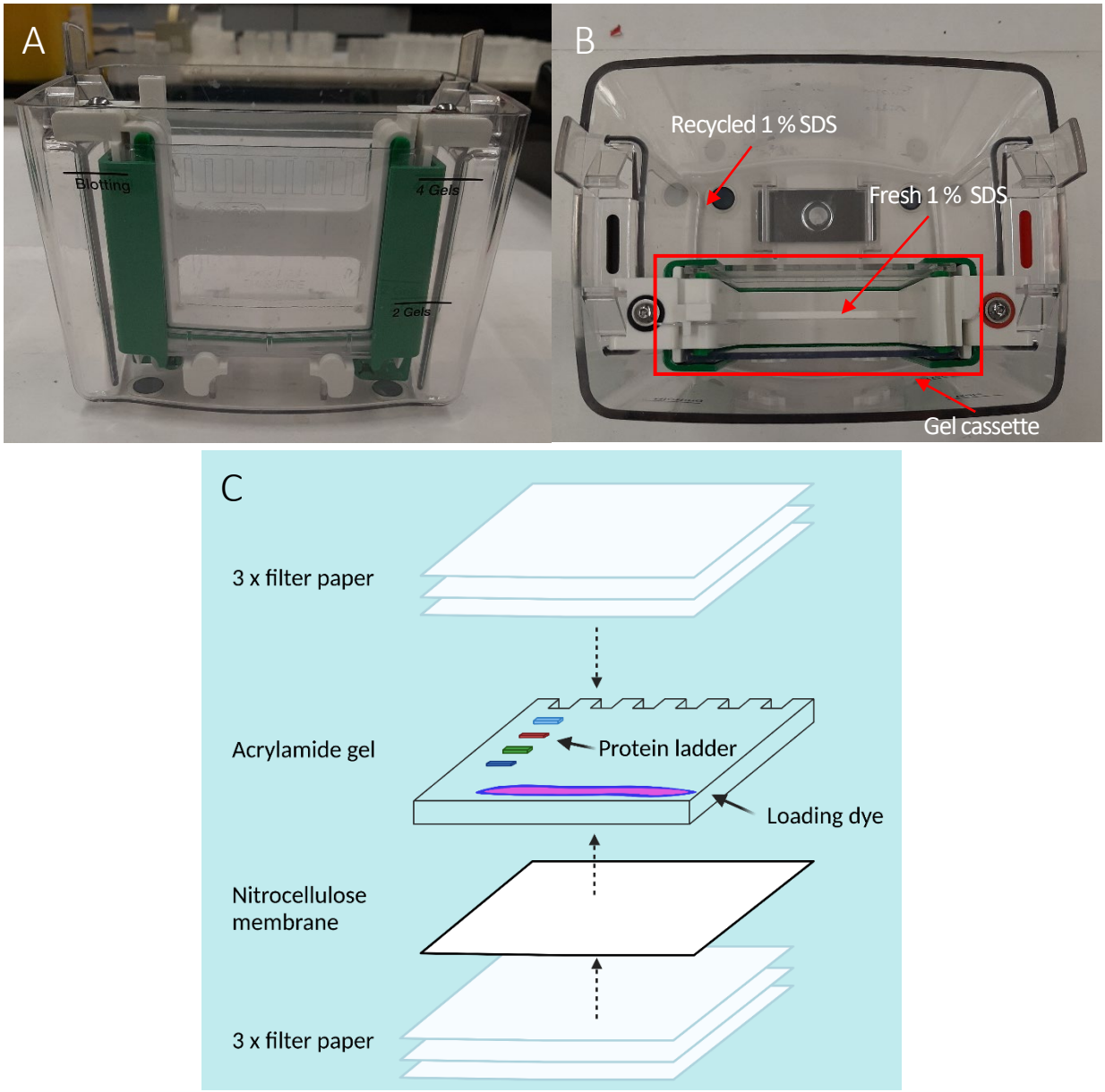

Figure 2.8. Western blotting equipment. (A) Gel electrophoresis tank used for western blotting. **(B)** The gel cassette would be filled with fresh 1 % SDS. **(C)** Schematic of how protein blots were transferred from an acrylamide gel to a nitrocellulose membrane.

2.4.5.4 Membrane staining

All membrane incubation steps were carried out in a sealed plastic tub either for one hour at room temperature on a SSL 4 see-saw rocker (SLS Scientific) or at 4 °C overnight in a fridge (BioCold, Polbeth, UK) on a SSL 4 see-saw rocker. Membranes were washed by the addition of 0.1 % TBS-tween 20; table 2.9) and 10 minutes of room temperature incubation. This wash buffer was then removed, and the wash step repeated another two times.

Freshly transferred membranes were first blocked by adding 5 % (w/v) dry milk powder or 5 % (w/v) BSA (depending on the buffer solution suggested by the antibodies manufacturers), both in 0.1 % (v/v) TBS, and washed. Following blocking, primary antibodies were applied to the blot and incubated for one hour or overnight. Following 3 washes in 0.1 % TBS-tween 20 for 10 minutes each, a secondary antibody conjugated to HRP was applied, the blot was incubated and washed. To quantify the amount of protein bound to the membrane, chemiluminescence solution (a 1:1 solution of Clarity Western Peroxide Reagent and Clarity Western Luminol/Enhancer Reagent (both Bio-Rad)), was added to the blot for 5 minutes and then removed. The membrane was then imaged on a C-Digit scanner (Li-Cor Biosciences, Cambridge, UK) for 12 minutes at a high sensitivity setting. Following imaging, the membrane was washed and the bound antibodies removed by 30 minutes of incubation with Western Blot Stripping Buffer (Abcam) that had been pre-warmed to 37 °C. Following antibody stripping, the membrane would be washed and blocked as before and could be re-probed with alternate antibodies.

2.4.5.5 Protein densitometry

Protein abundance was measured in a semi-quantitative manner via densitometry using the image software, Fiji (figure 2.9). Using the “rectangle” tool, equal areas across the same horizontal plane were selected around each lane of the image of the nitrocellulose membrane. Using the “plot lanes” feature in the “analyse” tool section of the program, histograms showing the relative density of the previously selected areas were generated. The area of the histogram represented the density of the band selected and the amount of protein present on the membrane. To subtract the background signal of the western blot, a line was drawn underneath the peak of each histogram and using the “wand” tool the area of each protein band was measured and normalised to the area of the corresponding loading control.

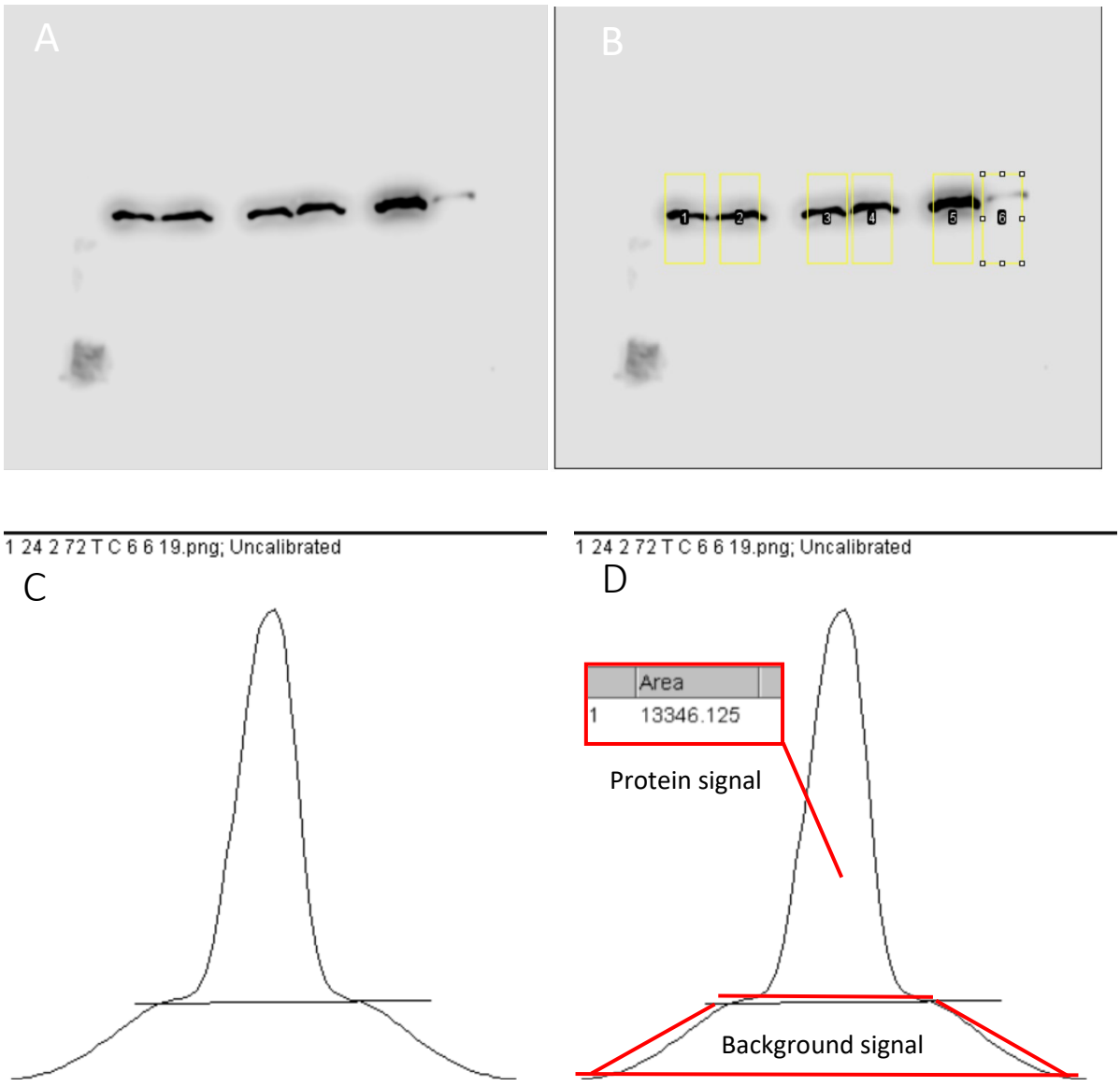

Figure 2.9. Western blot densitometry. (A) Example western blot stain for α-SMA. **(B)** Protein bands selected using the rectangle tool in Fiji. **(C)** Histogram generated by Fiji to visualise the density of a protein band. **(D)** The background signal was removed from density calculations.

2.4.5.6. Immunofluorescent imaging of myofibroblast protein

Microscope coverslips (19 mm; Thermo Fisher) were placed in wells of a 12 well-plate (Sarstedt) and sterilised in 1 ml of 100 % methanol for 15 minutes. Subsequently, these wells were washed three times in 1 ml of PBS. HDF were then seeded in these wells at 10,000 cells per well in 10 % D-MEM. After 24 hours, 10 % D-MEM was removed and replaced with serum free MesenPro for 24 hours to remove FCS from the fibroblasts. Serum free medium was then removed and replaced with serum free MesenPro containing 5 ng/ml of recombinant TGF-β1 and incubated for 72 hours. Following incubation, medium was removed, and the fibroblasts were fixed in 500 µl of 100 % methanol for 15 minutes. Cells were washed three times by adding and removing 1 ml of PBS to each well. After this, fibroblasts were permeabilized in 1 % v/v Triton X (Thermo Fisher) in PBS for 15 minutes and washed three times in PBS. The cells were then blocked for one hour in 2.5 % (w/v) BSA in PBS on a SLS 4 see-saw rocker, oscillating at 30 rpm for one hour at room temperature and were washed three times in PBS. Fibroblasts were then stained in one of two ways, depending on whether cells were being stained for α-SMA only or α-SMA and Ki-67.

α-SMA only

Fibroblasts were stained for one hour by adding anti-α-SMA-fluorescein isothiocyanate (FITC) conjugated antibody and DAPI stain both in 1.0 % BSA in PBS (table 2.13). Cells were incubated in this solution for one hour at room temperature on a rocker, oscillating at 30 rpm. Following incubation, this solution was removed, and wells were washed three times with PBS. Microscope coverslips were then removed from the well plate. The coverslip was then slowly placed cell side down onto a drop of DPX mountant (Thermo Fisher Scientific) on a microscope slide. Slides were imaged in a dark room on an 1x73 Inverted Olympus fluorescent microscope with a Retiga 6000 camera. Using a 69002 - ET - DAPI/FITC/Texas red filter to image coverslips. The filters allowed only light of specific wavelengths to reach the sample. These wavelengths were 405 nm (DAPI), 488 nm (FITC).

α-SMA and Ki-67

Fibroblasts were stained for one hour by adding Ki-67 and α-SMA antibodies in 1 % w/v BSA (table 2.13) and incubated at room temperature on a rocker. Following this, the antibodies were aspirated from the wells and secondary AlexaFluor® antibodies and DAPI were added in 1 % w/v BSA and incubated in wells for 1 hour at room temperature on a rocker while covered. Following incubation, this solution was removed, and wells were washed three times in PBS. Microscope coverslips were then removed from the well plate. The coverslip was then slowly placed cell side down onto a drop of DPX mountant on a microscope slide. Slides were imaged in a dark room on

using an upright LSM510 Meta Confocal microscope using the HeNe1 (543 nm), HeNe2 (633 nm), and Argon (458 nm) lasers to image coverslips.

In both instances, images were taken at x10 magnification as separate image files for each filter and later combined and analysed. Three images were taken for each microscope slide and a suitable image location was chosen by looking at slides with the DAPI filter so as to only see cell nuclei and not allow the presence of α-SMA to influence the choice of image location.

Cells were counted on ImageJ by their nuclei and the number of cells producing α-SMA was recorded (figure 2.10). Brightness was increased on images to aide visibility, this change was applied uniformly on all images in each respective set on ImageJ.

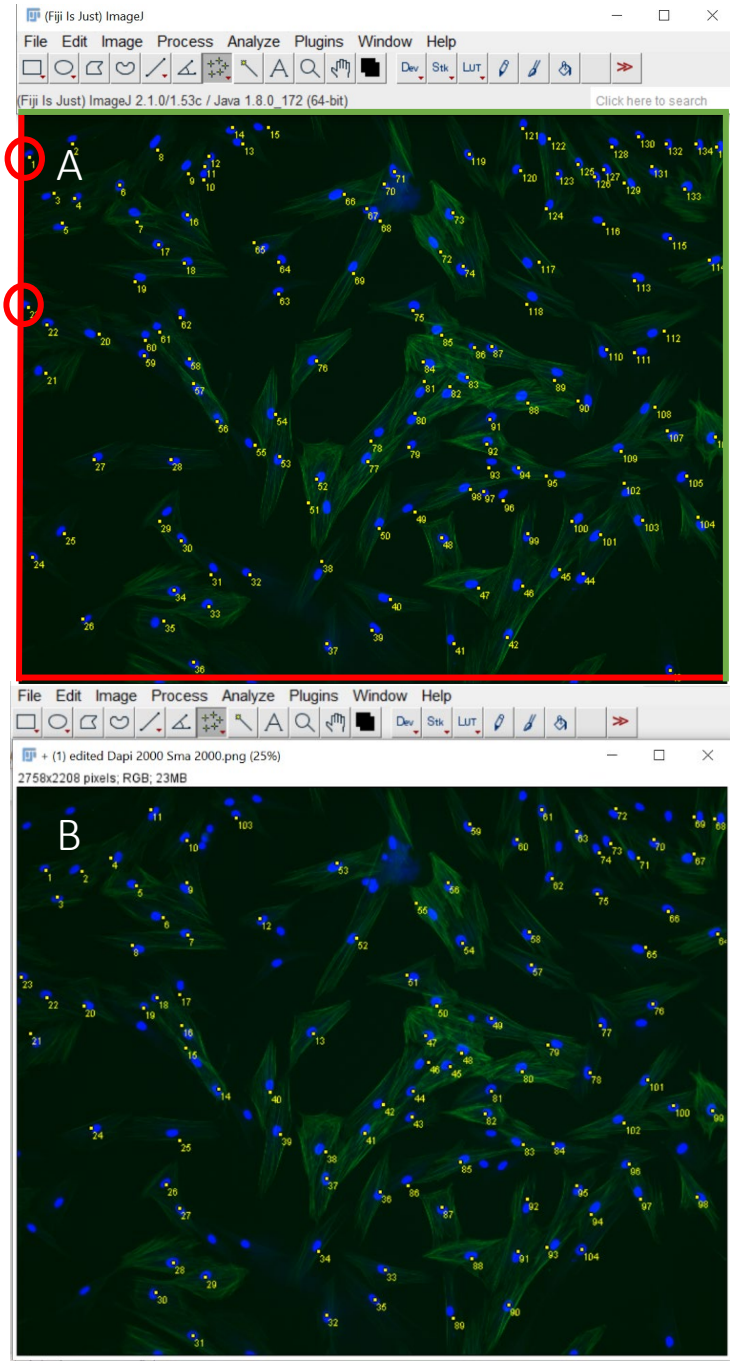

Figure 2.10. Example of image analysis. (A) All blue nuclei were counted in a field of view. If nuclei lay on the left or bottom edge they would be excluded from counting (see red lines and circles), if they lay on the right or top edge they would be counted (green line). **(B)** Nuclei laying on green α-SMA fibres would be counted to determine cells producing α-SMA.

2.4.6 Methods for examining the components of adipose tissue

2.4.6.1 Cytokine array

Adipose tissue conditioned medium was probed for a wide variety of different cytokines and growth factors using a Ray Bio® C-Series Human Cytokine Antibody Array (C5) (RayBiotech, Peterborough, UK). The array comprised 88 different antibodies (table 2.19) with binding sites to different cytokines collected in small circles across the blot. When conditioned medium or serum etc. are added, then proteins found in the solution will bind to the corresponding antibody if it is present on the membrane (figure 2.11). The amount of cytokine present can then be analysed using densitometry. Different samples of minced adipose tissue, lipoaspirate, emulsified fat, lipocondensate, ADSC, and lipid conditioned medium were selected for testing. Medium collected from three different patients' adipose tissue was used for each condition to limit the effect patient variation had upon results. A Pierce™ BCA assay was carried out as per the manufacturer's instructions to quantify total protein volume by generating a standard curve as in figure 2.7. The only difference to the procedure carried out in section 2.4.5.2 was that diluted serum free MesenPRO was used as the diluent. Serum free MesenPRO was diluted by a factor of 5 in deionised water as the phenol red contained in the MesenPRO RS™ basal medium interfered with absorbance readings at 562 nm. To ensure an equal volume of protein from each conditioned medium sample was added to the cytokine array, all different conditioned media were diluted in deionised water to the concentration of the lowest protein concentration sample. Different samples of the same formulation type of conditioned medium were then pooled together equally to make a 1 ml final mixture (333 µl of each patient sample). The samples were then run on the cytokine array.

All reagents in the C-Series Human Cytokine Antibody Array (C5) were made up as per the manufacturer's instructions and all incubation steps were carried out on an SSL 4 see-saw rocker oscillating at 30 rpm. Blocking buffer (2 ml) was added to each well to block binding sites present on the membrane to limit non-specific binding and incubated at room temperature for 30 minutes. This buffer was removed and the 1 ml solutions of conditioned media from minced adipose tissue, lipoaspirate, emulsified fat, lipocondensate, ADSC, and lipid were added to one blot each. Serum free MesenPRO was added to the final blot to act as a negative control. Once conditioned medium was added, the plate was incubated overnight at 4 °C.

Following this incubation, the conditioned medium was removed, and the membranes were washed three times by adding 2 ml of Wash Buffer I, incubating for 5 minutes at room temperature and then removing the buffer. This wash step was then repeated with Wash Buffer ll. After washing the membrane, 1 ml of biotinylated antibody cocktail was added to the membranes and left

overnight at 4 °C. This biotinylated antibody cocktail contains antibodies for the 88 cytokines tested by this membrane with biotin molecules attached, these antibodies bind to any cytokine that has been bound to the membrane (figure 2.11). After incubation, the membranes are washed again with Wash Buffer I and II before 2 ml of streptavidin conjugated to horseradish peroxidase was added and incubated on the membrane overnight at 4 °C. Streptavidin will bind to any biotin bound to the membrane and the conjugated horseradish peroxidase will luminesce when a chemiluminescent mixture is added to the membrane. The Streptavidin was removed, and the membranes washed a final time with wash buffer I and II following which, chemiluminescence detection mixture was applied to membranes for 2 minutes before the membranes were imaged at a high sensitivity setting on a C-Digit Scanner.

2.4.6.2 Array densitometry

Membrane images were analysed using the imaging software "Fiji" (figure 2.12). Using the "rectangle" tool, equal areas across the same horizontal plane were selected around each column of the image of the nitrocellulose membrane. Using the "plot lanes" feature in the "analyse" tool, histograms showing the relative density of the previously selected areas were generated. The area of the histogram represents the density of the band selected and the amount of protein present on the membrane. To subtract the background signal of the membrane a line was drawn underneath the peak of each histogram and using the "wand" tool the area of each protein circle was measured and equated to signal intensity.

The relative amount of cytokine present in conditioned medium was then calculated using the following equation and comparing to positive controls found on the membrane and serum free MesenPRO treated membranes.

$$Relative\ fold\ expression\ of\ cytokine\ X\ on\ membrane\ Y = \frac{Int.\ x\ (\frac{Pxy}{Pcont}.)}{Int.cont}$$

X = cytokine of choice
Y = membrane of choice
Int. = Pixel intensity of cytokine X on a membrane Y
Pxy = Average intensity of positive control spots on membrane Y
Pcont. = Average intensity of positive control spots on negative control membrane (serum free MesenPRO)
Int. cont. = Pixel intensity of cytokine X on negative control membrane

Equation 2.6. Densitometry calculation for a Ray BioTek cytokine array.

Table 2.21. Layout of the antibodies on the cytokine array. Antibodies for the cytokines probed for on the array were laid out in the manner described beneath.

	A	B	C	D	E	F	G	H	I	J	K
1	Positive control	Positive control	Positive control	Positive control	Negative control	Negative control	ENA-78 (CXCL5)	G-CSF	GM-CSF	GRO a/b/g	GRO alpha (CXCL1)
2	I-309 (CCL1)	IL-1 alpha (IL-1 F1)	IL-1 beta (IL-1 F2)	IL-2	IL-3	IL-4	IL-5	IL-6	IL-7	IL-8 (CXCL8)	IL-10
3	IL-12 p40/p70	IL-13	IL-15	IFN-gamma	MCP-1 (CCL2)	MCP-2 (CCL8)	MCP-3 (CCL7)	M-CSF	MDC (CCL22)	MIG (CXCL9)	MIP-1 beta (CCL4)
4	MIP-1 delta	RANTES (CCL5)	SCF	SDF-1 alpha	TARC (CCL17)	TGF beta 1	TNF alpha	TNF beta (TNFSF1B)	EGF	IGF-1	Angiogenin
5	OSM	TPO	VEGF-A	PDGF-BB	Leptin	BDNF	BLC (CXCL13)	Ck beta 8-1 (CCL23)	Eotaxin-1	Eotaxin-2	Eotaxin-3
6	FGF-4	FGF-6	FGF-7 (KGF)	FGF-9	FLT-3 Ligand	Fractalkine (CX3CL1)	GCP-2 (CXCL6)	GDNF	HGF	IGFBP-1	IGFBP-2
7	IGFBP-3	IGFBP-4	IL-16	IP-10 (CXCL10)	LIF	LIGHT (TNFSF14)	MCP-4 (CCL13)	MIF	MIP-3 alpha	NAP-2 (CXCL7)	NT-3
8	NT-4	OPN (SPP1)	OPG (TNFRSF11)	PARC	PLGF	TGF beta 2	TGF beta 3	TIMP-1	TIMP-2	Positive control	Positive control

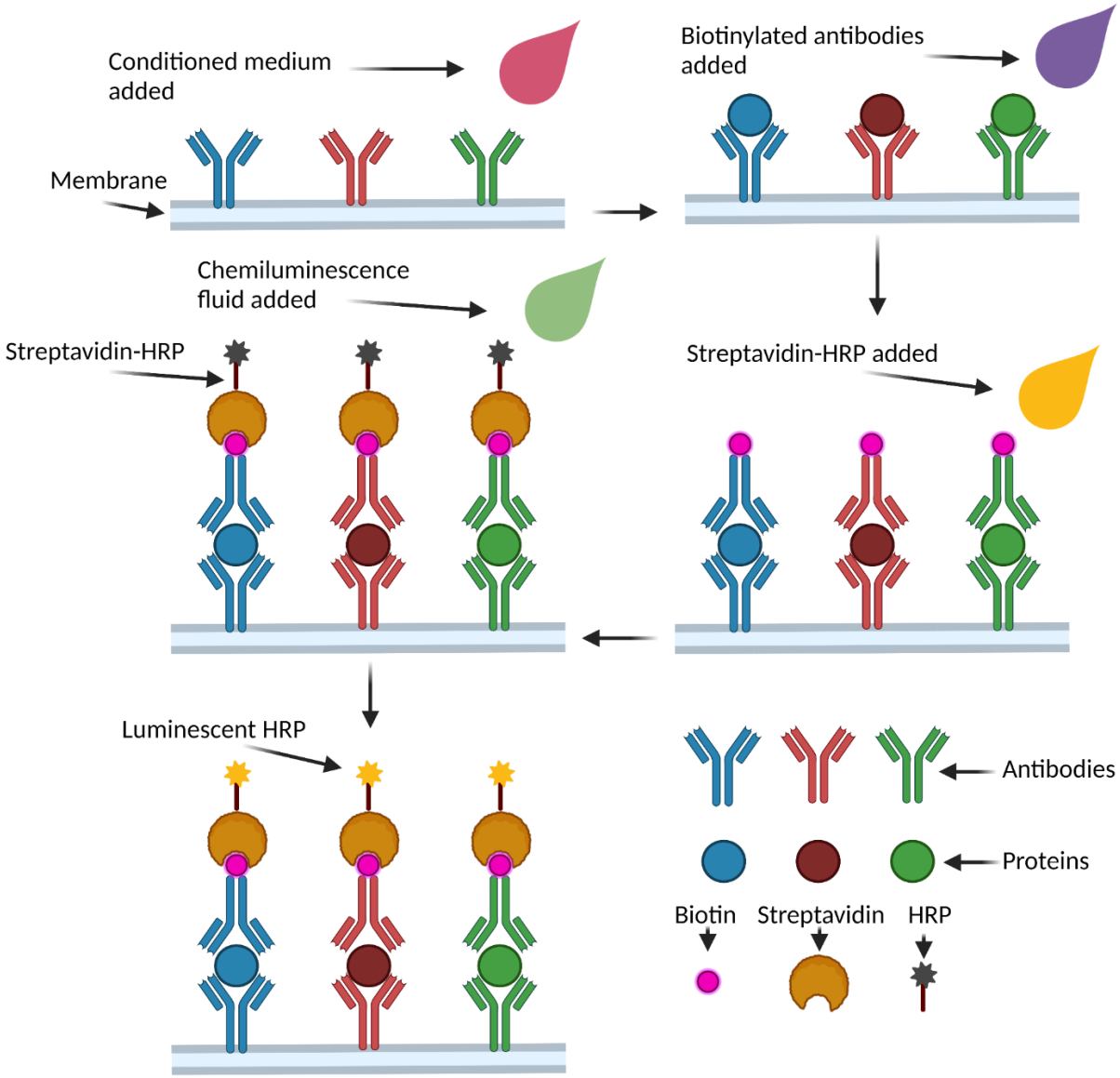

Figure 2.11. Schematic of cytokine array procedure. The cytokine array membrane contains a wide variety of different antibodies with binding sites for cytokines, if these are present in the medium added to the membrane they will bind and can be quantified by HRP densitometry.

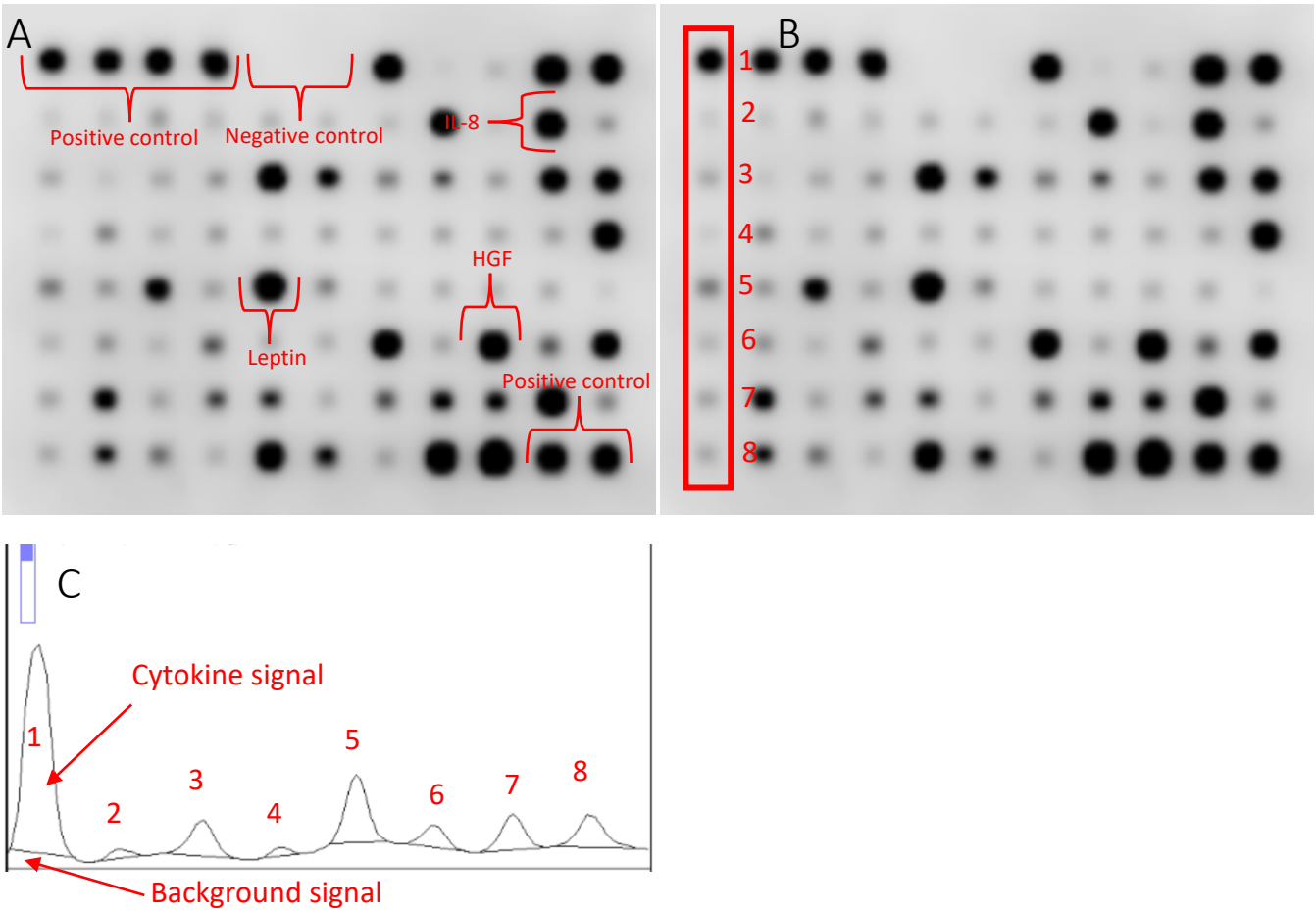

Figure 2.12. Densitometry analysis of cytokine array. (A) Example of the image produced using a C-Digit Scanner of a luminescent membrane and examples of the signal from select cytokines. **(B)** The rectangle tool was used to measure the pixel density of one column at a time, producing 8 peaks at once. **(C)** The background signal from the blot was subtracted from each peak to calculate relative density.

2.4.6.3 HGF ELISA

To quantify the specific concentration of hepatocyte growth factor found in conditioned media samples, an enzyme-linked immunosorbent assay (ELISA) was carried out. An ELISA works in a similar method to the cytokine array outlined above however it only contains antibodies for a specific, single protein, in this case HGF (figure 2.13).

Four different patient samples for each type of adipose tissue conditioned medium (minced adipose tissue, lipoaspirate, emulsified fat, lipocondensate, ADSC, and lipid conditioned medium) were analysed for HGF concentration via an ELISA. Where possible, samples that were tested using the cytokine array were also tested using the ELISA. The protein concentration of each different sample was quantified using a Pierce™ BCA assay as per the manufacturer's instructions to quantify total protein concentration by generating a standard curve as in figure 2.7. The only difference compared to section 2.4.5.2 was that diluted serum free MesenPRO was used as the diluent. Serum

free MesenPRO was diluted by a factor of 5 in deionised water as the phenol red contained in the MesenPRO RS™ basal medium interfered with absorbance readings at 562 nm.

Conditioned medium samples were then diluted with deionised water to a protein concentration of 25 µg/ml to match the concentration of the lowest protein sample. Conditioned medium (100 µl) was added to wells of a human HGF ELISA kit (Merck) and incubated overnight at 4 °C on a SLS 4 orbital rocker at 30 rpm. All reagents used in the ELISA were made up as per the manufacturer's instructions and all incubation steps were carried out on a rocker at 30 rpm. Wash steps were carried out by adding and then removing 1x Wash Buffer provided with the ELISA kit after 5 minutes on a rocker at 30 rpm.

The conditioned medium was removed following incubation and wells were washed with Wash Buffer after which, 100 µl of Detection Antibody was added to each well and incubated in the dark for 1 hour at room temperature. After incubation, wells were washed and 100 µl of streptavidin solution was added and incubated for 45 minutes in the dark at room temperature before the wells were washed again and 100 µl of TMB one-step substrate reagent was added. Wells were incubated in this solution for 30 minutes at room temperature in the dark before this was removed, wells were washed, and Stop Solution was added to halt the luminescence reaction. The absorbance of wells at 450 nm was then measured on a ELX800 photospectrometer (Agilent, Stockport, UK).

2.4.6.4 ELISA analysis

Alongside the conditioned medium samples, a standard curve was generated by diluting recombinant HGF provided with the ELISA kit to a known concentration and measuring the absorbance (as described in table 2.19). These absorbance values were plotted on GraphPad Prism 9 and using the "interpolate standard curve" and selecting "hyperbola" to generate a standard curve (figure 2.13). Absorbance values from conditioned medium samples were then compared to the standard curve by the GraphPad software and the concentration of HGF was calculated.

Table 2.22. HGF volumes used in standard curve generation.

Sample	Volume of Diluent (µl)	Volume of 2000 pg/µl HGF (µl)	Final concentration (pg/µl)
A	0	100	2000
B	66.6	33.4	666.7
C	88.9	11.1	222.2
D	96.3	3.7	74.07
E	98.77	1.23	24.7
F	99.59	0.41	8.23
G	99.86	0.14	2.74
H	100	0	0

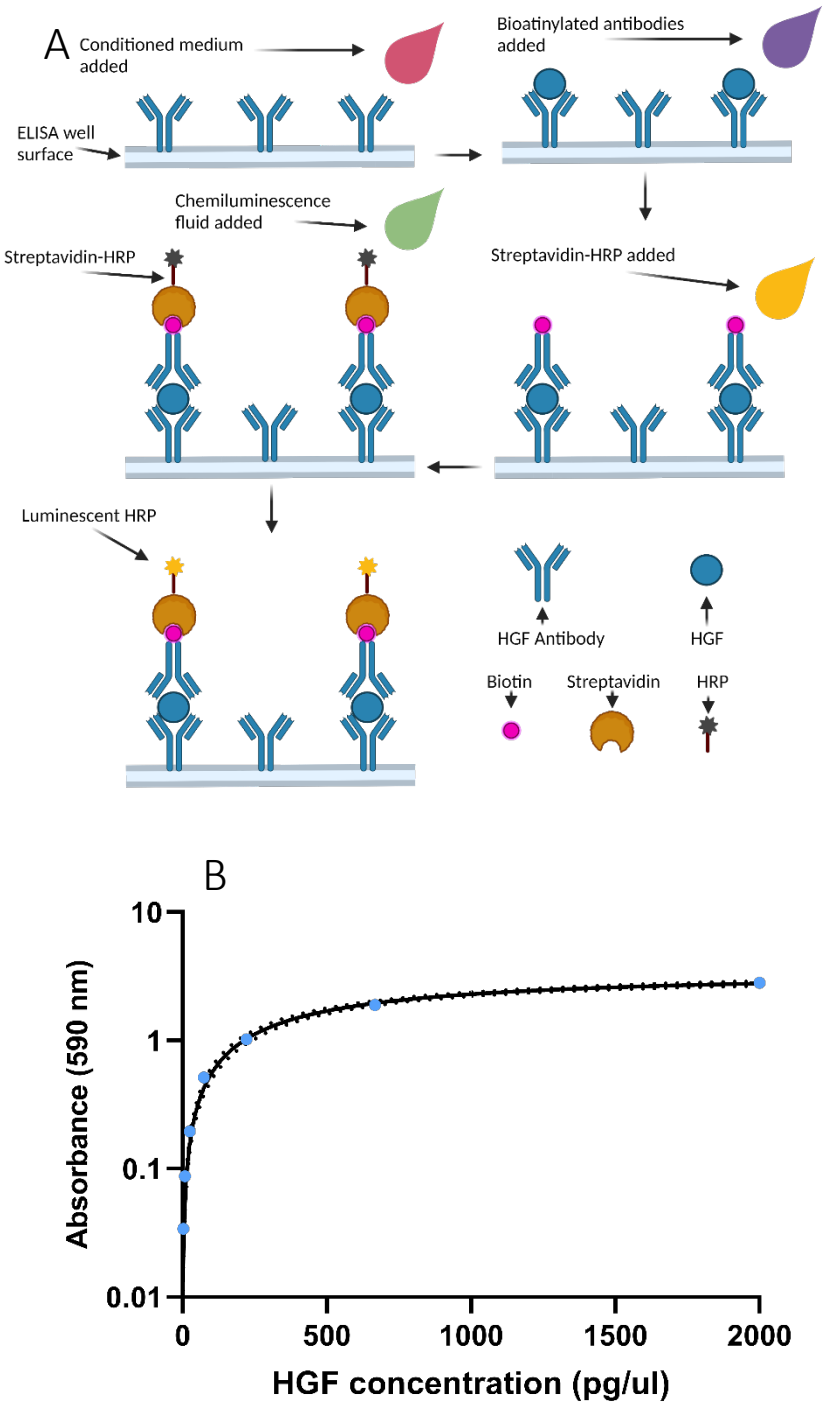

Figure 2.13. ELISA schematic. (A) Diagram of ELISA methodology. **(B)** Standard curve generated from HGF standards supplied with ELISA.

2.4.7 Assessing cellular metabolic activity

As a method of testing the cytotoxicity of a solution, a resazurin assay would be carried out on cells to examine the cell's metabolic activity following exposure to a given solution, a decrease in metabolic activity was an indicator of cytotoxicity.

HDF were seeded in a 12-well plate at 10,000 cells per well. Cells were seeded in 10 % D-MEM. After 24 hours, medium was removed and replaced with serum free media for 24 hours to starve the cells of serum. After 24 hours, serum free media was removed, wells washed with 1 ml of PBS, and 1 ml of filter sterilised 0.1 mM resazurin dye in serum free MesenPRO was added to wells. HDF in resazurin were then incubated in a 37 °C, 5 % CO_2 humidified incubator for 4 hours. Subsequently, 50 µl of this solution was removed and added to a 96-well plate. Fluorescence was measured at 570 nm/590 nm on an ELx800 photospectrometer and normalised to readings from 50 µl of 0.1 mM resazurin (equation 2.3).

2.5 Statistics

All statistical analysis was carried out on GraphPad Prism 7 software. This software was also used to assess whether data was normally distributed. Statistical significance was defined as $P \leq 0.05$. Errors bars represented standard deviation unless otherwise stated. Experiments were carried out at least in triplicate where possible. *N* was used to represent biological repeats where an experiment was carried out on different occasions using different samples. *n* was used to represent technical repeats where data was collected multiple times from the same biological sample and averaged to generate a mean of the technical repeats.

Given that most of the data presented in this thesis was comparing the values between different formulations of adipose tissue-derived conditioned medium, an ordinary one-way analysis of variance (ANOVA) was carried out to test significance between the different conditions. A Brown-Forsythe test, built into the ANOVA, was used to confirm data was standardly distributed and Tukey's multiple comparisons test was used to assess significance by pairwise mean comparison. These tests were used unless otherwise stated in the figure legends.

In graphs legends terms are used to represent cell culture medium conditioned with different formulations of adipose tissue were used. "Minced" represented minced adipose tissue conditioned, "lipoaspirate" represented lipoaspirate tissue conditioned, "emulsified" represented emulsified fat conditioned medium, "lipocondensate represented lipocondensate conditioned

medium, “ADSC” represented ADSC conditioned medium and “lipid” represented lipid conditioned medium.

Chapter 3: Characterisation of adipose tissue formulations

3.1 Introduction and aims

Subcutaneous injections of adipose tissue have been demonstrated to have an anti-fibrotic effect in skin and the ability to regenerate hypertrophic scars (Benjamin *et al.,* 2015; Bruno *et al.,* 2013). These autologous fat grafts have been shown to be effective at regenerating skin damaged from radiation (Rigotti *et al.,* 2007), burning (Klinger *et al.,* 2008), and surgery (Caviggioli *et al.,* 2011). Rigotti *et al*. (2007) were the first to demonstrate that autologous fat grafts could regenerate scar tissue. The group injected lipoaspirate under scars caused by repeated radiotherapy and observed an improvement in scar symptoms in 12 of the 13 patients. Klinger *et al*. (2008) followed this up with case studies on three patients with historic burns (between 2 and 13 years from initial injury) and found that following fat grafting the appearance, thickness, and elasticity of the scars were improved. Autologous fat grafting was also found to reduce the pain felt in patients following mastectomy (Caviggioli *et al.,* 2011).

While adipocytes make up roughly 90 % of the total volume of adipose tissue, a collection of stromal cells termed the "stromal vascular fraction" (SVF) make up the majority of the cellular population of adipose tissue (Cohen & Spiegelman, 2016). The SVF is composed of a wide variety of cell types such as endothelial cells, pericytes, fibroblasts and immune cells such as macrophages and leukocytes (Bourin *et al.,* 2013). Another large population of cells in the SVF are adipose derived stromal cells (ADSC). ADSCs were first observed in 2001 by Zuk *et al*. (2001) and are mesenchymal stromal cells that can differentiate into a variety of cells such as endothelial cells (Cao *et al.,* 2005), adipocytes, and osteoblasts (Gimble & Guilak, 2003). These cells also secrete growth factors such as vascular endothelial growth factor (VEGF) that increase vascularisation (Rehman *et al.,* 2004). The first papers investigating autologous fat grafting underneath scars suggested that the SVF was responsible for the regenerative properties observed with adipose tissue grafting techniques. Rigotti *et al*. (2007) found, by using ultrasound imaging, that neovascularisation at the wound site was increased following grafting. This was later confirmed by Klinger *et al*. (2008). Both papers suggested that cells in the SVF might be responsible. As a result, a major focus has been to identify methods to remove the other components of adipose tissue and thus concentrate the cells in the SVF (Alexander, 2016; Chen *et al.,* 2020; lo Furno *et al.,* 2017; Mashiko *et al.,* 2017; Qiu *et al.,* 2021; Sesé *et al.,* 2019, 2020; Tonnard *et al.,* 2013; Yao *et al.,* 2017).

While the SVF can be isolated enzymatically, this product is difficult to use clinically. Regulatory bodies, such as the Food and Drug Administration (FDA), regard enzymatic treatment of adipose tissue as more than "minimal manipulation" (U.S. Department of Health and Human Services Food and Drug Administration *et al.,* 2020, page 14) and thus these cells cannot be

transplanted into humans without additional approval. To address this issue, methods of isolating SVF cells mechanically have been investigated. One of the most well-known methods of emulsification is Nanofat, introduced by Tonnard *et al*. (2013). By passing lipoaspirate between two syringes, the adipose tissue has shear force applied to it and is broken down. The adipocytes in the adipose tissue are lysed and this forms a paste that is more easily injected using small gauge needles into areas such as the face. In addition to this, the SVF can be isolated mechanically by taking the fragmented adipose tissue used to make Nanofat and centrifuging it. This removes any lipid, liquid and cell debris, leaving mostly SVF cells (Sesé *et al.,* 2020; Yao *et al.,* 2017). These mixtures are termed 'SVF-gels' in the literature.

My research was focussed on the effect adipose tissue has on fibroblast to myofibroblast differentiation. One of the aims of my project was to test the effect of clinically relevant formulations of adipose tissue on myofibroblast differentiation. Another of the aims was to identify which components of adipose tissue are responsible for any effect observed on myofibroblast differentiation. To this end, it was chosen to investigate the effects of five different formulations of adipose tissue on myofibroblast differentiation. These formulations were termed minced adipose tissue, lipoaspirate, emulsified fat, lipocondensate, and ADSCs (figure 3.1). These formulations are already in clinical use by surgeons (Bhooshan *et al.,* 2018; Klinger *et al.,* 2008; Mashiko *et al.,* 2017; Yoshimura *et al.,* 2008) and their influence on myofibroblast differentiation are discussed in chapters 4 and 5.

While discussed in more detail in section 3.3.1, minced adipose tissue often had to be used as a substitute for lipoaspirate. It was considered minced adipose tissue and lipoaspirate were comparable because they both contain all the components of adipose tissue (Eto *et al.,* 2009). The only difference is that lipoaspirate has been broken apart during its surgical extraction and is in a liquid form, while minced adipose remains as a solid. Emulsified fat is similar to Nanofat described in Tonnard *et al*. (2013), with the macro structure of the adipose tissue fragmented and the adipocytes lysed. Lipocondensate is a formulation similar to other SVF-gels such as that described by technique used in Yang *et al*. (2021) and Yao *et al*. (2017). Processing to this formulation was expected to remove every component of the adipose tissue other than the SVF cells and extracellular matrix (ECM). Processing should also have had the effect of "concentrating" the SVF, as 10 ml of lipocondensate should contain more SVF cells than 10 ml of adipose tissue. Finally, enzymatic isolation of ADSCs removed nearly all other SVF cells. Each formulation was chosen because the processing steps between each formulation should remove at least one component of the adipose tissue (figure 3.2). This meant that the components responsible for any anti-fibrotic effects observed could be identified via a process of elimination. For example, if only ADSCs had any effect on

myofibroblast differentiation but no other formulation did, then it can be determined that ADSCs are the responsible component. Likewise, if an effect was seen in minced adipose tissue, lipoaspirate, emulsified fat, and lipocondensate but not ADSCs, then it was likely that cells from the SVF other than ADSCs were responsible for any effect observed on myofibroblast differentiation.

Before this was tested in later chapters however, characterisation of the adipose tissue formulations was carried out. The aim of this chapter was to characterise the clinical formulations used throughout the research for this thesis. This was achieved by:

-Optimising the processing techniques used to generate these formulations.

-Identifying the cellular populations contained within each formulation.

-Understanding how processing affects metabolic activity, lysis, and cell concentration within each formulation.

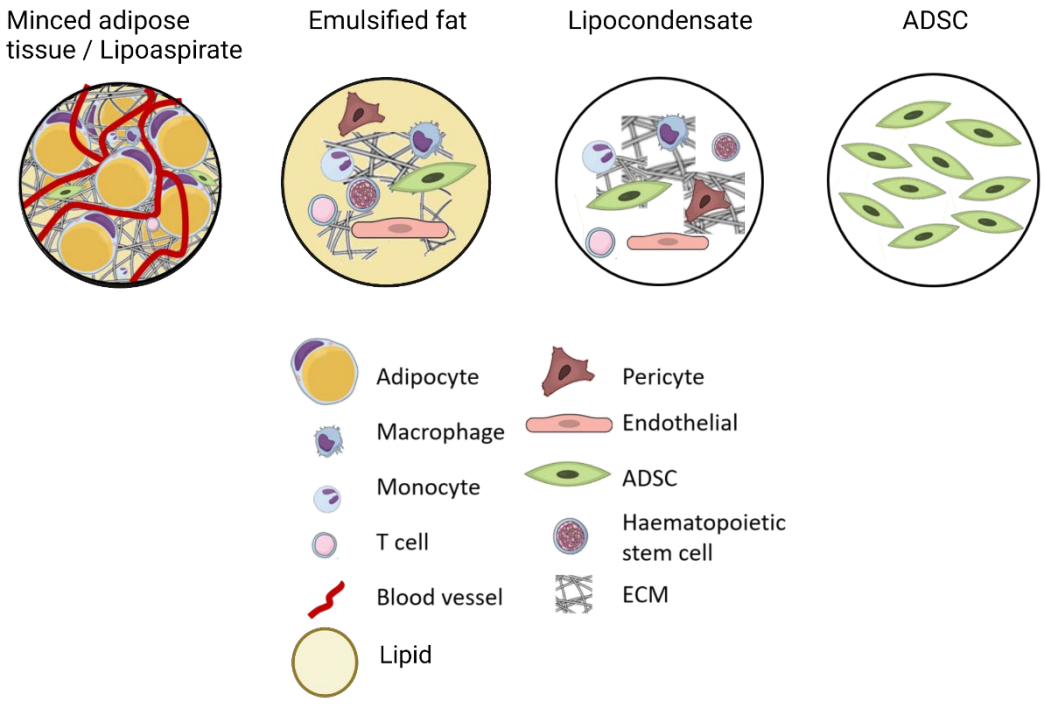

Figure 3.1 Formulations of adipose tissue. Outlined above are the formulations of adipose tissue used throughout this thesis and the components found within.

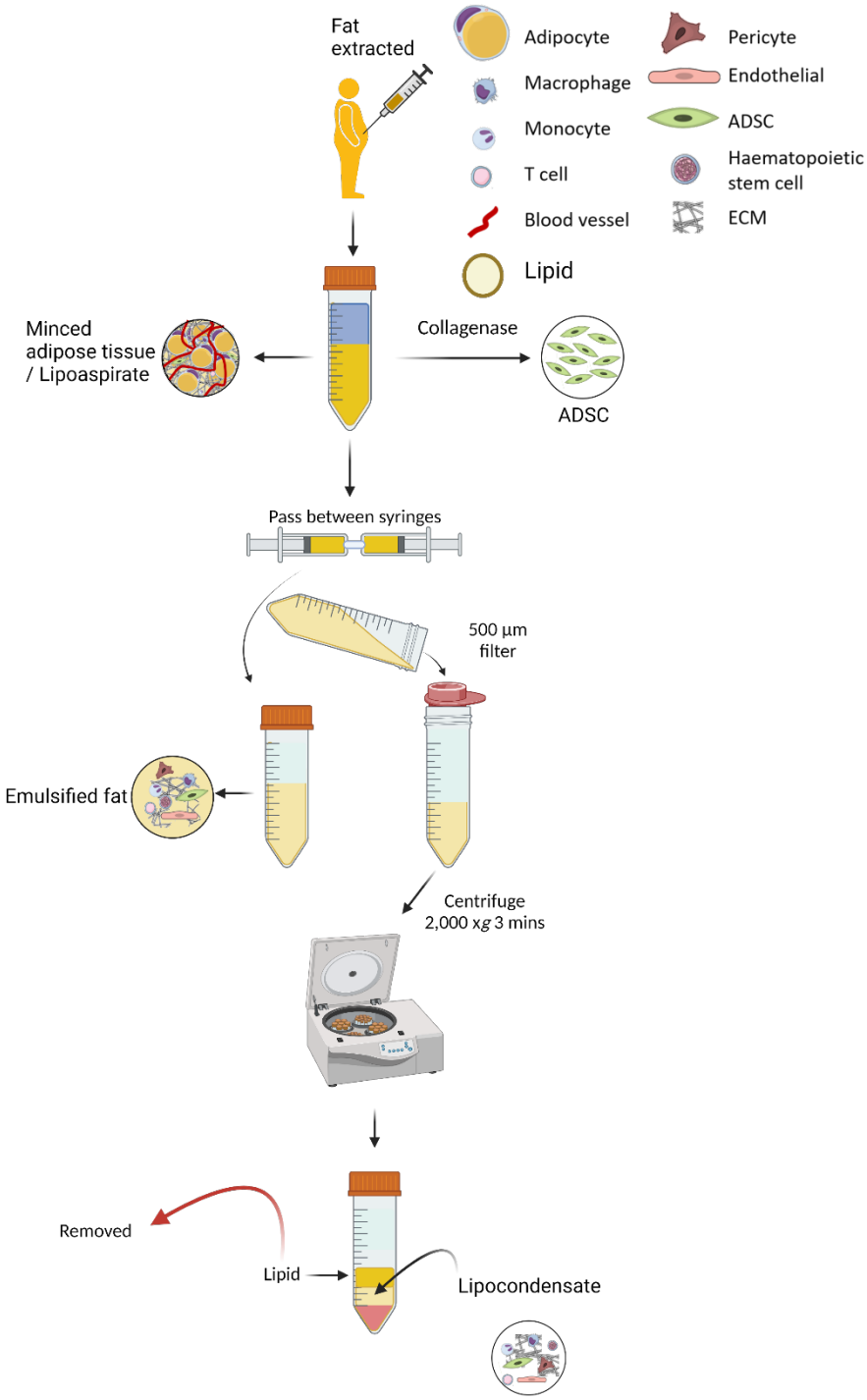

Figure 3.2. Composition of adipose tissue formulations. Schematic showing how adipose tissue is processed into different formulations and the components contained within. Fat is extracted as either minced adipose tissue or lipoaspirate containing all the components of adipose tissue. ADSCs are isolated via collagenase from this adipose tissue. Emulsified fat is generated, lysing adipocytes. This formulation is then filtered and centrifuged, and the lipid and lysed cells are removed, leaving the SVF and ECM.

3.2 Results

3.2.1 The appearance and form of adipose tissue formulations

Adipose tissue used in this research was obtained from the clinic, with informed consent, either as whole adipose tissue or lipoaspirate. Whole adipose tissue (figure 3.3A) had an orange appearance on the outer layers of the tissue. Once cut into, the adipose tissue within was a bright yellow colour. If cut into and subsequently left to oxidise this tissue would then also take on an orange colour. The tissue was coated in a moist and oily layer of liquid, but the tissue would dry out if left outside a sealed container for over an hour. Whole adipose tissue was easy to cut into with a scalpel and was composed of lobes of fat held together with connective tissue septa. If left to dry, the outer layer of adipose tissue was more difficult to cut with a scalpel. When generating minced adipose tissue from whole adipose tissue, long, red blood vessels were found and removed from the tissue. There were also collections of darker liquid that may have been pools of blood generated during surgery. Whole adipose tissue also contained larger segments of fascia that were difficult to slice with a scalpel. These sections would be cut away and removed. The tissue was overall oily to the touch, despite washing.

Minced adipose tissue appeared as a collection of small orange lobes of whole adipose tissue. The tissue had a wet consistency and was oily to the touch (figure 3.3B). If left in a liquid such as cell culture medium, lipid would leach out into the liquid and form droplets.

Lipoaspirate had the appearance of an orange slurry, similar to minced adipose tissue (figure 3.3C). The lipoaspirate behaved as a liquid however, there were small, solid lobes of adipose tissue within the lipoaspirate. This made transferring the tissue difficult as it could not be measured accurately as a liquid or transferred as a conventional solid. It had many of the properties of minced adipose tissue however, the segments of solid tissue were smaller than in minced adipose tissue. Lipoaspirate was less oily than minced adipose tissue and less lipid was observed to leach out if placed in liquid.

Emulsified fat was an orange paste with a pink hue. The tissue itself was very oily but behaved as a liquid. It was viscous, yet not enough to prevent emulsified fat being poured between containers. This viscosity was variable from sample to sample.

It was difficult to filter emulsified fat through a 500 µm filter to generate lipocondensate. The paste would flow through the filter slowly unless a pair of tweezers was rubbed round the filter in a circular manner to allow emulsified fat to transfer through the filter. After a time, there was an accumulation of fascia that would not pass through the filter and would collect around the tweezers.

This tissue was removed. Once formed, lipocondensate was a very viscous, yellow, gel. Its appearance was that of a gel and had no solid structure however, it would not flow as a liquid and was difficult to transfer between containers. Neither emulsified fat nor lipocondensate could be transferred with a Gilson micropipette and thus a Gilson Microman® positive displacement pipette was needed to measure volumes of emulsified fat and lipocondensate.

ADSCs were isolated from either whole adipose tissue or lipoaspirate. A fully confluent flask of ADSC would contain ~ 1.2 million cells and these would take on a spindle, fibroblast like morphology (figure 3.3F). Initial studies found problems with ADSC cell culture. Isolated ADSC were cultured in Dulbecco's Modified Eagles Medium (D-MEM) containing 10 % serum (referred to as 10 % D-MEM) and would grow as expected. However, after being passaged twice, the ADSC morphology changed becoming larger and wider, the cells would stretch, and stress fibres could be seen within the cells (figure 3.3G). In addition, proliferation stopped, and cells would begin to lyse. The problem was resolved by changing the culture medium to MesenPRO RS™ medium. The ADSCs reverted to their original growth rate and morphology and this medium was used to isolate and culture ADSCs for the remainder of the research.

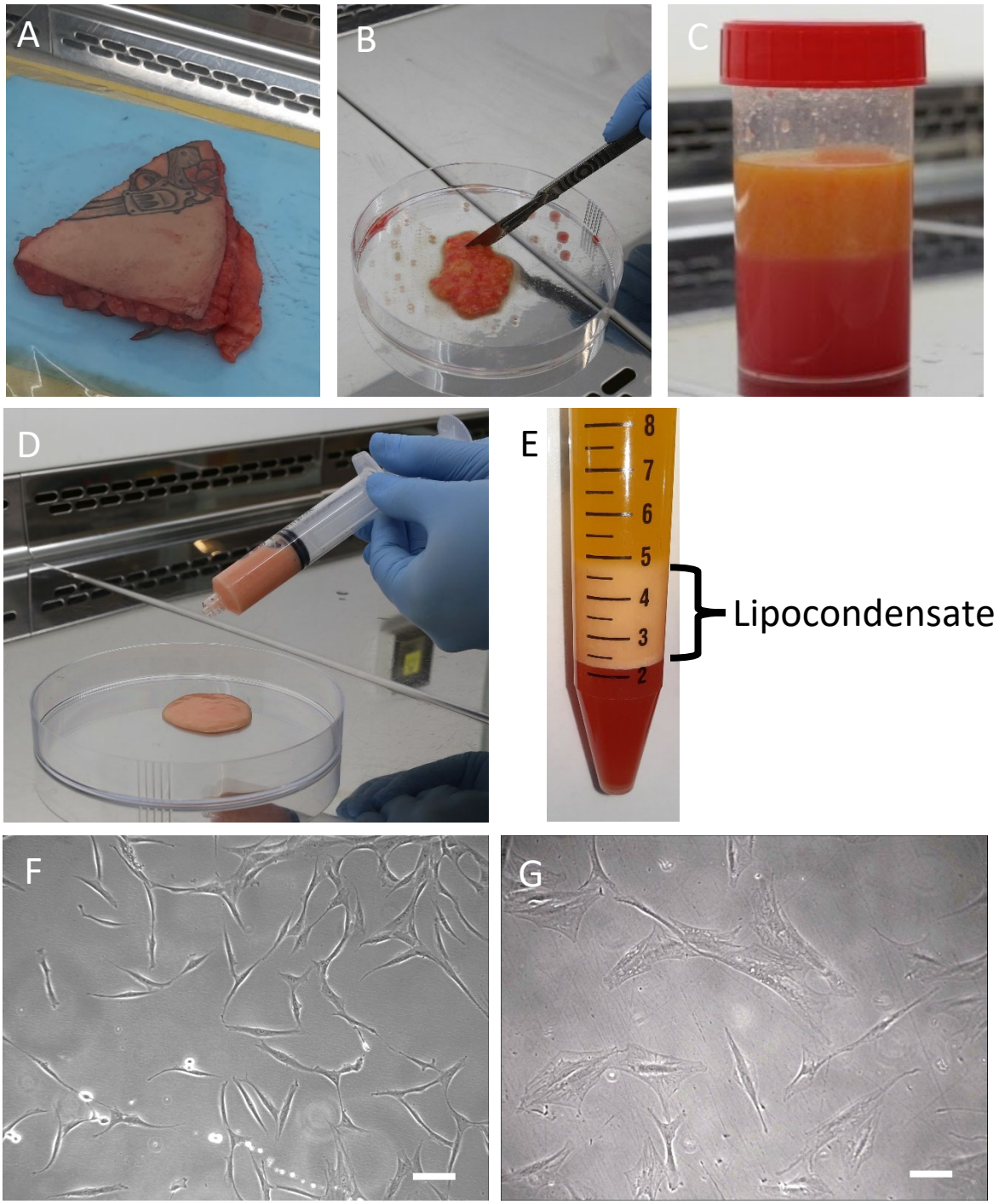

Figure 3.3. Adipose tissue formulations. (A) Whole adipose tissue. **(B)** Minced adipose tissue. **(C)** Lipoaspirate. **(D)** Emulsified fat. **(E)** Lipocondensate, black bracket denotes lipocondensate. **(F)** ADSCs cultured in MesenPRO RS™ Medium. **(G)** ADSCs cultured in 10 % D-MEM. Scale bars = 200 µm. Video of these processing techniques can be found at https://www.youtube.com/watch?v=EruoEy3QyUk.

3.2.2 ADSC surface marker characterisation

Due to the plasticity of ADSCs and because the ADSCs were isolated from tissue containing a wide variety of different cells, it was important to confirm that the cells being isolated and cultured were ADSCs. Flow cytometry was carried out as described in section 2.4.3 to measure the proportion of isolated cells expressing ADSC surface markers (figure 3.4). Cells isolated from two different patient samples were tested. The proportion of cell surface proteins was consistent between samples. A small number of cells were positive for CD31, CD34, CD45, or CD146 (0.23 %, 0.49 %, 0.56 %, and 0.06 % respectively). The number of cells that did not express control markers CD31 and CD45 was high with 99.50 % of cells CD31-/CD45- (figure 3.5). The proportion of CD73+ cells remained low (2.81 %, figure 3.4F). The number of CD90+ or CD105+ ADSCs was high with 91.50 % and 83.20 % expressing these markers respectively. The percentage of cells that were both CD90+/CD105+ was 80.10 % (figure 3.5).

3.2.3 ADSC adipogenic differentiation

Another marker of ADSCs is the ability to differentiate to adipocytes, which can be assessed by the formation of lipid droplets following incubation with adipogenic differentiation medium. ADSCs were cultured in adipogenic differentiation media as described in section 2.4.1.1, following which, oil red O staining was carried out on treated ADSCs (section 2.4.1.2). After being cultured in differentiation medium, cells had a visibly slower rate of proliferation compared to control ADSCs and some took on a circular form (Figure 3.6A-B). The number of lipid droplets present in differentiated ADSCs was calculated as described in section 2.4.1.2. Very few lipid droplets could be identified in control cells compared to differentiated ADSCs. Differentiated cells had visible lipid droplets and image analysis determined there was a mean of 128 lipid vesicles per field of view (figure 3.6C). This was significantly more lipid vesicles than control ADSCs (16, $p = 0.015$). This supported data outlined in 3.2.2. that the cells being isolated are ADSCs.

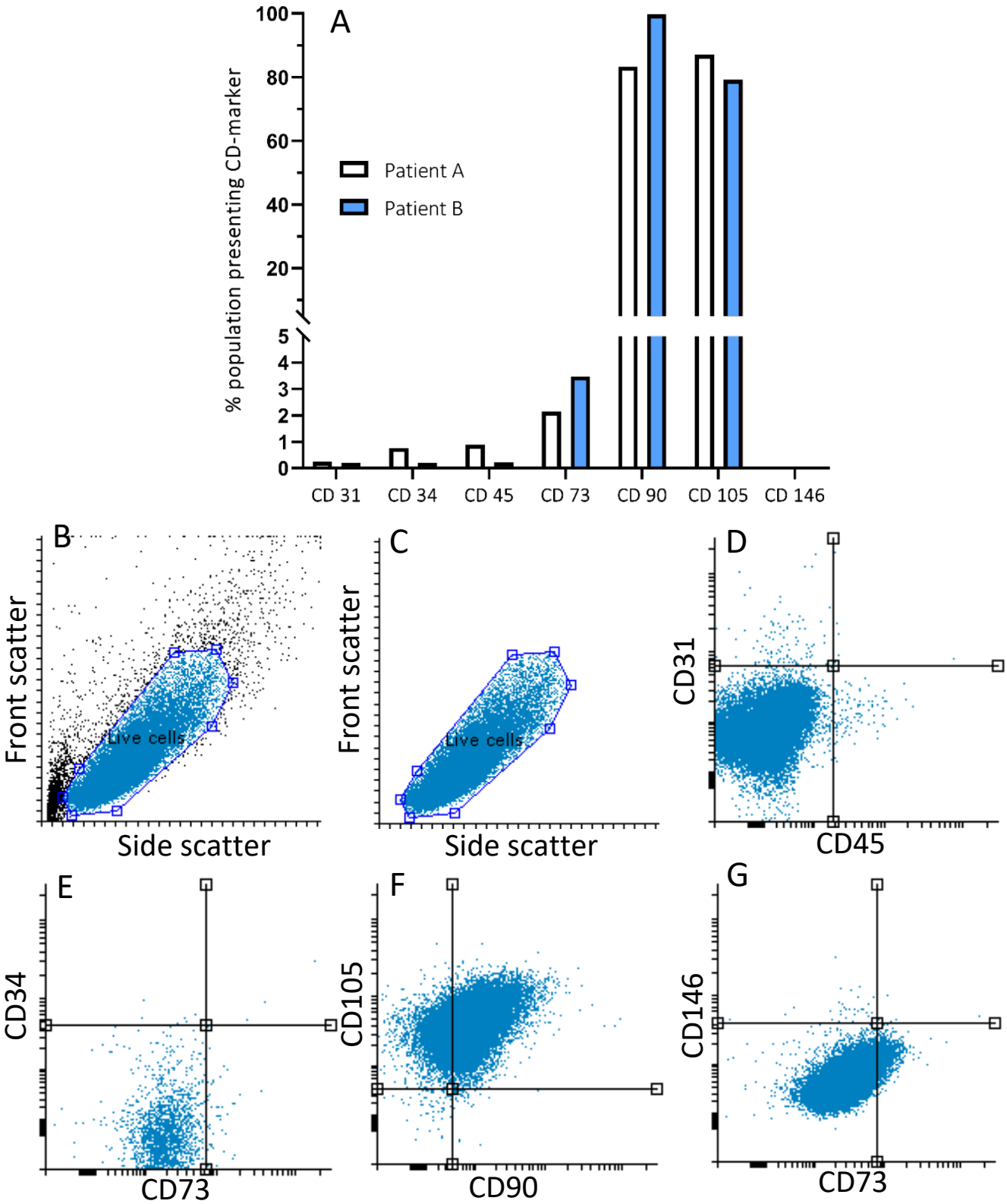

Figure 3.4. Flow cytometry analysis of ADSC surface marker expression. (A) Percentage population of cells from two patients expressing various CD surface markers. **(B-C)** Dot plots of cells sorted by FSC (front scatter) and SSC (side scatter). **(C)** singlet cells were identified based on their FSC and SSC and the expression on the surface of these cells was examined. **(D-G)** Dot plots showing the population of cells expressing a variety of cell surface markers were examined, **(D)** CD31/45, **(E)** CD34/73, **(F)** CD90/105, **(G)** CD73/146.

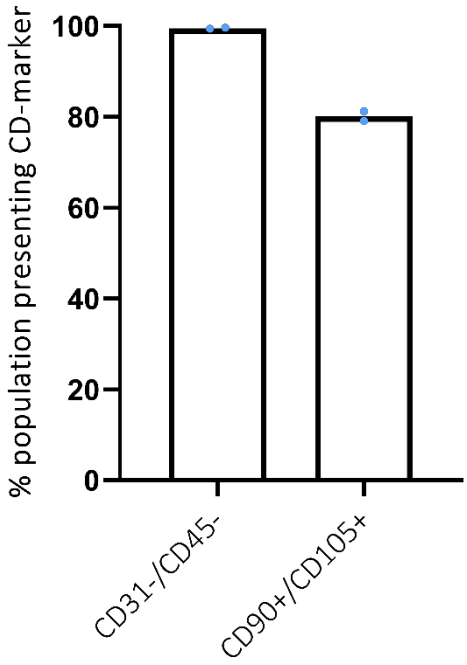

Figure 3.5. Analysis of markers characteristic of ADSCs. The percentage of cells expressing both markers of ADSCs CD90 and CD105 was calculated alongside the percentage of cells negative for markers of endothelial cells (CD31) and leukocytes (CD45). *N* = 2, *n* = 1.

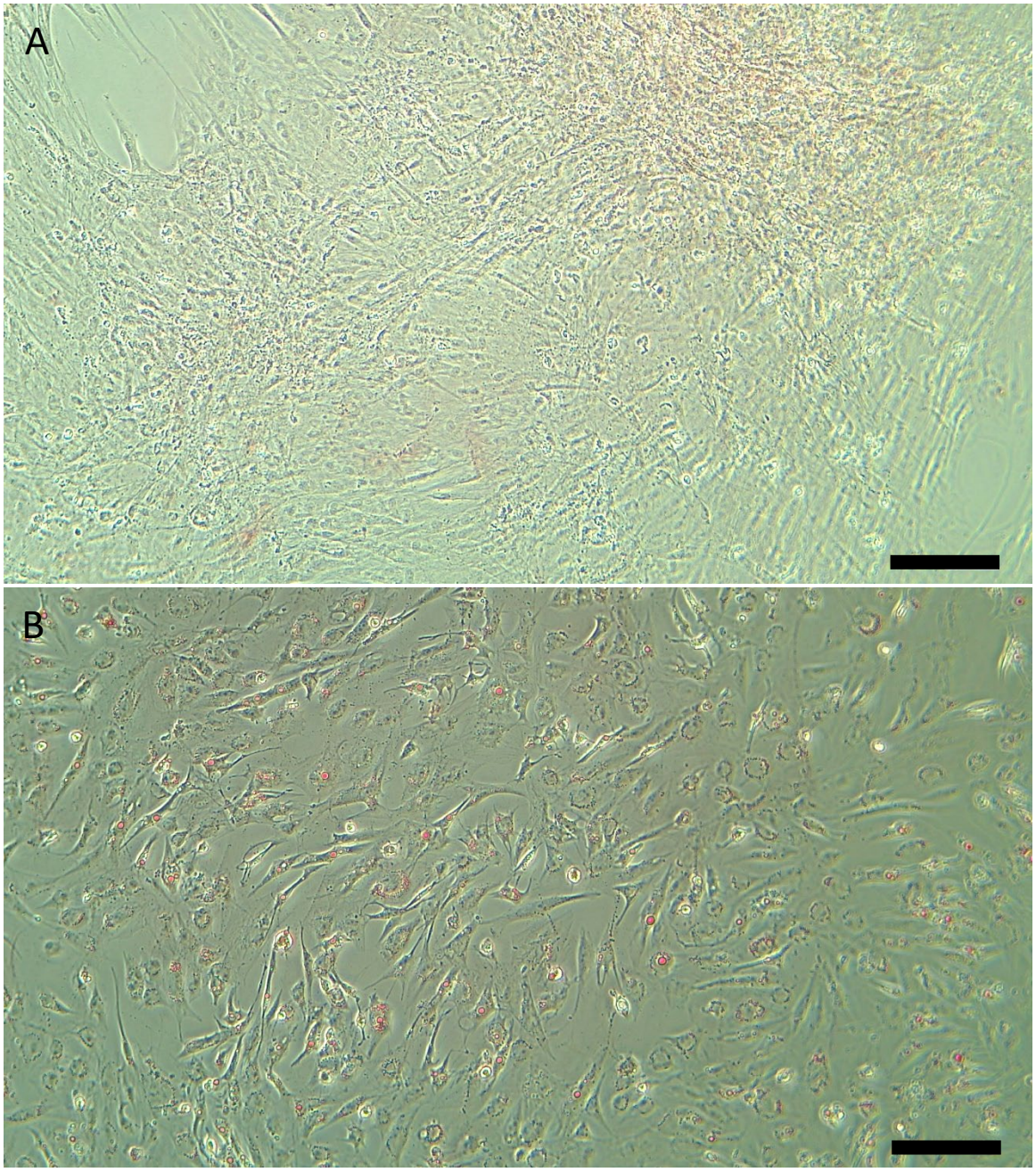

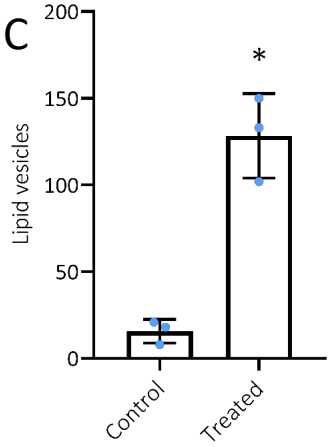

Figure 3.6. Analysis of ADSCs treated with adipogenic differentiation medium. (A-B) Light microscopy images of ADSCs stained with oil red O after 21 days of treatment with **(A)** serum free MesenPro, **(B)** adipogenic differentiation medium. Scale bar = 150 µm. **(C)** The number of lipid vesicles per field of view in treated and control cells. *N* = 3, *n* = 1. Bars = standard deviation, * = $p < 0.05$. Significance measured with an unpaired T test. Images taken by Rachel Furmidge and used in this thesis with her permission.

3.2.4. Optimisation of adipose tissue processing techniques

3.2.4.1 Does pass number affect the metabolic activity of emulsified fat and lipocondensate?

In Tonnard *et al*.'s original Nanofat paper in 2013, the authors passed lipoaspirate between syringes 30 times to lyse the adipocytes contained within. Since then, there has been little experimentation using different pass numbers and 30 passes has become the standard for Nanofat generation and other emulsification techniques (Bhooshan *et al.,* 2018; Kemaloğlu, 2016; lo Furno *et al.,* 2017; Sesé *et al.,* 2019; Yu *et al.,* 2018). There has only been a little work examining the effect of altering pass number in Nanofat generation (Osinga *et al.,* 2015). Nanofat has been used in surgery because of the regenerative effects of the cells found within the emulsion (Bhooshan *et al.,* 2018; Kemaloğlu, 2016). Thus, it was decided to test whether the number of times adipose tissue was passed between syringes had any effect on the metabolic activity of the cells found in emulsified fat or lipocondensate using a resazurin assay. Emulsified fat was generated as described in section 2.2.3 with a varying number of passes between syringes (10, 30, 100) and a resazurin assay carried out (section 2.4.1.4). The fluorescence value of the emulsified adipose tissue and lipocondensate was normalised against either the minced adipose tissue or lipoaspirate that the sample was processed from. One "pass" was defined as adipose tissue being transferred from one syringe to the other.

Following emulsification, there was no change in metabolic activity between samples passed between syringes 10 and 30 times (0.69 and 0.73 fluorescence relative to either minced adipose tissue or lipoaspirate respectively). When passed 100 times, metabolic activity decreased (0.29 relative fluorescence) however, this was not significant (figure 3.7A, $p > 0.05$). Additionally, lipocondensate was generated from this emulsified fat (section 2.2.4) and the metabolic activity of lipocondensate was measured *via* resazurin assay. Pass number was found to have little influence on cellular metabolic activity. All conditions were within 0.7 relative fluorescence units of each other and were not significantly different (figure 3.7B). This data shows the metabolic activity of the cellular population of emulsified fat and lipocondensate was not affected by altering the pass number in emulsified fat generation.

3.2.4.2 Does pass number effect cell lysis in emulsified fat and lipocondensate?

Given that the metabolic activity of the emulsified fat and lipocondensate was not affected by pass number, it was decided to test whether the change in pass number was affecting the degree of cell lysis in the emulsified fat and lipocondensate. To test this, an LDH assay (section 2.4.1.3) was carried out on emulsified fat and lipocondensate and normalised against the minced adipose tissue or the lipoaspirate that the sample was generated from.

The degree of cell lysis remained the same between emulsified fat generated from 10 and 30 passes between syringes at 1.74, and 1.63 relative absorbance respectively (figure 3.7C). When passed between syringes 100 times, there was an increase in relative absorbance to 2.10 however, this was not significant ($p > 0.3$). When this emulsified fat was processed into lipocondensate, there was little difference in the amount of cell lysis between samples. When passed between syringes 10 times, lipocondensate had 2.67 times greater relative absorbance compared to the adipose tissue it was generated from. This was the same as lipocondensate generated from emulsified fat that had been passed between syringes 30 times (2.71 times relative absorbance, figure 3.7D). There was a slight increase in relative absorbance in lipocondensate generated from 100 pass emulsified fat (3.12 times relative absorbance) however, this was not significant ($p > 0.89$). Furthermore, pass number did not affect the consistency of the emulsified fat formed, implying changing pass number had little impact on adipose tissue fragmentation. Taken together, data from figure 3.7 shows that the pass number of emulsified fat had no influence on the metabolic activity of the product and no effect on the number of cells lysed during the generation of these products. Going forward, emulsified fat and lipocondensate was passed between syringes 30 times. This was because pass number was found to have no effect on the variables measured and thus there was no reason not to use the literature standard.

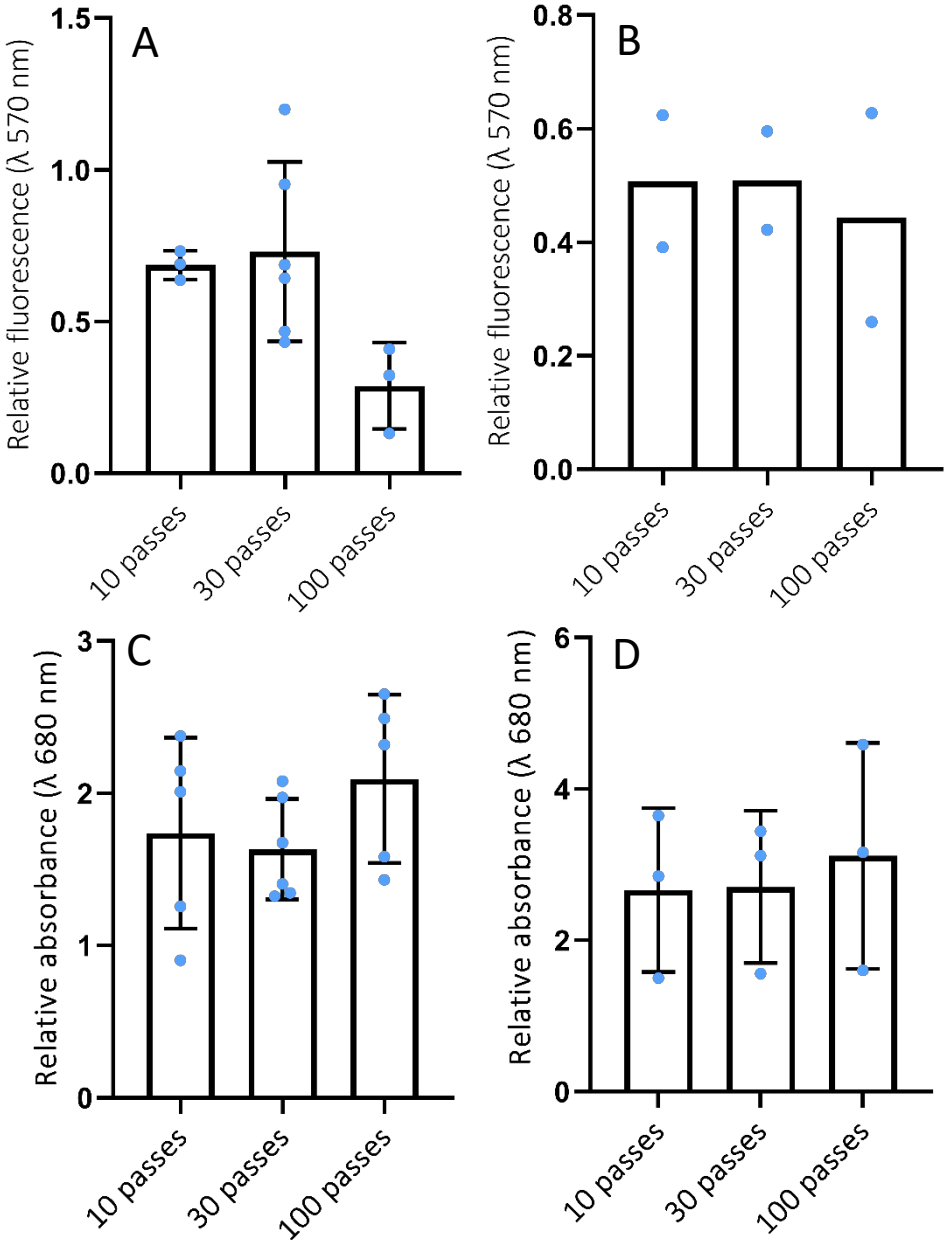

Figure 3.7. Pass number does not affect the cellular metabolic activity or the amount of cell lysis in emulsified fat or lipocondensate. (A-B) Cellular metabolic activity was measured using resazurin assays on **(A)** emulsified fat and **(B)** lipocondensate. Metabolic activity was assessed by measuring fluorescence values and normalising them to the fluorescence values of the minced adipose tissue or lipoaspirate the sample was generated from. **(C-D)** The amount of cell lysis following different pass numbers was measured using an LDH assay on **(C)** emulsified fat and **(D)** lipocondensate. *N* = 5 (A, C) / 3 (B, D), *n* = 3. Bars = standard deviation. Ordinary one-way analysis of variances (ANOVA) were carried out on B, C, and D. A Kruskal-Wallis test was carried out on A.

3.2.5 Does emulsifying adipose tissue with a "Microlyzer" lead to increased cell lysis?

Following centrifugation of emulsified fat to generate lipocondensate (section 2.2.4), a two-phase solution would form consisting of waste liquid below, and an emulsion of lipid in water on top (figure 3.8A). However, in the research describing the generation of "SVF-gel" that my protocol was based upon, Yao *et al*. (2013) described a tri-layered sample, with waste liquid at the bottom, an SVF layer above this and the free lipid oil on top. Thus, troubleshooting methods to generate separation between the SVF and free lipid layer was carried out.

It was considered that the processing pre-centrifugation may not be causing sufficient adipocyte lysis, resulting in the SVF and free lipid layers in the lipocondensate not separating consistently. To try and increase cell lysis, a commercial product known as a "Microlyzer", was trialled. This product is reported to increase adipocyte lysis and separate the SVF from adipose tissue for generating emulsified fat products (PRP First, 2021; Zocchi *et al.,* 2019) such as Nanofat. It consists of a compartment housing a filter with sharp blades that is attached between the syringes when generating emulsified fat. Adipose tissue is passed between filters 30 times, the blade filter is removed and replaced with a smaller blade filter and the process repeated. This should ensure complete lysis of adipocytes (figure 3.8). I hypothesised that the Microlyzer would lead to increased adipocyte lysis and thus more free lipid being present in the lipocondensate. This could lead to more consistent separation between the SVF and lipid layer.

To test the effect of the Microlyzer on lipocondensate cellular metabolic activity and cell lysis, lipocondensate was generated as in section 2.2.4 however instead of using a Luer-lock, a Microlyzer was fitted between the syringes (figure 3.8E). Following processing, a resazurin and LDH assay was carried out on the product. The metabolic activity of lipocondensate generated using the Microlyzer was greater than lipocondensate generated without the device (0.98 times relative fluorescence compared to 0.66, figure 3.9A). The amount of cell lysis occurring when lipocondensate was generated using the Microlyzer was lower than lipocondensate generated without the device (0.74 times relative absorbance compared to 3.62, figure 3.9B).

While using the Microlyzer, experimentation with techniques to disrupt the free lipid and SVF emulsification was carried out. In Yao *et al*. the authors state that, when generating SVF-gel, the free lipid and SVF emulsion must be flocculated to achieve full separation. To this end, unseparated lipocondensate generated by the Microlyzer was taken and stored at 4 °C until the emulsion had solidified. Following this, the emulsion was removed and warmed at room temperature until it had melted. This solution was then disrupted using a Pasteur pipette and recentrifuged the lipocondensate. This method caused a tri-layered sample to form and generate a separated solution

as seen in figure 3.10A. As a result, this technique was used for the remainder of the project to generate lipocondensate (figure 3.10B). Additionally, this separation occurred in lipocondensate generated without the Microlyzer. The Microlyzer resulted in less cell death assessed by the LDH assay, therefore it was not used in future work to generate lipocondensate.

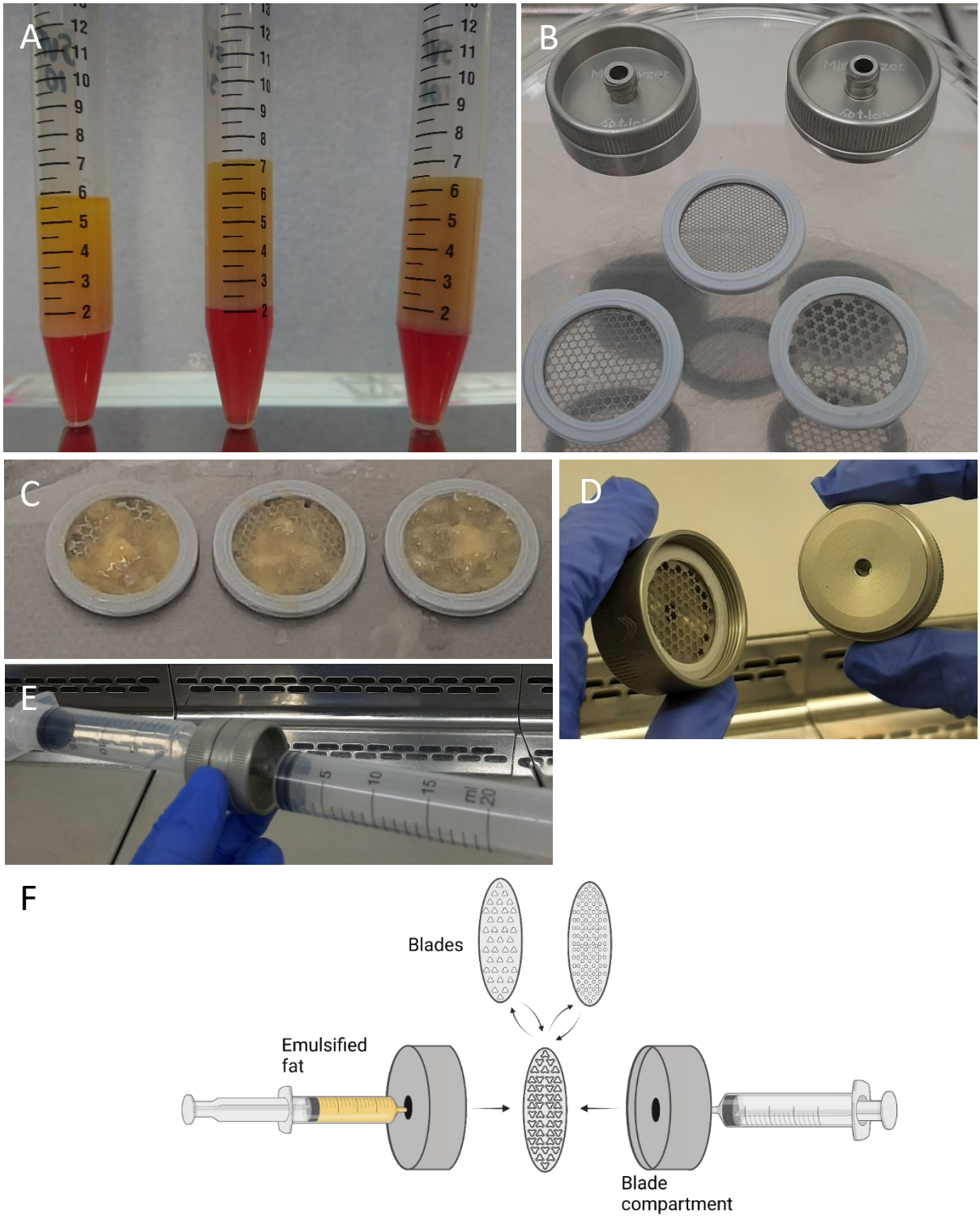

Figure 3.8. Using the Microlyzer to process adipose tissue. (A) Unseparated lipocondensate generated from emulsified fat made with varying pass number, (left-right) 10 passes, 30 passes, 100 passes. **(B)** Picture of Microlyzer blades. Blades were sized at 2400, 1200, and 600 µm. **(C)** Microlyzer blades after use to disrupt adipose tissue. **(D)** Microlyzer casing. **(E)** Microlyzer fully assembled with syringes attached. **(F)** Schematic of Microlyzer.

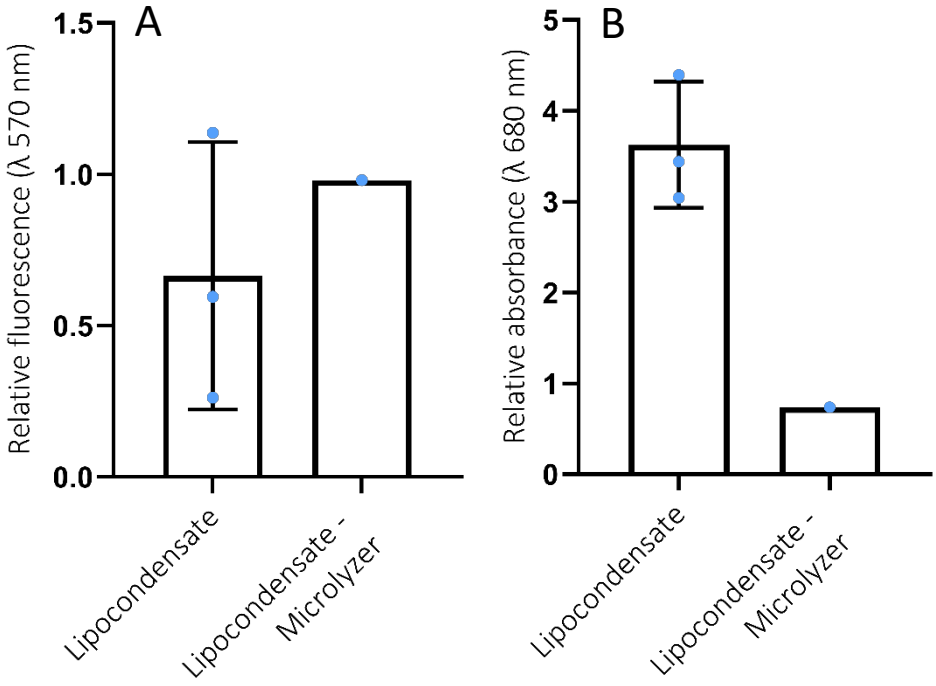

Figure 3.9. The effect of a Microlyzer on lipocondensate metabolic activity and cell lysis. (A) Relative cellular metabolic activity of lipocondensate generated with a Microlyzer**. Metabolic activity was calculated by measuring fluorescence values and normalising to the fluorescence values of the minced adipose tissue or lipoaspirate the same was generated from. (B)** Relative cell lysis of lipocondensate generated using a Microlyzer. *N* = 3 (lipocondensate) / 1 (lipocondensate - Microlyzer). Error bars = standard deviation.

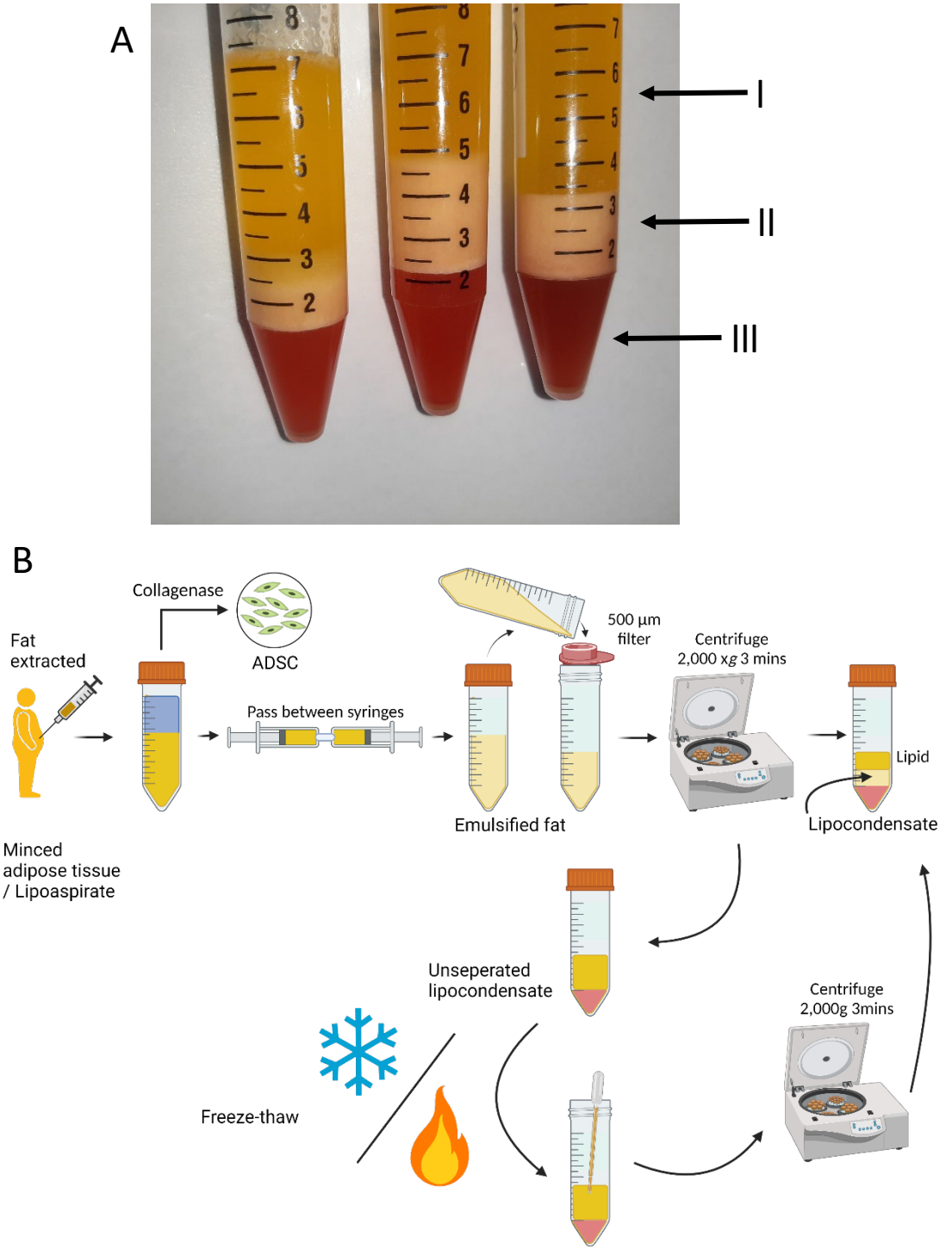

Figure 3.10. Separated lipocondensate. (A) Images of lipocondensate separated into a tri-layered sample. The three layers were (I) free lipid, (II) SVF/lipocondensate, (III) waste liquid. **(B)** Schematic of how lipocondensate was treated if it did not separate following centrifugation.

3.2.6 The effect of processing on the structure of adipose tissue

One of the purposes of using different formulations of adipose tissue in this work was to observe the effect of removing different components of adipose tissue when its anti-fibrotic abilities were tested in later chapters. These components were removed by the processing steps outlined in section 2.2. Processed adipose tissue was stained with various dyes (section 2.4.2) to analyse the effect of processing on the structure and cellular populations of the resulting adipose formulations. The tissue was stained with 4,4-difluoro-5-(2-Thienyl)-4-Bora-3a,4a-diaza-s-indacene-3-dodecanoic acid (BODIPY), Membrite 640/660, and DAPI to stain lipid, cell membrane, and nuclei respectively. These stains allowed for the identification of adipocytes and blood vessels. Adipocytes would present as large lipid droplets surrounded by a cell membrane and a nucleus associated with the membrane. Vessels would present as membranous tubules with multiple nuclei within the membrane.

Stained adipose tissue was imaged on a Zeiss LSM 880 AiryScan confocal microscope. A single image was taken of minced adipose tissue and Z-stack images were taken of lipoaspirate, emulsified fat, and lipocondensate and were combined into a maximal projection as described in section 2.4.2 (figure 3.11). This allowed the structure of adipose tissue to be analysed visually. Z-stack images were processed into orthogonal projections to allow the 3D structure of the adipose tissue to be examined (section 2.4.2, figure 3.12). Minced adipose tissue was found to be organised in a tightly packed structure containing adipocytes and blood vessels. All BODIPY staining was confined to lipid contained within a cell membrane and nuclei were associated with this membrane, marking them as adipocytes. Most adipocytes were large (~ 100 µm diameter). Blood vessels were identified and could be clearly visualised (figure 3.11A). In lipoaspirate, there were large droplets of lipid contained within cell membranes with nuclei associated, indicating these lipid droplets were adipocytes. Most adipocytes were large with a diameter of roughly 100 µm however, there were smaller (25 µm diameter) adipocytes present. There were vessels present as well and although there were clearly defined cell membranes, there were also collections of broken cell membranes with no nuclei associated, indicating the presence of debris from cell lysis (figure 3.11B). Lipoaspirate had a three-dimensional structure. Adipocytes could be seen to be present at different depths throughout the tissue on orthogonal projections (figure 3.12A).

Emulsified fat contained lipid droplets however, there was increased variation in the size of these collections compared to minced adipose tissue and lipoaspirate. Sizes ranged from between 100 and 5 µm in diameter. There were fewer clearly defined cell membranes surrounding lipid. There were large (100 µm) droplets of lipid present without any cell membrane indicating adipocyte lysis (figure 3.11C). No vessels could be identified and there was more cell debris present than in

minced adipose tissue and lipoaspirate. The three-dimensional structure of the tissue had been broken down (figure 3.12B). All structure in the emulsified fat was observed along one flat plane.

Processing adipose tissue to lipocondensate broke down the structure of the tissue. There were lipid droplets (50 µm – 100 µm) bound by a membrane and nuclei indicating the presence of adipocytes however, there were also large (100 µm – 150 µm) droplets of free lipid from lysed adipocytes (figure 3.11D, IV). The tissue contained vessels that could be identified however, there was also noticeable cell debris and unorganised membrane staining, indicating a high degree of cell lysis from processing. The three-dimensional structure of lipocondensate was similar to that of emulsified fat (figure 3.12C). Any cellular structure present was in a single layer at the bottom of the plane however, free lipid had risen to the surface of the gel used for mounting.

These images visualise how the structure of adipose tissue changes at a cellular level as it is processed into the formulations outlined in this work and suggests adipocyte lysis is occurring during processing.

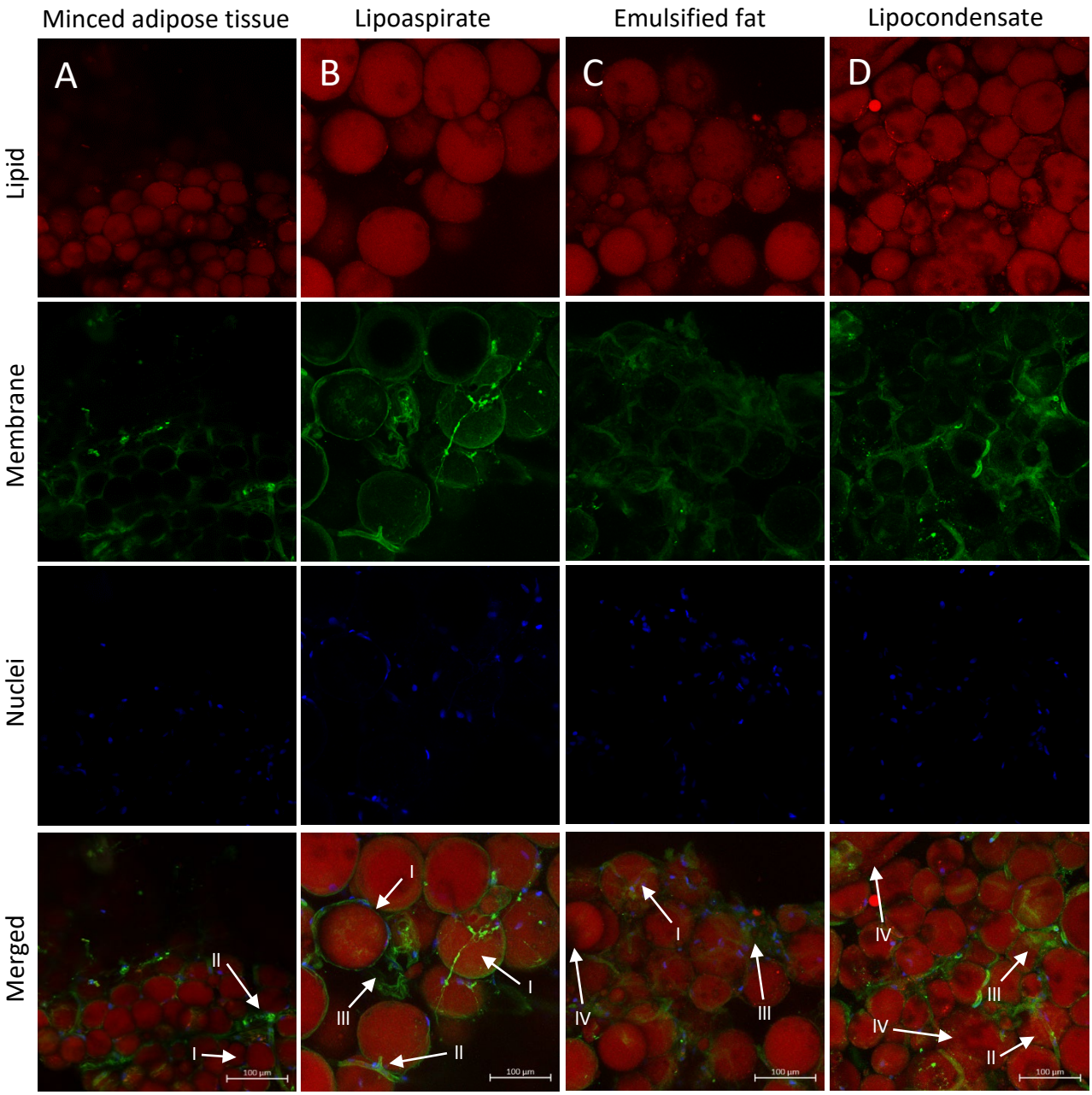

Figure 3.11. Staining of formulation of adipose tissue. (A-D) Fluorescent staining of adipose tissue. Adipose tissue was stained with BODIPY (lipid, red), Membrite 640/660 (cell membrane, green) and DAPI (cell nuclei, blue) and images merged. Images show **(A)** minced adipose tissue, **(B)** lipoaspirate, **(C)** emulsified fat, **(D)** lipocondensate. Arrows indicate **(I)** adipocytes, **(II)** vessels, **(III)** cell debris, **(IV)** free lipid.

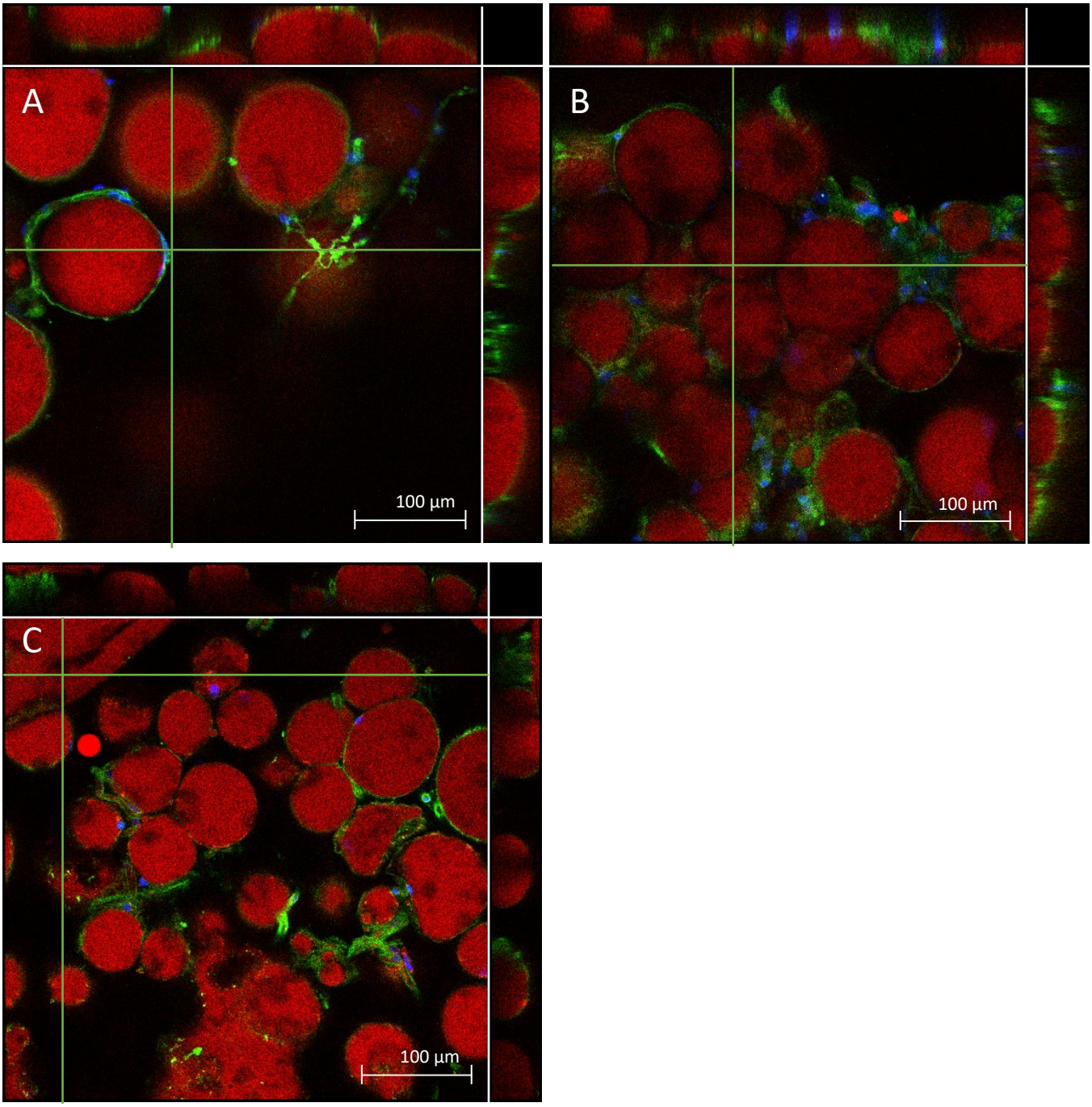

Figure 3.12. Orthogonal projections of adipose tissue. (A-C) Fluorescent staining of adipose tissue. Adipose tissue was stained with BODIPY (lipid, red), Membrite 640/660 (cell membrane, green) and DAPI (cell nuclei, blue) and orthogonal projections generated. An image of the Z-stack was chosen and a point along both X and Y axis selected (green lines). An image of all staining along the Z axis was then generated combining all the images of the Z-stack at that point along the X axis (right rectangle) and the Y axis (top rectangle) to give a three-dimensional structure to the image. **(A)** lipoaspirate, **(B)** emulsified fat, **(C)** lipocondensate. Scale bars = 100 µm.

3.2.7. Does processing adipose tissue cause cell lysis?

Fluorescent images in figures 3.11 and 3.12 imply that the mature adipocyte population is being removed as processing is carried out. To confirm if processing is removing adipocytes, the cellular metabolic activity of the adipose tissue formulations (generated as in section 2.2) was assessed by a resazurin assay and fluorescence normalised to a blank resazurin control (section 2.4.1.4).

The cellular metabolic activity of minced adipose tissue, lipoaspirate, emulsified fat, and lipocondensate was similar between groups (1.0, 1.0, 0.73, 0,66 times relative fluorescence to blank resazurin respectively, figure 3.13A). There was no significant change in metabolic activity between forms of processed adipose tissue ($p > 0.3$). Since there was no discernible difference in the metabolic activity of the forms of adipose tissue, an LDH assay was carried out to assess whether processing steps were causing cell lysis (section 2.4.1.3).

The amount of cell lysis occurring after processing in minced adipose tissue, lipoaspirate and emulsified fat was roughly equal. Minced adipose tissue had an absorbance value of 1.54 times that of the positive control, lipoaspirate 1.11 times the control and emulsified fat had a relative absorbance value of 1.77 times the positive control. However, when processed to lipocondensate there was a significant increase in the amount of cell lysis compared to all other groups ($P \leq 0.001$). Lipocondensate had a relative absorbance value of more than double the other forms of adipose tissue, at 3.63 times that of the positive control (figure 3.13B). This data shows that increased processing of adipose tissue leads to increase cell lysis however, this has no effect on the overall metabolic activity of the remaining adipose tissue cells.

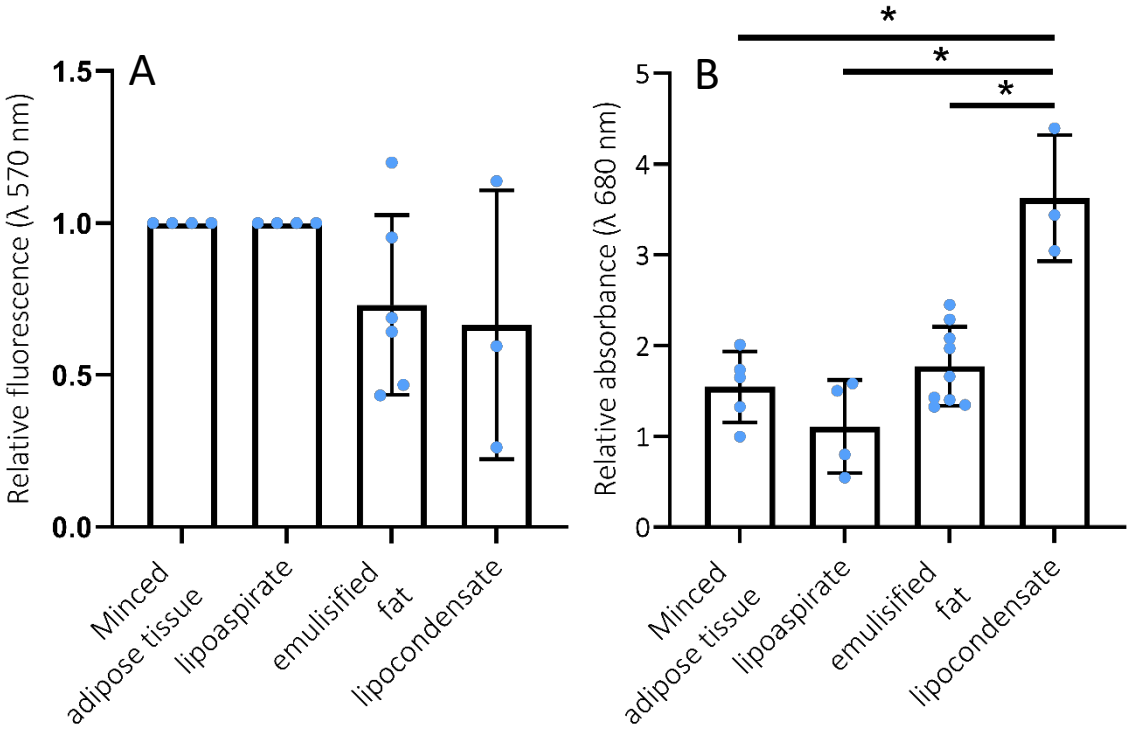

Figure 3.13. The effect of processing on adipose tissue metabolic activity or cell lysis. (A) Metabolic activity of processed adipose tissue. Fluorescence at 570 nm normalised to a fluorescence value of the minced adipose tissue/ lipoaspirate the samples were generated from (*N* = 4 (minced adipose tissue, lipoaspirate) / 8 (emulsified fat) / 3 (lipocondensate), error bars = standard deviation). **(B)** Cell lysis of adipose tissue following processing. Absorbance at 680 nm was measured and normalised to a positive control provided with the assay. (*N* = 5 (minced adipose tissue) / 4 (lipoaspirate) / 9 (emulsified fat) / 3 (lipocondensate). Ordinary one-way ANOVAs were carried out, bars = standard deviation, * = P ≤ 0.001).

3.2.8 Does adipose tissue origin affect metabolic activity and cell lysis of emulsified fat?

The supply of adipose tissue became limited at various points during the project and often whole adipose tissue was supplied as opposed to lipoaspirate. Lipoaspirate is more clinically relevant as surgeons almost exclusively use lipoaspirate (Bhooshan *et al.,* 2018; Caviggioli *et al.,* 2011; Klinger *et al.,* 2008; Rigotti *et al.,* 2007; Tonnard *et al.,* 2013; van Dongen *et al.,* 2016), however whole adipose tissue often had to be used as a substitute in my work. The previous experiments show that processing adipose tissue to emulsified fat did not affect cell metabolic activity or increase cell lysis. This data was generated by combining data from emulsified fat made from minced adipose tissue and lipoaspirate. It was decided to investigate whether the form of adipose tissue emulsified fat was generated from affected the cell metabolic activity or amount of cell lysis in the subsequent emulsified fat.

Resazurin data from emulsified fat generated from minced adipose tissue or from lipoaspirate was plotted separately (figure 3.14). Emulsified fat from minced adipose had a lower metabolic activity than emulsified fat generated from lipoaspirate (0.69 times fluorescence relative to minced adipose tissue/ lipoaspirate fluorescence values compared to 0.74 times fluorescence, figure 3.14A). Cell lysis data from emulsified fat generated from minced adipose tissue or from lipoaspirate was plotted separately (figure 3.14). Cell death in emulsified fat generated from minced adipose tissue was higher than that in emulsified fat generated from lipoaspirate (1.90 times absorbance relative to a positive control compared to 1.62 times absorbance). However, this was not significant ($p > 0.35$, figure 3.14B). This data suggests that minced adipose tissue is a suitable substitute for lipoaspirate for processing to emulsified fat.

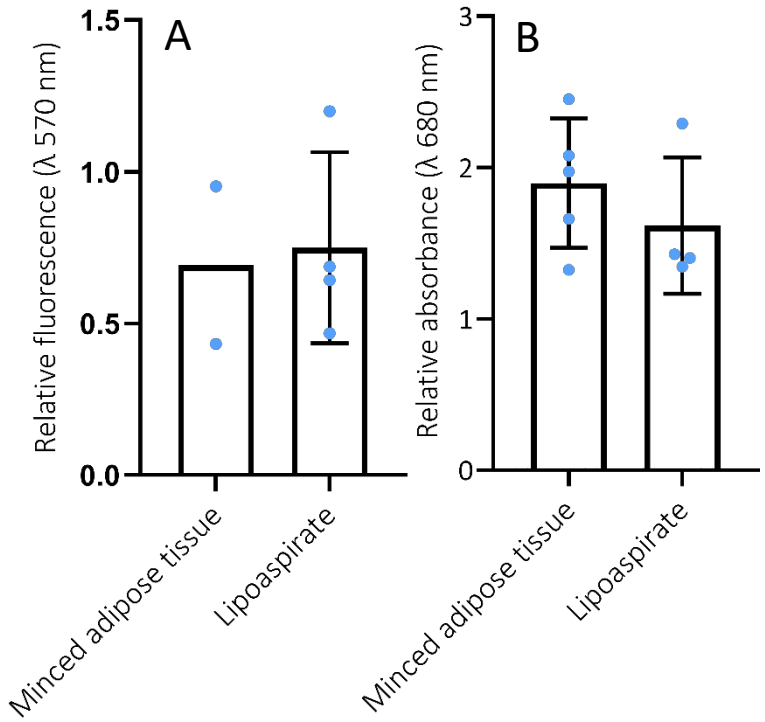

Figure 3.14. The effect of adipose tissue source on emulsified fat metabolic activity and cell lysis. (A) Metabolic activity of emulsified fat generated from either minced adipose tissue or lipoaspirate. Fluorescence at 570 nm normalised to the fluorescence values of the minced adipose tissue or lipoaspirate the samples were generated from (*N* = 4, bars = standard deviation). **(B)** Cell lysis in emulsified fat generated from either minced adipose tissue or lipoaspirate (*N* = 5 (minced adipose tissue) / 4 (lipoaspirate), bars = standard deviation, ordinary one-way ANOVAs were used to test significance).

3.2.9 Do adipose tissue processing methods concentrate SVF cells?

SVF-gels, such as lipocondensate, are used clinically because it is thought that adipocytes are being removed and the cells of the SVF are being concentrated, which in turn leads to a greater regenerative effect (Yao *et al.,* 2017). The above data outlined in section 3.2.5 demonstrates that processing adipose tissue to lipocondensate causes cell lysis, which may be the adipocytes lysing. Therefore, to test whether tissue processing concentrates cells, it was examined whether the number of cells present per gram of lipocondensate was altered compared to other formulations. By examining the amount of DNA present in lipoaspirate, emulsified fat and lipocondensate, the number of cells present in these formulations was calculated (section 2.4.1.5). Before and after processing, the mass of adipose tissue was measured to allow for the calculation of the number of cells in each formulation per gram of adipose tissue started with.

Lipoaspirate contained a mean of $7.85x10^6$ cells for every gram of adipose tissue before washing. After processing to emulsified fat, there was an increase in cell number to $8.57x10^6$ for every gram of starting adipose tissue. When processed to lipocondensate there was a large decrease in cell number to $1.11x10^6$ cells per gram of starting adipose tissue however, this decrease was not significant ($p = 0.057$, figure 3.15A). When the number of cells per gram of formulation was calculated, all formulations appeared to contain a roughly equal number of cells. Lipoaspirate contained $7.85x10^6$ cells per gram, emulsified fat $9.98x10^6$ cells per gram, and lipocondensate contained $9.75x10^6$ cells per gram. This shows that while processing the adipose tissue to lipocondensate does remove cells, when normalised against the mass of the formulation, lipocondensate contains a similar number of cells compared to lipoaspirate. Given that images in figure 3.11D show fewer intact adipocytes, it is likely that it is mostly SVF cells that remain and that processing was concentrating these SVF cells.

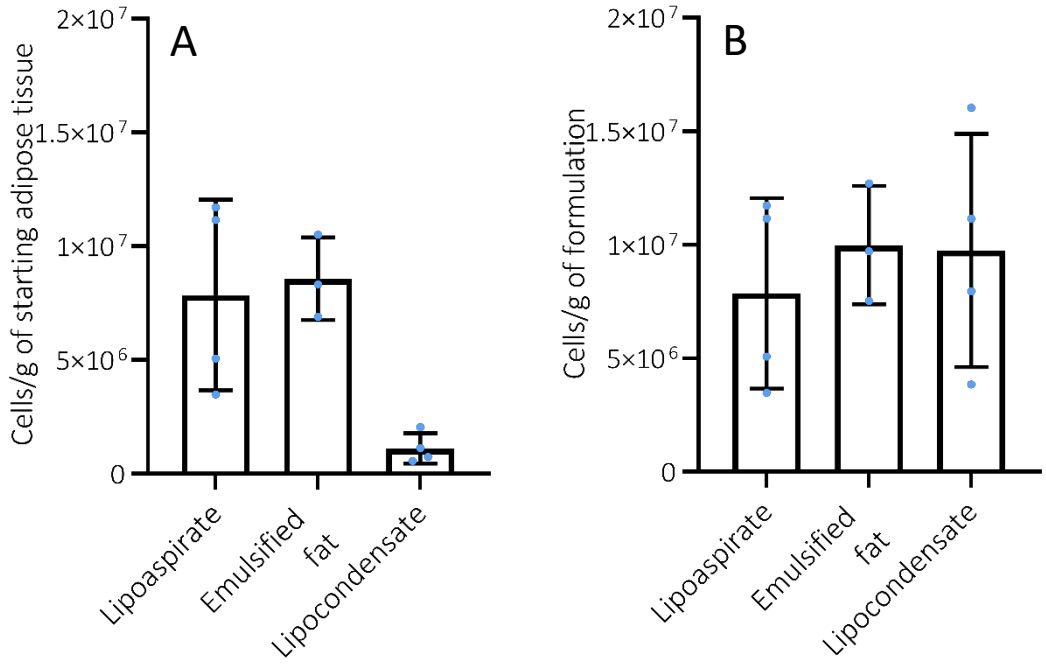

Figure 3.15. Quantification of adipose tissue cell number following processing. (A-B) Adipose tissue cell number calculated by quantification of DNA present. (A) Cell number per gram of starting adipose tissue. **(B)** Cell number per gram of formulation. *N* = 3/4 (lipocondensate), *n* = 3. Bars = standard deviation. A Kruskal-Wallace test was performed on figure A and an ordinary one-way ANOVA was carried out on figure B. DNA analysis was carried out by Dr. Victoria Workman and the data is presented with her permission.

3.3 Discussion

The aim of this chapter was to characterise the clinical formulations used throughout the research for this thesis. This was achieved by:

-Optimising the processing techniques used to generate these formulations.

-Identifying the cellular populations contained within each formulation.

-Understanding how processing affects metabolic activity, lysis, and cell concentration within each formulation.

Autologous fat grafting has been shown to regenerate damaged skin (Caviggioli *et al.,* 2011; Klinger *et al.,* 2008; Rigotti *et al.,* 2007). The mechanism behind this remains unknown. Further complicating this unknown is that adipose tissue is complex, with many different cell types and components (Eto *et al.,* 2009). In order to elucidate the mechanisms behind adipose tissue's regenerative action, a variety of different formulations of adipose tissue with different components, were tested in chapters 4 and 5. By removing components and testing these new formulations, it was hypothesised that the cellular population responsible for any regenerative effect could be identified. Furthermore, there are a wide variety of different adipose tissue formulations, generated *via* different processing methods, that are being used to treat damaged skin by clinicians (lo Furno *et al.,* 2017; Mashiko *et al.,* 2017; Tonnard *et al.,* 2013; Yao *et al.,* 2017). Thus, it was important to test the regenerative ability of other clinically relevant adipose tissue formulations as well as lipoaspirate. The formulations selected for use in chapters 4 and 5 were minced adipose tissue, lipoaspirate, emulsified fat, lipocondensate, and ADSCs. The work in this chapter was focussed on characterising these formulations for future work later in the thesis.

3.3.1 Minced adipose tissue and lipoaspirate

Minced adipose tissue and lipoaspirate were considered as "unaltered" adipose tissue, with all the components of adipose tissue present. Minced adipose tissue was generated from whole adipose tissue by fragmenting the tissue with a scalpel to a consistency similar to that of lipoaspirate (figure 3.3B). The characteristics of the two formulations were tested. Using stains for lipid, cell membrane, and cell nuclei, the structure of the two formulations was examined and compared. Both minced adipose tissue and lipoaspirate had a similar appearance (figure 3.11A-B). Both the tissues had a structured appearance with mostly uniform lipid droplets, surrounded by membranes and nuclei, which were most likely adipocytes. There were large vessel structures throughout the tissue showing that any endothelial structures present had not been completely broken apart. Fluorescent images taken of the two different formulations showed the tissues shared a similar structure post

processing. Resazurin and LDH assays were carried out on the formulations of adipose tissue generated for this work. When examining minced adipose tissue and lipoaspirate to judge the amount of cell lysis processing caused, here was no significant difference in cell lysis between the two formulations (figure 3.13B, $p = 0.54$). Additionally, emulsified fat generated from minced adipose tissue and lipoaspirate was compared. There was no difference in cellular metabolic activity and cell lysis. Taken together, this data shows that minced adipose tissue and lipoaspirate are functionally identical formulations. The same cellular components are present in the tissue and processing whole adipose tissue to minced adipose tissue results in a similar amount of cell lysis to lipoaspirate. Furthermore, products generated from the tissues are functionally the same with the metabolic activity and cell lysis during processing the same in emulsified fat generated with lipoaspirate or minced adipose tissue.

Following the standardisation of autologous fat grafting by Dr. Coleman (Coleman, 1998, 2002), lipoaspirate has been almost exclusively used over solid adipose tissue by clinicians (Caviggioli *et al.,* 2011; Klinger *et al.,* 2008; Rigotti *et al.,* 2007; Yoshimura *et al.,* 2008). Processing techniques such as Nanofat, SVF-gel, and other techniques such as “squeezed fat” (Mashiko *et al.,* 2017) also use lipoaspirate as standard (Sesé *et al.,* 2020; Tonnard *et al.,* 2013; Yao *et al.,* 2017). This is because these procedures are designed to be easy and quick for surgeons to carry out and be completed during one operation. Lipoaspiration has been shown to fragment adipose tissue slightly. The overall structure is maintained however, following liposuction the adipocytes are less densely packed and some larger vessels and ECM have been degraded (Eto *et al.,* 2009; Matsumoto *et al.,* 2006). Furthermore, there are reports that liposuction alters the cellular yield and composition of adipose tissue compared to whole adipose tissue. Von Heimburg *et al.,* (2004) demonstrated that aspirated fat contained a higher number of SVF cells per gram in comparison to whole, excised adipose tissue. This indicates that liposuction causes lysis of some adipocytes and changes the proportion of SVF cells in the tissue compared to excised adipose tissue. This is supported by Eto *et al.,* (2009) who saw a similar number of cells overall, but a higher proportion of SVF cells compared to adipocytes in lipoaspirate.

Lipoaspirate is often used by surgeons as it is quick to extract and then re-insert in one operation. Mincing adipose tissue with a scalpel, in the way I do in this study, would take more time than surgeons have, thus lipoaspirate is used as standard. The adipose tissue supplied to me, with informed consent, was excess waste surgical tissue and liposuction was carried out to collect lipoaspirate, only the amount needed for the surgery was extracted and used on the patient. Thus, there was often little excess lipoaspirate and I might only receive 2/3 ml of lipoaspirate per operation. However, when whole adipose tissue was removed from patients there was often little

use for this tissue and when I was supplied with whole adipose tissue it was often in large quantities. Consequently, most of the useable tissue received was whole adipose tissue as opposed to lipoaspirate. As such, it was decided to test and compare minced adipose tissue to lipoaspirate to examine whether minced adipose tissue could act as a substitute for lipoaspirate. The data gathered from confocal images show minced adipose tissue had a similar structure to lipoaspirate. Furthermore, these images show a tissue similar in structure to lipoaspirate in immunofluorescence and scanning electron microscope images shown in Eto *et al.* (2009) and Matsumoto *et al.* (2006). Minced adipose tissue showed bundled adipocytes with vessels running throughout similar to those in the literature. While the number of cells throughout minced adipose tissue compared to lipoaspirate was not quantified, LDH data demonstrated that there was not a difference in cell death between the formulation. This implies that cell number will not be widely different between the two formulations. This is also supported by the literature with data showing there is a slight alteration in the proportion of cell populations between lipoaspirate and whole fat but little substantial difference (Eto *et al.,* 2009; von Heimburg *et al.,* 2004).

This data supports little difference exists between whole adipose tissue and lipoaspirate to begin with but, that mincing adipose tissue in the method outlined in this chapter generates a formulation functionally identical to lipoaspirate. This data establishes a baseline formulation used in the clinic that more processed formulations such as emulsified fat and lipocondensate can be compared to.

3.3.2 Emulsified fat

Nanofat was originally developed to help treat volume loss in smaller and more delicate areas in the body (Tonnard *et al.,* 2013). The authors found that adipocytes were lysed whilst mechanically breaking down the adipose tissue, and further experimentation has shown that the remaining SVF is still associated with the surrounding ECM (Alexander, 2016). It was decided to use a formulation "emulsified fat" that was styled upon Tonnard's Nanofat. This formulation was used as it would remove the adipocyte population from the adipose tissue and allow me to see the effect of adipocytes *in vitro* by comparing emulsified fat to the minced adipose tissue or lipoaspirate. The processing technique to generate emulsified fat was optimised and the formulation characterised.

Generating emulsified fat with 10 and 30 passes between syringes did not lead to a change in cell metabolic activity or cell lysis (figure 3.7A, C). When generated using 100 passes there was a decrease in the mean metabolic activity combined with an increase in mean LDH presence however, neither of these data were significant ($p = 0.1$ and 0.32 respectively). The metabolic activity of emulsified fat was similar to that of minced adipose tissue and lipoaspirate. The cell lysis that

occurred during processing was also the same as during minced adipose tissue or lipoaspirate processing as well (figure 3.13). Confocal images revealed that some adipocytes were still present following emulsified fat processing (figure 3.11). However, vessels were fragmented, and large lipid vesicles (indicating adipocyte lysis) were present throughout. Finally, emulsified fat contained a similar number of cells per gram of starting adipose tissue compared to lipoaspirate. However, per gram of formulation emulsified fat contained a higher mean number of cells in comparison to lipoaspirate. This data showed that increasing pass number did not lead to increased cell lysis and thus 30 passes was used to generate emulsified fat as this is what is used in the literature. Confocal images showed that adipocytes were being lysed however, this was not reflected in a significant decrease in metabolic activity or increase in cell lysis compared to lipoaspirate. An explanation for the lack of change in metabolic activity and cell death may be that adipocytes only contribute 10 % of the total cell number of adipose tissue (Alexander, 2016). There is more than 10 % variation in this metabolic activity and cell lysis data (standard deviation was more than 35 % of the mean averages) and thus lysing this relatively small population may not alter the metabolic activity of the adipose tissue enough to impact a resazurin assay or LDH assay. Supporting this is that the mean number of cells per gram of formulation in emulsified fat increased compared to lipoaspirate. This implies that the larger adipocytes are being lysed and thus per gram, there are more, smaller, SVF present. This data indicates emulsified fat is being generated as expected.

When Tonnard *et al*. (2013) first generated Nanofat, the purpose was to break down the adipose tissue so that it could be implanted using 27-gauge needles that were smaller than the previously used 23-gauge. This would mean lipofilling could be carried out more accurately in smaller, delicate, areas of the body. To do this, the authors passed adipose tissue between syringes 30 times. The shear force applied to adipose tissue while shifting between syringes in Nanofat generation is the force that is reported to lyse any viable adipocytes (Tonnard *et al.,* 2013). 30 passes has become the industry standard (Bhooshan *et al.,* 2018; Kemaloğlu, 2016; lo Furno *et al.,* 2017; Sesé *et al.,* 2019; Yu *et al.,* 2018). There has been some experimentation to investigate how different methods of Nanofat generation alter the formulation's efficacy or ADSC yield (Gentile *et al.,* 2017; lo Furno *et al.,* 2017; Yang *et al.,* 2021). By filtering the Nanofat after its formation, centrifuging half of the Nanofat to isolate the SVF and then adding this SVF back into the Nanofat Gentile *et al*. (2017) generated "supercharged Nanofat". This increased the number of cells found in the formulation and when injected underneath burns the thickness, pliability, and vascularisation of the skin was increased. Alternatively, it has been shown that by not filtering Nanofat following formation, SVF cells in the Nanofat have increased proliferation after the first week when cultured (lo Furno *et al.,* 2017). Despite this experimentation however, to my knowledge there has been no investigation into

whether increasing pass number during Nanofat generation increases cell lysis. Chen *et al.,* (2020) and Qiu *et al*. (2021) both found that decreasing the size of the aperture adipose tissue is passed through to generate Nanofat increased cell lysis however, with a significant decrease in the viable cell population. The number of cells per gram of emulsified fat/Nanofat etc. has been reported as between $6x10^6$ (Sesé *et al.,* 2019) and $4x10^4$ (Yang *et al.,* 2021).

When analysing the cell lysis that had occurred during emulsified fat generation, increasing pass number did not lead to increased cell lysis. This is slightly unexpected as it is logical that applying more shear force by passing the adipose tissue more times would lead to increased cell death however, the data suggests this is not the case. However, for this work a 3.6 mm Luer-Lock was used. This generated the lowest shear force on adipose tissue when used by Qiu *et al*. (2021) compared to smaller apertures. This data, combined with this analysis in the literature suggests that the size of the aperture adipose tissue is passed through is more important for lysing adipocytes than pass number as pass number had little influence on cell lysis, whereas aperture did (Qiu *et al*., 2021). It may be that after a few passes, any cells that are going to lyse from the shear force have, and smaller cells can pass through the aperture undisrupted. In future I would generate emulsified fat with progressively smaller Luer-Locks to ensure complete adipocyte lysis.

In confocal images in figure 3.11, it can be hard to distinguish between live adipocytes, and lipid vesicles. Tonnard *et al*. (2013) used live/dead staining to show there were no viable adipocytes in Nanofat (figure 3.16). In the images used in the paper there is calcein AM staining of smaller cells (which usually indicates live cells) in between large, dark, circles where there is no staining present. These dark circles are lipid vesicles as the calcein AM and propidium iodine stains used in live/dead staining do not stain lipid. This shows that even when adipocytes are lysed by shear force the lipid contained within the now burst adipocytes remains in droplet form. This appears to be occurring in the emulsified fat generated for this work. There is some specific staining for cell membrane around lipid droplets which shows the presence of some adipocytes. However, most staining appears nonspecific, in gaps between the lipid droplets, or in clumps of cellular debris. This indicates that most adipocytes are lysed but even so, Nanofat is not completely devoid of adipocytes (figure 3.13C) with images from Sesé *et al.* (2019) showing some adipocytes present in their Nanofat formulation.

Finally, the number of cells per gram of emulsified fat is consistent with figures reported in the literature with the 8.5 $x10^6$ cells per gram aligning with figures from Sesé *et al.* (2019). The numbers recorded in this paper put the number of cells per gram at around $6x10^6$, which is slightly lower than those recorded in this work. This perhaps indicates slightly less lysis is occurring during emulsified fat processing however, this was within acceptable variation.

The processing technique used to generate a Nanofat-like formulation “emulsified fat” have been optimised. These formulations were then characterised with the metabolic activity and cell number present being similar to minced adipose tissue and lipoaspirate. There is evidence that the adipocyte population has been removed, as would be expected based upon the literature.

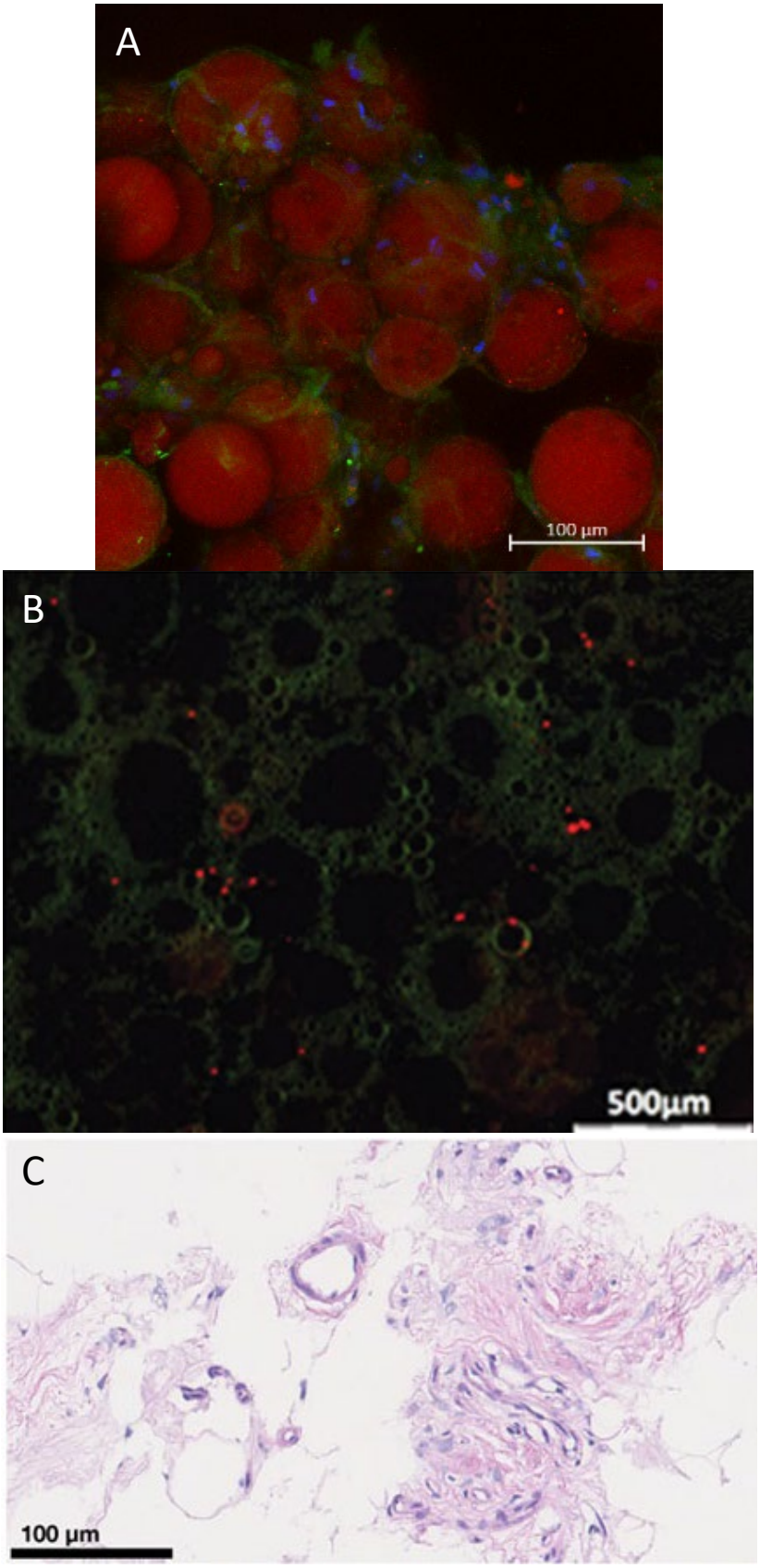

Figure 3.16. Adipocytes in formulations of emulsified fat. Staining of adipose tissue from **(A)** emulsified fat generated by myself (confocal microscopy), **(B)** Nanofat from Tonnard *et al*. (2013) (live dead staining), **(C)** Nanofat from Sesé *et al*. (2019), (haematoxylin and eosin staining). Images used with permission from Copyright Clearance Centre using licence 5324931343530 and 5324940022993.

3.3.3 Lipocondensate

Clinicians have developed different processing techniques for lipoaspirate to condense the SVF fraction of adipose tissue to achieve better therapeutic outcomes (Mashiko *et al.,* 2017; Sesé *et al.,* 2020; van Dongen *et al.,* 2016; Yao *et al.,* 2017). The "lipocondensate" used in this work was based on the "SVF-gel" generated in Yao *et al*. (2017). The theory behind this condensation of the SVF is that the majority of adipose tissue volume is made up of adipocytes, yet these cells encompass a small number of the total cells of adipose tissue (Alexander, 2016). By disrupting adipocytes by mechanical processing and removing oil and water via centrifugation, it is theorised to dramatically increase the number of SVF cells present per gram of adipose tissue. In this chapter, the processing technique to generate lipocondensate was optimised, the cellular composition of the formulation was characterised and finally, the metabolic activity and cell number post processing was compared to lipoaspirate.

Alterations to the emulsified fat generation process had no effect on the subsequent lipocondensate generated (figure 3.7B, D). Metabolic activity and cell lysis was unchanged regardless of pass number used on emulsified fat implying that changing the pass number in our method of generating emulsified fat causes little additional lysis of SVF cells as the metabolic activity of the lipocondensate (which contains only SVF cells) is unchanged. The initial attempts to generate lipocondensate using the technique in Yao *et al.* yielded little success. Centrifugation would often not result in separation between the lipocondensate layer and the top, free lipid layer (figure 3.8A). Instead, an oily emulsion of both layers would be present, as opposed to two clearly defined and separate layers. Several different methods to flocculate the emulsion and cause separation were trialled but emulsion separation was effectively achieved via freezing the emulsion in a 4 °C fridge, thawing the mixture and disturbing with a Pasteur pipette and re-centrifuging the solution. This allowed for consistent lipocondensate formation with the lipid layer separating from the lipocondensate. A commercial Microlyzer product was trialled to increase cell lysis during lipocondensate processing. However, cellular metabolic activity was higher and cell lysis lower in lipocondensate generated with the Microlyzer and thus it was discarded. In confocal images (figure 3.11D), the structure of lipocondensate appears disrupted compared to lipoaspirate and minced adipose tissue. There are few adipocytes present and most of the lipid stained is not bound within a membrane and smeared across the image into large vesicles. The formulation did still contain vessels however, there was also a high degree of cell debris, indicating increased breakdown of the tissue. This indicates the adipose tissue is becoming more fragmented the more processing occurs. When analysed via a resazurin and LDH assay, there was significantly increased cell lysis present in the lipocondensate compared to all other formulations (figure 3.13B, $P \leq 0.001$) however, there is no

change in the levels of metabolic activity in comparison to the other formulations (figure 3.13A). In addition to this, for every gram of starting adipose tissue there were $1.10x10^6$ cells found in lipocondensate, much lower than in emulsified fat and lipoaspirate. Whereas, when measuring cells per gram of formulation there were $9.75x10^6$ cells in lipocondensate, a similar number to emulsified fat and lipoaspirate. Taken together, this data shows that lipocondensate processing is causing adipocyte lysis and removal from the formulation. This is because LDH levels indicate increased cell lysis however, metabolic activity is comparable to other formulations because there are still the same number of cells per gram present in the formulation. The adipocytes are being replaced by a higher concentration of SVF cells.

The layer of oil and lipocondensate that formed in figure 3.8A were acting as an emulsion. Emulsions are a stable solution of two liquids that are immiscible. If the emulsion becomes unstable the two liquids will begin to separate and form two distinct phases (reviewed in Goodarzi & Zendehboud (2019)). Under certain conditions, an emulsion can become stable and will remain as droplets of one component in another component which is immiscible to the first. One of the most important factors in the stability of an oil/water emulsion is the size of the oil droplets (Rousseau, 2000). Yao *et al*. (2017) recommends that should the SVF-gel fail to separate from the oil layer then extra oil should be added and force used to "flocculate" the emulsion. The process of flocculation is a recognised technique used to destabilise emulsions. The theory behind the process itself is that by adding lipids or disrupting the emulsion in other ways, the droplets of one phase that exist in the emulsion start to group together where they then coalesce and join (figure 3.17). This causes the stability of the emulsion to be lost, and the two phases to separate (Degner *et al.,* 2014). Lipid oil is released from lysed adipocytes (Qiu *et al.,* 2021). Qiu *et al.,* (2021) examined the amount of oil generated from producing Nanofat with different sized Luer-locks and found that Nanofat generated with the largest connector had the lowest lipid oil content of the all the Nanofat formulations made. Since the initial development of Nanofat, commercial products to streamline and speed up the process of mechanically emulsifying the adipose tissue have been developed (Bianchi *et al.,* 2013; TULIP Aesthetics, 2022). The Tulip system is one such product. The device is designed to transfer lipoaspirate between syringes and through a mesh as part of a closed system that can be used quickly during surgery (TULIP Aesthetics, 2022) and is used to generate Nanofat (Sesé *et al.,* 2019). The Microlyzer is a similar system and is designed to isolate SVF cells from adipose tissue by using blades of 2.4, 1.2, and 0.6 µm diameter to mechanically emulsify the adipose tissue (PRP First, 2021). Imaging of lipocondensate-like formulations has demonstrated the removal of adipocytes. Live/dead imaging, scanning electron microscopy, and confocal imaging has shown even the fragmentation of adipocytes or no adipocyte presence at all (Wang *et al.,* 2019; Yang *et al.,* 2021; Yao *et al.,* 2017).

The formulation appears to be composed to SVF cells and disrupted ECM (Sesé *et al.,* 2020; Yao *et al.,* 2017). The removal of these adipocytes leads to a concentration of the SVF, with the large volume of adipocytes removed, a higher number of SVF cells per gram can be realised. In lipocondensate/ SVF-gel formulations, the number of cells per gram of formulation has been reported as $5x10^5$ (Yang *et al.,* 2021), $4x10^4$ (Yao *et al.,* 2017), $3x10^6$ (van Dongen *et al.,* 2016), and the highest reported value being $3x10^7$ (Sesé *et al.,* 2020). Despite the wide range of values, all of these SVF-gels were found to have a similar or higher number of cells per gram than lipoaspirate and are thus successfully condensing the SVF population.

Lipocondensate was failing to separate from lipid oil as described in Yao *et al.* (2017). Several mechanisms were trialled to "flocculate" the emulsion such as adding more lipid, disruption with a Pasteur pipette, and re-centrifugation. The use of the Microlyzer was an attempt to generate more lipid with the hope of stabilising the emulsion. When generating emulsified fat, a 3.6 mm Luer-Lock was used, this generated the lowest amount of lipid when different size Luer-Locks were tested in Qiu *et al.,* (2021). It was hoped that by using the Microlyzer, more adipocytes would lyse and release more lipid, destabilising the emulsion. This was not the case however, with the Microlyzer leading to less cell death in lipocondensate generated with the Microlyzer. Consistent lipocondensate separation was achieved by freeze/thawing the lipocondensate mixture. It was then noticed that the lipocondensate emulsion would solidify in a 4 °C fridge, above the freezing point of water. Thus, the mixture of lipid in the unseparated lipocondensate must have a different freezing point to the water phase of the emulsion. The mixture was then thawed, disturbed with a Pasteur pipette and re-centrifuged. This technique then led to phase separation and the successful formation of lipocondensate every time it was used. This occurs because when frozen in an emulsion, oil droplets undergo a process known as "partial coalescence", whereby the oil droplets begin to partially crystallise and fuse together. When thawing begins the now fused droplets join. This joining decreases the stability of the emulsion causing it to become unstable and eventually the phases separate out (Degner *et al.,* 2014). Following this finding, if lipocondensate did not separate following initial centrifugation, it was treated with this freezing technique, and this allowed consistent formation of lipocondensate. The cellular structure and makeup of my lipocondensate is consistent with that of the literature. The fragmented formulation in Yao *et al*. looks very similar to my lipocondensate with a few adipocytes and mostly disrupted cell debris and vessels. In theory, processing to lipocondensate should remove all adipocytes (Wang *et al.,* 2019). In reality however, images do show a few adipocytes still remaining, both in my work and others (Sesé *et al.,* 2020; Yao *et al.,* 2017). It is likely that this is down to the method of image capture which may be adding bias to the fluorescent images. It is impossible to take an image of an artifact that is not present. Given

that the structure of emulsified fat and lipocondensate have been broken down to an almost liquid form, there is little to view under a microscope. Thus, the images taken will be of the most structured elements remaining, which are more likely to contain the few adipocytes present. Despite this, my data agrees with the literature that processing to lipocondensate concentrates the SVF cells in lipocondensate-like formulations. The number of cells per gram of lipocondensate was $9.75x10^6$. This is between values reported by Sesé *et al.* (2020), at $3x10^7$ and van Dongen *et al.* (2016) at $3x10^6$. As in these papers, the cells per gram of lipocondensate was similar or higher than the number of cells per gram of lipoaspirate while adipocytes were removed, showing that processing to lipocondensate is concentrating the SVF cells in adipose tissue. The work in this chapter has optimised the processing technique for my lipocondensate formulation, characterised the cellular structure of the formulation, and compared the metabolic activity, cell lysis, and cell number to the other formulations used in this work.

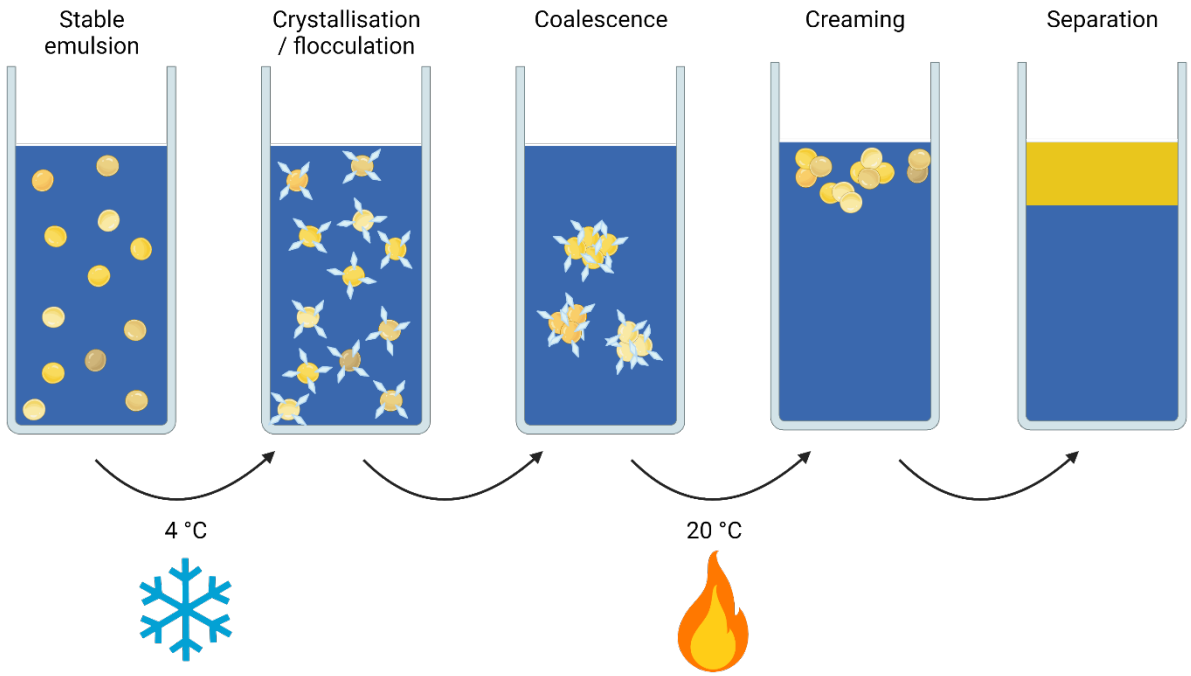

Figure 3.17. Separating a stable emulsion. Lipid in a stable oil/water emulsion can be separated by freezing the lipid until crystallisation. This crystallisation causes the lipid to fuse together, destabilising the emulsion upon thawing and leading to separation.

3.3.4. ADSC

Finally, enzymatically isolated ADSCs were characterised via flow cytometry and an oil red O assay. Overall, the ADSCs isolated were positive for markers CD90 and CD105 (figure 3.4). Across the cellular population isolated, 80.50 % of cells were CD90+/CD105+ (figure 3.5). There was little expression of CD34, CD73, and CD146 (less than 0.50 %). Expression of control markers CD31 and CD45 was low (figure 3.4) with 99.50 % of cells being CD31-/CD45- (figure 3.5). ADSCs treated with differentiation media showed a substantial change in morphology with significantly more lipid vesicles present compared to untreated ADSCs (figure 3.6). During the initial months of this project, isolated ADSC were cultured in 10 % D-MEM. However, these cells did not grow in a reliable manner. Cells frequently stopped proliferating and slowly died after two weeks. Cell cultures died before they became confluent enough to reach a second passage, and thus, no quantitative measure or assay of their viability could be carried out to investigate this phenomenon. A variety of factors were investigated ranging from collagenase A concentration during isolation, seeding density, and incubator environment. However, changing the culture medium to MesenPro led to ADSC survival to at least passage six. The flow cytometry data along with oil red O staining supports that ADSCs isolated are in fact ADSCs and following the use of MesenPro growth medium, ADSCs are behaving as would be expected.

ADSCs are frequently cited as the cellular component in adipose tissue responsible for its regenerative properties (Cao *et al.,* 2005; Rehman *et al.,* 2004; Rigotti *et al.,* 2007; Spiekman *et al.,* 2014). ADSCs are a dynamic cell, share many properties with mesenchymal stem cells (MSCs) and can differentiate into multiple cell lineages (Cao *et al.,* 2005; Gimble & Guilak, 2003; Zuk *et al.,* 2001). Guidelines have been set by the “International Federation for Adipose Therapeutics and Science” and the “International Society for Cellular Therapy”. The groups recommend that ADSCs can be classed as such if they are expressing two CD markers found to be present in ADSCs and are tested for two negative CD markers (Bourin *et al.,* 2013). CD90, referred to as Thy-1 (Shi *et al.,* 2019), and CD105 (referred to as Endoglin; Fonsatti & Maio, 2004) are markers of MSCs (Dominici *et al.,* 2006) and are frequently cited as being expressed by ADSC, (Bourin *et al.,* 2013; Gimble & Guilak, 2003; Huang *et al.,* 2013; Mildmay-White & Khan, 2017). As such, the presence of these markers is a strong indicator that the isolated cells are ADSCs. CD31 (Platelet Endothelial Cell Adhesion Molecule) is a marker found in endothelial cells (reviewed in Rakocevic *et al.* 2017) and CD45 (leukocyte common antigen) acts as a marker for hematopoietic stem cells (Nakano *et al.,* 1990). CD31 and CD45 are used as a negative control for MSCs (Dominici *et al.,* 2006) and ADSCs are found to not express these surface proteins (Bourin *et al.,* 2013; Huang *et al.,* 2013). CD146 is considered a marker of ADSCs by some (Gimble & Guilak, 2003; Huang *et al.,* 2013) however, others have found

little expression of CD146 in ADSCs (Mildmay-White & Khan, 2017; Pachón-Peña *et al.,* 2011). ADSCs have been shown to exist in distinct sub-populations, with Borrelli *et al*. (2020) able to find large populations of CD146- ADSCs while also finding CD146+ ADSCs when isolating SVF cells. CD34 is another protein with no clear scientific consensus as to whether it is a marker of ADSCs. The transmembrane phosphoglycoprotein has been found to be present in ADSCs (Gronthos *et al.,* 2001; Mildmay-White & Khan, 2017) and is even considered a marker in the International Federation for Adipose Therapeutics and Science and the International Society for Cellular Therapy (Bourin *et al.,* 2013). However, other researchers have found MSCs and ADSCs to be CD34- (Dominici *et al.,* 2006; Huang *et al.,* 2013; Zuk *et al.,* 2002). Additionally, ADSCs have been shown to lose the expression of markers such as CD34 over time as the cells are passaged in culture (Mitchell *et al.,* 2006).

ADSCs can differentiate into adipogenic, osteogenic, and chondrogenic cell lineages (Gimble & Guilak, 2003). Because of this ability, other standard tests for ADSC purity are assays for adipogenic (oil red O), osteogenic (alkaline phosphatase), and chondrogenic (alcian blue) differentiation (Bianchi *et al.,* 2013; Bourin *et al.,* 2013; *et al.,* 2001). Finally, different culture medium has been used for growth of isolated ADSC (al Battah *et al.,* 2011; Fadel *et al.,* 2011; Francis *et al.,* 2010; Roxburgh *et al.,* 2016). Roxburgh *et al*. (2016) investigated the effect of culturing ADSCs in various cell culture media on their proliferation and ability to differentiate. They found that ADSCs cultured in 10 % D-MEM had one of the highest rates of proliferation however, they did also observe a high rate of spontaneous osteogenic differentiation when cultured in 10 % D-MEM. Other groups have cultured isolated ADSCs successfully in 10 % D-MEM (Baptista *et al.,* 2009; Francis *et al.,* 2010; Sherman *et al.,* 2019) but it was noted by Baptista *et al*. (2009) and Sherman *et al*. (2019) that some ADSC cultures would halt proliferation and the population would spontaneously decrease. This observation, combined with the spontaneous differentiation seen in Roxburgh *et al*. (2016) and my own observations indicates that 10 % D-MEM might not be the most suitable medium to culture ADSCs in. Fadel *et al*. (2011) isolated ADSCs in Alpha-MEM supplemented with 15 % foetal calf serum however, most of their isolation techniques failed with ADSCs halting proliferation and dying. Other commercial media was examined in Roxburgh *et al*. (2016) and “Advanced D-MEM” by Invitrogen and “Pre-adipocyte media” from Lonza was found to lead to low rates of proliferation in ADSCs. The group did find however that ADSCs cultured in MesenPRO medium remained healthy and proliferated at a high rate.

This project involved isolating ADSCs from human tissue. Primary cell isolates will show patient-patient variation and are, by definition, uncharacterised. In addition to this, the ethical approvals in place for this work do not allow for the disclosure of relevant demographic information such as: patient age, smoker status, or weight. All these factors can affect the characteristics of the

ADSCs isolated (reviewed in Varghese *et al.,* 2017). Additionally, ADSCs have been shown to have different characteristics depending on the donor site (Engels *et al.,* 2013; Padoin *et al.,* 2008), another piece of information that was not accessible. For these reasons, isolated ADSCs from two patients were characterised and the expression of common surface protein markers was examined. Overall, the ADSCs isolated matched the criteria established by the International Federation for Adipose Therapeutics and Science with the vast majority of ADSCs positive for CD90+/CD105+, with adipogenic differentiation capabilities and little CD31 and CD45 contamination. There are mixed reports of ADSCs expressing CD146 and CD34 and the International Federation for Adipose Therapeutics and Science accepts that there is a high degree of heterogeneity between individuals ADSCs. Thus, these two markers alone are not essential for ADSC classification (Bourin *et al.,* 2013). The lack of CD146 in my isolated ADSCs may be a result of a combination of patient variation and heterogeneity in adipose tissue isolated. By chance cells could have isolated from a region of adipose tissue with a high population of CD146- ADSCs identified by Borrelli *et al.* (2020a). Given that the cells used in flow cytometry had been in culture for at least two weeks, a possible explanation for why the ADSCs isolated have low expression of marker CD34 is that as in Mitchell *et al.* (2006) the ADSCs may have lost the expression of this marker. Based on experience and reports in the literature, it is likely that culturing ADSCs in 10 % D-MEM leaves the user open to issues with batch variation. The spontaneous halting of proliferation in some ADSC cultures described in Baptista *et al*. (2009) and Sherman *et al*. (2019) and the fact that changing culture medium to MesenPRO instantly removed my own issues, indicates that it is likely some batches of FCS serum used in 10 % D-MEM were lacking an element essential to ADSC growth. The composition of serum supplement must be different in MesenPRO resulting in more reliable growth in ADSC culture.

The ADSCs used in this project have been characterised the evidence suggests that the isolation technique used is leading to ADSC cultures. Furthermore, this culturing process has been optimised by altering the medium used to ensure ADSC growth and survival for use in this research.

In conclusion, the formulations I will be using to test on myofibroblast differentiation have established. These are formulations used today in a clinical setting and work in this chapter has demonstrated these formulations behave as the literature expects. This work has optimised the processing techniques used to generate these formulations, identified the cellular populations contained within each formulation, and demonstrated how processing affects metabolic activity, lysis, and cell concentration within each formulation.

Chapter 4: Investigating the ability of factors from adipose tissue to inhibit a myofibroblast phenotype

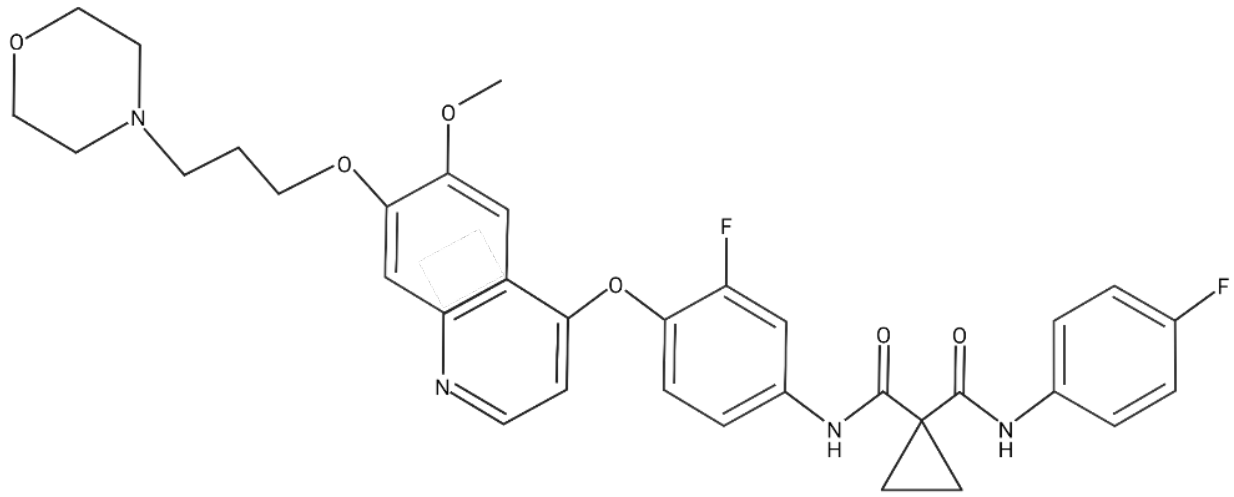

4.1. Introduction and aims

Hypertrophic scars are caused by excessive deposition of collagen following traumatic or repeated injury. These injuries lead to dysregulation of extracellular matrix (ECM) synthesis and excessive production of ECM from myofibroblasts. At the same time, the breakdown of collagen by matrix metalloproteinases is decreased. The myofibroblast is a key effector cell in this process due to their ability to produce increased amounts of ECM components such as collagen. As such, one of the key stages in the formation of hypertrophic scars is the differentiation of fibroblasts to myofibroblasts by transforming growth factor-β (TGF-β) 1 via the SMAD signalling pathway.

Significant research has been carried out to investigate whether it is possible to disrupt the TGF-β1/SMAD signalling pathway in fibrosis. Ai *et al.* (2015) used the molecule GQ5 from the resin of the plant *Toxicondendron vernicifluum* to disrupt the phosphorylation of SMAD3. When used in a rat model GQ5 was able to reduce the expression of fibrotic genes. The molecule hepatocyte growth factor (HGF) has been found to inhibit SMAD signalling in multiple ways; for example, by blocking SMAD2/3 translocation into the nucleus, stabilising the SMAD co-repressor transforming growth interacting factor, and by inducing the expression of the SMAD co-repressor SnoN (Dai & Liu, 2004; J. Yang *et al.,* 2003, 2005). As well as this, Hou *et al.* (2005) found that by increasing expression of SMAD7, which in turn inhibits SMAD3 phosphorylation, they were able to prevent fibrosis from developing in rat kidneys.

Since the discovery by Rigotti *et al.* (2007) that subcutaneous injections of adipose tissue can lead to tissue regeneration, research has been carried out to investigate the underlying mechanisms behind these observations, much of which has centred around ADSC. Spiekman *et al.* (2014) demonstrated that paracrine factors secreted from ADSC were able to inhibit myofibroblast differentiation and other groups have since demonstrated that factors from ADSC can influence the TGF-β1 signalling pathway (Ejaz *et al.,* 2019; Ma *et al.,* 2020; Rathinasabapathy *et al.,* 2016). Despite this, there has been little interest as to whether paracrine factors from adipose tissue, as opposed to monocultured ADSC, can interfere with the TGF-β1 signalling pathway.

In the previous chapter, various formulations of adipose tissue were characterised and the cellular components present post processing were described. The aims of the chapter were to:

- Test whether growth factors released by adipose tissue-derived conditioned medium inhibit TGF-β1 dependent myofibroblast differentiation.
- Elucidate the mechanism behind any inhibitory effect.
- Examine which component(s) of adipose tissue are responsible for any inhibition?

4.2 Results

4.2.1 Analysing the effect of TGF-β1 on fibroblasts

4.2.1.1 Gene expression of myofibroblast markers following TGF-β1 treatment

Myofibroblasts are often characterised by an increase in α-smooth muscle actin (α-SMA) and ECM production (Hinz *et al.,* 2001). TGF-β1 has long been reported to induce differentiation of fibroblasts to a myofibroblast phenotype (Desmouliere *et al.,* 1993). To test whether TGF-β1 is a suitable molecule for inducing myofibroblast differentiation in fibroblasts, the gene expression of three characteristic myofibroblast markers were examined in fibroblasts incubated with TGF-β1 for 24, 48, or 72 hours. Human dermal fibroblasts were treated with TGF-β1 as described in section 2.4.4.1 and gene expression of Col1A1, FN1-EDA, and α-SMA was quantified as described in section 2.4.4.2 and 2.4.4.3. Gene expression was compared to the housekeeping gene RNU6-1.

The expression of α-SMA remained similar at all time points in TGF-β1 treated and untreated cells, relative to RNU6-1 (figure 4.1). There was a small increase in the mean α-SMA expression when fibroblasts were treated with TGF-β1 for 48 hours (2.6 times the expression of RNU6-1 compared to 2.0 in untreated cells), however this difference was not significant ($p = 0.70$). There was an increase in the mean fibronectin expression in TGF-β1 treated fibroblasts compared to untreated cells at the 24 hour time point which was not significant ($p = 0.55$). After 48 hours of TGF-β1 treatment, there was a significant increase in fibronectin expression compared to untreated cells (0.9 to 7.1 times expression relative to RNU6-1, $p < 0.05$). Fibronectin mRNA expression in fibroblasts treated with TGF-β1 for 72 hours was unchanged compared to untreated cells. The addition of TGF-β1 to fibroblasts increased collagen l expression relative to RNU6-1 when compared to untreated fibroblasts. This increase was found after 24, and 48 hours and there was a significant increase of 1.1 to 4.9 times relative expression after 72 hours of TGF-β1 treatment compared to untreated cells ($p < 0.05$).

These results show that fibroblasts treated with TGF-β1 express increased amounts of collagen l and fibronectin mRNA, which is characteristic of a myofibroblast phenotype. TGF-β1 treatment did not significantly alter α-SMA expression at the time points measured. However, mRNA can be present for short time periods (Yang *et al.,* 2003) and thus mRNA expression may not fully reflect cell phenotype. To further test whether TGF-β1 can alter α-SMA expression, protein analysis was carried out.

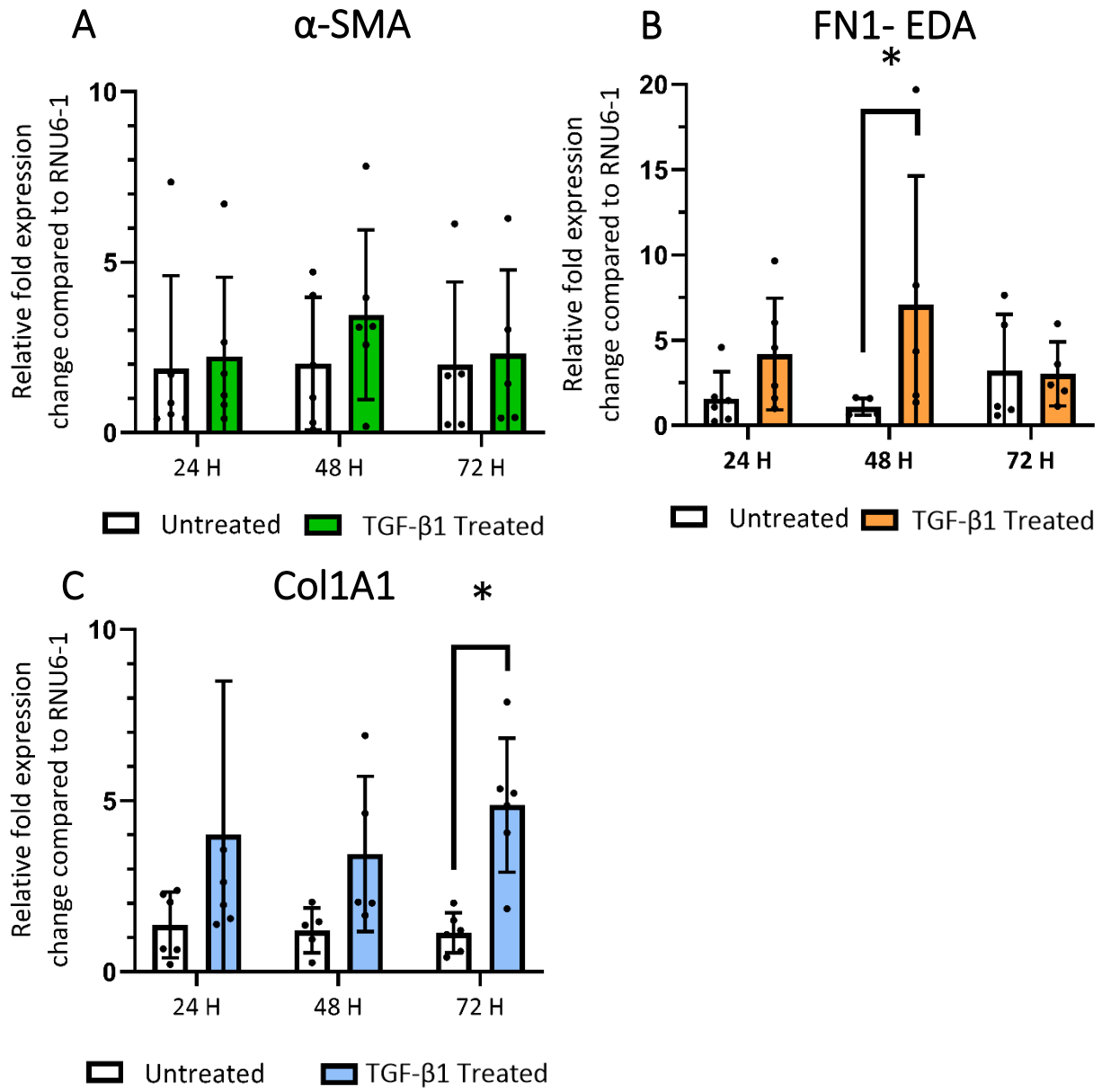

Figure 4.1. Expression levels of mRNA characteristic of a myofibroblast phenotype relative to RNU6-1. (A) α-SMA expression **(B)** FN1-EDA expression **(C)** COL 1-A1 expression. Gene expression was calculated using the $2^{-\Delta\Delta CT}$ method, normalising to RNA expression levels from RNU6-1. A two-way analysis of variance (ANOVA) was carried out comparing the expression of TGF-β1 treated and untreated fibroblasts. *N* = 6 (24 hours), 5 (48 and 72 hours), *n* = 3. Error bars = standard deviation. * = $p < 0.05$.

4.2.1.2 Protein analysis of TGF-β1 treated fibroblasts

To examine the effect of TGF-β1 on α-SMA protein expression in fibroblasts, western blotting analysis was carried out on protein lysate from fibroblasts treated with TGF-β1 for 24 and 72 hours. HDF were passaged as described in section 2.3.2 and seeded at 35,000 cells per well. Cells were treated with TGF-β1, and a western blot was carried out as described section 2.4.5. The amount of α-SMA protein present in the protein lysate was compared to the constitutively expressed protein, GAPDH, by densitometry (see section 2.4.5.5). There was no change in the amount of α-SMA protein expressed by untreated cells compared with cells treated with TGF-β1 for 24 hours (figure 4.2A). At the 72-hour timepoint, untreated cells expressed 0.3 times as much α-SMA protein as GAPDH. When TGF-β1 was added to fibroblasts for 72 hours, α-SMA expression relative to GAPDH protein was significantly increased compared to untreated cells (1.3 times that of GAPDH, $P < 0.03$, figure 4.2B).

Taken together, the increase in gene expression of collagen and fibronectin and protein expression of α-SMA shows TGF-β1 treatment increases markers of myofibroblast differentiation in fibroblasts. Henceforth, TGF-β1 was used to simulate scar induced myofibroblast differentiation in fibroblasts. Incubation with TGF-β1 for 72 hours was used to examine the effects paracrine factors from adipose tissue had on myofibroblast differentiation.

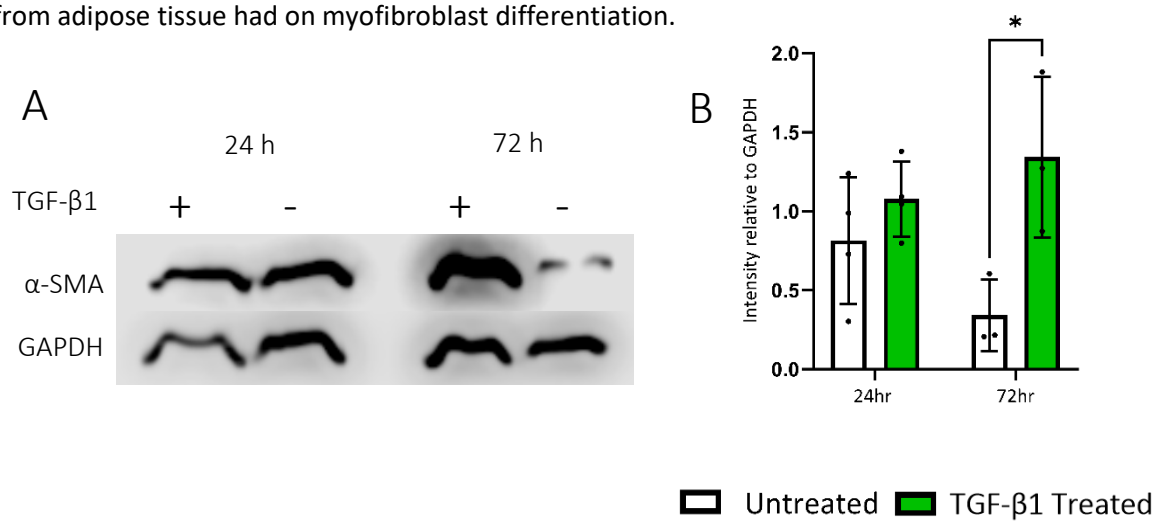

Figure 4.2. α-SMA protein expression following treatment with TGF-β1. (A) Representative western blots probed for α-SMA and loading control GAPDH. **(B)** Relative densitometry values of protein bands. *N* = 4 (24 hours) / 3 (72 hours) *n* = 1, error bars = standard deviation. A two-way ANOVA was carried out to compare the relative intensity of protein bands in TGF-β1 treated and untreated cells. * = P > 0.03.

4.2.2 The effect of adipose tissue-derived conditioned medium on myofibroblast markers in cells treated with TGF-β1

To examine the effect that paracrine factors from adipose tissue have on the TGF-β1/SMAD signalling pathway, adipose tissue was used to condition cell culture medium. TGF-β1 was added to fibroblasts alongside adipose tissue-derived conditioned medium. Medium was conditioned with either minced adipose tissue, lipoaspirate, emulsified fat, lipocondensate, ADSCs, lipid. A control of serum free MesenPRO alongside TGFβ-1 and free lipid added on top was also used. Changes to the levels of markers of myofibroblast differentiation: collagen, fibronectin and α-SMA, were used to quantify the impact of paracrine factors from adipose tissue on myofibroblast differentiation (figure 4.3).

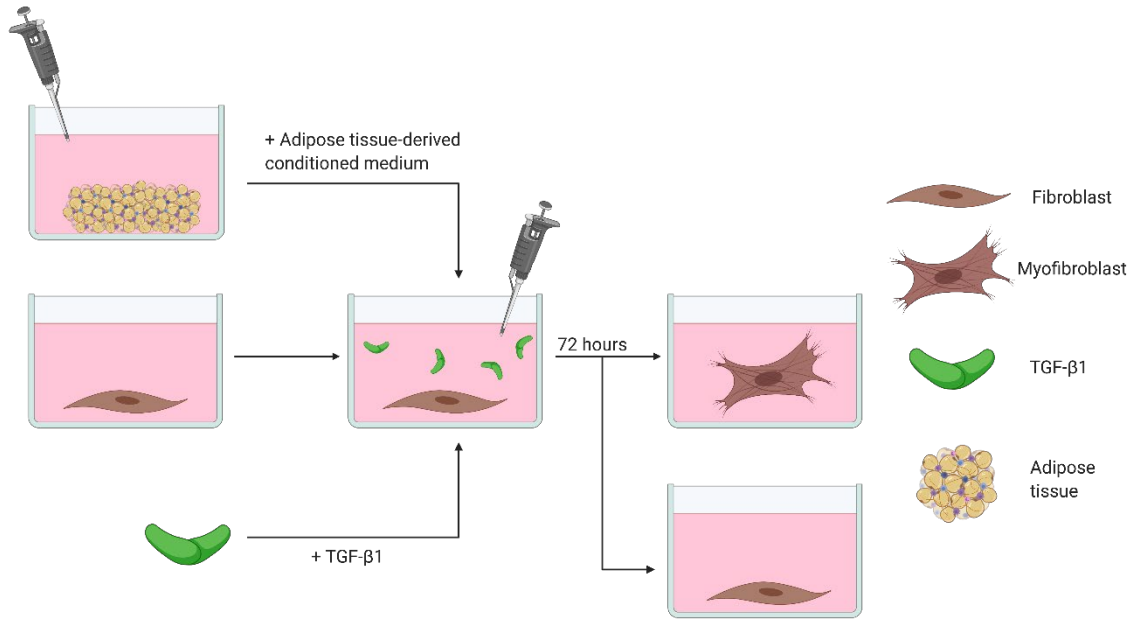

Figure 4.3. Experimental design for examining the effect of adipose tissue-derived conditioned medium on TGF-β1 induced myofibroblast differentiation.

4.2.2.1 Gene expression of myofibroblast markers following TGF-β1 treatment alongside adipose tissue-derived conditioned medium

To examine the effect of adipose tissue-derived conditioned medium upon TGF-β1 treatment of fibroblasts, gene expression levels of fibronectin and collagen were examined (section 2.4.4). Medium conditioned with either minced adipose tissue, emulsified fat, lipocondensate, or free lipid was tested alongside a control containing serum free MesenPRO, TGF-β1 and free lipid added on top of the medium.

There was a large increase in expression levels of fibronectin compared to RNU6-1 in cells treated with TGF-β1 (10.5 times expression of RNU6-1) relative to untreated, control cells ($p = 0.44$). This increase was also present when free lipid was added alongside TGF-β1 (16.1 times expression

compared to RNU6-1, p = 0.09). When medium conditioned with either minced adipose tissue, emulsified fat, or lipocondensate was added to fibroblasts in combination with TGF-β1, there was a decrease in the mean fibronectin expression in comparison to TGF-β1 treated cells (6.1, 7.8, 8.7 times expression respectively, figure 4.4A). However, this expression was still increased compared to the expression of fibronectin in untreated fibroblasts. The only condition under which there was not an increase in fibronectin when cells were treated with TGF-β1 was when fibroblasts were treated with lipid medium and TGF-β1, with the expression of fibronectin at 0.6 times expression relative to RNU6-1.

When examining gene expression levels of collagen compared to RNU6-1, fibroblasts treated with: TGF-β1, TGF-β1 and free lipid, and TGF-β1 and lipid conditioned medium, there was an increase in the mean collagen expression levels compared to untreated fibroblasts (2.6, 4.3, 1.8 times expression compared to RNU6-1 respectively). However, mean expression levels of collagen in cells treated with TGF-β1 and minced adipose tissue, emulsified fat, and lipocondensate were either equal with untreated cells (minced adipose tissue conditioned medium, figure 4.4B) or were decreased. Emulsified fat conditioned medium and TGF-β1 treated fibroblasts expressed 0.8 times the amount of collagen as untreated cells. Lipocondensate conditioned medium and TGF-β1 treated fibroblasts expressed 0.7 times the amount of mRNA relative to RNU6-1 although this decrease in both conditions was not significant compared to TGF-β1 treated cells (p = 0.21 and 0.17 respectively).

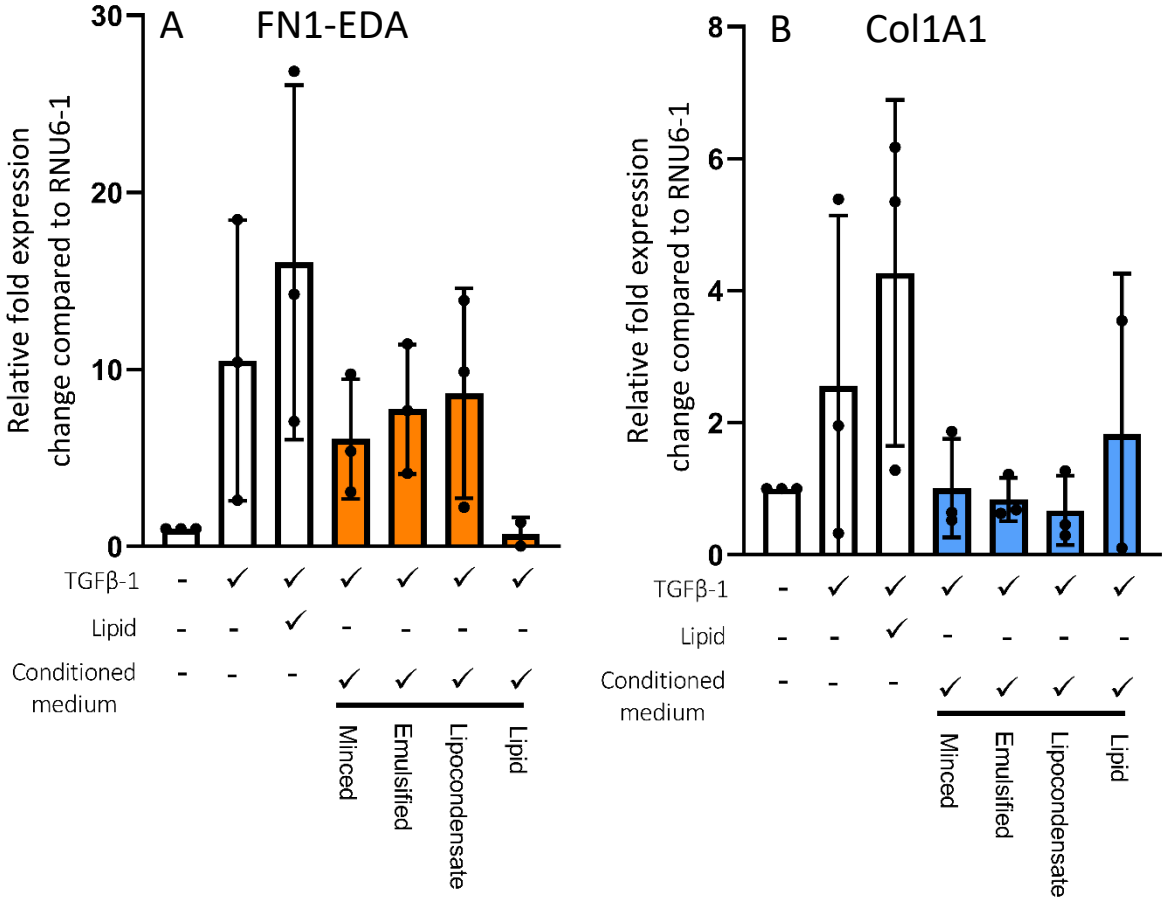

Figure 4.4. Expression levels of mRNA of myofibroblast markers in adipose tissue-derived conditioned medium and TGF-β1 treated fibroblasts. (A) FN1-EDA expression and **(B)** COL1A1 expression. Gene expression was calculated using the $2^{-\Delta\Delta CT}$ method, normalising to RNA expression levels from RNU6-1. Coloured bars represent cells treated with conditioned medium. A One-way ANOVA was carried out comparing the expression of fibroblasts treated with TGF-β1 and various adipose tissue-derived conditioned medium *N* = 3 (*N* = 2 for lipid medium + TGF-β1), *n* = 3. Error bars = standard deviation.

4.2.2.2 Analysis of α-SMA protein expression following treatment of fibroblasts with TGF-β1 and adipose tissue-derived conditioned medium

Following gene expression analysis, the impact that paracrine factors had on TGF-β1 dependent α-SMA expression was measured via western blotting and fluorescent immunocytochemistry (section 2.4.5). Medium conditioned with either minced adipose tissue, emulsified fat, lipocondensate, ADSC, or free lipid was tested alongside a control containing TGF-β1 and free lipid added on top of the medium.

Using western blotting and densitometry analysis, the amount of α-SMA protein expressed by fibroblasts was compared to levels of GAPDH, a constitutively expressed protein (figure 4.5A). Adding TGF-β1 to fibroblasts led to a significant increase in α-SMA expression compared to untreated cells (1.0 to 0.2 times α-SMA protein compared to GAPDH, $p < 0.001$). When fibroblasts were treated with TGF-β1 and either: minced adipose tissue, emulsified fat, or lipocondensate conditioned medium, there was a significant decrease in the levels of α-SMA relative to GAPDH compared to TGF-β1 treated cells (0.1, 0.02, 0.02 relative intensity respectively, $p < 0.001$, figure 4.5B). There was a significant increase in the levels of α-SMA protein levels relative to GAPDH in fibroblasts treated with TGF-β1 and free lipid when compared to untreated cells ($p < 0.001$). There was an increase in the mean expression of α-SMA protein in fibroblasts treated with lipid and TGF-β1 or ADSC conditioned medium compared to untreated cells (1.2 and 0.7 relative intensity respectively) however, this increase was not significant.

Immunofluorescent staining of cells with 4',6-diamindino-2-phenylindole (DAPI) stain and an anti-α-SMA- Fluorescein isothiocyanate (FITC) conjugated antibody was used to assess the percentage population of cells expressing α-SMA protein. In untreated cells, 2.0 % of the cellular population were expressing α-SMA protein (figure 4.6A). There was an increase in the mean percentage of α-SMA positive cells when treated with TGF-β1 (52.5 %). When cells were treated with TGF-β1 and conditioned medium from either minced adipose tissue, emulsified fat, or lipocondensate there was a decrease in the mean percentage population of cells expressing α-SMA. Only 0.5 % of minced adipose tissue and TGF-β1 treated cells expressed α-SMA, 2.5 % of emulsified fat and TGF-β1 treated cells expressed α-SMA, and 0.87 % of lipocondensate and TGF-β1 treated cells expressed α-SMA (figure 4.6C-E). There was an increase in the mean percentage population of α-SMA expressing cells when cells were treated with TGF-β1 and either free lipid, lipid conditioned medium or ADSC conditioned medium at 26.6 %, 40.3 %, and 42.7 % respectively. Following a Kruskal-Wallace test, there was a significant difference between the means in this data set ($p = 0.036$), however there was no significance between individual means (discussed later in section 4.3.2).

Taken together, the α-SMA protein and fibronectin and collagen mRNA expression data appears to show that paracrine factors from minced adipose tissue, emulsified fat, and lipocondensate can inhibit the characteristic increase in myofibroblast markers from TGF-β1 dependent differentiation of fibroblasts. This poses the question as to which factors from the adipose tissue-derived conditioned medium are responsible for this effect?

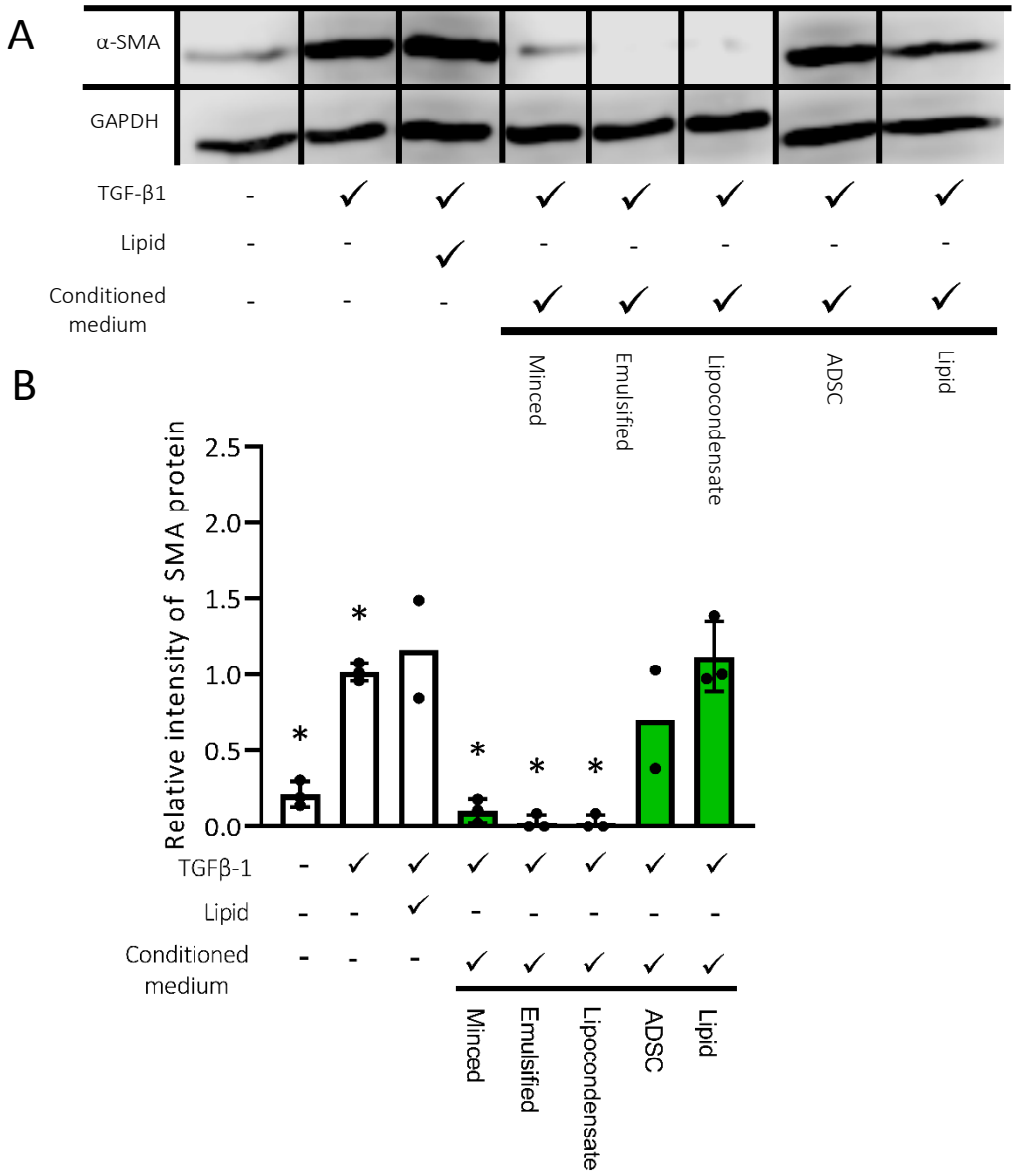

Figure 4.5. α-SMA protein expression following treatment with TGF-β1 and adipose tissue-derived conditioned medium. **(A)** Representative western blots of fibroblasts treated with TGF-β1 and various forms of adipose tissue-derived conditioned medium stained for α-SMA and loading control GAPDH. **(B)** Relative densitometry values of protein bands. Coloured bars represent cells treated with conditioned medium. *N* = 3 (*N* = 2 for Lipid medium + TGF-β1 and ADSC + TGF-β1) *n* = 1. Error bars = standard deviation. * = $p < 0.05$ compared to TGF-β1 positive control.

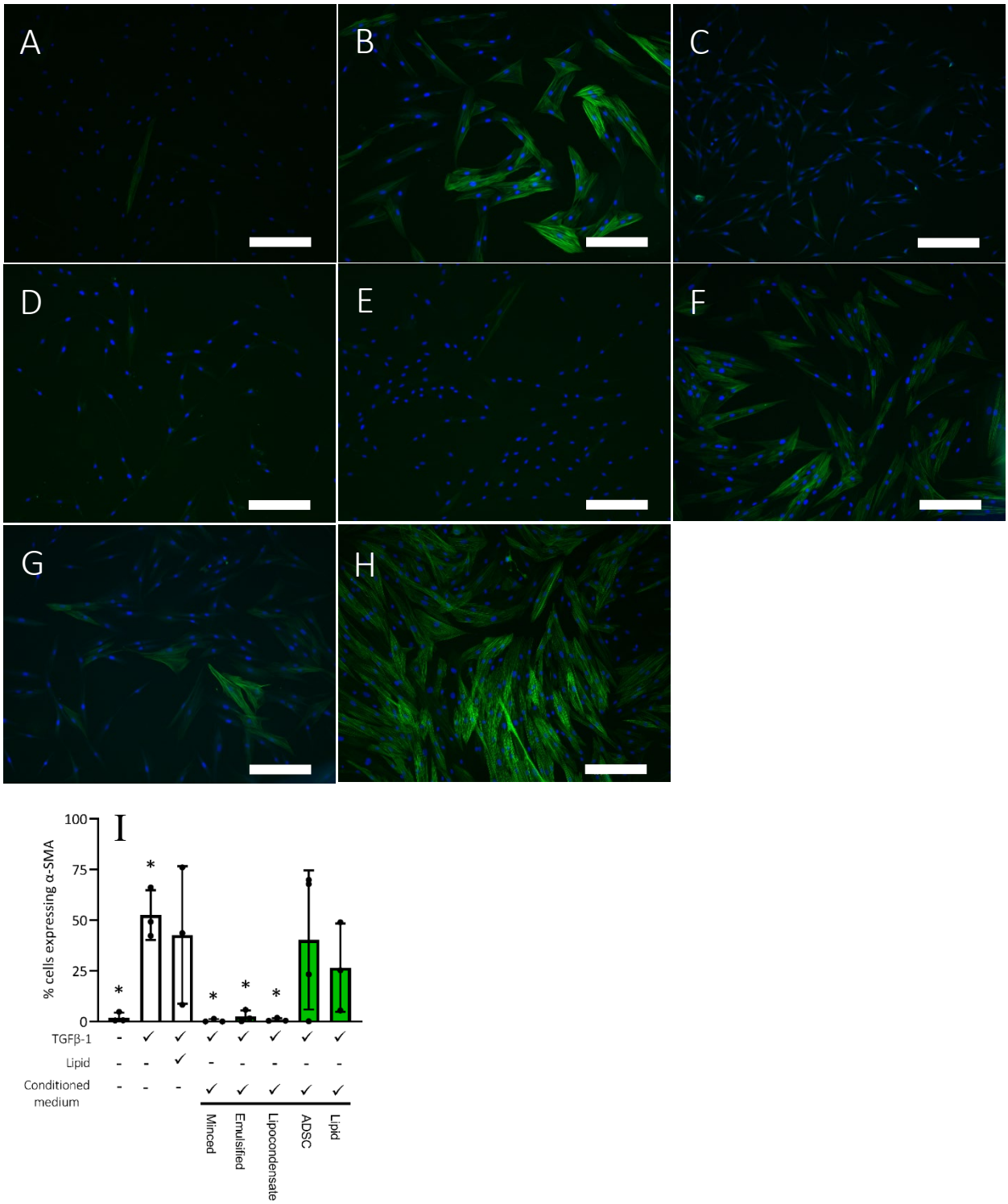

Figure 4.6. Immunofluorescence analysis of the effect of adipose tissue-derived conditioned medium on TGF-β1 dependent α-SMA expression. (A-H) Representative immunofluorescence images of cells stained for nuclei (blue) and α-SMA fibres (green). Fibroblasts were treated with **(A)** untreated, **(B)** TGF-β1, **(C)** TGF-β1 + minced adipose tissue-derived conditioned medium, **(D)** TGF-β1 + emulsified fat conditioned medium, **(E)** TGF-β1 + lipocondensate conditioned medium, **(F)** TGF-β1 + ADSC conditioned medium, **(G)** TGF-β1 + Lipid conditioned medium, **(H)** and TGF-β1 + free lipid. **(I)** The percentage of the cellular population per field of view was calculated from images and tabulated. Scale bar = 200 μm, *N* = 3 (N = 4 for ADSC + TGF-β1), *n* = 3. Coloured bars represent cells treated with conditioned medium. Error bars = standard deviation. * = $p < 0.04$ compared to TGF-β1 positive control.

4.2.3 Analysis of cytokines present in adipose tissue-derived conditioned medium

4.2.3.1 Examination of conditioned medium via cytokine array

Data from section 4.2.2 suggests that adipose tissue-derived conditioned medium can inhibit TGF-β1 dependent fibroblast differentiation. A cytokine array was used to identify which paracrine factors were present in the adipose tissue-derived conditioned medium and thus may be responsible for the above effect. A cytokine array containing various molecules implicated in the inhibition of TGF-β1 signalling was selected. Conditioned medium from minced adipose tissue, lipoaspirate, emulsified fat, lipocondensate, ADSC, and free lipid was applied to the array. The relative abundance of target cytokines compared to serum free MesenPRO was calculated by densitometry of the antibody dots in each blot (section 2.4.6.1 and 2.4.6.2). Groups of cytokines were analysed first with fibroblast growth factor (FGF) proteins, interleukin (IL) proteins, and TGF-β1 proteins assessed. The cytokine array only contained enough reagents to test adipose tissue-derived conditioned medium once and thus significance cannot be drawn from the data. In an attempt to minimise the effect of patient-to-patient variation, media was collected from three different patients and pooled together before testing.

FGF proteins were found in relatively low quantities (figure 4.7A), FGF-4, -6, -7, and -9 were found to be present at baseline levels in all conditioned media except for FGF-9 from emulsified fat conditioned medium (2.2 times relative intensity compared to serum free MesenPRO). TGF-β1, -2, and -3 were found to be present however, in concentrations similar to that of serum free MesenPRO (figure 4.7B).

Most ILs were present in similar quantities in conditioned medium compared to serum free MesenPRO. Notable exceptions to this were IL-6, -7, -8, -10, and -16 (figure 4.7C). IL-7, -10 and -16 had high quantities present in only one form of conditioned medium. IL-7 was found to be present in lipocondensate conditioned medium at 6.7 times the amount found in serum free MesenPRO. Levels of IL-10 were found to be high in minced adipose tissue conditioned medium (3.2 times relative intensity to serum free MesenPRO) and emulsified fat conditioned medium contained 4.6 times the amount of IL-16 relative to serum free MesenPRO. Concentrations of IL-8 increased as adipose tissue was processed from minced adipose tissue to emulsified fat to lipocondensate as the relative concentration of IL-8 increased from 4.6 times that of serum free MesenPRO in minced adipose tissue to 10.0 in lipocondensate conditioned medium. IL-8 concentrations then dropped in ADSC conditioned medium with 3.5 times relative intensity compared to serum free MesenPRO and was found to be present at lower levels than baseline in lipid conditioned medium. The highest concentration of any cytokine tested on the array was IL-6. The relative intensity of spots from

minced adipose tissue, lipoaspirate, emulsified fat, lipocondensate, and ADSC conditioned medium was exceptionally high (29.3, 39.2, 49.3, 59.7, 34.3 times relative to serum free MesenPRO respectively). However, the amount of IL-6 found in lipid conditioned medium was lower than that of serum free MesenPRO with 0.5 times the intensity relative to the serum free media.

To select target factors for further analysis, cytokines present in amounts more than 10 times that of serum free MesenPRO were selected and analysed (figure 4.8). A brief search of the literature was carried out on these molecules to identify if any anti-fibrotic effects had been previously observed (table 4.1). Cytokines IL-6, angiogenin, tissue inhibitor of metalloproteinases (TIMP)-2, and HGF were found in the highest abundance out of all cytokines across the array with a relative intensity of 59.7, 40.4, 33.5, and 28.0 times that of serum free MesenPRO respectively. The highest concentration of IL-6 was found in lipocondensate conditioned medium, the highest TIMP-2 concentration was found in lipoaspirate conditioned medium and the highest angiogenin and HGF levels were found in emulsified fat conditioned medium.

Following the literature search, CXCL1 (18.1 times relative intensity compared to serum free medium), CXCL9 (12.5 times relative intensity compared to serum free medium) and HGF were found to have recorded anti-fibrotic properties or mechanisms in fibroblasts. Given the high levels of abundance found in conditioned medium isolated from minced adipose tissue, emulsified fat, and lipocondensate, which were found to inhibit TGF-β1 dependent fibroblast differentiation, and well recorded anti-fibrotic properties in the literature, HGF was chosen for further tests as to whether it is responsible for the anti-fibrotic effects of adipose tissue-derived conditioned media.

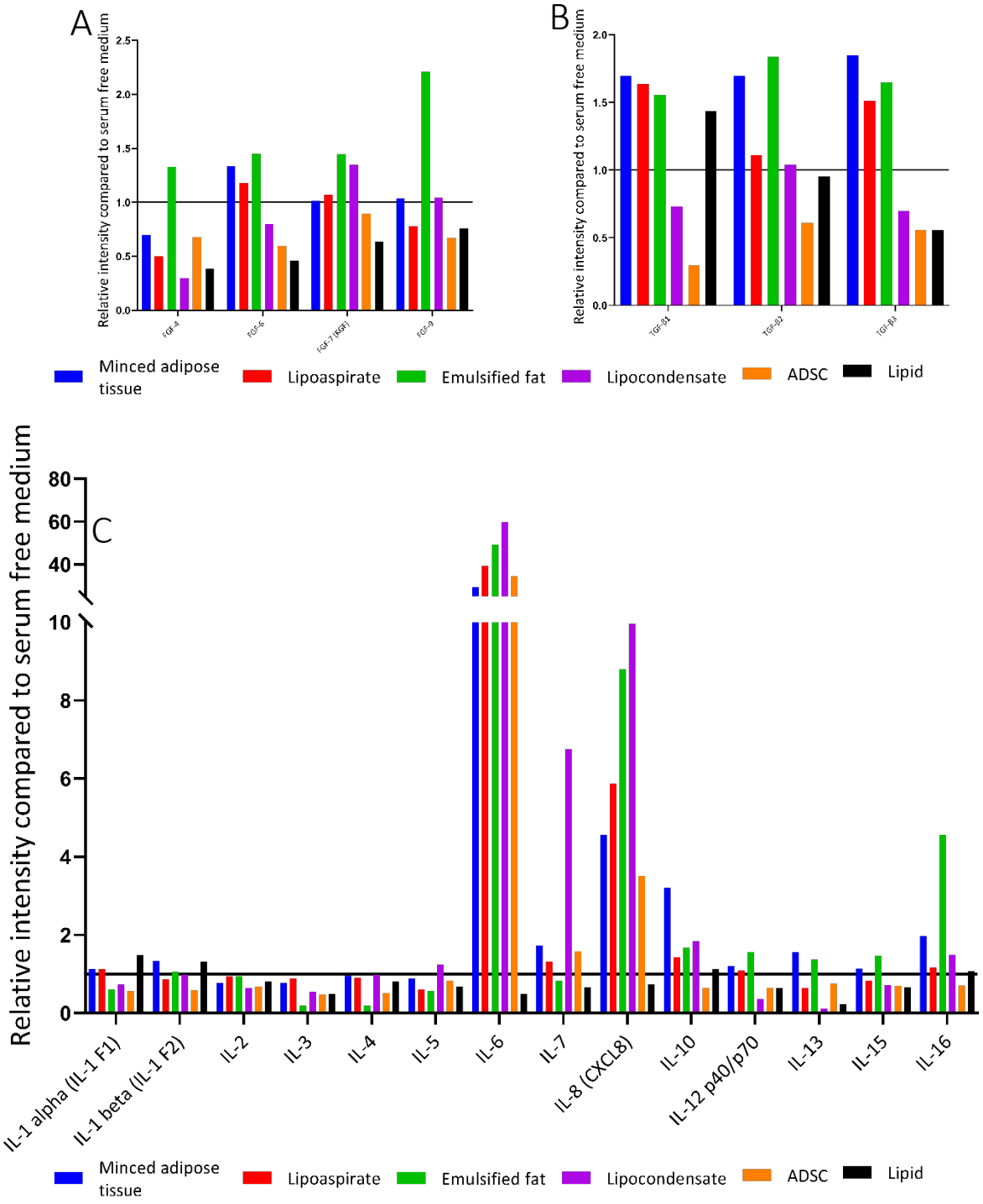

Figure 4.7. Cytokine array analysis of FGF, TGF-β1 and IL proteins. (A-C) Conditioned medium was probed on a cytokine array to assess the abundance of **(A)** FGF, **(B)** TGF-β, **(C)** and IL proteins present in the conditioned medium relative to serum free MesenPRO. *N* = 1, *n* = 1. Black line represents the concentration of the cytokine present in serum free MesenPRO.

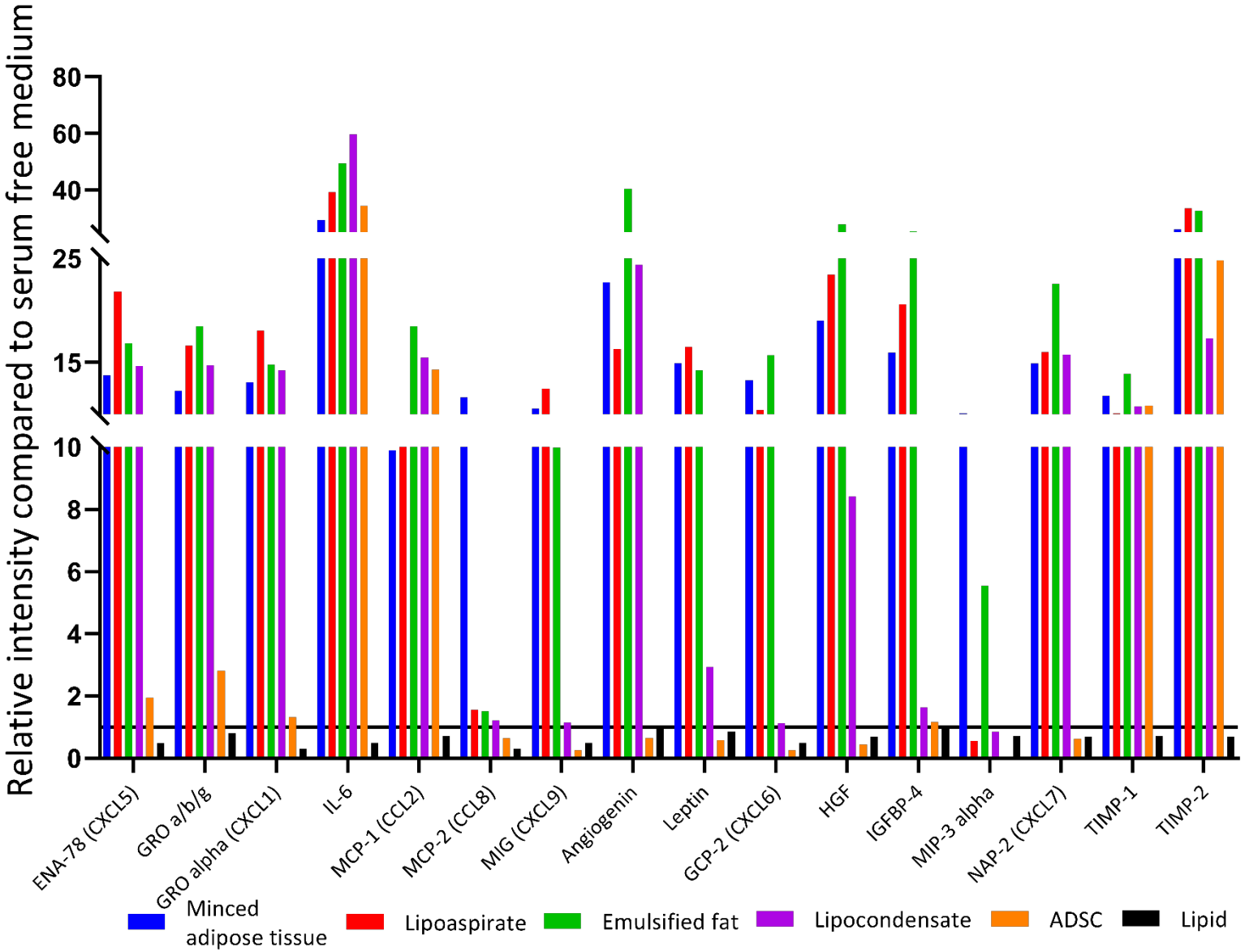

Figure 4.8. Cytokines present in high abundance compared to serum free MesenPRO. Conditioned medium was probed on a cytokine array to assess the abundance of a wide variety of proteins relative to serum free MesenPro. Cytokines present in amounts more than 10 times that of Serum free MesenPRO were plotted in the graph above. *N* = 1, *n* = 1. Black line represents the concentration of the cytokine present in serum free MesenPRO.

Table 4.1. High abundance cytokines. Table of all cytokines from figure 4.8. and literature supporting their pro- and or anti- fibrotic function.

Cytokine	Basic function	Pro or Anti-fibrotic function	Reference
ENA-78 (CXCL5)	Stimulates chemotaxis of neutrophils with angiogenic function.	Pro fibrotic, ENA-78 found in high concentrations in people with idiopathic pulmonary fibrosis.	Keane, *et al.,* (2001)
GRO alpha (CXCL1)	Chemoattractant for neutrophils.	Produced by myofibroblasts in cancer associated fibroblasts, inverse correlation between TGF-β1 signalling and CXCL-1.	Zou, *et al.,* (2014)
IL-6	Pro-inflammatory cytokine, inhibits tumour necrosis factor alpha and IL-1 and IL-10.	Stimulates proliferation and migration of fibroblasts via JAK/STAT and mitogen associated protein kinase pathways. Can stimulate differentiation to myofibroblasts via JAK/ERK Induces Bcl2 in fibroblasts which makes resistant 2 apoptosis.	Johnson, *et al.,* (2020)
MCP-1 (CCL2)	Chemokine responsible for recruiting osteoclasts to bone.	Profibrotic, secreted in high amounts by hepatic myofibroblasts.	Dagouassat, *et al.,* (2009)
MCP-2 (CCL8)	Activates immune cells.	Little evidence of antifibrotic activity. Increases myofibroblast migration.	Torres, *et al.,* (2013)
MIG (CXCL9)	Inflammatory chemokine associated with the function of T-cells.	Found to have general antifibrotic effects in human livers. Can inhibit SMAD signalling via promoting SMAD7 expression.	Wasmuth, *et al.,* (2009) O'Beirne, *et al.,* (2015)
Angiogenin	Promotes angiogenesis and blood vessel growth.	N/A	N/A
Leptin	Adipose hormone, primarily involved in energy regulation.	Increases SMAD2/3 activation in conjunction with TGF-β1 in mice, knockout downplays fibrotic response. Generally, seems to be pro-fibrotic by increasing the differentiation of cells to myofibroblasts via TGF-β1 pathway.	Yang, *et al.,* (2007)
GCP-2 (CXCL6)	Mediates angiogenesis and a chemoattractant to neutrophil granulocytes.	Found in high levels in fibrosis patients promotes fibrosis through JAK-STAT.	Cai, *et al.,* (2018) Sun, *et al.,* (2019)
HGF	Secreted by mesenchymal cells, promotes motility and cellular cascades. Important for organ regeneration.	Inhibits TGF-β1 activation of rat myofibroblasts via inhibition of SMAD2/3 translocating into the cell nucleus, does it by activating ERK signalling, sequestering activated SMAD2/3 away. Down regulates IL proteins.	Yang, *et al.,* (2003) Schievenbusch, *et al.,* (2009)
IGFBP-4	Can act as an apoptotic factor in cancer. Binds insulin like growth factors.	Potentially antifibrotic, reduces connective tissue growth factor and collagen expression in TGF-β1 treated fibroblasts.	Su, *et al.* (2019)
MIP-3 alpha	Activator of immune cells (dendrites and neutrophils).	Produced in high amounts post TGF-β1 activation, acts downstream of SMAD signalling.	Brand, *et al.,* (2015)
NAP-2 (CXCL7)	Mediates neutrophil recruitment.	N/A	N/A
TIMP-1	Inhibit metalloprotease function.	Pro-fibrotic.	Johnston & Gillis, (2017)
TIMP-2	Inhibit metalloprotease function.	Pro-fibrotic.	Johnston & Gillis, (2017)
PDGF-BB	Stimulates angiogenesis and granulation tissue.	Profibrotic, stimulates migration of myofibroblasts and may encourage their proliferation.	Tangkijvanuch, *et al.,* (2002)

4.2.3.2 Examination of conditioned medium via HGF ELISA

Cytokine array analysis of conditioned medium used in the preceding section calculates cytokine concentration in a semi-quantitative fashion. Having chosen to investigate the effect of HGF further, a more accurate measure of the concentration of HGF in adipose tissue-derived conditioned medium was required. This would be used to identify the form of conditioned medium containing the highest concentration of HGF to use in future experiments.

To this end, a HGF enzyme-linked immunosorbent assay (ELISA) was carried out as described in section 2.4.6.3 to quantify HGF concentration in conditioned medium from minced adipose tissue, lipoaspirate, minced adipose tissue, emulsified fat, ADSC and lipid. Conditioned medium from minced adipose tissue contained 2.8 ng/ml of HGF (figure 4.9). The highest concentration of HGF was found in lipoaspirate conditioned medium at 6.4 ng/ml which fell to 2.4 ng/ml in emulsified fat. Lipocondensate conditioned medium contained 0.4 ng/ml which was significantly lower than the concentration in lipoaspirate conditioned medium ($p < 0.01$) and ADSC and lipid conditioned medium did not contain enough HGF to give a reading on the ELISA. HGF was found at more than double the concentration in lipoaspirate conditioned medium than that of the next highest condition and thus in future experiments, where possible, lipoaspirate conditioned medium would be used to test the effect of HGF on fibroblast differentiation.

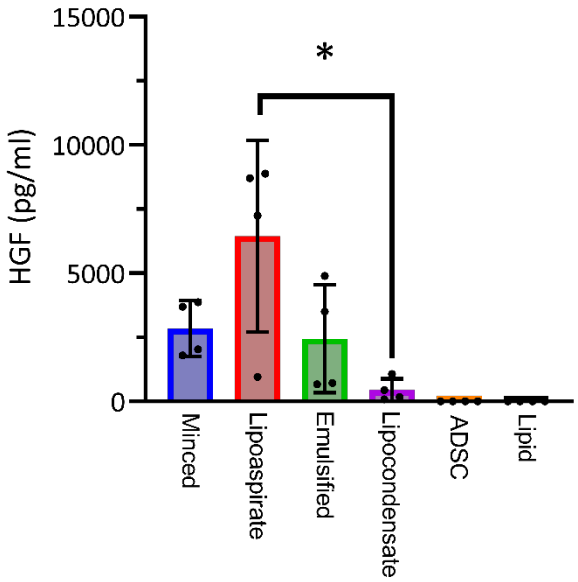

Figure 4.9. Quantification of HGF concentration present in adipose tissue-derived conditioned medium. HGF concentration was quantified via an HGF-ELISA. *N* = 4, *n* = 2, error bars = standard deviation, * = $p < 0.01$ between selected conditions.

4.2.4 Can foretinib restore myofibroblast differentiation from adipose tissue-derived conditioned medium?

Hepatocyte growth factor was identified as one of a number of candidate molecules that may be responsible for adipose tissue-derived conditioned medium's ability to inhibit myofibroblast differentiation. To test whether this is the case, the inhibitor molecule foretinib was used alongside TGF-β1, adipose tissue-derived conditioned medium, and recombinant HGF. Foretinib acts as a competitive inhibitor on the C-Met receptor (figure 4.10), which is the receptor through which HGF acts. Adipose tissue-derived conditioned medium was added to fibroblasts alongside TGF-β1 as described previously in this chapter (section 4.2.2); however, foretinib was added alongside the medium and TGF-β1 (figure 4.11). Markers of myofibroblast differentiation were measured to examine whether foretinib could prevent the inhibitory effect of adipose tissue-derived conditioned medium with the ultimate aim of understanding the molecular mechanism of action.

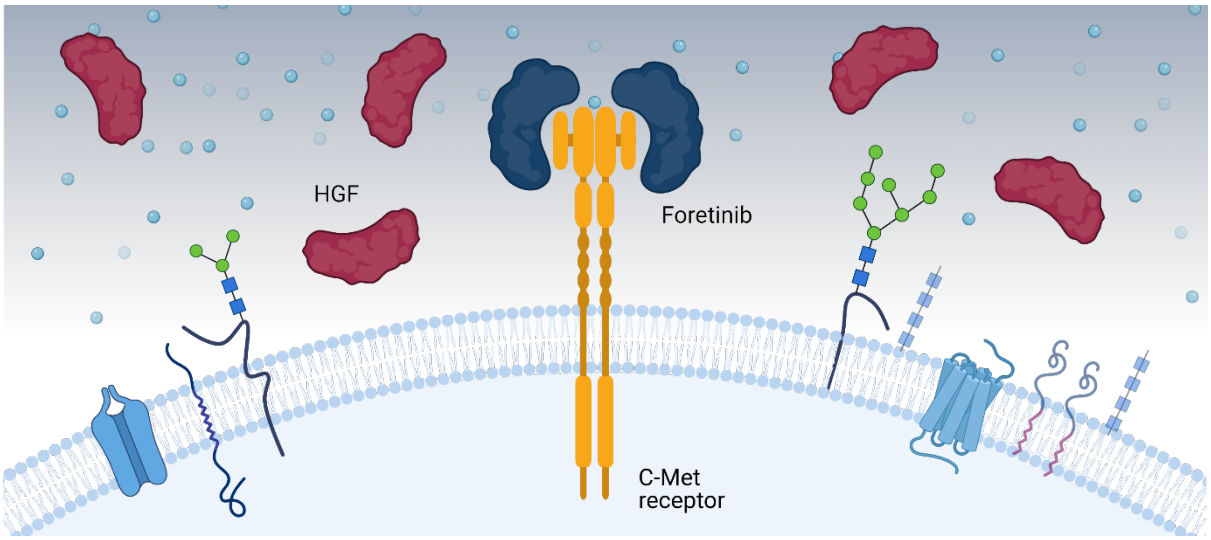

Figure 4.10. Foretinib inhibition of the C-Met receptor. Foretinib acts as a competitive inhibitor to HGF by binding with the C-Met receptor, blocking the binding site from HGF (Sohn et al., 2020; Zillhardt et al., 2011) .

4.2.4.1 Testing the cytotoxicity of foretinib and its solvent vehicle on fibroblasts

Before testing the effect of foretinib on the adipose tissue-derived conditioned medium, it was first required to test whether foretinib, or the concentration of solvent needed to solubilise the foretinib was cytotoxic to fibroblasts. Human dermal fibroblasts were cultured in serum free MesenPRO and 100 % ethanol (1 or 2.5 µl/ml) or dimethyl sulfoxide (DMSO; 1.0, 2.5, or 5.0 µl/ml) were added. A resazurin assay (section 2.4.7) was carried out to examine the effect of the solvent on fibroblast metabolic activity. Fluorescent values at 570 nm were normalised to those of a negative control containing cells cultured in only serum free MesenPRO. A positive control of fibroblasts cultured in 2 % serum MesenPRO saw an increase in the mean fluorescence value to 1.2 times that of the serum free MesenPRO control (figure 4.12A). Fibroblasts were cultured in 1, 2.5, and 5 µl/ml of DMSO following which their metabolic activity was unchanged relative to fibroblasts in serum free MesenPRO (1.0 times fluorescence compared to the negative control in all conditions). When cultured with ethanol there was no change in cell metabolic activity. Fibroblasts cultured in 1 µl/ml absolute ethanol had a relative fluorescent value of 0.9 times that of the negative control as did fibroblasts cultured in 2.5 µl/ml absolute ethanol. Due to this, it was decided to solubilise foretinib in DMSO; as at the concentrations chosen there was little or no effect on cell metabolic activity. While only by a small degree, fibroblasts cultured in 2.5 µl/ml of DMSO had the highest mean metabolic activity of the cells cultured in solvent, thus foretinib was solubilised in 2.5 µl/ml DMSO.

Following this, fibroblasts were cultured in serum free MesenPRO and various concentrations of foretinib. A resazurin assay was carried out to assess the metabolic activity of cells cultured in foretinib to assess the impact of foretinib on fibroblast metabolic activity. Compared to cells cultured in serum free MesenPro, cells cultured in 2 % serum MesenPRO produced fluorescence values of 1.2 times that of the negative control. All cells cultured in foretinib produced similar fluorescence values than the negative control. The metabolic activity of cells was the same regardless of foretinib concentration (figure 4.12B). Cells cultured in 0.4 nM foretinib had a relative fluorescence value of 0.9 times that of cells cultured in serum free MesenPRO. Fibroblasts in 4, 40, and 400 nM foretinib had relative fluorescence values of 0.90 times that of cells cultured in serum free MesenPRO respectively and no concentrations were significantly lower than the negative control. Taken together, these results suggest foretinib is not significantly cytotoxic to fibroblasts. As all concentrations of foretinib resulted in a similar metabolic activity then foretinib was used at 1nM, which is the highest working concentration suggested by the manufacturers.

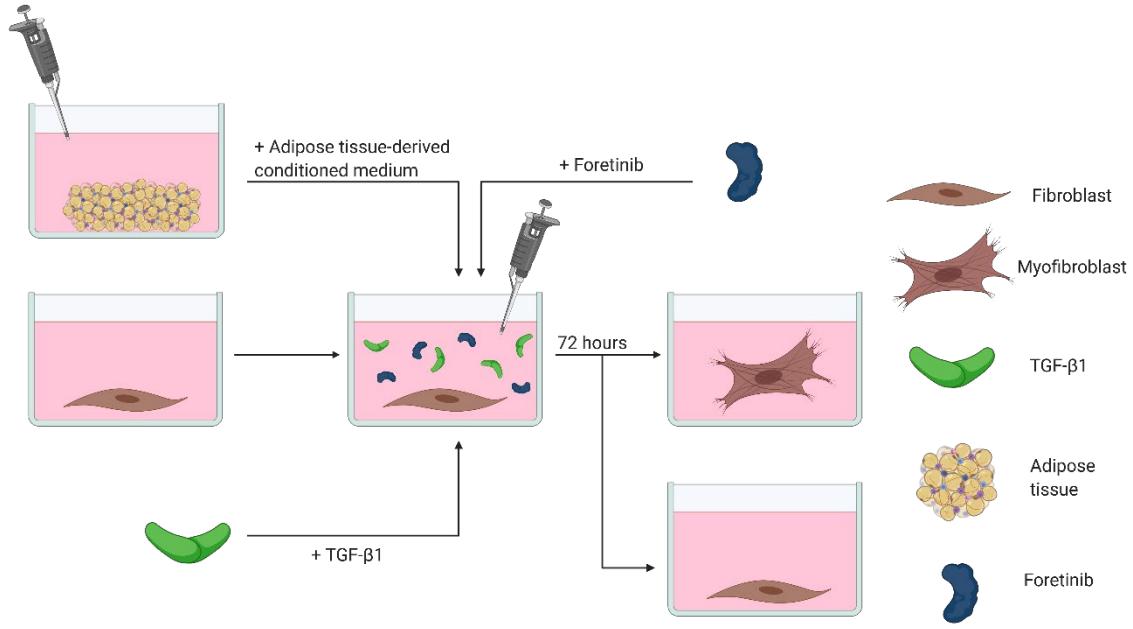

Figure 4.11. Can foretinib restore fibroblast differentiation? Schematic of experimental design to test the effect of foretinib on adipose tissue-derived conditioned medium dependent inhibition of myofibroblast differentiation.

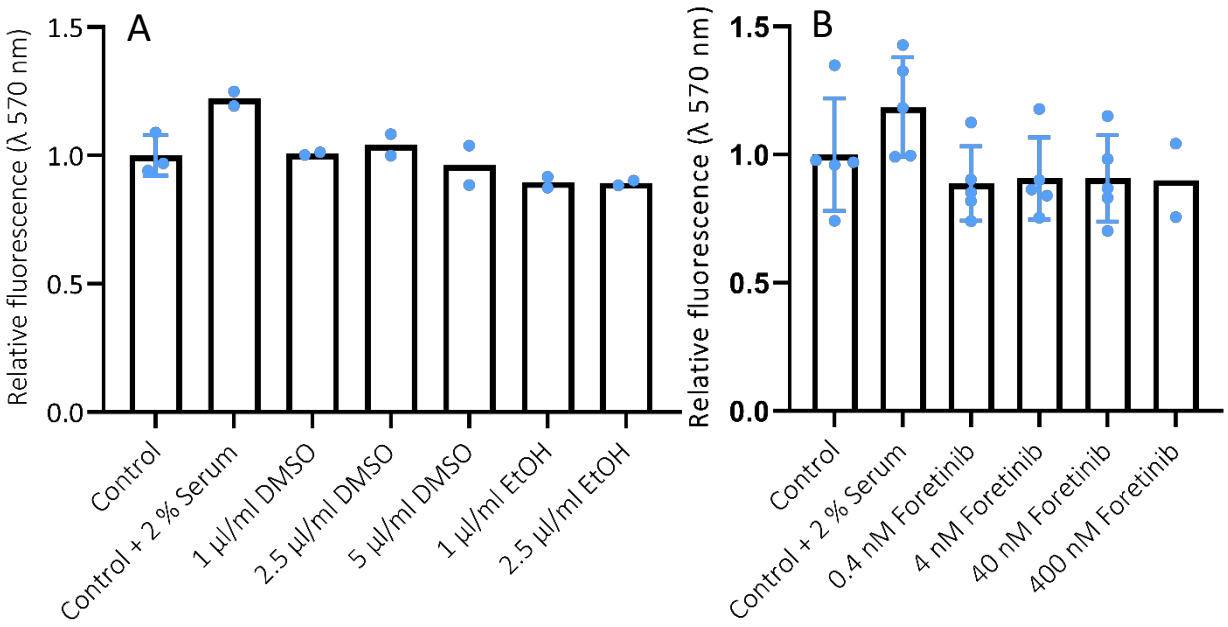

Figure 4.12. Assessing the cytotoxicity of foretinib and its solvent vehicles. (A-B) Fibroblasts were treated with various concentrations of **(A)** DMSO and ethanol and **(B)** foretinib and were incubated with resazurin dye to assess cell metabolic activity. The fluorescence at 570 nm was recorded and normalised to untreated fibroblasts (control). **(A)** *N* = 2 / 3 (Control), *n* = 3. **(B)** *N* = 5 / 2 (400 nM foretinib), *n* = 3, error bars = standard deviation.

4.2.4.2 Does foretinib remove adipose tissue-derived conditioned medium dependent inhibition of α-SMA expression in TGF-β1 treated fibroblasts?

The ability of HGF and adipose tissue-derived conditioned medium to inhibit fibroblast differentiation and for foretinib to remove this inhibitory effect, was tested by analysing the expression of α-SMA protein. HDF were seeded and treated with TGF-β1 as in section 2.4.5.1. Combinations of 40 ng/ml of HGF, 1 nM foretinib, and adipose tissue-derived conditioned medium was added concurrently with TGF-β1. Fluorescent immunocytochemistry and western blotting were carried out to assess α-SMA protein expression. When TGF-β1 treated cells were stained for nuclei and α-SMA fibres, 48.7 % of cells were expressing α-SMA, which was significantly higher than untreated fibroblasts (15.4 %, figure 4.13B, $p < 0.05$). When cells were treated with TGF-β1 and 40 ng/ml of HGF the percentage of cells expressing α-SMA increased to 64.1 % which was also significantly higher than untreated cells ($p < 0.01$). When 1 nM foretinib was added to fibroblasts alongside HGF and TGF-β1, 46.7 % of cells expressed α-SMA, this decrease in the mean was not significant compared to TGF-β1 treated cells ($p = 0.66$). When lipoaspirate conditioned medium was added to fibroblasts in combination with TGF-β1 there was a significant decrease in the percentage of cells expressing α-SMA compared to TGF-β1 treated fibroblasts (48.7 % to 8.8 %, $p < 0.05$, figure 4.13H). When foretinib and lipoaspirate conditioned medium were added to cells alongside TGF-β1 the percentage of cells expressing α-SMA was 20.7 %. This was significantly lower than the percentage of cells expressing α-SMA following TGF-β1 and HFG treatment (64.1 %, $p < 0.01$).

Using western blotting techniques, the amount of α-SMA protein being expressed by fibroblasts relative to the constitutive protein β-actin was assessed. When treated with TGF-β1, there was an increase in the mean α-SMA protein expressed compared to untreated fibroblasts (0.5 to 1.2 times relative intensity to β-actin, $p = 0.17$, figure 4.14B). Fibroblasts treated with TGF-β1 and 40 ng/ml of HGF expressed a similar amount of α-SMA protein to TGF-β1 treated fibroblasts relative to β-actin (1.0 times relative intensity to β-actin). The mean α-SMA expression was lower when fibroblasts were treated with TGF-β1, HGF and 1 nM foretinib (0.7 times relative intensity) however, this was not significant compared to TGF-β1 treated cells ($p = 0.3$). When lipoaspirate conditioned medium was added alongside TGF-β1 to fibroblasts there was a decrease in mean α-SMA expression to 0.4 times relative intensity to β-actin but once again, this was not significant ($p = 0.06$). The cells with the lowest expression of α-SMA protein were fibroblasts treated with TGF-β1, fat conditioned medium, and 1 nM foretinib at 0.14 times relative intensity to β-actin, this was significantly lower than cells treated with TGF-β1 and cells treated with TGF-β1 and HGF ($p < 0.05$).

Taken together, the immunofluorescence and western blotting data suggests that HGF does not play a role in TGF-β1 dependent differentiation of fibroblasts to myofibroblasts under the

conditions tested and that foretinib is not capable of restoring myofibroblast differentiation in adipose tissue conditioned media treated fibroblasts.

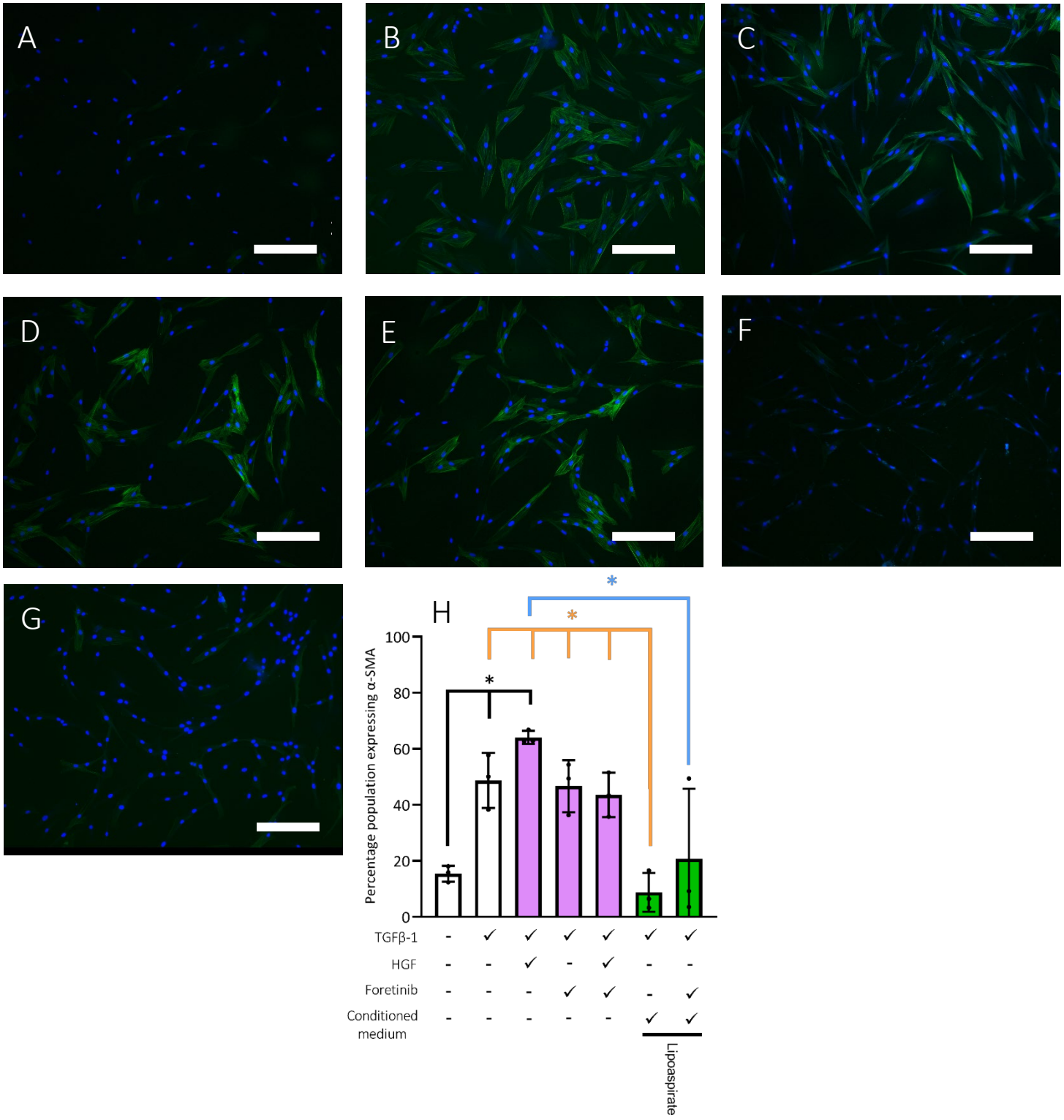

Figure 4.13. Fluorescent staining of α-SMA following TGF-β1 and foretinib treatment. (A-H) Representative immunofluorescence images of cells stained for nuclei (blue) and α-SMA fibres (green). Fibroblasts were treated with **(A)** nothing / control, **(B)** TGF-β1, **(C)** TGF-β1 + 40 ng/ml HGF, **(D)** TGF-β1 + 1 nM foretinib, **(E)** TGF-β1 + 40 ng/ml HGF + 1 nM foretinib, **(F)** TGF-β1 + lipoaspirate conditioned medium, **(G)** and TGF-β1 + lipoaspirate conditioned medium + 1 nM foretinib. **(H)** The percentage of the cellular population per field of view was calculated from images and tabulated. Scale bar = 200 µm. *N* = 3, *n* = 3. Error bars = standard deviation. Purple coloured bars represent cells treated with HGF and/or foretinib, green coloured bars represent cells treated with conditioned medium. Black * = $p < 0.05$ compared to basal medium control, orange * = $p < 0.05$ compared to TGF-β1 and lipoaspirate conditioned medium treated cells, blue * = $p < 0.01$ compared to TGFβ-1, lipoaspirate conditioned medium and foretinib treated cells.

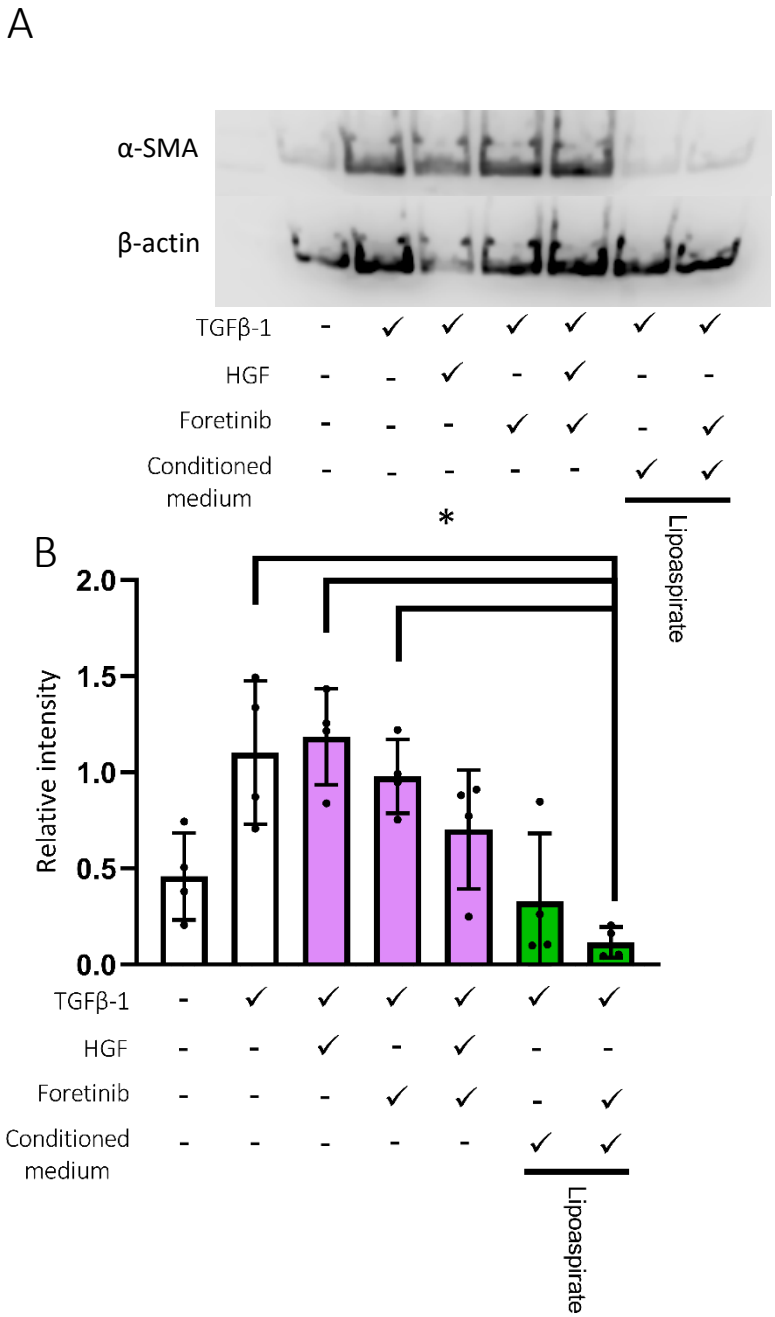

Figure 4.14. α-SMA protein expression following treatment with TGF-β1 and adipose tissue-derived conditioned medium. (A) Representative western blots of fibroblasts treated with TGF-β1, HGF, foretinib, and adipose conditioned medium stained for α-SMA and loading control β-actin. **(B)** Relative densitometry values of protein bands. $N = 3$, $n = 1$. Error bars = standard deviation. Purple bars represent cells treated with HGF and/or Foretinib, green bars represent cells treated with conditioned medium. * = $p < 0.05$ compared to cells treated with TGF-β1, foretinib and conditioned medium.

4.3 Discussion

The aims of this chapter were to:

- Test whether growth factors released by adipose tissue-derived conditioned medium inhibit TGF-β1 dependent myofibroblast differentiation.
- Elucidate the mechanism behind any inhibitory effect.
- Examine which component(s) of adipose tissue are responsible for any inhibition

4.3.1 Differentiation of fibroblasts to myofibroblasts

The work in this chapter has demonstrated that the addition of adipose tissue-derived conditioned medium to TGF-β1 treated dermal fibroblasts inhibited myofibroblast differentiation. Firstly, a model for myofibroblast differentiation was established. The addition of TGF-β1 led to an increase in myofibroblast differentiation. When cells were treated with TGF-β1, there was a significant increase in fibronectin and collagen gene expression (figure 4.1B-C) implying fibroblasts are undergoing differentiation upon TGF-β1 treatment. Although it should be noted that α-SMA mRNA expression in TGF-β1 treated fibroblasts did not differ from that of untreated cells (figure 4.1A). Of the time points examined, fibronectin gene expression relative to untreated cells was highest at 48 hours, while collagen gene expression compared to untreated cells was unchanged after 24 hours before increasing after 48 hours. When examining protein data, western blotting showed that after 72 hours of TGF-β1 treatment there was a significant increase in α-SMA expression compared to untreated cells (figure 4.2).

One of the difficulties that investigators face when carrying out research on myofibroblasts is the lack of definition as to what a myofibroblast is. There are many different markers used in the literature however none are unique to the myofibroblast. A common compromise to this problem is to use a combination of different markers to define whether a fibroblast has differentiated to a myofibroblast. Markers of myofibroblast differentiation range from cytoskeletal proteins, surface markers, and ECM proteins (reviewed in Hinz, 2007).

The markers initially chosen to characterise TGF-β1 dependent differentiation of fibroblasts in this work were α-SMA, collagen 1, and fibronectin EDA splice variant. Myofibroblasts produce increased amounts of ECM proteins compared to fibroblasts. Two of these proteins are fibronectin and collagen 1 and thus increases in the expression of the genes Col1A1 and FN1-EDA are an effective method of measuring myofibroblast differentiation, furthermore, FN1-EDA is an essential component of TGF-β1 myofibroblast differentiation (Serini *et al.,* 1998).

A cytoskeletal marker of myofibroblast differentiation is α-SMA. This is the most commonly used marker in the literature, responsible for myofibroblasts contractile ability and regarded by some as the minimum requirement to confirm myofibroblast differentiation (Li *et al.,* 2021; Hu *et al.,* 2020; Plikus *et al.,* 2017; Speight *et al.,* 2013; Hecker *et al.,* 2011; Hinz, 2007; Hinz *et al.,* 2001). The main hesitancy in the literature to use α-SMA as a myofibroblast marker is that it does not distinguish between myofibroblasts and other smooth muscle cells (Zalewski *et al.,* 2002). This however, is not an issue with the research carried out for this thesis as differentiating between smooth muscle cells and myofibroblasts is not required, as this work is comparing the effect TGF-β1 has on dermal fibroblasts.

The expression of α-SMA in TGF-β1 treated cells did not differ from untreated fibroblasts, implying that fibroblasts might not be differentiating. However, the turnover of mRNA to protein can be very quick in cells, and the half-life of mRNA can be very short and influenced by the surrounding environment of the cell (reviewed in more detail by Yang *et al.,* 2003). it was decided to investigate whether TGF-β1 treated fibroblasts were producing increased levels of α-SMA protein, as this would be another method to demonstrate increased levels of α-SMA gene expression. Given the increase seen in the above data, the evidence suggests TGF-β1 is differentiating dermal fibroblasts to myofibroblasts.

Interestingly, after 24 hours untreated cells were shown to be expressing similar levels of α-SMA protein compared to TGF-β1 treated cells. There is likely to be slight activation of some fibroblasts regardless of TGF-β1 treatment as serum starvation has been shown to increase fibroblast ECM production and there is evidence that seeding fibroblasts onto cell culture plastic promotes fibroblast contraction, likely caused by increased α-SMA (Leicht *et al.,* 2001; Grinnell, 2000). Given that α-SMA protein expression in untreated cells had decreased by 72 hours, and that α-SMA protein expression (figure 4.2) and collagen expression (figure 4.1) was highest after 72 hours of TGF-β1 treatment, it was decided that going forward in future experiments, fibroblasts would be treated with TGF-β1 for 72 hours. This would in theory allow for greater TGF-β1 dependent differentiation and allow time for untreated cells to adjust to serum starvation and cell culture plastic and allow α-SMA expression back to basal levels.

Measuring and assessing levels of markers of contraction (α-SMA) and increased ECM production (collagen and fibronectin) is useful because hypertrophic scars are produced by excessive ECM deposition and contraction (Evans *et al.,* 2003; Ehrlich *et al.,* 1994). By measuring markers that lead to scarring, any decrease adipose tissue-derived conditioned medium causes in the expression of these markers not only shows myofibroblast differentiation is inhibited, but also that any future

treatment based on adipose tissue-derived conditioned medium is likely to be therapeutically beneficial.

4.3.2 The effect of adipose tissue-derived conditioned medium on fibroblast differentiation

Following on from this, data clearly showed that paracrine factors from adipose tissue-derived conditioned medium can inhibit myofibroblast differentiation. The data in figures 4.4, 4.5, and 4.6 show that factors released from adipose tissue reduces the expression of myofibroblast markers in fibroblasts treated with TGF-β1 in a paracrine fashion. Conditioned medium from minced adipose tissue, emulsified fat, and lipocondensate was not able to significantly reduce ECM gene expression relative to TGF-β1 treated fibroblasts however, mean collagen 1 expression was either the same or lower than in untreated fibroblasts. In protein data in figures 4.4 and 4.5 α-SMA protein expression is almost completely removed when TGF-β1 is applied to fibroblasts alongside minced adipose tissue, emulsified fat, and lipocondensate conditioned medium.

While western blotting data showed a significant decrease in the amount of α-SMA protein produced when TGF-β1 was added alongside minced adipose tissue, emulsified fat, and lipocondensate conditioned medium there was no significant decrease in the population of α-SMA producing cells in immunofluorescence images. It is possible that this is due to variance in other data sets. In figure 4.6, the mean average population of cells expressing α-SMA protein when treated with TGF-β1 and minced adipose tissue, emulsified fat, or lipocondensate conditioned medium was 0.5 %, 2.5 %, and 0.9 % respectively. It appears in these conditions, α-SMA expression is inhibited when compared to the 52.5 % of cells producing α-SMA when treated with only TGF-β1. However, there was large variation in other conditions tested (TGF-β1 and free lipid, ADSC conditioned medium, or lipid conditioned medium). This resulted in the data for figure 4.6 not being standardly distributed and thus a Kruskal-Wallis test was the most suitable test to analyse statistical significance. The Kruskal-Wallis test is less sensitive than a one-way ANOVA because it is not assumed that the data is parametric. The Kruskal-Wallis test showed there was statistical significance overall between the mean averages in the data set ($p = 0.036$) however, when pair-wise comparisons were carried out between the individual mean averages in the data set, no significance was found between any individual conditions. Although no RNA or immunofluorescence data was significant compared to TGF-β1 treated fibroblasts when combined with protein data, the evidence supports the conclusion that adipose tissue-derived conditioned medium inhibits myofibroblast differentiation in TGF-β1 treated fibroblasts.

When minced adipose tissue, emulsified fat, and lipocondensate conditioned medium was added alongside TGF-β1 to fibroblasts α-SMA protein expression was removed and the mean average of

collagen 1 gene expression was identical to untreated fibroblasts. Adipose tissue-derived conditioned medium was always added in conjunction with TGF-β1 and thus, it is likely that it is the adipose tissue-derived conditioned medium that is inhibiting the expression of these genes and proteins.

Given that myofibroblast differentiation was inhibited by minced adipose tissue, emulsified fat, and lipocondensate conditioned medium it is possible to speculate on the source of these inhibitory molecules. All three of these formulations contain the stromal vascular fraction (SVF) and ECM implying these components are responsible for the inhibitory effect of these conditioned media. Because ADSC conditioned medium did not lead to myofibroblast inhibition then it could be considered that other cells in the SVF are producing the growth factors responsible for inhibition or that the growth factors are being released from the adipose tissue ECM.

Myofibroblast differentiation has been inhibited by a range of molecules via the TGF-β1/SMAD pathway and factors produced by adipose tissue such as FGF (Cushing *et al.,* 2008; Liguori *et al.,* 2018) and HGF (Hu *et al.,* 2020a) have been shown to be very effective at this. There is significant literature that shows ADSCs alleviate the symptoms of hypertrophic scarring and can inhibit myofibroblast differentiation (Li *et al.,* 2016*; Spiekman *et al.,* 2014; Uysal *et al.,* 2014). The only evidence however, of *in vitro* inhibition of myofibroblast differentiation was demonstrated by Spiekman *et al.* (2014). The group showed that fibroblasts treated with TGF-β1 and cell culture medium conditioned with ADSCs was able to inhibit expression of α-SMA and collagen and prevent TGF-β1 dependent contraction of fibroblasts. This contradicts the results obtained in figures 4.4, 4.5, and 4.6 as conditioned medium from minced adipose tissue, emulsified fat, and lipocondensate was able to inhibit myofibroblast differentiation however, ADSC conditioned medium did not. The differences in results may be explained by how conditioned medium was generated. In Spiekman *et al.* the exact number of cells used to condition cell culture medium is not described and thus they may have used more ADSCs and had an increased concentration of paracrine factors than in the conditioned medium I used. Alternatively, the differences between our data may be a result of patient-to-patient variation. It has been demonstrated that sub-populations of ADSCs exist that have different secretory profiles properties (Borrelli *et al.,* 2020). There is no flow cytometry characterisation of the ADSCs used in Spiekman *et al.* and thus it is impossible to know if there existed different populations in their ADSC culture compared to mine. This is further reinforced by a paper from the same group as Spiekman *et al.* They found it possible to inhibit myofibroblast differentiation with HGF but found ADSC conditioned medium had little effect on cardiac fibroblast differentiation (Liguori *et al.,* 2018). The inconsistency between their results and those in this thesis may be as a result of patient-to-patient variation in isolated ADSCs.

*See appendix

The lipid conditioned medium and the control + TGF-β1 and free lipid controls served important yet distinct roles. Lipid droplets contain protein and are capable of exchanging proteins and ions with other organelles (Olzmann & Carvalho, 2019). It was considered possible that proteins released from lipid droplets may inhibit TGF-β1 dependent differentiation. Thus, lipid conditioned medium was used to observe whether any paracrine factors were released from the adipose tissue lipid which may interfere with SMAD signalling. The TGF-β1 and free lipid control was used because lipid droplets are hydrophobic environments. When left in the cell culture medium to generate conditioned medium, lipid droplets were released from the adipose tissue and stayed in the conditioned medium. It was considered possible that recombinant TGF-β1 added to the cell culture medium may be sequestered and trapped in the droplet, preventing TGF-β1 dependent differentiation. Thus, the free lipid control was used to test whether any large lipid vesicles found in the conditioned medium were sequestering TGF-β1 added to culture medium. Fibronectin expression levels following TGF-β1 and lipid medium conditioned medium treatment implied lipid medium may be able to effect fibronectin gene expression (figure 4.4). However, neither control showed any ability to inhibit α-SMA protein expression of TGF-β1 treated fibroblasts. Cells treated with TGF-β1 and free lipid had similar levels of myofibroblast markers α-SMA, collagen, and fibronectin compared to TGF-β1 treated fibroblasts. Similar controls are not present in other *in vitro* work and when combined with data from this thesis it appears free lipid has no effect on TGF-β1 entry into fibroblasts *in vitro*.

The demonstration that paracrine factors from adipose tissue can inhibit myofibroblast differentiation is useful for clinicians. Primarily this data aides understanding as to why adipose tissue can inhibit fibrosis but also suggests anti-fibrotic treatments. Having surgery is a major risk factor in developing fibrosis (Delavary *et al.,* 2012) with 35 % of people developing scars from fibrosis. Elective surgery could be preceded by liposuction to generate an adipose tissue-derived conditioned medium based therapeutic, or a cell free therapy could be developed from the constituent components of the medium. Furthermore, it could be used in combination with surgical techniques to remove the scar and prevent a new one forming. A drug that aimed to prevent fibrosis has already been trialled and combined with surgical revision (So *et al.,* 2011) and while it failed at a later clinical trial there is obvious desire for an anti-fibrotic drug to inhibit fibrotic development. Furthermore, the knowledge that the paracrine factors responsible for this inhibition are likely being generated from the SVF or ECM of adipose tissue justifies the use of formulations such as Nanofat and SVF-gel techniques (van Dongen *et al.,* 2021; Gentile *et al.,* 2017; Tonnard *et al.,* 2013). These techniques are used to concentrate the SVF in these formations and in theory should have a greater anti-fibrotic effect.

4.3.3 Cytokines present in adipose tissue-derived conditioned medium

A RayBio® cytokine array was used to probe the conditioned medium from minced adipose tissue, lipoaspirate, emulsified fat, lipocondensate, ADSC and lipid. This was carried out to identify cytokines present in adipose tissue-derived conditioned medium. An array containing 88 different cytokines (see section 2.4.6.1), most with links to immunomodulation, ECM remodelling or with noted antifibrotic effect was selected and the medium probed.

The cytokine array chosen contained four FGF proteins. FGF-4, -6, -7, and -9 were all found to be present in adipose tissue-derived conditioned medium, in low amounts relative to serum free medium (figure 4.7A). FGFs were consistently found to be highest in medium conditioned with emulsified fat, suggesting that perhaps FGFs are found in adipocytes and upon their lysis are released. TGF-β1 was found to be present in minced adipose tissue, lipoaspirate, emulsified fat and lipid conditioned medium at a higher concentration than serum free medium however, it was in lower concentrations when compared to other cytokines (figure 4.7B). This supports the idea that adipose tissue-derived conditioned medium is antifibrotic as it contains little TGF-β1. Additionally, TGF-β1 was found to be present at lower amounts in ADSC conditioned medium compared to serum free medium (figure 4.7B). The profile of TGF-β3 followed that of TGF-β1, the cytokine was found in the highest amounts in minced adipose tissue, lipoaspirate, and emulsified fat conditioned medium. Although the concentration of TGF-β3 in all conditioned media was on a par with, or below TGF-β3 levels in serum free MesenPRO medium (figure 4.7B). The concentration of ILs were very low in adipose tissue-derived conditioned medium relative to serum free medium, except for in the case of IL-6 and IL-8 (figure 4.7C).

The SVF has been shown to secrete FGFs, vascular endothelial growth factors, and insulin-like growth factor (Grasys *et al.,* 2016) and ADSCs secrete high concentrations of these factors as well (Pallua, *et al.,* 2014b). However, none of the work by Spiekman *et al.* probes what paracrine signals are being secreted by the ADSCs and which factors may be responsible for inhibiting myofibroblast differentiation. To elucidate a mechanism behind this inhibition, these secreted paracrine factors were investigated.

While promoting fibroblast migration and reducing their apoptosis, some members of the FGF family have been found to protect from fibrosis or can inhibit fibroblast to myofibroblast differentiation so in this context can be considered anti-fibrotic (Joannes *et al.,* 2016; Shams *et al.,* 2015; Yao *et al.,* 2013; Ramos *et al.,* 2006). Due to the nature of the cytokine array used, the concentration of FGFs found in the conditioned medium used in this work to that found by Grasys *et al.,* (2016) cannot be directly compared. Given the low amounts that FGFs were found in, especially

compared to other growth factors, it was decided it was unlikely that FGFs were responsible for the anti-fibrotic effects of adipose tissue-derived conditioned medium. The concentration of various TGF-β proteins were assessed on the cytokine array (figure 4.7B).

Cell culture serum has been found to contain TGF-β1 (Danielpour *et al.,* 1989). Given that TGF-β1 was used in these experiments to cause myofibroblast differentiation, it was important to control when cells were exposed to TGF-β1. To this end, cells were cultured in serum free medium to remove any TGF-β1 found in serum. ADSC conditioned medium did not inhibit myofibroblast differentiation. One hypothesis as to why, is that ADSCs produce TGF-β1 (Heo *et al.,* 2016) and thus ADSC conditioned medium may be exogenously activating the fibroblasts. Given the low concentration of TGF-β1 in ADSC conditioned medium, it can be ruled out that ADSC production of TGF-β1 being responsible for the lack of inhibition in ADSC conditioned medium treated cells in section 4.2.2.

Ferguson *et al.* (So *et al.,* 2011; Shah, Foreman, & Ferguson, 1995; Whitby & Ferguson, 1991) have carried out extensive work into the anti-fibrotic action of TGF-β3. With that in mind, levels of TGF-β3 found in adipose tissue-derived conditioned medium was investigated. TGF-β3 was also found in low concentrations relative to serum free medium and was not chosen as a target going forward due to the low concentration found in the conditioned medium.

Interleukins make up a broad family of cytokines with a wide variety of immunomodulatory effects. Some interleukins are directly able to cause differentiation of fibroblasts to myofibroblasts (Ma *et al.,* 2012; Murray *et al.,* 2008). It has been suggested that IL-1 can inhibit TGF-β1 dependent α-SMA expression in fibroblasts (Zhang *et al.,* 1997, Shephard *et al.,* 2004) however, other literature indicates that IL-1 is in fact pro-fibrotic and leads to an increase in fibroblast collagen production similar to that of myofibroblast activation (Wilson *et al.,* 2010; Zhang *et al.,* 1993). IL-6 has been shown to cause differentiation of fibroblasts to myofibroblasts in the literature (Ma *et al.,* 2012). Thus, it is contradictory that IL-6 is the most concentrated cytokine found on the array used, given that adipose tissue-derived conditioned medium appears to be inhibiting and not promoting fibroblast differentiation. A reason for this contradiction may be that the cytokines through which adipose tissue-derived conditioned medium inhibits fibroblast differentiation are many times more potent than the activating capacity of IL-6. Alternatively, cytokines from adipose tissue-derived conditioned medium may inhibit IL-6 dependent differentiation through the same mechanism it inhibits TGF-β1 dependent activation (this would make sense as IL-6 dependent myofibroblast activation also occurs through the SMAD signalling pathway (Ma *et al.,* 2012)). Additionally, the lack of effect of IL-6 on fibroblasts in this data highlights a limitation of this *in vitro* work. IL-6 has been

found to have different effects on fibrosis in different environments. In healthy patients IL-6 appears to be anti-fibrotic however, in patients suffering from idiopathic pulmonary fibrosis IL-6 is a profibrotic marker (Moodley *et al.,* 2003). Furthermore, when co-cultured with activated M1 macrophages, fibroblasts secreted significantly more IL-6 and the cross talk between fibroblasts and macrophages led to an increased pro-fibrotic environment (Ma *et al.,* 2012). This highlights how adipose tissue-derived conditioned medium is effectively inhibiting myofibroblast differentiation in an *in vitro* monoculture of fibroblasts however, it may not be as effective when applied to a more complex fibrotic model such as a bleomycin challenge in an animal (Lagares *et al.,* 2017). The high concentrations of IL-6 may not be having any effect on healthy, isolated dermal fibroblasts, but may be much more potent if applied to fibroblasts in a scar or fibrotic environment.

To decide on a target from adipose tissue-derived conditioned medium to examine further for an ability to inhibit myofibroblast differentiation, the cytokines found in the highest concentration were selected. This was because it was theorised these cytokines would be having the largest effect on fibroblast differentiation. Cytokines found at concentrations at least 10 times that of serum free medium were selected for further screening (figure 4.8). Evidence of anti-fibrotic effects from these cytokines was investigated. Some cytokines were pro-fibrotic or caused differentiation of fibroblasts to myofibroblasts, such as leptin (Kü *et al.,* 2007) and IL-6 (Ma *et al.,* 2012). Some cytokines, such as MIP3-Alpha, were found to act downstream of SMAD signalling and thus would have no effect on TGF-β1 dependent myofibroblast differentiation (Brand *et al.,* 2015). However, two cytokines found in high concentrations in adipose tissue-derived conditioned medium have previously been reported to inhibit myofibroblast differentiation. CXCL-9 has been shown to promote SMAD7 expression, which in turn suppresses SMAD2/3 phosphorylation and translocation into the nucleus (O'Beirne *et al.,* 2015; Wasmuth *et al.,* 2009). HGF has been frequently reported to have anti-fibrotic effects in a variety of different mechanisms (Dai & Liu, 2004; Shams *et al.,* 2015; Yang *et al.,* 2003, 2005). Due to the frequency with which HGF is cited in the literature for its ability to inhibit myofibroblast differentiation, it was decided to test whether HGF was the factor present in adipose tissue-derived conditioned medium for inhibiting myofibroblast differentiation.

HGF was found in high concentrations in minced adipose tissue (2.8 ng/ml), lipoaspirate (6.4 ng/ml), and emulsified fat conditioned medium (2.4 ng/ml; figure 4.9). HGF concentration was highest in lipoaspirate while ADSC and lipid conditioned medium did not contain enough HGF to record a reading on the ELISA. The lack of HGF in ADSC and lipid conditioned medium perhaps offers an explanation as to why there was no myofibroblast inhibition from these conditioned media, as there was little HGF present.

4.3.4 The effect of foretinib and HGF on adipose tissue-derived conditioned medium inhibition of myofibroblast differentiation

Foretinib was designed as an anti-cancer drug due to its ability to inhibit the C-Met receptor and is known to be cytotoxic to human cells (Simiczyjew *et al.,* 2018). In addition to this, foretinib needs to be dissolved in solvents. These solvents are cytotoxic agents and for this reason, the effect of foretinib and the solvents on the metabolic activity of fibroblasts was tested. This data was used to ensure that foretinib or the solvents used did not have a significant cytotoxic effect on dermal fibroblasts. When solvents were added to fibroblasts in concentrations that would be used to solubilise foretinib, there was no difference in metabolic activity relative to a control treated with only serum free medium. A decision needed to be made as to which solvent was used to solubilise foretinib in. While not significant, fibroblasts cultured in ethanol had a slightly lower metabolic activity than those cultured in DMSO when tested, so going forward it was decided to use DMSO to solubilise foretinib. Realistically, there was no difference in metabolic activity and these solvents had no effect on the fibroblasts. Likewise, all foretinib concentrations had no effect on cell metabolic activity at any of the concentrations tested. With that being the case, the highest concentration recommended by the manufacturers (1.0 nM) was selected for use on fibroblasts.

HDF were treated with TGF-β1, HGF, and foretinib (figure 4.11). Levels of α-SMA protein following this treatment was examined via western blotting and immunofluorescence. Treating cells with HGF alongside TGF-β1 did not lead to a decrease in α-SMA expression compared to TGF-β1 treated cells (figures 4.13 and 4.14). Once again, adipose tissue-derived conditioned medium significantly reduced the expression of α-SMA when HDF were treated with adipose tissue-derived conditioned medium and TGF-β1. When foretinib was added alongside the adipose tissue-derived conditioned medium and TGF-β1 HDF also produced significantly less α-SMA, showing the inhibitory effect of adipose tissue-derived conditioned medium was not blocked by foretinib (in figure 4.14B, adipose tissue-derived conditioned medium, foretinib, and TGF-β1 treated fibroblasts had the lowest amount of α-SMA protein present). This data appears to indicate that HGF is not capable of inhibiting myofibroblast differentiation *in vitro* under the conditions tested. This conclusion can be reached because cells treated with HGF and TGF-β1 still expressed high levels of α-SMA protein. Furthermore, foretinib was not able to remove the inhibitory effect of adipose tissue-derived conditioned medium on α-SMA expression, showing that factors in the medium are still inhibiting α-SMA protein expression.

It has been demonstrated that HGF added to fibroblasts alongside TGF-β1 is able to inhibit α-SMA expression *in vitro* (Yang *et al.,* 2003). Yang *et al.* found that a concentration of 40 ng/ml was able to prevent the translocation of SMAD2/3 into the nucleus and prevent fibroblast differentiation. HGF

was used at the same concentration as Yang *et al.* and did not elicit a similar effect, recombinant HGF and HGF from adipose tissue-derived conditioned medium could not inhibit α-SMA expression. This may be a result of using a higher TGF-β1 concentration. In this work, 5 ng/ml of TGF-β1 were added to fibroblasts whereas, Yang *et al.* added 2 ng/ml, a higher concentration of HGF may have been required to inhibit differentiation from a higher concentration of TGF-β1. Furthermore, the concentration of HGF needed to inhibit SMAD signalling may vary between cell population and a higher concentration may have been required compared to the cells used by Yang *et al.* However, data from figure 4.9 suggest that the concentration of HGF used was not an issue as the concentration of HGF in lipoaspirate conditioned medium was at roughly 5.5 ng/ml. This is much lower than the 40 ng/ml of HGF added to the fibroblasts but lipoaspirate conditioned medium was still able to inhibit myofibroblast differentiation. Future work could determine whether the HGF was activating the C-Met receptor or whether the foretinib supplied was inhibiting the C-Met receptor of cultured fibroblasts. It may simply be that the inhibitory ability of adipose tissue-derived conditioned medium is a result of a wide range and combination of different inhibitory factors present in the medium. As mentioned earlier, an anti-fibrotic therapeutic aimed at inhibiting scarring via the addition of a single molecule was developed (So *et al.,* 2011). However, when used in patients on a much larger scale was not seen to have as great an effect as in small scale wounds (McKee, 2011). A combination of different molecules may be needed to effectively inhibit myofibroblast differentiation *in vitro*.

To conclude, this chapter has demonstrated that paracrine factors from adipose tissue-derived conditioned medium can inhibit myofibroblast differentiation via the SMAD signalling pathway. This work is the first *in vitro* evidence that adipose tissue used by clinicians can inhibit myofibroblast differentiation, providing evidence for adipose tissue's antifibrotic abilities and future therapeutics. The ability to inhibit the formation of myofibroblasts in those at risk of scarring could prevent excessive hypertrophic scarring. This work has provided evidence that the paracrine factors that inhibit this differentiation are likely being produced by the SVF or ECM of adipose tissue and thus methods that concentrate these populations in adipose tissue should be encouraged and developed further. In the conditions tested, HGF was unable to inhibit myofibroblast differentiation and further work to elucidate the precise mechanism behind adipose tissue inhibition of myofibroblast differentiation should be investigated further.

Chapter 5: Investigating the ability of factors from adipose tissue to reverse a myofibroblast phenotype

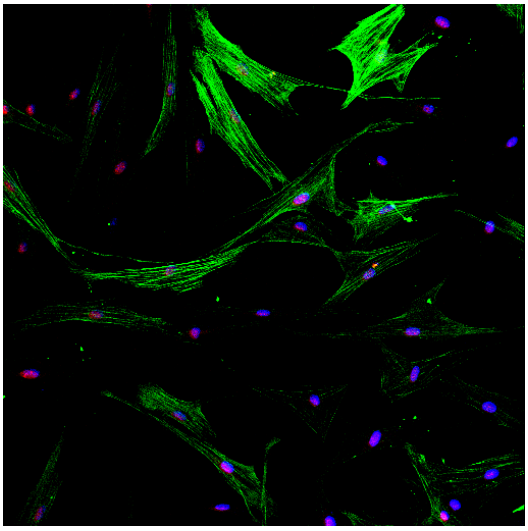

5.1 Introduction and aims

In the preceding chapter, it was demonstrated that factors from adipose tissue-derived conditioned media can inhibit transforming growth factor-β (TGF-β) 1 dependent myofibroblast differentiation. This knowledge could be used to generate therapeutics delivered to groups at risk of fibrosis and those who know they will be undergoing surgery or radiotherapy. By taking these therapeutics, the development of fibrosis could be prevented by inhibiting myofibroblast differentiation.

However, this does little to clarify the role of adipose tissue in regenerating already formed scars. In literature showing adipose tissue-based regeneration of hypertrophic scars, these wounds have often been formed for years (Bruno *et al.,* 2013; Byrne *et al.,* 2016; Klinger *et al.,* 2008). In these cases, the inhibition of myofibroblast differentiation would not be particularly useful, as this differentiation has already occurred.

It has historically been considered that myofibroblasts are terminally differentiated (Bayreuther *et al.,* 1988; Evans *et al.,* 2003) and that unless they undergo apoptosis, these cells are not capable of differentiation to other cell types or back to quiescent fibroblasts (Hinz, 2007). In more recent times however, research groups have demonstrated that myofibroblasts can undergo adipogenic differentiation (el Agha *et al.,* 2017; Plikus *et al.,* 2017). Additionally, factors from adipocytes have also been shown to cause myofibroblast de-differentiation (Hoerst *et al.,* 2019). Following adipose tissue grafting underneath scars, it is often reported that contraction is decreased, excessive extracellular matrix (ECM) is removed, and collagen deposition remodelled (Bruno *et al.,* 2013; Caviggioli *et al.,* 2011; Maione *et al.,* 2014). It is likely that this is a result of factors from the adipose tissue causing the myofibroblasts activated during scar formation to de-differentiate to another cell type, or to undergo apoptosis. Thus, the aims of this chapter were to:

- Measure α-smooth muscle actin (α-SMA) expression in TGF-β1 differentiated myofibroblasts following the addition of adipose tissue-derived conditioned medium (figure 5.1) to examine whether factors within the conditioned medium could reverse myofibroblast differentiation.

- Elucidate the mechanism behind any reversal effect.

- Examine whether addition of adipose tissue-derived conditioned medium could reverse myofibroblast differentiation in hypertrophic scar myofibroblasts.

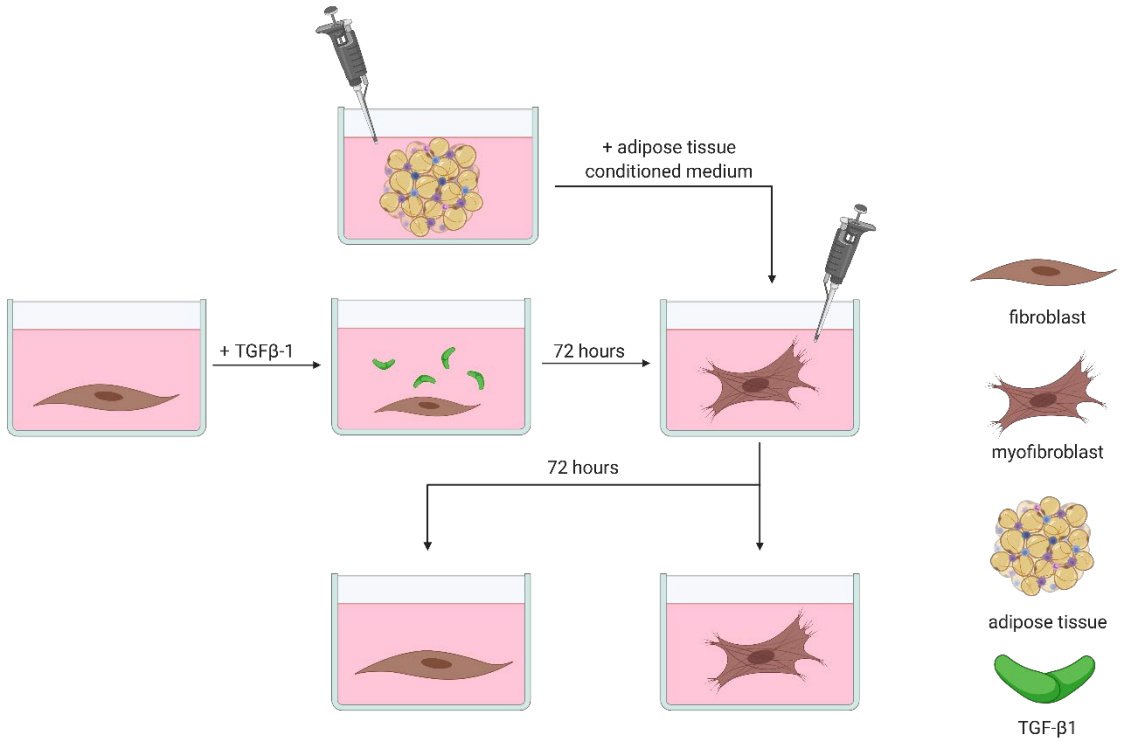

Figure 5.1. Schematic of protocol to investigate the ability of adipose tissue-derived conditioned medium to reverse a TGF-β1 induced myofibroblast phenotype. Fibroblasts were activated to myofibroblasts via TGF-β1 incubation for 72 hours. Following this, cells were treated with adipose tissue-derived conditioned medium for 72 hours. Markers of a myofibroblast phenotype were then investigated.

5.2 Results

5.2.1 Do myofibroblasts remain differentiated if TGF-β1 is removed?

Before testing whether adipose tissue-derived conditioned medium was capable of reversing myofibroblast differentiation, it was important to examine whether TGF-β1 treated fibroblasts still displayed markers of myofibroblast differentiation following the removal of TGF-β1. This was to ensure that any decrease found in myofibroblast markers was a result of the addition of adipose tissue-derived conditioned medium and not a consequence of removing TGF-β1 from the fibroblasts. To test whether markers of myofibroblast differentiation remain following the removal of TGF-β1, fibroblasts were treated with TGF-β1 for various time periods using the methods described in section 2.4.4.1. Medium containing TGF-β1 was removed and replaced with serum free MesenPRO for 72 hours, following which gene expression of collagen and fibronectin was quantified as described in section 2.4.4.2 and 2.4.4.3. Gene expression was normalised to the house-keeping gene RNU6-1 and compared to the gene expression of untreated fibroblasts.

Fibronectin expression in fibroblasts treated with TGF-β1 and then serum free media was higher than untreated cells. In all time periods tested, the mean fibronectin expression was higher than untreated cells (figure 5.2A). The relative fibronectin expression in TGF-β1 treated cells was significantly higher than untreated cells after 24 and 72 hours of TGF-β1 treatment (6.9-times and 6.6-times relative gene expression compared to 0.9 and 1.0 respectively, $p < 0.01$).

Likewise, collagen expression in fibroblasts treated with TGF-β1 and then serum free media was higher than untreated cells. Mean collagen expression was higher than untreated cells at all time points and significantly higher after 24 hours of TGF-β1 treatment (figure 5.2B). Untreated cells expressed 1.0-times as much collagen as RNU6-1 while cells treated with TGF-β1 for 24 hours and then serum free medium for 72 hours expressed 4.8-times as much collagen as RNU6-1 ($p = 0.02$).

Given that collagen and fibronectin expression is significantly higher than untreated cells after TGF-β1 is removed for 72 hours, this gave confidence going forward that any effect on myofibroblast markers is in response to adipose tissue-derived conditioned medium and not the removal of TGF-β1. For the sake of consistency with previous sections, it was decided to treat fibroblasts with TGF-β1 for 72 hours.

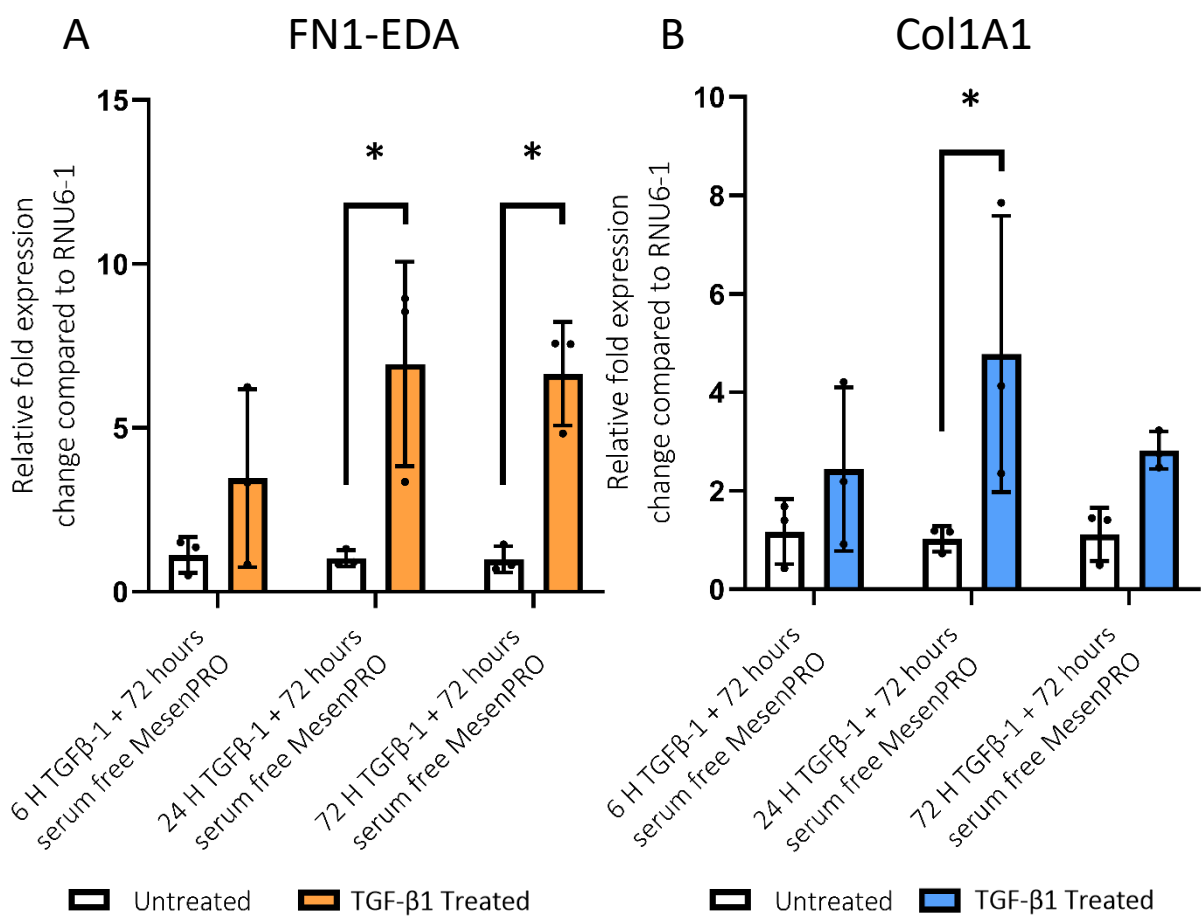

Figure 5.2. Expression levels of mRNA characteristic of a myofibroblast phenotype following TGF-β1 treated followed by 72 hours of serum free media treatment. (A) FN1-EDA expression **(B)** COL1A1 expression. Gene expression was calculated using the $2^{-\Delta\Delta CT}$ method, normalising to RNA expression levels from RNU6-1. A two-way analysis of variance (ANOVA) was carried out comparing the expression of fibroblasts treated with TGF-β1 for 6,24, and 72 hours. *N* = 3, *n* = 3. Error bars = standard deviation. * = $p < 0.02$.

5.2.2. Can adipose tissue-derived conditioned medium reduce α-SMA protein expression in fibroblasts previously treated with TGF-β1?

To examine whether factors from adipose tissue-derived conditioned medium could reverse the expression of α-SMA protein induced by TGF-β1 treatment, immunofluorescence of fibroblasts treated with TGF-β1 for 72 hours and then adipose tissue-derived conditioned medium for 72 hours (figure 5.1) was carried out. Fibroblasts were seeded on coverslips and treated with TGF-β1, or left untreated, for 72 hours as described in section 2.4.5.6. This medium was then removed, and fibroblasts were treated with adipose tissue-derived conditioned medium for 72 hours. Following which, medium was removed, cells were fixed and immunofluorescence staining of cell nuclei and α-SMA was carried out as described in section 2.4.5.6. Once again, there was a control to examine the effect of lipid on α-SMA protein expression. In this condition, fibroblasts were treated with TGF-β1 for 72 hours which was then replaced with serum free medium with lipid added for 72 hours.

Before fixation for immunofluorescence, light microscopy images were taken of cells (figure 5.3). There was a noticeable visual difference in cell morphology in cells treated with adipose tissue-derived conditioned medium compared to only TGF-β1 treated cells. TGF-β1 treated cells were large and had a stretched appearance (figure 5.3B), and immunofluorescence images indicated actin fibres across the cell. While nonquantitative, this implies that TGF-β1 treated cells had a myofibroblast morphology and maintained it after TGF-β1 was removed for 72 hours. In comparison, cells treated with TGF-β1 and either minced adipose tissue, emulsified fat, or lipocondensate had a more spindle like appearance, matching the literature description of fibroblasts (Fortier *et al.,* 2021; figures 5.3C-E). These images suggest that following TGF-β1 treatment and then exposure to adipose tissue-derived conditioned medium, cells had a fibroblast like morphology.

In immunofluorescence images, less than 1 % of untreated fibroblasts expressed any detectable α-SMA protein (0.9 %, figure 5.4A). There was a significant increase in the percentage of cells expressing α-SMA in fibroblasts treated with TGF-β1 and then serum free media as 41.0 % of cells expressed α-SMA protein ($p < 0.01$, figure 5.4 B, I). The percentage of α-SMA expressing fibroblasts was significantly lower than TGF-β1 treated cells when fibroblasts were treated with TGF-β1 and then either minced adipose tissue, emulsified fat, or lipocondensate conditioned medium (4.5, 3.4, and 11.3 % respectively, $p < 0.02$, figure 5.4C-E). When treated with TGF-β1 and then adipose derived stromal cell (ADSC) conditioned medium there was no change in the percentage of cells expressing α-SMA compared to only TGF-β1 treated cells (41.7 %). When fibroblasts were treated with TGF-β1 and then lipid conditioned medium, there was a significantly lower percentage of cells expressing α-SMA compared to TGF-β1 treatment (16.0 %, $p = 0.03$). When treated with TGF-β1 and then serum free medium and lipid 32.7 % of cells expressed α-SMA.

Taken together, this data shows that paracrine factors from adipose tissue-derived conditioned medium can lower the expression α-SMA, a key marker myofibroblast differentiation and suggests that these factors are reversing myofibroblast differentiation.

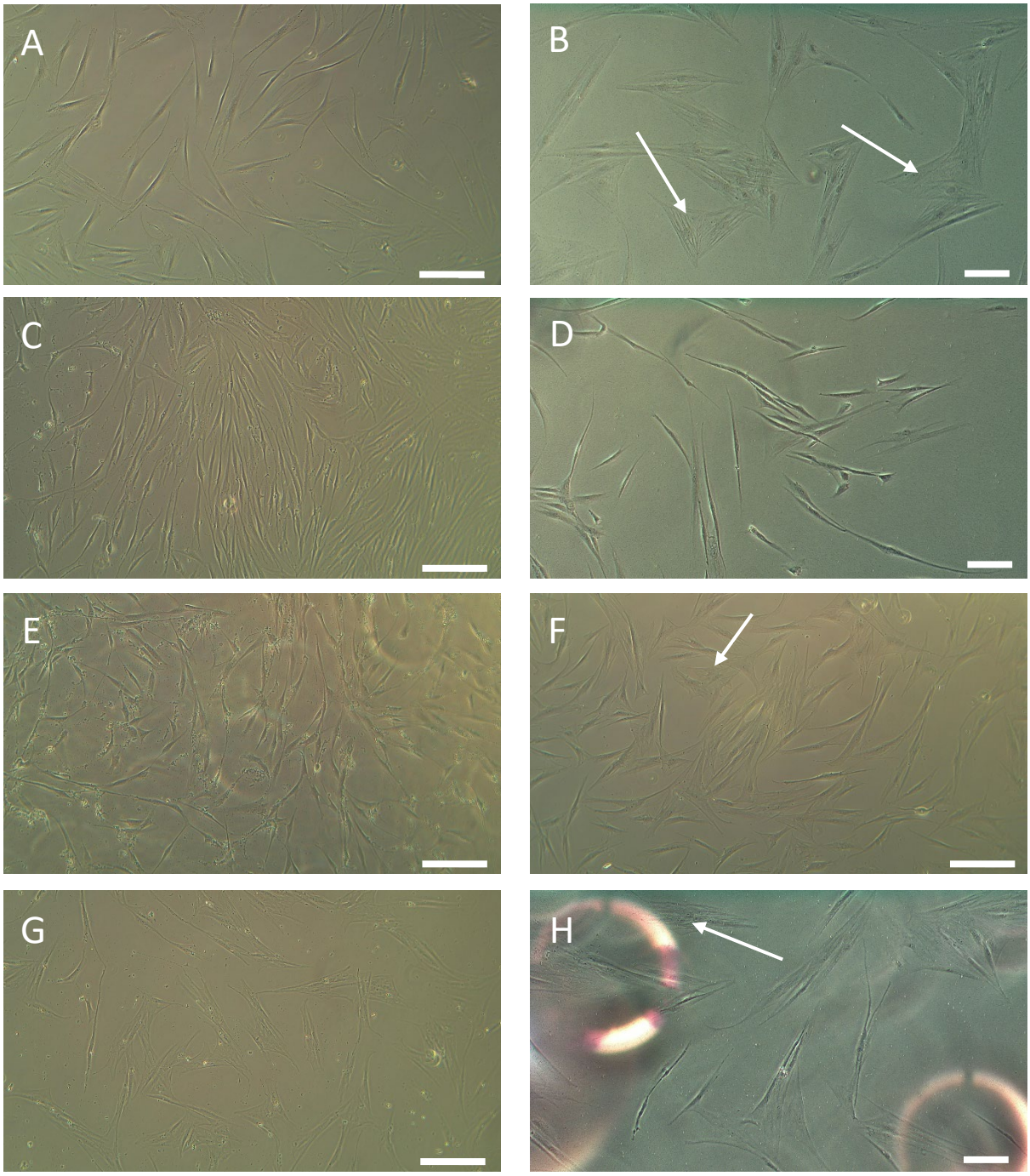

Figure 5.3. Morphological analysis of adipose tissue-derived conditioned medium on TGF-β1 treated fibroblasts. (A-H) Light microscopy images were taken at x10 magnification on an AE 2000 inverted light microscope**.** Cells were treated with **(A)** untreated, **(B)** TGF-β1 and then serum free medium, **(C)** TGF-β1 and then minced adipose tissue conditioned medium, **(D)** TGF-β1 and then emulsified fat conditioned medium, **(E)** TGF-β1 and then lipocondensate conditioned medium, **(F)** TGF-β1 and then ADSC conditioned medium, **(G)** TGF-β1 and then lipid conditioned medium, **(H)** TGF-β1 and then serum free medium and lipid. Scale bars = 100 μM. Arrows indicate visible α-SMA stress fibres.

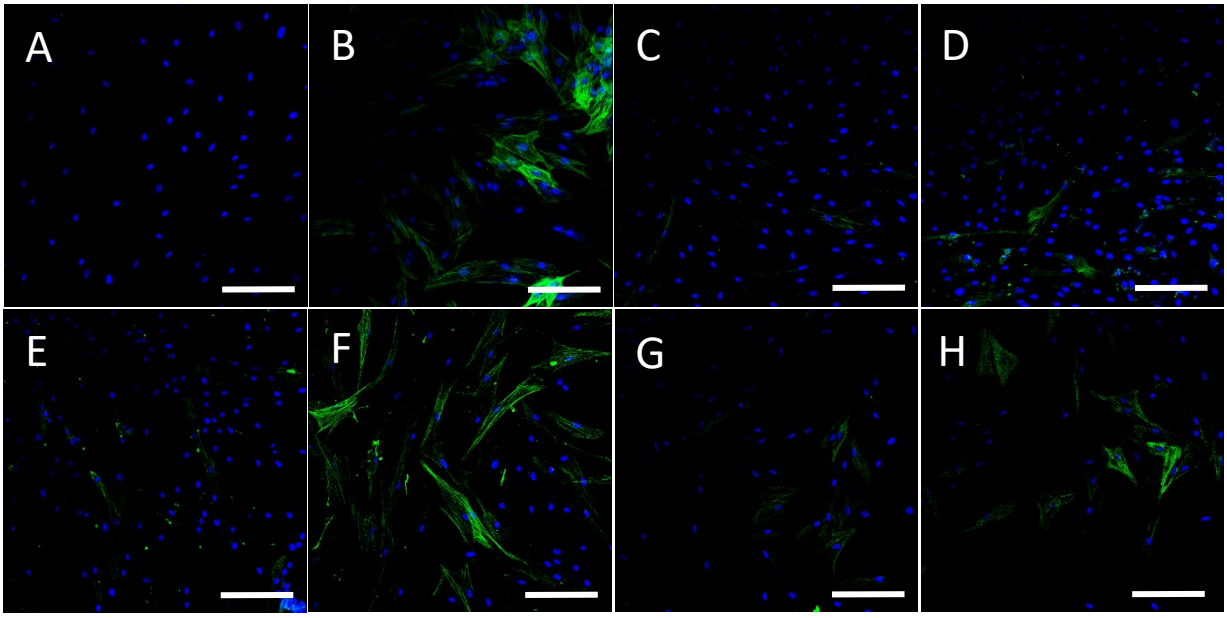

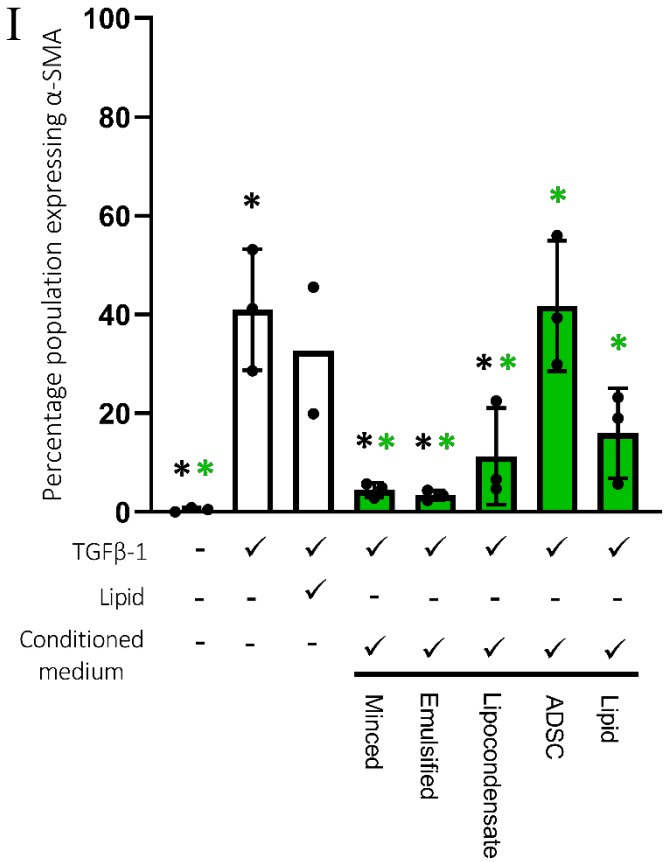

Figure 5.4. Analysis of α-SMA production in TGF-β1 activated myofibroblasts following treatment with adipose tissue-derived conditioned medium. (A-H) Fluorescent images taken on an upright LSM510 Meta confocal microscope. Cells were stained for nuclei (blue) and α-SMA fibres (green). Cells were treated with **(A)** untreated, **(B)** TGF-β1 and then serum free medium, **(C)** TGF-β1 and then minced adipose tissue conditioned medium, **(D)** TGF-β1 and then emulsified fat conditioned medium, **(E)** TGF-β1 and then lipocondensate conditioned medium, **(F)** TGF-β1 and then ADSC conditioned medium, **(G)** TGF-β1 and then lipid conditioned medium, **(H)** TGF-β1 and then serum free medium and lipid. Scale bars = 100 µM. **(I)** The percentage of cells producing α-SMA was calculated. *N* = 3 / 2 (control + TGF-β1 + lipid), *n* = 3. Green bars represent cells treated with conditioned medium. Error bars = standard deviation. An ordinary one-way ANOVA was carried out to test for significance. Black * = $p < 0.037$ compared to TGF-β1 treated control, green * = $p < 0.037$ compared to TGF-β1 and ADSC treated cells.

5.2.3 Does adipose tissue-derived conditioned medium increase myofibroblast proliferation?

5.2.3.1 Immunofluorescence cell count

It was noticed anecdotally in immunofluorescence images from figures 5.3 and 5.4 that images of cells treated with adipose tissue-derived conditioned media contained more cells than other conditions. Mitogens such as fibroblast growth factor (FGF)-2 have been shown to cause myofibroblast de-differentiation via activating the mitogen activated protein kinase (MAPK) signalling cascade and causing myofibroblasts to proliferate into fibroblasts (Fortier *et al.,* 2021; Hecker *et al.,* 2011). It was considered that that this may be the mechanism through which adipose tissue-derived conditioned medium was lowering α-SMA expression in TGF-β1 treated fibroblasts. To examine if images taken of adipose tissue-derived conditioned medium treated fibroblasts contained more cells, the number of cells per image were counted as in section 2.4.5.6 using the number of DAPI stained nuclei to count cell number.

Images of control fibroblasts, not treated with TGF-β1, contained on average 59 cells per mm^2. Treating cells with TGF-β1 and then serum free media did not affect the number of cells present in images (79 cells per mm^2, $p = 0.99$, figure 5.5A). Likewise, treating cells with TGF-β1 and lipid conditioned medium or TGF-β1, serum free media and free lipid had no effect on the number of cells present, with 75 and 68 cells per mm^2 respectively. There was an increase in the mean number of cells present when fibroblasts were treated with TGF-β1 and lipocondensate or ADSC conditioned medium however, this was not significant (161 and 123 cells per mm^2, $p > 0.08$). When cells were treated with TGF-β1 and then minced adipose tissue or emulsified fat conditioned medium, there were significantly more cells present in images. Images of cells treated with TGF-β1 and then minced adipose tissue contained on average, 191 cells per mm^2 and images of cells treated with TGF-β1 and then emulsified fat conditioned medium contained 222 cells per mm^2. This was significantly higher than the number of cells present in images of untreated fibroblasts, TGF-β1 treated fibroblasts, and TGF-β1 and lipid conditioned medium treated fibroblasts ($p < 0.05$).

Given that images were taken in an unbiased manner (detailed in section 2.4.5.6) and the same number of cells are seeded for all conditions at the beginning of each experiment, these results suggest that minced adipose tissue and emulsified fat conditioned medium were affecting the number of cells present when imaged.

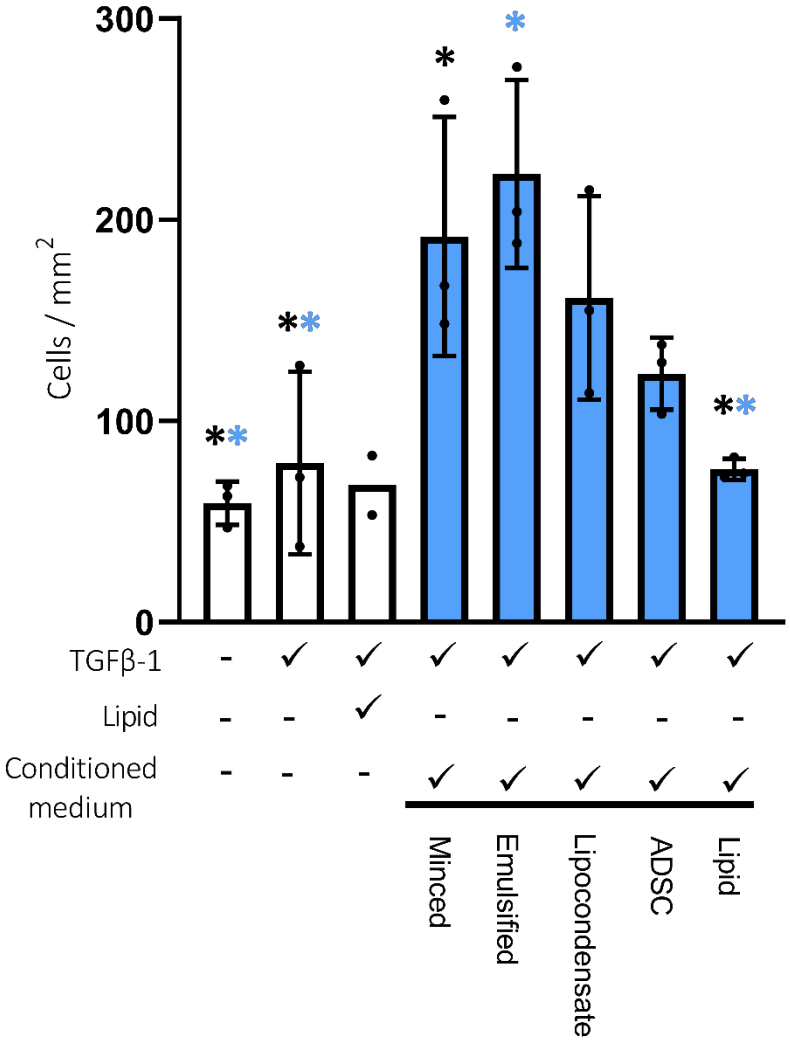

Figure 5.5. The effect of adipose tissue-derived conditioned medium on the number of cells in fluorescent images. Using images in figure 5.4, the number of cells per mm^2 in images was counted. *N* = 3 / 2 (control + TGF-β1 + lipid), *n* = 3. Error bars = standard deviation. Coloured bars represent cells treated with conditioned medium. An ordinary one-way ANOVA was carried out to test for significance. Black * = $p < 0.042$ compared to TGF-β1 and minced adipose tissue conditioned medium treated cells. Blue * = $p < 0.042$ compared to TGF-β1 and emulsified fat conditioned medium treated cells.

5.2.3.2 Cellular metabolic activity of adipose tissue-derived conditioned medium treated cells

Immunofluorescence images of cells treated with TGF-β1 and adipose tissue-derived conditioned medium showed that there were more cells present in images taken of cells following treatment with adipose tissue-derived conditioned medium. To examine whether adipose tissue-derived conditioned medium was causing an increase in the number of cells present, a resazurin assay was carried out on fibroblasts treated with adipose tissue-derived conditioned medium. Fibroblasts were seeded in 12 well plates and were treated with TGF-β1 for 72 hours (or just serum free medium in the case of the negative control condition) as described in section 2.4.5.1. A resazurin assay (section 2.4.7) was then carried out on the cells. Fibroblasts were washed in phosphate buffered saline (PBS) and treated for 72 hours in adipose tissue-derived conditioned media. A control condition of cells treated in 2 % serum medium for 72 hours following TGF-β1 treatment was also added. Another resazurin assay was then carried out and the fluorescence values normalised to the negative control following the first 72 hours of serum free medium culture (figure 5.6A).

Following 72 hours in serum free medium, control cells had a relative metabolic activity of 0.9-times that of control fibroblasts after the first 72 hours of serum free medium incubation. TGF-β1 treated cell metabolic activity was unchanged at 0.9-times that of untreated fibroblasts. Cells treated with minced adipose tissue, lipocondensate, ADSC, or lipid conditioned medium all had a higher mean metabolic activity at 1.2-, 1.0-, 1.0-, and 1.0-times that of untreated fibroblasts however, this was not significant. Cells treated with TGF-β1 and then emulsified fat had a cellular metabolic activity of 1.3-times that of untreated cells and this was significantly higher than control fibroblasts, TGF-β1 and serum free medium treated fibroblasts, and TGF-β1, serum free medium and lipid treated fibroblasts ($p < 0.04$). Control cells treated with only 2 % serum medium had a relative metabolic activity of 1.3-times that of untreated fibroblasts, which was also significantly higher than control fibroblasts, TGF-β1 and serum free medium treated fibroblasts, and TGF-β1, serum free medium and lipid treated fibroblasts ($p < 0.05$). This data shows that adipose tissue-derived conditioned medium increases the cellular metabolic activity of fibroblasts and implies the presence of an increased number of cells.

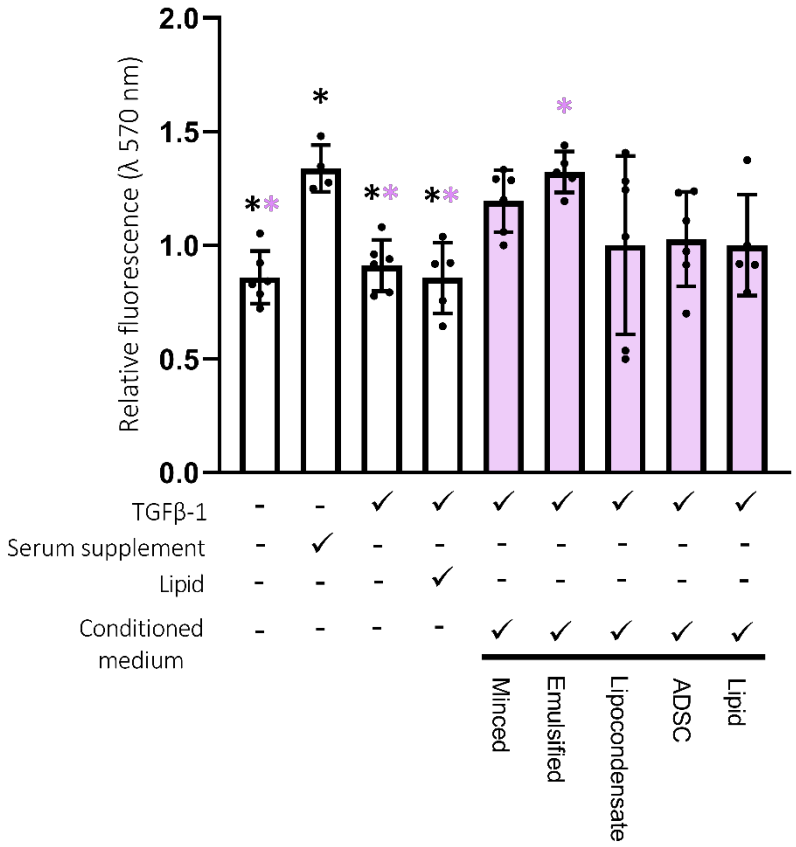

Figure 5.6. The effect of adipose tissue-derived conditioned medium on relative metabolic activity in TGF-β1 activated myofibroblasts. A resazurin assay was carried out on cells following treatment with TGF-β1 and then repeated following treatment with adipose tissue-derived conditioned medium. Relative metabolic activity was calculated by normalizing the fluorescence of resazurin at 570 nm after adipose tissue conditioned media to fluorescence values following 72 hours of TGF-β1 treatment**.** *N* = 6 (control, control + TGF-β1, TGF-β1 + minced adipose tissue, TGF-β1 + lipocondensate, TGF-β1 + ADSC) / 5 (TGF-β1 + emulsified fat, TGF-β1 + lipid medium, control + TGF-β1 + lipid) / 4 (control + 2 % serum), *n* = 3. Error bars = standard deviation. Coloured bars represent cells treated with conditioned medium. An ordinary one-way ANOVA was carried out to test for significance. Black * = $p < 0.043$ compared to cells treated with medium containing 2 % serum supplement. Pink * = $p < 0.043$ compared to cells treated with TGF-β1 and emulsified fat conditioned medium.

5.2.3.3 Examination of Ki-67 expression following TGF-β1 and adipose tissue-derived conditioned medium treatment

While increased cellular metabolic activity does not definitively indicate that there are more cells present, this data does imply that adipose tissue-derived conditioned medium is increasing the number of cells present. Combined with data from section 5.3.2.1 and 5.2.2.2, this data suggests that factors from adipose tissue-derived conditioned media may be giving the appearance of decreasing myofibroblast number by causing increased proliferation of cells. To examine further whether adipose tissue-derived conditioned medium was increasing cellular proliferation, fibroblasts were treated with TGF-β1 for 72 hours and then adipose tissue-derived conditioned medium and were stained for 4',6-diamindino-2-phenylindole (DAPI), α-SMA and Ki-67 as described in section 2.4.5.6. Confocal microscopy and immunofluorescence analysis was then carried out on these cells (section 2.4.5.6). Ki-67 is a marker of cellular proliferation (Davey *et al.,* 2021; Sun & Kaufman, 2018) and any cell expressing the protein was considered to be proliferating.

In untreated fibroblasts, 14.6 % of cells were expressing Ki-67 (figure 5.7A, I). There was an increase in the mean percentage of cells expressing Ki-67 when treated with TGF-β1 and then serum free media to 23.2 % however this was not a significant increase (figure 5.7B, $p = 0.99$). Likewise, there was no change in the percentage of Ki-67 expressing cells in populations treated with TGF-β1 and then either minced adipose tissue or emulsified fat conditioned medium (27.3 and 28.9 % respectively, figures 5.7C-D, $p > 0.95$). Fibroblasts treated with TGF-β1 and then either lipocondensate or ADSC conditioned medium expressed Ki-67 in 56.1 % of the cellular population examined, this was not significantly higher than any other condition examined ($p > 0.19$). In cells treated with TGF-β1 and then lipid conditioned medium, 11.6 % of cells were expressing Ki-67 and 10.1 % of cells treated with TGF-β1 and then serum free media and lipid were expressing Ki-67. Taken together, no adipose tissue conditioned media significantly altered the expression of Ki-67 in TGF-β1 treated fibroblasts.

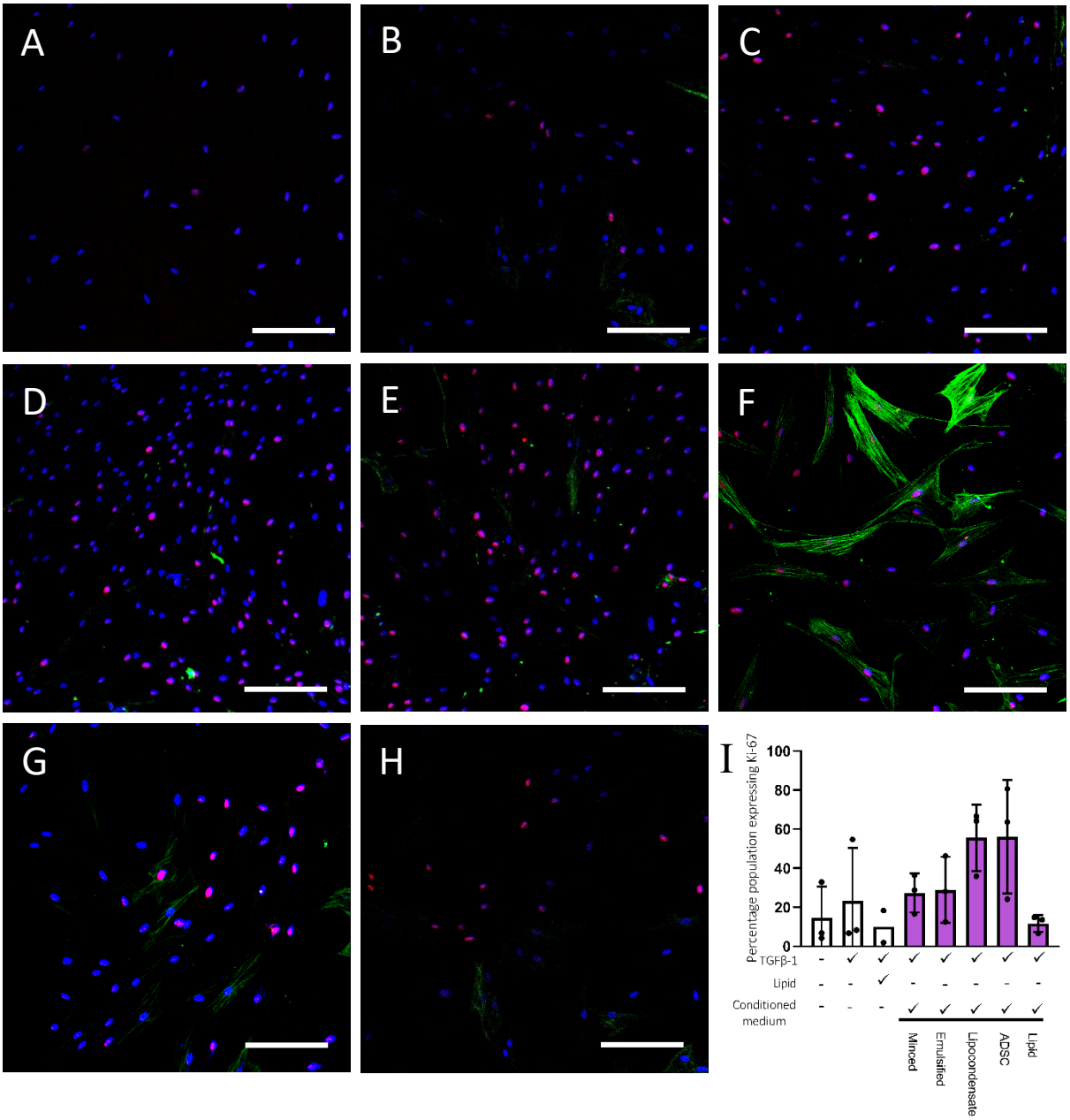

Figure 5.7. Analysis of Ki-67 expression in TGF-β1 activated myofibroblasts following treatment with adipose tissue - derived conditioned medium. (A-H) Fluorescent images taken on an upright LSM510 Meta confocal microscope. Cells were stained for nuclei (blue), α-SMA fibres (green), and Ki-67 (purple). Cells were treated with **(A)** untreated, **(B)** TGF-β1 and then serum free medium, **(C)** TGF-β1 and then minced adipose tissue conditioned medium, **(D)** TGF-β1 and then emulsified fat conditioned medium, **(E)** TGF-β1 and then lipocondensate conditioned medium, **(F)** TGF-β1 and then ADSC conditioned medium, **(G)** TGF-β1 and then lipid conditioned medium, **(H)** TGF-β1 and then serum free medium and lipid. Scale bars = 100 μM. **(I)** The percentage of cells expressing Ki-67 was calculated. *N* = 3 / 2 (control + TGF-β1 + lipid), *n* = 3. Coloured bars represent cells treated with conditioned medium. Error bars = standard deviation. An ordinary one-way ANOVA was carried out to test for significance.

5.2.3.4 Does adipose tissue-derived conditioned medium illicit adipogenic differentiation in TGF-β1 treated fibroblasts

Data to examine whether adipose tissue-derived conditioned medium causes proliferation of myofibroblasts was inconclusive however, another mechanism behind reversible myofibroblast differentiation has been reported. There is evidence to suggest that myofibroblasts can undergo adipogenic differentiation following wounding (el Agha *et al.,* 2017; Plikus *et al.,* 2017). To examine if factors from adipose tissue-derived conditioned medium were causing adipogenic differentiation of fibroblasts, cells were treated as described in section 5.2.2 except following fixation, an oil red O assay was carried out as described in section 2.4.1.2. The presence of oil red O stain indicates the presence of lipid and adipogenic differentiation. Oil red O stain was quantified by absorbance at 492 nm.

There was no difference in the amount of oil red O staining in any condition ($p > 0.45$). Untreated, TGF-β1 and serum free media, and TGF-β1 and minced adipose tissue conditioned medium treated cells had a similar mean absorbance (0.29, 0.25, and 0.28 respectively, figure 5.8). TGF-β1 and emulsified fat conditioned medium treated cells had an absorbance of 0.50, as did TGF-β1 and lipocondensate conditioned medium treated cells. Cells treated with TGF-β1 and ADSC conditioned medium had an absorbance value of 0.38 and TGF-β1 and lipid conditioned medium cells had an absorbance value of 0.55. Fibroblasts treated with TGF-β1 and then serum free media and lipid had the highest mean absorbance value (0.65) but this is not significantly higher than any other condition ($p > 0.14$). This data suggest that adipose tissue-derived conditioned medium is not causing adipogenic differentiation of myofibroblasts. Following this, it was decided to examine whether adipose tissue-derived conditioned medium could reverse myofibroblast differentiation in fibroblasts isolated from hypertrophic scars.

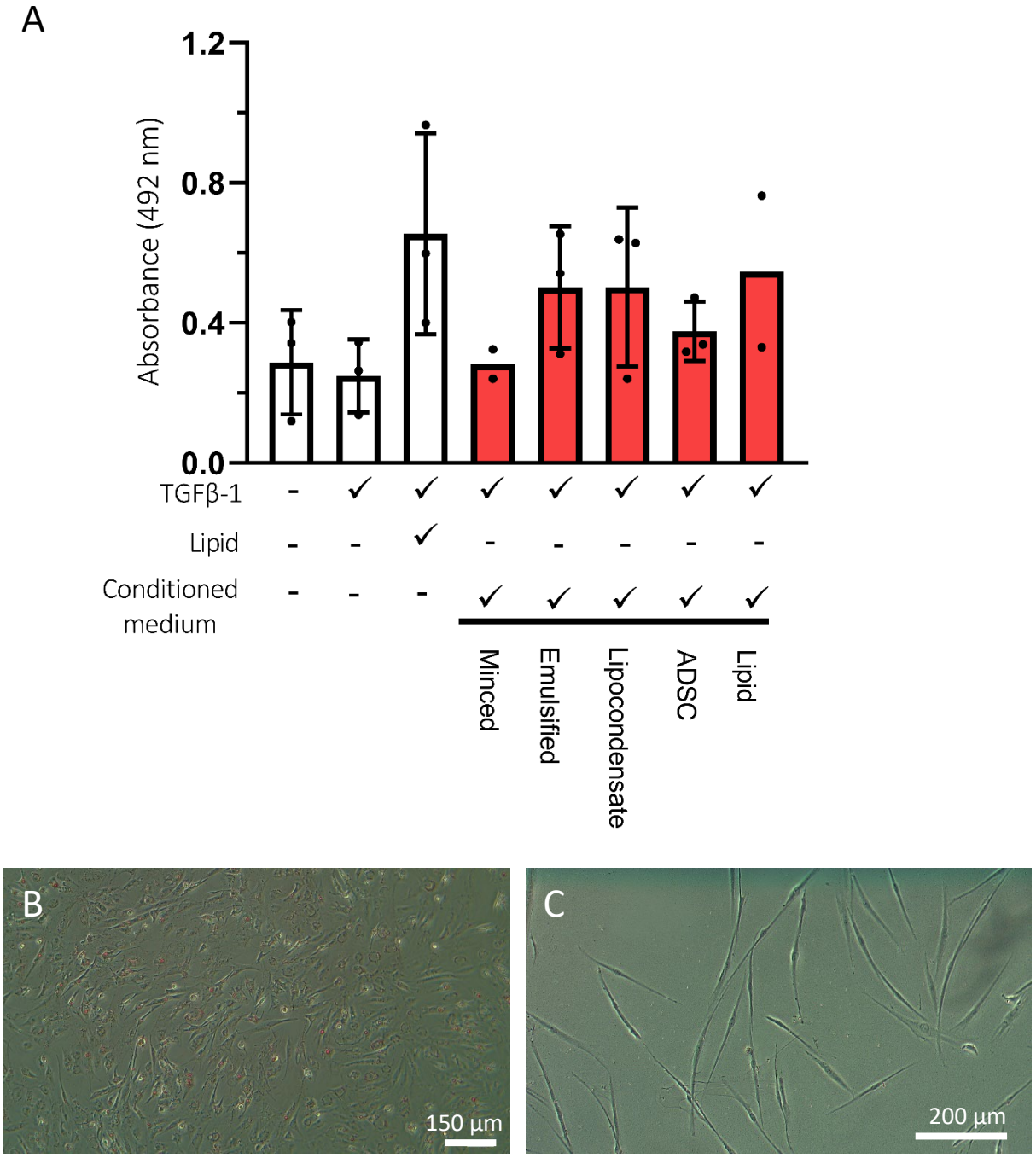

Figure 5.8. Does adipose tissue conditioned medium induce adipogenic differentiation in TGF-β1 activated myofibroblasts. (A) Adipogenic differentiation was assessed by the presence of Oil red O dye following staining after TGF-β1 and adipose tissue conditioned media treatment. *N* = 3 / 2 (TGF-β1 + minced adipose tissue and TGF-β1 + lipid medium), *n* = 3. Coloured bars represent cells treated with conditioned medium. Error bars = standard deviation. An ordinary one-way ANOVA was carried out to test for significance. **(B)** Representative image of ADSCs treated with adipogenic differentiation medium. Red droplets indicate lipid presence and adipogenic differentiation. Image taken at x4 magnification, scale bar = 150 µm. **(C)** Representative image of TGF-β1 treated myofibroblasts following the addition of minced adipose tissue conditioned medium. Few lipid droplets can be seen. Image taken at x10 magnification, scale bar = 200 µm.

5.2.4 Does adipose tissue-derived conditioned medium reduce α-SMA expression in scar fibroblasts?

To test the ability of adipose tissue conditioned media to reduce the expression of α-SMA in already differentiated myofibroblasts, fibroblasts isolated from scars were cultured as described in section 2.3.1.4. These scar fibroblasts were then seeded on coverslips and as described in section 2.4.5.6, serum starved, and then cultured with TGF-β1, adipose tissue-derived conditioned medium, or lipid for 72 hours. These cells were then stained for cell nuclei and α-SMA, as described in section 2.4.5.6, and immunofluorescence analysis carried out.

In populations of untreated, control, scar fibroblasts, 46.5 % of cells were expressing α-SMA (figure 5.9E). This significantly increased to 97.4 % of cells expressing α-SMA when TGF-β1 was added to scar fibroblasts for 72 hours (figure 5.9B, $p = 0.005$). The percentage of cells expressing α-SMA when treated with minced adipose tissue conditioned medium was 32.7 %, significantly lower than TGF-β1 treated scar fibroblasts ($p < 0.001$). However, this was not significantly lower than untreated scar fibroblasts ($p > 0.65$). The mean percentage of cells expressing α-SMA when treated with ADSC conditioned medium or lipid was higher than untreated scar fibroblasts (62.7 % and 68.8 % respectively) but was not significantly higher ($p < 0.35$). This data shows that under the conditions tested, adipose tissue-derived conditioned medium did not reduce α-SMA expression in scar fibroblasts.

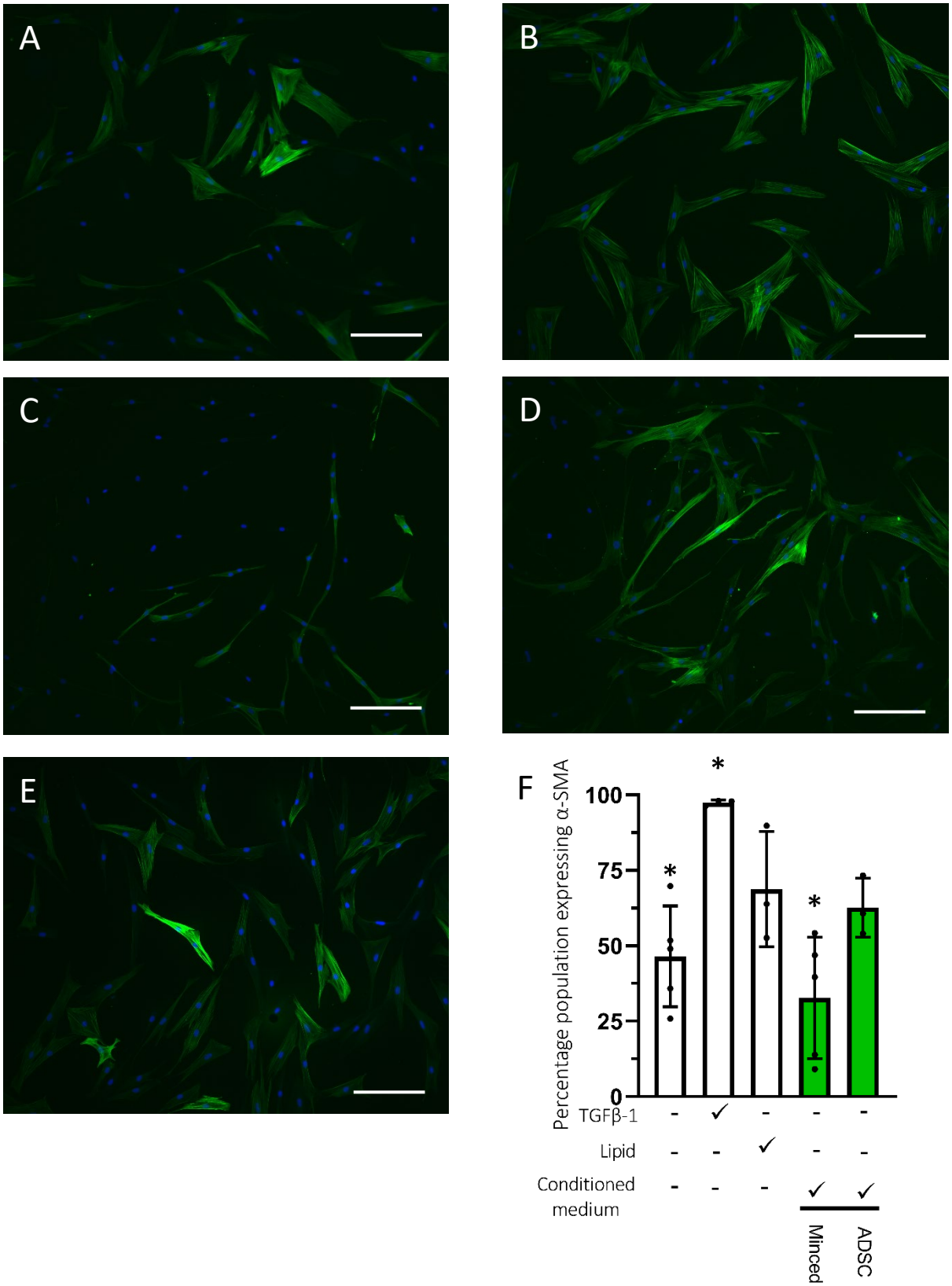

Figure 5.9. α-SMA production in adipose tissue conditioned media treated scar fibroblasts. (A-E) Representative images of α-SMA and DAPI stained scar fibroblasts, **(A)** untreated, **(B)** TGF-β1 treated, **(C)** minced adipose tissue conditioned medium treated, **(D)** ADSC conditioned medium treated, **(E)** Lipid treated. X10 magnification, scale bar = 200 µm. **(F)** The percentage of cells expressing α-SMA. Significance calculated by an ordinary one-way ANOVA. *N* = 3, *n* = 3. Coloured bars represent cells treated with conditioned medium. * = $p < 0.005$ compared to TGF-β1 treated cells.

5.3 Discussion

The aims of this chapter were to:

- Measure α-smooth muscle actin (α-SMA) expression in TGF-β1 differentiated myofibroblasts following the addition of adipose tissue-derived conditioned medium (figure 5.1) to examine whether factors within the conditioned medium could reverse myofibroblast differentiation.

- Elucidate the mechanism behind any reversal effect.

- Examine whether addition of adipose tissue-derived conditioned medium could reverse myofibroblast differentiation in hypertrophic scar myofibroblasts.

5.3.1 Paracrine reversal of myofibroblast differentiation

To test whether factors from adipose tissue-derived conditioned medium could reverse myofibroblast differentiation, gene expression data was used to ensure that the removal of TGF-β1, was not causing spontaneous de-differentiation. 72 hours after TGF-β1 removal, cells treated with TGF-β1 for 24 and 72 hours expressed significantly higher fibronectin compared to untreated fibroblasts. Collagen expression was also significantly higher in cells following TGF-β1 removal after 24 hours of TGF-β1 treatment compared to untreated fibroblasts (figure 5.2). This demonstrated that TGF-β1 treated cells maintain their phenotype for 72 hours if cultured in serum free medium after the addition of TGF-β1. For consistency with the work in chapter 4 and because fibronectin expression remained increased, in this chapter, TGF-β1 was added for 72 hours to activate myofibroblasts. Adipose tissue-derived conditioned medium was also added for 72 hours for the sake of consistency with chapter 4.

Paracrine factors in adipose tissue-derived conditioned medium were able to reverse the myofibroblast phenotype in fibroblasts treated with TGF-β1 for 72 hours. Immunofluorescence showed a significant decrease in the expression of α-SMA fibres in cells treated first with TGF-β1, and then minced adipose tissue, emulsified fat, lipocondensate, or lipid conditioned medium (figure 5.3). As in chapter 4, ADSC conditioned medium had no effect on α-SMA expression. Light microscopy images supported this data with cells treated with TGF-β1 having a wide and stretched appearance. Within the cytoplasm, actin stress fibres could be seen to be causing contraction of the outer membrane of the myofibroblasts as described in the literature. On the other hand, fibroblasts treated first with TGF-β1 and then minced adipose tissue or emulsified fat conditioned medium had a thin, spindle-like appearance with no visible stress fibres. These data indicate that paracrine factors from adipose tissue-derived conditioned medium can reverse the myofibroblast phenotype.

Given that factors from minced adipose tissue, emulsified fat, or lipocondensate conditioned medium reversed the differentiation of myofibroblasts, it could be suggested that as in chapter 4, the stromal vascular fraction (SVF) or ECM is the responsible component for this de-differentiation. This is because these are the components of adipose tissue found in all these formulations. However, factors from lipid conditioned medium were also able to reduce the expression of α-SMA in TGF-β1 differentiated myofibroblasts (figure 5.3). Lipid is also found in minced adipose tissue and emulsified fat however, not in lipocondensate. Thus, there may be two different mechanisms causing myofibroblast de-differentiation, one dependent on factors released from lipid and another dependent on factors released from the SVF.

A significantly increased number of cells was found in immunofluorescence images of cells treated with TGF-β1 and then minced adipose tissue, emulsified fat, or lipocondensate conditioned medium. There were a similar number of cells after incubation with lipid medium as in samples incubated with only TGF-β1. This is further suggestive of two separate mechanisms of myofibroblast de-differentiation. Because, if myofibroblast de-differentiation is working via increasing proliferation (mentioned later) then there is little to suggest that lipid conditioned medium is increasing myofibroblast proliferation.

The ability of adipose tissue-derived conditioned medium to increase TGF-β1 treated fibroblast proliferation was examined via Ki-67 staining and resazurin assay. Cell counts of fluorescent images in figure 5.4 showed that when treated with TGF-β1 and minced adipose tissue or emulsified fat conditioned medium, a significantly higher number of cells were present (figure 5.5). However, these images were just random selections of the larger cellular population in each well plate. The resazurin assay on the other hand, gave information about the whole cellular population present in a particular well. Cells treated with TGF-β1 and then emulsified fat conditioned medium were significantly more metabolically active than control cells. No other condition was significantly higher than the control however, cells treated with TGF-β1 and then minced adipose tissue-derived conditioned medium had a higher mean average than all conditions other than emulsified fat conditioned medium ($p = 0.11$). When stained for Ki-67, there was no significant difference in Ki-67 expression in any condition tested and thus the number of proliferating cells were not different between conditions when stained with Ki-67. While not a quantitative measure of cell number, resazurin data implies that following treatment with emulsified fat conditioned medium a higher number of cells were present. Ki-67 expression did not show increased proliferation of myofibroblasts, but Ki-67 only has a half-life of 6-9 hours (Davey *et al.,* 2021). Given that TGF-β1 treated myofibroblasts are being incubated with adipose tissue-derived conditioned media for 72 hours, it is likely that by the time cells are fixed and stained most of the

Ki-67 expression in proliferating cells has been missed. Taken together resazurin, and Ki-67 data shows that in the conditions tested adipose tissue-derived conditioned medium did not lead to increased myofibroblast proliferation. However, cell counts and resazurin data on emulsified fat conditioned medium imply there might be adipose tissue growth factor dependent increased proliferation occurring. If timings for Ki-67 staining are optimised and more objective measures of cell counts are used, then this hypothesis could be confirmed.

In all conditions tested via oil red O staining, there was no significant difference in absorbance. This showed there was not an increased lipid presence in cells treated with TGF-β1 and then adipose tissue-derived conditioned medium. These results confirmed that adipose tissue-derived conditioned medium was not causing myofibroblasts to undergo adipogenic differentiation.

Finally, immunofluorescence staining of α-SMA was carried out on fibroblasts isolated from scars and treated with TGF-β1, minced adipose tissue, or ADSC conditioned medium. In control scar fibroblast populations, 45.6 % of cells expressed α-SMA. Cells treated with TGF-β1 expressed significantly more α-SMA than all other conditions. Minced adipose tissue conditioned medium treated scar fibroblasts had a lowest mean expression of α-SMA however this was not significantly lower than control scar fibroblasts. This data shows that in the conditions tested, factors from adipose tissue-derived conditioned medium cannot reverse the differentiation of scar-derived myofibroblasts.

5.3.2 Myofibroblast plasticity

Historically, myofibroblast differentiation has been considered a terminal stage in the fibroblast lifecycle (Bayreuther *et al.,* 1988; Evans *et al.,* 2003; Hinz, 2007). In more recent times however, it has become increasingly apparent that myofibroblast differentiation is not necessarily terminal and can be reversed *in vitro* (el Agha *et al.,* 2017; Fang *et al.,* 2012; Fortier *et al.,* 2021; Hecker *et al.,* 2011; Maltseva *et al.,* 2001; Melling *et al.,* 2018; Sieber *et al.,* 2018; Walker *et al.,* 2020). Furthermore, it has been suggested that myofibroblasts may differentiate into adipocytes to resolve wound healing (Plikus *et al.,* 2017).

Evans *et al.,* (2003) was one of the first research groups to demonstrate the involvement of SMAD proteins in TGF-β1 induced myofibroblast differentiation. This work is frequently cited as demonstrating that myofibroblasts are a terminally differentiated cell (Garrison *et al.,* 2013; Hecker *et al.,* 2011; Kato *et al.,* 2020; Sieber *et al.,* 2018). To the best of my understanding however, there are no experiments carried out in this research paper to demonstrate that these myofibroblasts are in fact terminally differentiated. Bayreuther *et al.,* (1988) was cited by Evans *et al.,* (2003) as demonstrating that myofibroblasts are terminally differentiated. The group does demonstrate that

serially passaged fibroblasts demonstrate a myofibroblast phenotype and halt proliferation. However, it is possible the inability of these myofibroblasts to de-differentiate is a result of myofibroblast senescence from serial passaging and not something intrinsic to myofibroblast differentiation as Kato *et al.,* (2020) were able to cause de-differentiation of TGF-β1 induced myofibroblasts but not in senescent myofibroblasts. Myofibroblast de-differentiation has been demonstrated since 2001 (Maltseva *et al.,* 2001), but in the past decade there has been an increasing acceptance that myofibroblasts are still a plastic cell type (Fortier *et al.,* 2021; Hinz, 2015; Sieber *et al.,* 2018).

It has been reported that removing TGF-β1 and culturing with media containing 10 % serum induces the reversal of the myofibroblast phenotype (Hecker *et al.,* 2011; Kato *et al.,* 2020). However, multiple papers have demonstrated that myofibroblasts activated with TGF-β1 maintain their myofibroblast phenotype following culture in serum free media. Hecker *et al.,* (2011) showed that myofibroblasts remain activated for longer than 72 hours after TGF-β1 is removed and Fortier *et al.,* (2021), Garrison *et al.,* (2013), and Kato *et al.,* (2020) have shown activation 120 hours post TGF-β1 removal.

There are several mechanisms thought to be responsible for the removal of myofibroblasts from wound tissue. Hecker *et al.,* (2011) demonstrated that myofibroblast de-differentiation is a result of increased MAPK signalling. Mitogens are molecules that stimulate mitosis *via* various signalling pathways (reviewed in McCubrey *et al.,* (2007)) and Hecker *et al.,* showed that increased MAPK activity decreased α-SMA expression *via* downregulating the protein MyoD and caused myofibroblast proliferation. They also suggested that MAPK activity caused disassembly of α-SMA fibres, which results in a loss of the myofibroblast phenotype. The mitogen FGF-2 has been shown to de-differentiate myofibroblasts (Koo *et al.,* 2018; Maltseva *et al.,* 2001) and it has been suggested that FGF-2 may act by causing myofibroblast proliferation through the MAPK pathway (Fortier *et al.,* 2021). Treating TGF-β1 activated myofibroblasts with FGF-2 caused upregulation of proliferative genes, caused increased proliferation, and resulted in a morphological change wherein myofibroblasts lost their stress fibres and became elongated and thin as if untreated with TGF-β1 (Fortier *et al.,* 2021). It was suggested that for myofibroblasts to proliferate it is required that their cytoskeleton is re-structured, and the α-SMA stress fibres are broken down, leading to a loss of phenotype upon proliferation and de-differentiation back to a fibroblast state.

Alternatively, it has been suggested that myofibroblasts may undergo adipogenic differentiation. It is thought that in the dermis, the differentiation of myofibroblasts to adipocytes is a key stage in the resolution of wound healing (Plikus *et al.,* 2017). The research of Plikus *et al.,*

demonstrated that myofibroblasts around hair follicles can differentiate into adipocytes *via* bone morphogenic protein (BMP)-2 or 4 stimulation. In addition to the work by Plikus *et al.,* (2017), it has been shown that lung myofibroblasts can be differentiated into a cell termed a lipofibroblast (el Agha *et al.,* 2017). These cells (reviewed in McGowan, 2019) are fibroblasts containing lipid vesicles found in lung tissue. This differentiation was found to be regulated *via* peroxisome proliferator-activated receptor-γ (PPARγ; el Agha *et al.,* 2017). Myofibroblasts from systemic sclerosis skin (a fibrotic skin disease) were found to express less collagen following treatment with adiponectin (Fang *et al.,* 2012). Adiponectin is a downstream product of PPARγ and if those myofibroblasts had been tested for lipid vesicles, they may have been found to have differentiated due to the adiponectin. In fact, Plikus *et al.* (2017) found that the removal of PPARγ prevents adipogenic differentiation of myofibroblasts, further highlighting PPARγ's importance in this differentiation.

Finally, prostaglandin E_2 (PGE_2) is an inflammatory mediator that also plays a role in female reproduction (Niringiyumukiza *et al.,* 2018). It has also been found to cause the removal of myofibroblasts (Sieber *et al.,* 2018). The mechanistic action behind this effect was investigated (Fortier *et al.,* 2021) and it was discovered that PGE_2 promoted the production of cyclic adenosine monophosphate and poly ADP ribosome polymerase, both markers of apoptosis (Kondo *et al.,* 2010; Zhou *et al.,* 2005). It was concluded that PGE_2 was promoting apoptosis in myofibroblasts, which caused a decrease of myofibroblast markers such as α-SMA and collagen in cells (Fortier *et al.,* 2021). Upon the resolution of normal wound healing, myofibroblasts undergo apoptosis (Desmoulire *et al.,* 1995). In fibrosis, this does not occur for reasons not fully understood (Hinz, 2007). It appears that PGE_2 restores this programmed cell death in TGF-β1 treated myofibroblasts.

While the process behind hypertrophic scarring is not fully understood, it is clear that fibroblasts isolated from hypertrophic scars behave differently from normal fibroblasts (Chun *et al.,* 2016; Tuan & Nichter, 1998; Ţuţuianu *et al.,* 2019). As a result of long term and repeated exposure to inflammatory signals such as TGF-β1, these cells have been constitutively activated to myofibroblasts and express α-SMA even when isolated and not treated with TGF-β1 (Kumai *et al.,* 2010; Ţuţuianu *et al.,* 2019). Furthermore, several other proteins are expressed differentially compared to normal, healthy, fibroblasts (Tuan & Nichter, 1998; Zhang *et al.,* 2012).

There has been some investigation into whether factors from adipose tissue can alter the phenotype of scar fibroblasts. Kumai *et al.* (2010) found that ADSC conditioned medium lowered the expression of α-SMA in ferret scar fibroblasts and Li *et al.* (2016) * found ADSC conditioned medium lowered expression of α-SMA and collagen in human scar fibroblasts, while also decreasing scar fibroblast migration. Factors from monocultured adipocytes have been shown to lower the

*See appendix

expression of α-SMA and ECM markers of a myofibroblast phenotype (Hoerst *et al.,* 2019). The authors suggest that BMP-4 secreted by ADSCs activated PPARγ caused this effect. Spiekman *et al.,* (2014), demonstrated that ADSC conditioned medium could inhibit TGF-β1 induced fibroblast differentiation and applied this medium to activated myofibroblasts from keloid scars. However, they only saw a partial decrease in the myofibroblast markers of keloid fibroblasts. Finally, co-culture of ADSCs with scar fibroblasts has been demonstrated to reverse the myofibroblast phenotype of these scar fibroblasts with α-SMA, fibronectin, and collagen expression decreased alongside myofibroblast contractile ability (Deng *et al.,* 2018)*. Although, the authors do not suggest a specific paracrine mechanism for this observation.

5.3.3 Adipose tissue based myofibroblast reversal

It appears there are three mechanisms behind the removal of myofibroblasts in a wound setting; apoptosis of myofibroblasts (Fortier *et al.,* 2021; Sieber *et al.,* 2018), adipogenic differentiation (el Agha *et al.,* 2017; Plikus *et al.,* 2017), and myofibroblast proliferation (Fortier *et al.,* 2021; Hecker *et al.,* 2011). After the resolution of wound healing, myofibroblasts normally undergo apoptosis however, in fibrosis this seems to be dysregulated (Desmoulire *et al.,* 1995). The addition of PGE_2 appears to restore this apoptosis (Sieber *et al.,* 2018), potentially removing the myofibroblast population from scars. Unfortunately, the cytokine array in section 2.4.6.1 did not test for the levels of PGE_2 in adipose tissue-derived conditioned medium. However, there is evidence of adipose tissue secreting this factor (Hu *et al.,* 2016). In figure 5.3, in light microscopy images, cell debris can be seen in fibroblasts treated with TGF-β1 and then lipid conditioned medium. Furthermore, cells appear sparser in these images, perhaps indicating that some cells have undergone apoptosis. There could be PGE_2 being released from lipid conditioned medium leading to increased myofibroblast apoptosis meaning there appears to be less α-SMA in figure 5.4. However, it would then be expected that cell counts were lower in figure 5.5 and this isn't the case. Further investigation is needed to identify whether this is the method of action lipid conditioned medium is causing myofibroblast removal through.

Another mechanism of myofibroblast removal is adipogenic differentiation. Myofibroblasts have been shown to undergo adipogenic differentiation following wound healing in response to PPARγ (el Agha *et al.,* 2017). It was noticed that myofibroblasts treated with adipose tissue-derived conditioned medium seemed to contain lipid vesicles, a marker of adipogenic differentiation (Gimble & Guilak, 2003). Plikus *et al.* found that following wounding, as myofibroblasts differentiated to adipocytes, oil red O staining showed that lipid presence increased and α-SMA expression decreased in wounds. If my myofibroblasts were undergoing adipogenic differentiation, then it would explain

*See appendix

why α-SMA expression decreased in figure 5.4 when adipose tissue-derived conditioned medium was added. In Hoerst *et al.* (2019), the authors found that myofibroblast de-differentiation was induced by PPARγ signalling with a decrease in α-SMA and collagen expression. PPARγ signalling acts upstream of adiponectin signalling (Plikus *et al.,* 2017) and is highly expressed in adipose tissue (Torre-Villalvazo *et al.,* 2018). It was hypothesised that adiponectin secreted by adipose tissue-derived conditioned medium may have been acting downstream of PPARγ signalling and causing adipogenic differentiation in myofibroblasts. Myofibroblasts were stained with oil red O which binds to lipid in cells (Mehlem *et al.,* 2013) however, as in Hoerst *et al.* there was no observed increase in lipid droplet formation in any conditions. The literature, along with data discussed above indicates that adipokine induced PPARγ signalling in myofibroblasts is still not fully understood and the decrease in α-SMA expression observed in TGF-β1 treated myofibroblasts is not a result of adipogenic differentiation.

Finally, mitogens (specifically FGF-2) cause myofibroblasts to proliferate (Fortier *et al.,* 2021). For this proliferation to occur, the actin cytoskeleton must be disassembled and thus myofibroblasts lose their contractile phenotype and α-SMA fibres when proliferating, resulting in them no longer being considered myofibroblasts (Hecker *et al.,* 2011). FGF proteins were found to be present in my adipose tissue-derived conditioned medium in section 4.2.3, and adipose tissue has been found to secrete high volumes of FGF-2 (Mydlo *et al.,* 1998). While resazurin and Ki-67 staining did not show increased myofibroblast proliferation I believe there are mitigating factors that explain this (mentioned in section 5.3.1). The α-SMA in myofibroblasts give the cells the wide, splayed appearance (figure 5.3). When treated with FGF-2 and proliferation has occurred, the cytoskeleton has disassembled and myofibroblasts return to the thin and elongated fibroblast (Fortier *et al.,* 2021). The images in this paper are very similar to my light microscopy images in figure 5.3, (figure 5.10). This gives me reason to believe one of the main mechanisms through which my adipose tissue-derived conditioned medium reverses myofibroblast differentiation is through increased proliferation. Further optimisation and objective testing would have been used to test this hypothesis however, time constraints meant this unfortunately could not happen.

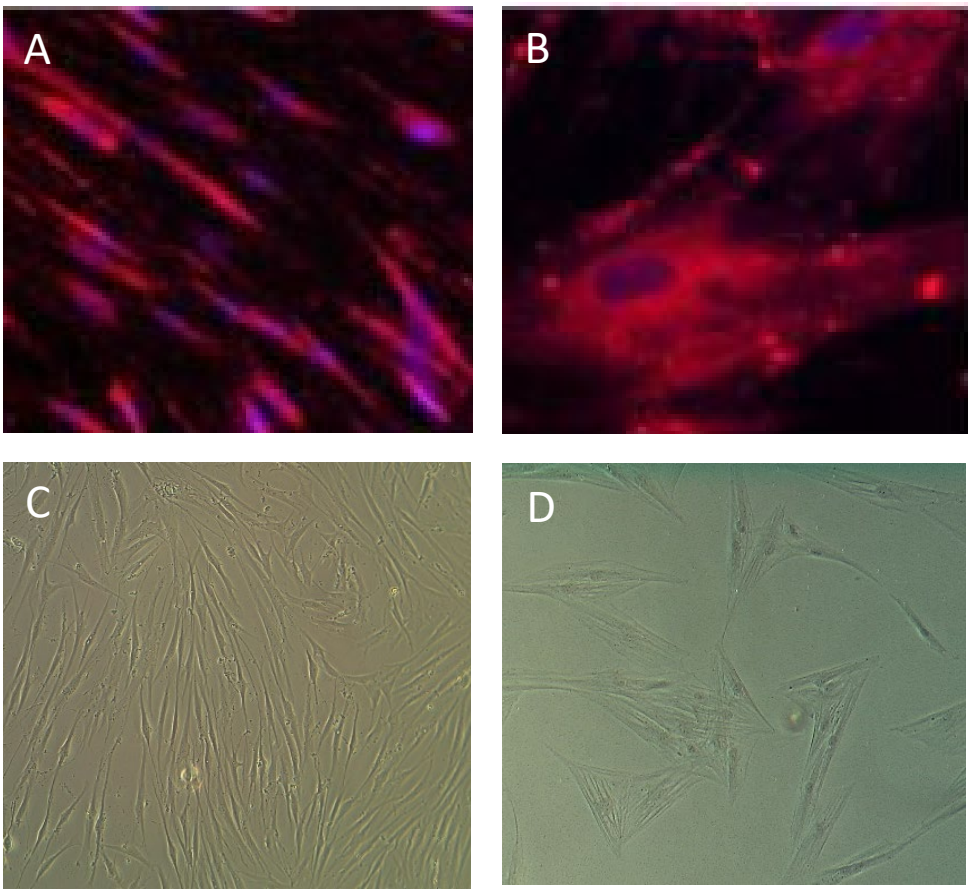

Figure 5.10. Change in myofibroblast morphology following FGF-2 and adipose tissue conditioned medium treatment. (A-B) Images of TGF-β1 treated fibroblasts and stained for α-SMA from Fortier *et al.*, (2021). Images used with permission from Creative Commons using the following license https://creativecommons.org/licenses/by/4.0/. **(A)** TGF-β1 and then FGF-2 treated myofibroblasts, cells have a spindle-like morphology. **(B)** TGF-β1 treated fibroblasts, cells are wide and stretched, characteristic of a myofibroblast phenotype. **(C-D)** Light microscope images of TGF-β1 treated fibroblasts. **(C)** Cells treated with minced adipose tissue. Cells have a long, spindle morphology. **(D)** Untreated myofibroblasts, cells are stretched and α-SMA fibres are visible.

My work is the first to show that paracrine factors from clinically relevant formulations of adipose tissue can reverse the differentiation of myofibroblasts following TGF-β1 differentiation *in vitro*. It has been previously demonstrated that paracrine factors from adipocytes can reverse myofibroblast differentiation (Hoerst *et al.,* 2019). The work by Hoerst *et al.* also agreed with my results as their ADSC conditioned medium could not reverse myofibroblast differentiation. The group do not mention the concentration of ADSCs per ml of conditioned medium, but they seeded cells at 100,000 cells per well of a 6-well plate. This is more than double the number of cells I seed per well for my ADSC conditioned medium (45,000 cells per well of a 6-well plate) and is suggestive that ADSC concentration is not why ADSC conditioned medium had no influence on myofibroblast phenotype. Their work also suggests that the adipocyte population in minced adipose tissue is responsible for the anti-fibrotic effect from the conditioned medium. Factors secreted from adipocytes will also be present in emulsified fat and lipid conditioned medium as these factors will have been stored in the lipid of these formulations.

This work was unable to demonstrate that adipose tissue-derived conditioned medium was able to reverse the differentiation of scar fibroblasts. This aligns with some data from Spiekman *et al.* testing their ADSC conditioned medium on fibroblasts isolated from keloid scars. There was some responsiveness to ADSC conditioned medium with a decrease in collagen type lll expression but there was no other decrease compared to baseline keloid scar fibroblasts. The α-SMA expression in their article matches that of figure 5.9, with TGF-β1 increasing α-SMA expression significantly and their conditioned medium able to bring this expression to baseline levels. However, this expression never went lower than that of the untreated scar fibroblasts. Kumai *et al.* (2010) were able to show a decrease in α-SMA expression in scar fibroblasts via ADSC co-culture but the decrease in the percentage of cells expressing α-SMA was smaller than the difference observed between the mean of α-SMA expressing cells in my untreated and minced adipose tissue conditioned medium treated scar fibroblasts. Likewise, Deng *et al.* (2018) have also suggested ADSC co-culture to be able to reverse myofibroblast differentiation. While this does disagree with the results of my work in this chapter co-culture experiments are different to using conditioned medium as paracrine signals will be being constantly secreted with co-culture, alongside the scar fibroblasts signalling to the ADSCs. Furthermore, Deng *et al.* (2018) cultured their scar fibroblasts in D-MEM containing 10 % serum. It has been demonstrated that culturing differentiated myofibroblasts in serum causes de-differentiation back to fibroblasts (Hecker *et al.,* 2011; Kato *et al.,* 2020). It is possible the de-differentiation that Deng *et al.* (2018) reported may be a result of the serum they added and not crosstalk from ADSCs.

This chapter has shown that paracrine factors from clinically used forms of adipose tissue can reverse myofibroblast differentiation *in vitro*. This work is supported by other results in the literature and goes some way to explaining why autologous fat grafting regenerates scar tissue. The reduced contraction and thickness of scars may be a result of myofibroblast de-differentiation/apoptosis around the scar tissue, removing the production of ECM and contractile forces on the tissue. While it was not possible to cause de-differentiation of scar fibroblasts in these conditions there is support from the literature and my *in vitro* work that this may be possible by causing apoptosis, adipogenic differentiation, or proliferation based de-differentiation. These results suggest that adipocytes or lipid, and the stromal vascular fraction are responsible for this effect. This highlights that while concentrating the SVF can be effective for regenerative grafting, adipocytes play an important role in this regeneration and should not necessarily be discarded. If the exact signalling mechanisms behind this response can be elucidated, then a cell free therapeutic could be developed to deliver subcutaneously to hypertrophic scars to reduce scar contraction.

6.0 Discussion

The aims set out at the beginning of this work were as follows:

1. Investigate whether paracrine factors from clinically relevant forms of adipose tissue can inhibit the differentiation of fibroblasts.

2. Examine whether paracrine factors from clinically relevant forms of adipose tissue can reverse the differentiation of myofibroblasts.

3. Identify the cellular components of adipose tissue responsible for any effect paracrine factors from clinically relevant forms of adipose tissue may have on myofibroblast differentiation

4. Elucidate the underlying mechanisms behind any effect paracrine factors from clinically relevant forms of adipose tissue may have on myofibroblast differentiation.

6.1 General discussion

6.1.1 Characterising adipose tissue formulations

The results in this thesis demonstrate that adipose tissue can inhibit myofibroblast differentiation and reverse myofibroblast differentiation *in vitro*. This work aimed to use formulations of adipose tissue that are used currently in a clinical setting. These formulations were minced adipose tissue, lipoaspirate, emulsified fat, lipocondensate and ADSCs. During this work, the processing steps used to generate emulsified fat and lipocondensate were optimised. In particular, the observation that freeze/thawing the lipocondensate formulation causes separation from the lipid oil is useful knowledge that may help other researchers and surgeons effectively generate their own lipocondensate-like formulation. Using confocal imaging, resazurin and LDH assays, and through cell counting the formulations were characterised and by comparing them to the literature it is likely the formulations used in this work matched those used by others. This data demonstrated that minced adipose tissue could be used as a substitute for lipoaspirate, adipocytes were being lysed during emulsified fat generation, lipocondensate formation was concentrating the SVF and that ADSCs had literature-established markers.

Clinicians use a wide variety of different adipose tissue formulations, similar to those used in this project, in regenerative surgeries. These include lipoaspirate (Caviggioli *et al.,* 2011; Klinger *et al.,* 2008), emulsified fat (Kemaloğlu, 2016), lipocondensate (Cao *et al.,* 2022), and adipose tissue supplemented with ADSCs (Carstens *et al.,* 2015). Processing adipose tissue from lipoaspirate into other formulations significantly alters the structure and the contents of the adipose tissue itself. For example, processing to Nanofat removes the adipocyte population of the adipose tissue (Tonnard *et*

al., 2013) and SVF-gel formulations have had the lipid removed (Yao *et al.,* 2017). Furthermore, because the use of enzymatically isolated ADSCs is restricted by regulatory bodies (U.S. Department of Health and Human Services *et al.,* 2020), these formulations are generated in an attempt to mechanically disrupt the adipose tissue and concentrate the population of SVF cells (and thus by extension, ADSCs). As a result of this, a wide range of different formulations have been developed in the literature using different processing techniques (Bianchi *et al.,* 2013; Mashiko *et al.,* 2017; Tonnard *et al.,* 2013; Yao *et al.,* 2017). Even within established techniques, there are often differences in processing steps with different versions of "Nanofat" (Gentile *et al.,* 2017; lo Furno *et al.,* 2017) and "SVF-gels" (Sesé *et al.,* 2020; van Dongen *et al.,* 2016; Yao *et al.,* 2017) cited in the literature. As a result, it was important to characterise the formulations used throughout this work and ensure they are functioning as intended in the literature they are based on.

To this end, confocal images of the formulations used in this work are comparable to images of clinically relevant formulations of adipose tissue (lipoaspirate (Eto *et al.,* 2009), emulsified fat (Tonnard *et al.,* 2013), and lipocondensate (Yao *et al.,* 2017)). These images show the well-structured adipose tissue becomes fragmented and the adipocyte population decreases and release lipid as the adipose tissue becomes more fragmented. Lipoaspirate images show tightly bundled adipocytes with vessels running throughout in a similar manner to Eto *et al.* (2009). Images of emulsified fat show the fragmented tissue structure with lipid vesicles in place of adipocytes as seen in the live/dead staining of Tonnard *et al.* (2013). These images also show the highly fragmented lipocondensate with few adipocytes but SVF cells still present is similar to the images in Yao *et al.* (2017). Furthermore, cell numbers in the formulation are in line with those in the literature. (Sesé *et al.,* 2019, 2020) and demonstrate that the more adipose tissue is processed, the more concentrated the SVF becomes. This data not only characterises the formulations used throughout this work but also confirms that the formulations are acting in an identical manner to the clinically relevant formulations they are based upon.

6.1.2 Myofibroblast differentiation inhibition and reversal

These formulations characterised in chapter 3 were used to generate "conditioned medium" containing paracrine factors from the adipose tissue formulations. These paracrine factors were able to inhibit TGF-β1 dependent myofibroblast differentiation with ECM expression and α-SMA production inhibited. These paracrine factors could also decrease the production of α-SMA in fibroblasts already differentiated to myofibroblasts. This indicates that myofibroblast de-differentiation was occurring following treatment with paracrine factors. In the conditions tested, HGF was unable to replicate the inhibition caused by adipose tissue-derived conditioned medium. Furthermore, the C-Met inhibitor, foretinib, was unable to prevent the inhibitory action of

lipoaspirate conditioned medium. This implies that HGF is not the paracrine factor in adipose tissue responsible for myofibroblast inhibition. Finally, paracrine factors from adipose tissue were unable to reverse the differentiation of myofibroblasts isolated from scar tissue in the conditions tested. Admittedly though, this was the last experiment carried out in this work and could definitely be optimised and tested in greater detail.

There is strong evidence that autologous fat grafting regenerates scar tissue (Klinger *et al.,* 2013; Rigotti *et al.,* 2007; van Dongen *et al.,* 2021). Alongside reducing pain and increasing elasticity, the stiffness of the scar tissue is decreased (Jaspers *et al.,* 2017; Maione *et al.,* 2014). Excessive ECM produced by myofibroblasts alongside contraction of the myofibroblasts themselves is responsible for this stiffness (Hinz *et al.,* 2001). In histological analysis of scars following autologous fat grafting, there is a decrease in the presence of α-SMA and a decreased myofibroblast population (Uysal *et al.,* 2014; Wang *et al.,* 2019). This suggests that autologous fat grafting is able to remove or cause de-differentiation of the myofibroblasts formed during scarring. It has become apparent that the myofibroblast is a plastic cell type and de-differentiation is possible (Fortier *et al.,* 2021; Hecker *et al.,* 2011). Furthermore, adipocytes (Hoerst *et al.,* 2019) and ADSCs (Li *et al.,* 2016; Deng *et al.,* 2018) have been observed to cause a reversal of the myofibroblast phenotype. Despite evidence suggesting autologous fat grafting removes myofibroblast cells from scars, there have been few *in vitro* studies on the ability of adipose tissue and these formulations to inhibit or reverse myofibroblast differentiation. ADSCs have been shown to inhibit (Spiekman *et al.,* 2014) and reverse myofibroblast differentiation *in vitro* (Deng *et al.,* 2018). However, the effectiveness of other formulations at inhibiting or reversing myofibroblast differentiation has never been compared *in vivo or in vitro*. Inhibition of the TGF-β1 pathway *in vitro* has been reported with numerous molecules implicated in SMAD inhibition. HGF (Yang *et al.,* 2003), FGF (Liguori *et al.,* 2018), and CXCL9 (Wasmuth *et al.,* 2009) have all been demonstrated to interfere with the TGF-β1 signalling pathway. Anti-scarring drugs have been designed and tested with the aim of inhibiting myofibroblast differentiation in scar tissue (So *et al.,* 2011). Clinical trials however, have been unsuccessful and anti-fibrotic treatments are in need of development (McKee, 2011).

In vitro inhibition of myofibroblast differentiation has been established by Spiekman *et al.,* however, this is the first demonstration that other formulations of adipose tissue used in clinic can inhibit differentiation. HGF has been shown to inhibit myofibroblast differentiation *in vitro* (Yang *et al.,* 2003). Despite this, in my research HGF from adipose tissue conditioned medium did not have this same affect. This highlights that one of the strengths of using adipose tissue in regenerative medicine is the variety of different factors it secretes (highlighted in chapter 4). Previous research has targeted myofibroblast differentiation using one molecule at a time (Liguori *et al.,* 2018; (HGF);

So *et al.,* 2011; (TGF-β3); Yang *et al.,* 2003; (HGF)). This was eventually shown to be ineffective in more complex models (McKee, 2011) despite early success. In the context of this thesis, HGF may not effectively inhibit myofibroblast differentiation on its own and adipose tissue-derived conditioned medium may inhibit myofibroblast differentiation *via* a combination of different factors at the same time. My work, in combination with the literature above highlights this. Finally, adipose tissue conditioned medium was unable to reverse myofibroblast differentiation in fibroblasts isolated from scar tissue. There is inconsistency in the literature regarding scar myofibroblast de-differentiation. Deng *et al.* showed that ADSC co-culture can reverse scar myofibroblast phenotype however, Spiekman *et al.* demonstrated that ADSC conditioned medium had little impact. This combined with my research implies scar myofibroblast de-differentiation is possible, but further testing is required to reveal how this can be achieved consistently with adipose tissue.

6.1.3 The components responsible for myofibroblast inhibition and reversal

ADSC conditioned medium was not able to inhibit or reverse myofibroblast differentiation in any measure tested during this work. All forms of conditioned medium apart from ADSC and lipid conditioned medium was able to inhibit myofibroblast differentiation. Thus, it can be concluded that the paracrine factors responsible for this inhibition are derived from the SVF or the ECM of adipose tissue as this is the only component present in minced adipose tissue, lipoaspirate, emulsified fat, and lipocondensate. ADSC conditioned medium was unable to inhibit or reverse myofibroblast differentiation in any condition tested. This is not indicative that ADSCs have no influence at all on myofibroblast differentiation. ADSCs will be present in all formulations bar lipid medium and as discussed in the upcoming section, it is possible that ADSC conditioned medium was generated with too low a concentration of ADSCs.

Interestingly, all forms of conditioned medium except ADSC conditioned medium caused reversal of the myofibroblast phenotype. This suggests at least two mechanisms of action behind myofibroblast de-differentiation as lipid conditioned medium does not contain SVF, ECM, or adipocytes, which are present in the other formulations.

Most work on the regenerative abilities of adipose tissue focus on ADSCs (Deng *et al.,* 2018; Ma *et al.,* 2020; Spiekman *et al.,* 2014; Uysal *et al.,* 2014). ADSCs have been shown to inhibit and reverse myofibroblast differentiation. However, little work has investigated what roles other components of adipose tissue can play in affecting fibroblast differentiation. Hoerst *et al.* has shown that factors released from adipocytes can reverse myofibroblast differentiation but, to my knowledge this is the only other research investigating myofibroblast reversal with any component of adipose tissue other than ADSCs. My data in chapter 5 indicates that paracrine factors from

adipose tissue conditioned medium can reverse myofibroblast differentiation. As stated in the above, the data implies two mechanisms of action as lipid conditioned medium and lipocondensate conditioned medium both had a similar affect but share none of the same cellular components. Given that lipocondensate only contains SVF and ECM it is likely that these components are responsible for one of the mechanisms of myofibroblast differentiation. Given that adipocyte conditioned medium has been observed to lead to myofibroblast de-differentiation (Hoerst *et al.,* 2019), It is likely that factors released from live adipocytes into the lipid of adipose tissue are responsible for this second mechanism. This is an important reminder that while ADSCs show regenerative potential, adipose tissue as a whole is a strong source of regenerative factors. My research shows that *in vitro* myofibroblast inhibition is likely from factors released by the ECM and SVF of adipose tissue, while myofibroblast reversal is likely from two different mechanisms, one from the ECM and SVF, the other from factors released into lipid.

6.1.4 Wider influence of this research

In vitro inhibition of myofibroblast differentiation has been established by Spiekman *et al.,* however, this is the first demonstration that other formulations used in clinic can inhibit differentiation. Taken together, this knowledge could help in the development of new anti-scarring therapeutics. There is currently no effective method of removing hypertrophic scars. Surgical resection of the scarring often leads to recurrence (Leventhal *et al.,* 2006) and therapeutics developed to inhibit scar formation such as mannose-6-phosphate (ClinicalTrials.gov, 2009) and metelimumab (Denton *et al.,* 2007) have proved ineffective. Furthermore, approximately 35 % of surgical skin wounds will develop into a hypertrophic scar (Delavary *et al.,* 2012). This data could form the basis of new anti-fibrotic treatments aimed at using therapeutics to inhibit myofibroblast differentiation and prevent scars forming. With elective surgeries, liposuction could be carried out days beforehand and the conditioned medium used alongside surgery to prevent hypertrophic scar formation following surgery. Furthermore, conditioned medium treatment could be provided alongside scar resection, removing the scar, and preventing its recurrence of a new scar. This would allow for the regeneration of already formed scars. If the growth factors responsible for this inhibition could be identified, a cell free therapeutic with the constituent molecules of adipose tissue-derived conditioned medium could also be developed for the same purpose. Alternatively, these therapeutics could be used to cause the reversal of myofibroblast differentiation. This would lead to the underlying ECM returning to a “normal” microenvironment and alleviate the contraction and stiffness felt in hypertrophic scars.

This data is also useful to the surgeons. Firstly, it demonstrates that it is not necessary to spend time processing adipose tissue down to only ADSCs. This work has shown that formulations

other than ADSCs, already in use, are capable of *in vitro* myofibroblast inhibition and reversal. Thus, the need to seek ethical approval for the use of enzymatically isolated ADSCs is removed and quick procedures such as generating Nanofat can be used in a clinical setting to achieve myofibroblast inhibition. This data also demonstrates that in a fibroblast inhibition setting, lipocondensate and emulsified fat are as effective as conventional lipoaspirate grafting. This means surgeons do not need to consider how effective a formulation is at inhibiting myofibroblast differentiation when selecting which formulation to use in the clinic, as they all seem equally effective. As a result, different formulations can be used depending on what the surgeon needs, small and delicate areas in need of regeneration can be treated with emulsified fat or lipocondensate and large areas can be treated with lipoaspirate with minimal manipulation required.

6.2 Limitations of this work

One of the main limitations of this work is that the physiological effects of adipose tissue conditioned medium on TGF-β1 treated fibroblasts was not examined. While factors from adipose tissue-derived conditioned medium reduced the production of α-SMA it was never examined what affect this would have on the contractile ability of these myofibroblasts. This work assumes that inhibiting or reversing the production of α-SMA would help alleviate the symptoms of hypertrophic scarring however, due to time constraints, this was never tested. It was originally planned to test the effect of adipose tissue conditioned medium on myofibroblast contraction using a collagen gel assay (Bell *et al.,* 1979; Spiekman *et al.,* 2014). Unfortunately, due to lab time lost during the COVID-19 pandemic, this work was never carried out.

TGF-β1 causes differentiation of fibroblasts via the SMAD pathway (figure 1.9). By observing a reduction in α-SMA when fibroblasts are treated with adipose tissue conditioned medium and TGF-β1 I have assumed that this reduction is a result of inhibiting the SMAD pathway. This is logical however, to further confirm this western blotting analysis could have been carried out to examine the levels of phosphorylated SMAD3 (p-SMAD3). If p-SMAD3 was found to also be present in decreased amounts when adipose tissue conditioned medium was added it would confirm that the SMAD pathway is being inhibited.

Fibrosis is a very complex disease and is a result of more than just the dysregulation of myofibroblast differentiation. Thus, using only monocultured fibroblasts, cultured in 2D, is a rather simple model of fibrosis with more thorough animal wound models available (Koo *et al.,* 2018; Wang *et al.,* 2019). Furthermore, fibroblasts differentiated to myofibroblasts with recombinant TGF-β1 will behave differently from fibroblasts isolated from scars that differentiated a long time ago. The results from this study should be interpreted with this in mind. However, when treated with TGF-β1

roughly 50 % of fibroblasts differentiated and expressed α-SMA (figures 4.5, 4.6, 5.3, 5.9). When fibroblasts were isolated from scar tissue and stained for α-SMA, the same proportion of these cells were constitutively expressing α-SMA compared to TGF-β1 treated fibroblasts. This supports the concept that TGF-β1 activated fibroblasts can be used as a substitute for scar myofibroblasts.

Fibroblasts can be differentiated into myofibroblasts *via* more than just TGF-β1 acting *via* the SMAD pathway. These non-canonical methods of activation are outlined in section 1.2.3. It could be argued that this work would have a greater impact if the ability of adipose tissue-derived conditioned medium to inhibit or reverse myofibroblasts activated *via* different mechanisms to TGF-β1, such as radiation induced fibrosis, were investigated.

Finally, if this work were to be repeated, the method with which adipose tissue-derived conditioned media was generated could be changed. The concentration at which adipose tissue was added to added to medium to "condition" the medium was decided early in the project. Minced adipose tissue and lipoaspirate were added to serum free medium at a concentration of 0.1 g/ml. This was an arbitrary starting point but by using a small volume of adipose tissue it was hoped that hypoxia in the tissue over the 72 hours of conditioning would be minimised. Initially, it was attempted to condition medium with an equivalent amount of adipose tissue for each condition. When converting minced adipose tissue or lipoaspirate to emulsified fat, there would be very little volume lost (and this is supported by DNA quantification showing that lipoaspirate and emulsified fat had almost the same number of cells per gram). As a result of this observation, 0.1 g/ml of emulsified fat was used when generating emulsified fat conditioned medium. However, during the early stages of the project, and before the lipocondensate processing had been fully optimised in section 2.2.4, it appeared that for every 10 g of lipoaspirate or minced adipose tissue processed, 5 g of lipocondensate and 5 g of lipid was generated. As a result, lipocondensate and lipid were added to medium at 0.05 g/ml as it appeared that processing to lipocondensate roughly halved the amount of adipose tissue remaining and that half of the mass of adipose tissue was lipid. Thus, halving the volume added to the medium made sense at the time. In hindsight and having carried out more characterisation work, this is now known to not be the case. Having fully optimised the lipocondensate procedure it is now known that for every 10 grams of lipoaspirate/minced adipose tissue I started with, roughly 1 g of lipocondensate was produced alongside roughly 7.5 g lipid. Additionally, DNA quantification in section 3.2.9 showed that lipocondensate had roughly a tenth of the number of cells of lipoaspirate and emulsified fat. Thus, if aiming to use equivalent amounts of adipose tissue, conditioned medium should have been generated with 0.01 g/ml of lipocondensate and 0.075 g/ml of lipid. This miscalculation resulted in lipocondensate being effectively 5 times more concentrated than it should have been if equivalent volumes of adipose tissue were being used. If

aware of this at the start of the work in chapter 4, medium would have been conditioned with these volumes of adipose tissue however, significant sections of this work had already been completed so no changes were made.

ADSC conditioned medium was generated by adding serum free medium to ADSCs seeded at a concentration of 4,500 cells per cm^2 in 6-well plates. This was because multiple people were examining the effects of ADSC conditioned medium in my lab group and to be consistent with their work I began seeding 45,000 cells per cm^2. A decision was made to decrease this to 4,500 cells per cm^2 (15,000 cells per ml of conditioned medium as I added 3 ml of serum free MesenPRO per well of a 6 well plate). This was because at 45,000 cells per cm^2 cells were overconfluent in the well plates and it was considered this would have an adverse effect on the factors in the conditioned medium. If this work were to be carried out again, medium would be conditioned in a T75 flask with 10 ml of serum free MesenPRO with 34,000 cells per ml of conditioned medium (4,500 cells per cm^2 in a T75 flask). This change is because following further characterisation, the number of cells per gram of lipoaspirate was calculated at 7.85 $x10^6$. For an equivalent number of ADSCs then the total number of cells used to condition lipoaspirate conditioned medium would be calculated (7.85 $x10^5$ cells in 0.1 g/ml) and this number divided by 23.3 (the percentage of cells in lipoaspirate that are ADSCs as calculated in Eto *et al.,* (2009)). This would give a total of ~34,000 cells per ml of conditioned medium.

6.3 Future work

To take this work further, the mechanistic action responsible for adipose tissue conditioned mediums ability to inhibit and reverse myofibroblast differentiation must be identified. One could examine the ability of different growth factors found in adipose tissue-derived conditioned medium to replicate this effect such as FGF-2, CXCL9, PGE_2, and adiponectin. Additionally, it would be possible examine the effect of adding several of these factors at once as adipose tissue-derived conditioned medium may work because it contains a multitude of different factors that may interact with one another. It would be interesting to examine whether the inhibition and reversal of α-SMA adipose tissue conditioned medium was having a physiological effect on myofibroblast contraction and ECM production using collagen contraction assays and Sirius red staining to quantify collagen production. Reducing the expression of α-SMA should lead to less contraction (Hinz *et al.,* 2001). it would also be useful to examine whether adipose tissue-derived conditioned medium could inhibit or reverse the differentiation of fibroblasts when treated with other myofibroblast inducing molecules or treatments such as connective tissue growth factor or radiation.

The use of extracellular vesicles (EVs) in therapeutic research has been rapidly increasing (Roy *et al.,* 2018). It has been shown that EVs from adipose tissue can have a significant impact on the surrounding environment (Crewe *et al.,* 2018; Gao *et al.,* 2017) and EVs from ADSCs have been shown to aide in cellular regeneration (Han *et al.,* 2020). EVs are an important part of paracrine signalling, and it will be likely that EVs from these formulations may be having an impact on myofibroblast differentiation. The growth factors contained in EVs will not have been identified on the cytokine array used and thus a large portion of the growth factors in my conditioned medium may not have been analysed. It would be interesting to isolate EVs from my conditioned medium and investigate whether these EVs alone could inhibit or reverse myofibroblast differentiation. It would then be possible to also compare the effect of EVs from adipose tissue as opposed to EVs from just ADSCs. This could be followed up with proteomic analysis to identify what signalling and growth factors may be present in the conditioned medium.

Finally, one could further examine whether adipose tissue-derived conditioned medium could reverse the differentiation of scar fibroblasts. It was hypothesised in chapter 5 that scar fibroblasts may need to be treated with adipose tissue-derived conditioned medium for a prolonged period of time. This is because in conditioned medium the concentration of paracrine factors will only decrease over time unless more conditioned medium is re-applied. Scar fibroblasts may need a higher concentration of paracrine factors or to be exposed to these factors for a longer period of time to cause de-differentiation, due to the increased time the cells have existed in a myofibroblast phenotype. In a co-culture set up, paracrine factors are being continuously released throughout the time period of the experiment. This constant release of factors may be why Deng *et al.* saw success at de-differentiation scar myofibroblasts. To replicate this, It would be possible to re-apply adipose tissue-derived conditioned medium to examine if increasing the concentration of paracrine factors and the length of time from adipose tissue has any effect on scar fibroblast phenotype.

6.4 Conclusions

To conclude, I have generated and characterised clinically relevant formulations of adipose tissue used in regenerative surgeries by clinicians. I optimised steps in the production of a Nanofat-like formulation and my technique of generating lipocondensate provides useful information into the mechanics of generating SVF-gel formulations. I compared these formulations to others in the literature and found that as processing steps were carried out the adipocyte population was removed and the number of SVF cells present was concentrated.

Using these formulations of adipose tissue, I revealed that paracrine factors from these formulations could inhibit α-SMA expression and TGF-β1 induced myofibroblast differentiation *in*

vitro. This was the first *in vitro* demonstration of inhibition of myofibroblast differentiation by factors from clinically relevant formulations of adipose tissue. I tested whether HGF was the paracrine factor responsible for this effect however I was unable to confirm this. The concentration of other paracrine factors secreted by adipose tissue was examined however and other potential therapeutic targets remain to be examined in the future.

I demonstrated that paracrine factors from adipose tissue could reverse the phenotype of TGF-β1 treated myofibroblasts. This was the first *in vitro* demonstration of reversal of myofibroblast differentiation by factors from clinically relevant formulations of adipose tissue. Paracrine factors from adipose tissue were able to inhibit α-SMA expression in fibroblasts already differentiated to myofibroblasts using TGF-β1. The mechanisms behind such actions were investigated and myofibroblast proliferation and adipogenic differentiation were examined however, neither of these mechanisms could be confirmed at this time. Further work needs to be carried out if the impact of paracrine factors from adipose tissue on scar fibroblasts phenotype is to be realised. I am the first to demonstrate that paracrine factors from adipose tissue itself, and not just ADSCs, are capable of both inhibiting and reversing myofibroblast differentiation.

7.0. Appendix

When drawing conclusions from these papers, the following must be considered.

Deng *et al.* (2018) – It has been noticed that in figure 1A of this paper the two left hand side panels showing what should be different cell cultures are likely the same image.

Li *et al.* (2016) – The paper is entitled “Adipose tissue-derived stem cells suppress hypertrophic scar fibrosis via the p38/MAPK signaling pathway”. It has been noticed a paper entitled “Adipose tissue-derived stem cells inhibit hypertrophic scar (HS) fibrosis via p38/MAPK pathway” was published in 2018 with similar sections of text and similar figures. (DOI: 10.1002/jcb.27689).

7.1 References

Abe, M., Oda, N. & Sato, Y. (1998). Cell-Associated Activation of Latent Transforming Growth Factor-β by Calpain. *Journal of Cellular Physiology*, 174(2), 186–193.

Aberle, H., Bauer, A., Stappert, J., Kispert, A. & Kemler, R. (1997). β-Catenin Is a Target for the Ubiquitin-Proteasome Pathway. *EMBO Journal*, 16(13), 3797–3804.

Adachi, Y., Mio, T., Takigawa, K., Striz, I., Romberger, D. J., Spurzem, J. R. & Rennard, S. I. (1998). Fibronectin Production by Cultured Human Lung Fibroblasts in Three-Dimensional Collagen Gel Culture. *In Vitro Cellular & Developmental Biology. Animal*, 34(3), 203–210.

Ai, J., Nie, J., He, J., Guo, Q., Li, M., Lei, Y., Liu, Y., Zhou, Z., Zhu, F., Liang, M., Cheng, Y. & Hou, F. F. (2015). GQ5 Hinders Renal Fibrosis in Obstructive Nephropathy by Selectively Inhibiting TGF-β-Induced SMAD3 Phosphorylation. *Journal of the American Society of Nephrology*, 26(8), 1827–1838.

Aida-Yasuoka, K., Peoples, C., Yasuoka, H., Hershberger, P., Thiel, K., Cauley, J. A., Medsger, T. A. & Feghali-Bostwick, C. A. (2013). Estradiol Promotes the Development of a Fibrotic Phenotype and Is Increased in the Serum of Patients with Systemic Sclerosis. *Arthritis Research and Therapy*, 15(1), 1-10.

Akasaka, Y., Ono, I., Tominaga, A., Ishikawa, Y., Ito, K., Suzuki, T., Imaizumi, R., Ishiguro, S., Jimbow, K. & Ishii, T. (2007). Basic Fibroblast Growth Factor in an Artificial Dermis Promotes Apoptosis and Inhibits Expression of α-Smooth Muscle Actin, Leading to Reduction of Wound Contraction. *Wound Repair and Regeneration*, 15(3), 378–389.

Akhmetshina, A., Palumbo, K., Dees, C., Bergmann, C., Venalis, P., Zerr, P., Horn, A., Kireva, T., Beyer, C., Zwerina, J., Schneider, H., Sadowski, A., Riener, M. O., MacDougald, O. A., Distler, O., Schett, G. & Distler, J. H. W. (2012). Activation of Canonical Wnt Signalling Is Required for TGF-β-Mediated Fibrosis. *Nature Communications*, 3(735), 1-12.

Al Battah, F., de Kock, J., Ramboer, E., Heymans, A., Vanhaecke, T., Rogiers, V., & Snykers, S. (2011). Evaluation of the multipotent character of human adipose tissue-derived stem cells isolated by Ficoll gradient centrifugation and red blood cell lysis treatment. *Toxicology in Vitro*, 25(6), 1224–1230.

Alexander, R. W. (2016). Understanding Mechanical Emulsification (Nanofat) Versus Enzymatic Isolation of Tissue Stromal Vascular Fraction (tSVF) Cells from Adipose Tissue: Potential Uses in Biocellular Regenerative Medicine. *Journal of Prolotherapy*, 8, 947–960.

Allen, J. L., Cooke, M. E. & Alliston, T. (2012). ECM Stiffness Primes the TGFβ Pathway to Promote Chondrocyte Differentiation. *Molecular Biology of the Cell*, 23(18), 3731–3742.

Amin, K. (2012). The Role of Mast Cells in Allergic Inflammation. *Respiratory Medicine*, 106(1), 9–14.

Amos, P. J., Shang, H., Bailey, A. M., Taylor, A., Katz, A. J. & Peirce, S. M. (2008). IFATS Collection: The Role of Human Adipose-Derived Stromal Cells in Inflammatory Microvascular Remodeling and Evidence of a Perivascular Phenotype. *Stem Cells*, 26(10), 2682–2690.

Anderson, J. M., Rodriguez, A. & Chang, D. T. (2008). Foreign Body Reaction to Biomaterials. *Seminars in Immunology*, 20(2), 86–100.

Andersson, J. & Melcherst, F. (1981). T Cell-Dependent Activation of Resting B Cells: Requirement for Both Nonspecific Unrestricted and Antigen-Specific Ia-Restricted Soluble Factors. *Immunology*, 78(4), 2497–2501.

Andersson, M., Blanc, P. D., Torén, K. & Järvholm, B. (2021). Smoking, Occupational Exposures, and Idiopathic Pulmonary Fibrosis among Swedish Construction Workers. *American Journal of Industrial Medicine*, 64(4), 251–257.

Angmalisang, E. C., Sukmawati, D., Damayanti, L., Eryani, A. & Pawitan, J. A. (2018). Adipose-Derived Stem Cell Condition Medium Enhances Expression of Ephrin-B2 Related to Neovascularization in Burn Wound Tissue. *Advanced Science Letters*, 24(8), 6168–6172.

Asahara, T., Masuda, H., Takahashi, T., Kalka, C., Pastore, C., Silver, M., Kearne, M., Magner, M. & Isner, J. M. (1999). Bone Marrow Origin of Endothelial Progenitor Cells Responsible for Postnatal Vasculogenesis in Physiological and Pathological Neovascularization. *Circulation Research*, 85, 221-228.

Assoian, R. K., Komoriya, A., Meyers, C. A., Miller, D. M. & Sporn, M. B. (1983). Transforming Growth Factor-β in Human Platelets. Identification of a Major Storage Site, Purification, and Characterization. *Journal of Biological Chemistry*, 258(11), 7155–7160.

Avouac, J., Pezet, S., Gonzalez, V., Baudoin, L., Cauvet, A., Ruiz, B., Boleto, G., Brandely, M. L., Elmerich, M. & Allanore, Y. (2020). Estrogens Counteract the Profibrotic Effects of TGF-β and Their Inhibition Exacerbates Experimental Dermal Fibrosis. *Journal of Investigative Dermatology*, 140(3), 593-601.

Azzam, O. A., Atta, A. T., Sobhi, R. M. & Mostafa, P. I. N. (2013). Fractional CO(2) Laser Treatment vs Autologous Fat Transfer in the Treatment of Acne Scars: A Comparative Study. *Journal of Drugs in Dermatology,* 12(1), 7–13.

van Baar, M. E., Essink-Bot, M. L., Oen, I. M. M. H., Dokter, J., Boxma, H. & van Beeck, E. F. (2006). Functional Outcome after Burns: A Review. *Burns*, 32(1), 1–9.

Baker, R. H. J., Townley, W. A., Mckeon, S., Linge, C. & Vijh, V. (2007). Retrospective Study of the Association Between Hypertrophic Burn Scarring and Bacterial Colonization. *Journal of Burn Care & Research*, 28(1), 152–156.

Bank, R. A., Zandstra, J., Room, H., Petersen, A. H. & van Putten, S. M. (2017). Biomaterial Encapsulation Is Enhanced in the Early Stages of the Foreign Body Reaction during Conditional Macrophage Depletion in Transgenic Macrophage Fas-Induced Apoptosis Mice. *Tissue Engineering - Part A*, 23(19–20), 1078–1087.

Baptista, L. S., do Amaral, R. J. F. C., Carias, R. B. V., Aniceto, M., Claudio-Da-Silva, C., & Borojevic, R. (2009). An alternative method for the isolation of mesenchymal stromal cells derived from lipoaspirate samples. *Cytotherapy*, 11(6), 706–715.

Barfod, K. W. & Blønd, L. (2019). Treatment of Osteoarthritis with Autologous and Microfragmented Adipose Tissue. *Dan Med J*, 66, 1–5.

Barlian, A., Judawisastra, H., Alfarafisa, N. M., Wibowo, U. A. & Rosadi, I. (2018). Chondrogenic Differentiation of Adipose-Derived Mesenchymal Stem Cells Induced by L-Ascorbic Acid and Platelet Rich Plasma on Silk Fibroin Scaffold. *PeerJ*, 1-20.

Baryza, M. J. & Baryza, G. A. (1995). The Vancouver Scar Scale: An Administration Tool and Its Interrater Reliability. *Journal of Burn Care & Rehabilitation*, 16(5), 535–538.

Bauer, E. A., Stricklin, G. P., Jeffrey, J. J. & Eisen, A. Z. (1975). Collagenase Production by Human Skin Fibroblasts. *Biochemical and Biophysical Research Communications*, 64(1), 232–240.

Baumann, L. S., Spencer, J. M. & Spencer, J. (1999). The Effects of Topical Vitamin E on the Cosmetic Appearance of Scars Diagnosing the Baumann Skin Type View Project Mechanism of Action for PMMA Collagen-Gel View Project the Effects of Topical Vitamin E on the Cosmetic Appearance of Scars. *Dermatologic Surgery*, 25(4), 311-315.

Bayat, A., Bock, O., Mrowietz, U., Ollier, W. E. R. & Ferguson, M. W. J. (2003). Genetic Susceptibility to Keloid Disease and Hypertrophic Scarring: Transforming Growth Factor B1 Common Polymorphisms and Plasma Levels. *Plastic and Reconstructive Surgery*, 111(2), 535–543.

Bayreuther, K., Peter Rodemann, H., Hommel, R., Dittmann, K., Albiez, M., & Francz, P. I. (1988). Human skin fibroblasts in vitro differentiate along a terminal cell lineage (cell types/stem cell system/cellular aging/two-dimensional gel electrophoresis). *Proceedings of the National Academy of Sciences of the United States of America*, 85, 5112-5116.

Bell, E., Ivarsson, B., & Merrill, C. (1979). Production of a Tissue-Like Structure by Contraction of Collagen Lattices by Human Fibroblasts of Different Proliferative Potential in vitro. *Proceedings of the National Academy of Sciences of the United States of America*, 76(3), 1274-1278.

Bell, L. N., Cai, L., Johnstone, B. H., Traktuev, D. O., March, K. L. & Considine, R. v. (2008). A Central Role for Hepatocyte Growth Factor in Adipose Tissue Angiogenesis. *American Journal of Physiology-Endocrinology & Metabolism*, 294, 336–344.

Bellini, E., Grieco, M. P. & Raposio, E. (2017a). A Journey through Liposuction and Liposculture: Review. *Annals of Medicine and Surgery*, 24, 53–60.

Bellini, E., Grieco, M. P. & Raposio, E. (2017b). The Science behind Autologous Fat Grafting. *Annals of Medicine and Surgery*, 24, 65–73.

Benjamin, M. A., Schwarzman, G., Eivazi, M., & Zachary, L. (2015). Autologous staged fat tissue transfer in post-traumatic lower extremity reconstruction. *Journal of Surgical Case Reports*, 11, 1-3.

Berman, B. & Bieley, H. C. (1996). Adjunct Therapies to Surgical Management of Keloids. *Dermatologic Surgery*, 22(2), 126–130.

Berman, B., Perez, O. A., Konda, S., Kohut, B. E., Viera, M. H., Delgado, S., Zell, D. & Li, Q. (2007). A Review of the Biologic Effects, Clinical Efficacy, and Safety of Silicone Elastomer Sheeting for Hypertrophic and Keloid Scar Treatment and Management. *Dermatologic Surgery*, 33(11), 1291–1303.

Berry, D. C., Stenesen, D., Zeve, D. & Graff, J. M. (2013). The Developmental Origins of Adipose Tissue. *Development*, 140(19), 3939–3949.

Bertola, A., Ciucci, T., Rousseau, D., Bourlier, V., Duffaut, C., Bonnafous, S., Blin-Wakkach, C., Anty, R., Iannelli, A., Gugenheim, J., Tran, A., Bouloumié, A., Gual, P. & Wakkach, A. (2012). Identification of Adipose Tissue Dendritic Cells Correlated with Obesity-Associated Insulin-Resistance and Inducing Th17 Responses in Mice and Patients. *Diabetes*, 61(9), 2238–2247.

Bhooshan, L. S., Geetha Devi, M., Aniraj, R., Binod, P., & Lekshmi, M. (2018). Autologous emulsified fat injection for rejuvenation of scars: A prospective observational study. *Indian Journal of Plastic Surgery*, 51(1), 77–83.

Bianchi, F., Maioli, M., Leonardi, E., Olivi, E., Pasquinelli, G., Valente, S., Mendez, A. J., Ricordi, C., Raffaini, M., Tremolada, C., & Ventura, C. (2013). A new nonenzymatic method and device to obtain a fat tissue derivative highly enriched in pericyte-like elements by mild mechanical forces from human lipoaspirates. *Cell Transplantation*, 22(11), 2063–2077.

Bjarnegård, M., Enge, M., Norlin, J., Gustafsdottir, S., Fredriksson, S., Abramsson, A., Takemoto, M., Gustafsson, E., Fässler, R. & Betsholtz, C. (2004). Endothelium-Specific Ablation of PDGFB Leads to Pericyte Loss and Glomerular, Cardiac and Placental Abnormalities. *Development*, 131(8), 1847–1857.

Bjørndal, B., Burri, L., Staalesen, V., Skorve, J. & Berge, R. K. (2011). Different Adipose Depots: Their Role in the Development of Metabolic Syndrome and Mitochondrial Response to Hypolipidemic Agents. *Journal of Obesity*, 2011, 1–15.

Bornstein, S. R., Abu-Asab, M., Glasow, A., Päth, G., Hauner, H., Tsokos, M., Chrousos, G. P. & Scherbaum, W. A. (2000). Immunohistochemical and Ultrastructural Localization of Leptin and Leptin Receptor in Human White Adipose Tissue and Differentiating Human Adipose Cells in Primary Culture. *Diabetes*, 49, 532–538.

Borrelli, M. R., Patel, R. A., Blackshear, C., Vistnes, S., Diaz Deleon, N. M., Adem, S., Shen, A. H., Sokol, J., Momeni, A., Nguyen, D., Longaker, M. T., & Wan, D. C. (2020a). CD34+CD146+ adipose-derived stromal cells enhance engraftment of transplanted fat. *Stem Cells Translational Medicine*, 1-12.

Borrelli, M. R., Patel, R. A., Adem, S., Diaz Deleon, N. M., Shen, A. H., Sokol, J., Yen, S., Chang, E. Y., Nazerali, R., Nguyen, D., Momeni, A., Wang, K. C., Longaker, M. T. & Wan, D. C. (2020b). The Antifibrotic Adipose-Derived Stromal Cell: Grafted Fat Enriched with CD74+ Adipose-Derived Stromal Cells Reduces Chronic Radiation-Induced Skin Fibrosis. *Stem Cells Translational Medicine*, 1-13.

Borthwick, L. A., Wynn, T. A. & Fisher, A. J. (2013). Cytokine Mediated Tissue Fibrosis. *Biochimica et Biophysica Acta - Molecular Basis of Disease*, 1832(7), 1049–1060.

Bourin, P., Bunnell, B. A., Casteilla, L., Dominici, M., Katz, A. J., March, K. L., Redl, H., Rubin, J. P., Yoshimura, K., & Gimble, J. M. (2013). Stromal cells from the adipose tissue-derived stromal vascular fraction and culture expanded adipose tissue-derived stromal/stem cells: A joint statement of the International Federation for Adipose Therapeutics and Science (IFATS) and the International Society for Cellular Therapy (ISCT). *Cytotherapy*, 15(6), 641–648.

Bowles, A. C., Wise, R. M., Gerstein, B. Y., Thomas, R. C., Ogelman, R., Febbo, I. & Bunnell, B. A. (2017). Immunomodulatory Effects of Adipose Stromal Vascular Fraction Cells Promote Alternative Activation Macrophages to Repair Tissue Damage. *Stem Cells*, 35(10), 2198–2207.

Brand, O. J., Somanath, S., Moermans, C., Yanagisawa, H., Hashimoto, M., Cambier, S., Markovics, J., Bondesson, A. J., Hill, A., Jablons, D., Wolters, P., Lou, J., Marks, J. D., Baron, J. L. & Nishimura, S. L. (2015). Transforming Growth Factor-β and Interleukin-1β Signaling Pathways Converge on the Chemokine CCL20 Promoter. *Journal of Biological Chemistry*, 290(23), 14717–14728.

Brown, J. C., Shang, H., Shang, H., Yang, N., Pierson, J., Ratliff, C. R., Prince, N., Roney, N., Chan, R., Hatem, V., Gittleman, H., Barnholtz-Sloan, J. S., Vincek, V., Katz, A. J. & Katz, A. J. (2020). Autologous Fat Transfer for Scar Prevention and Remodeling: A Randomized, Blinded, Placebo-Controlled Trial. *Plastic and Reconstructive Surgery - Global Open*, 1-20.

Bruno, A., Delli Santi, G., Fasciani, L., Cempanari, M., Palombo, M., & Palombo, P. (2013). Burn scar lipofilling: Immunohistochemical and clinical outcomes. *Journal of Craniofacial Surgery*, 24(5), 1806–1814.

Byrne, M., O'Donnell, M., Fitzgerald, L., & Shelley, O. P. (2016). Early experience with fat grafting as an adjunct for secondary burn reconstruction in the hand: Technique, hand function assessment and aesthetic outcomes. *Burns*, 42(2), 356–365.

Cao, Y., Sun, Z., Liao, L., Meng, Y., Han, Q., & Zhao, R. C. (2005). Human adipose tissue-derived stem cells differentiate into endothelial cells in vitro and improve postnatal neovascularization in vivo. *Biochemical and Biophysical Research Communications*, 332(2), 370–379.

Cao, Z., Li, H., Wang, Z. H., & Liang, X. Q. (2022). High-Density Fat Grafting Assisted Stromal Vascular Fraction Gel in Facial Deformities. *Journal of Craniofacial Surgery*, 33(1), 108–111.

Carmeliet, P. & Jain, R. K. (2011). Molecular Mechanisms and Clinical Applications of Angiogenesis. *Nature*, 473(7347), 298–307.

Carraro, R., Lil, Z.-H., Johnson, J. E. & Gregerman, R. I. (1991). Cell and Tissue Research Islets of Preadipocytes Highly Committed to Differentiation in Cultures of Adherent Rat Adipocytes Light-and Electron-Microscopic Observations. *Cell and Tissue Research*, 264, 243-251.

Carstens, M. H., Correa, D., Llull, R., Gomez, A., Turner, E., & Socorro Valladares, L. (2015). Subcutaneous reconstruction of hand dorsum and fingers for late sequelae of burn scars using adipose-derived stromal vascular fraction (SVF). *CellR4*, 3(5), 1–9.

Carstens, M. H., Pérez, M., Briceño, H., Valladares, S. & Correa, D. (2017). Treatment of Late Sequelae of Burn Scar Fibrosis with Adipose-Derived Stromal Vascular Fraction (SVF) Cells: A Case Series. *CellR4*, 5(3), 1–16.

Caruso, R. A., Fedele, F., Finocchiaro, G., Pizzi, G., Nunnari, M., Gitto, G., Fabiano, V., Parisi, A. & Venuti, A. (2009). Ultrastructural Descriptions of Pericyte Endothelium Peg-Socket Interdigitations in the Microvasculature of Human Gastric Carcinomas. *Anticancer Research*, 29, 449–454.

Caviggioli, F., Maione, L., Forcellini, D., Klinger, F., & Klinger, M. (2011). Autologous fat graft in postmastectomy pain syndrome. *Plastic and Reconstructive Surgery*, 128(2), 349–352.

Cederberg, A., Gronning, L. M., Ahren, B., Tasken, K., Carlsson, P. & Enerback, S. (2001). FOXC2 Is a Winged Helix Gene That Counteracts Obesity Hypertriglyceridemia and Diet Induced Insulin Resistance. *Cell*, 106, 563–573.

Chae, D. S., Han, S., Son, M. & Kim, S. W. (2017). Stromal Vascular Fraction Shows Robust Wound Healing through High Chemotactic and Epithelialization Property. *Cytotherapy*, 19(4), 543–554.

Chen, L., Guo, S., Ranzer, M. J. & Dipietro, L. A. (2013). Toll-like Receptor 4 Has an Essential Role in Early Skin Wound Healing. *Journal of Investigative Dermatology*, 133(1), 258–267.

Chen, L., Wang, J., Li, S., Yu, Z., Liu, B., Song, B. & Su, Y. (2019). The Clinical Dynamic Changes of Macrophage Phenotype and Function in Different Stages of Human Wound Healing and Hypertrophic Scar Formation. *International Wound Journal*, 16(2), 360–369.

Chen, M. M., Lam, A., Abraham, J. A., Schreiner, G. F. & Joly, A. H. (2000). CTGF Expression Is Induced by TGF- β in Cardiac Fibroblasts and Cardiac Myocytes: A Potential Role in Heart Fibrosis. *Journal of Molecular and Cellular Cardiology*, 32(10), 1805–1819.

Chen, X., Hong, S., Hong, F., Yang, B., Tong, C., & Zhang, J. (2020). Mechanical emulsification of lipoaspirate by different Luer-Lok connector changes the viability of adipose derived stem cells in Nanofat. *Journal of Plastic Surgery and Hand Surgery*, 54(6), 344–351.

Chen, Y. W., Scutaru, T. T., Ghetu, N., Carasevici, E., Lupascu, C. D., Ferariu, D., Pieptu, D., Coman, C. G. & Danciu, M. (2017). The Effects of Adipose-Derived Stem Cell-Differentiated Adipocytes on Skin Burn Wound Healing in Rats. *Journal of Burn Care and Research*, 38(1), 1–10.

Chiaverina, G., di Blasio, L., Monica, V., Accardo, M., Palmiero, M., Peracino, B., Vara-Messler, M., Puliafito, A. & Primo, L. (2019). Dynamic Interplay between Pericytes and Endothelial Cells during Sprouting Angiogenesis. *Cells*, 8(9), 1-13.

Chinnapaka, S., Katherine, Y., Epperly, M., Wen, U., Greenberger, J., Rubin, P. (2021) Allogenic Adipose Tissue-Derived Matrix Mitigate Radiation-Induced Fibrosis (RIF), *18th Annual IFATS Conference*. Florida, USA, IFATS.

Choi, J. S., Chae, D. S., Ryu, H. A. & Kim, S. W. (2019). Transplantation of Human Adipose Tissue Derived-SVF Enhance Liver Function through High Anti-Inflammatory Property. *Biochimica et Biophysica Acta - Molecular and Cell Biology of Lipids*, 1864(12), 1-11.

Choi, Y. H., Kim, K. M., Kim, H. O., Jang, Y. C. & Kwak, I. S. (2013). Clinical and Histological Correlation in Post-Burn Hypertrophic Scar for Pain and Itching Sensation. *Annals of Dermatology*, 25(4), 428–433.

Chun, Q., Zhiyong, W., Fei, S., & Xiqiao, W. (2016). Dynamic biological changes in fibroblasts during hypertrophic scar formation and regression. *International Wound Journal*, *13*(2), 257–262.

Cinti, S. (2009). Reversible Physiological Transdifferentiation in the Adipose Organ. *Proceedings of the Nutrition Society*, 68, 340-349.

ClinicalTrials.gov (2006) *Juvidex (Mannose-6-Phosphate) in Accelerating the Healing of Split Thickness Skin Graft Donor Sites*. www.clinicaltrials.gov/ct2/show/study/NCT00664352 (Accessed: 15 April 2022).

Cohen, P., & Spiegelman, B. M. (2016). Cell biology of fat storage. *Molecular Biology of the Cell,* 27(16), 2523-2527.

Coleman, S. R., (2002). Hand Rejuvenation with Structural Fat Grafting. *Plastic and Reconstructive Surgery*, 110(7), 1731–1744.

Coleman, S. R. (1995). Long-Term Survival of Fat Transplants: Controlled Demonstrations. *Aesthetic Plastic Surgery*, 19, 421–425.

Coleman, S. R., (1998). Structural Fat Grafting. *Aesthetic Surgery Journal*, 18(5), 387–388.

Coleman, S. R. (2006). Structural Fat Grafting: More Than a Permanent Filler. *Plastic and Reconstructive Surgery*, 118(3), 108-120.

Craig, R. D. P., Schofield, J. D. & Jackson, S. S. (1975). Collagen Biosynthesis in Normal Human Skin, Normal and Hypertrophic Scar and Keloid. *European Journal of Clinical Investigation*, 5(1), 69–74.

Crewe, C., Joffin, N., Rutkowski, J. M., Kim, M., Zhang, F., Towler, D. A., Gordillo, R., & Scherer, P. E. (2018). An Endothelial-to-Adipocyte Extracellular Vesicle Axis Governed by Metabolic State. *Cell*, 175(3), 695-708.

Cushing, M. C., Mariner, P. D., Liao, J., Sims, E. A. & Anseth, K. S. (2008). Fibroblast Growth Factor Represses SMAD-mediated Myofibroblast Activation in Aortic Valvular Interstitial Cells. *The FASEB Journal*, 22(6), 1769–1777.

Cushman, S. W. (1970). Structure-Function Relationships in the Adipose Cell. *The Journal of Cell Biology*, 46, 326–341.

Dai, C. & Liu, Y. (2004). Hepatocyte Growth Factor Antagonizes the Profibrotic Action of TGF-β1 in Mesangial Cells by Stabilizing SMAD Transcriptional Corepressor TGIF. *Journal of the American Society of Nephrology*, 15(6), 1402–1412.

Darland, D. C., Massingham, L. J., Smith, S. R., Piek, E., Saint-Geniez, M. & D'amore, P. A. (2003). Pericyte Production of Cell-Associated VEGF Is Differentiation-Dependent and Is Associated with Endothelial Survival. *Developmental Biology*, 264, 275-288.

Danielpour, D., Kim, K. Y., Dart, L. L., Watanabe, S., Roberts, A. B. & Sporn, M. B. (1989). Sandwich Enzyme-Linked Immunosorbent Assays (Selisas) Quantitate and Distinguish Two Forms of Transforming Growth Factor-Beta (TGF-β1 and TGF-β2) in Complex Biological Fluids. *Growth Factors*, 2(1), 61–71.

Davey, M. G., Hynes, S. O., Kerin, M. J., Miller, N., & Lowery, A. J. (2021). Ki-67 as a prognostic biomarker in invasive breast cancer. *Cancers* 13(17), 1-19.

Degner, B. M., Chung, C., Schlegel, V., Hutkins, R., & Mcclements, D. J. (2014). Factors influencing the freeze-thaw stability of emulsion-based foods. *Comprehensive Reviews in Food Science and Food Safety*, 13(2), 98–113.

Delavary, B, M., van der Veer, W. M., Ferreira, J. A. & Niessen, F. B. (2012). Formation of Hypertrophic Scars: Evolution and Susceptibility. *Journal of Plastic Surgery and Hand Surgery*, 46(2), 95–101.

Deleon, N. M. D., Adem, S., Lavin, C. v., Abbas, D. B., Griffin, M., King, M. E., Borrelli, M. R., Patel, R. A., Fahy, E. J., Lee, D., Shen, A. H., Momeni, A., Longaker, M. T. & Wan, D. C. (2021). Angiogenic CD34+CD146+ Adipose-Derived Stromal Cells Augment Recovery of Soft Tissue after Radiotherapy. *Journal of Tissue Engineering and Regenerative Medicine*, 15(12), 1105–1117.

Deng, J., Shi, Y., Gao, Z., Zhang, W., Wu, X., Cao, W., & Liu, W. (2018). Inhibition of Pathological Phenotype of Hypertrophic Scar Fibroblasts Via Coculture with Adipose-Derived Stem Cells. *Tissue Engineering - Part A*, 24(5–6), 382–393.

Denton, C. P., Merkel, P. A., Furst, D. E., Khanna, D., Emery, P., Hsu, V. M., Silliman, N., Streisand, J., Powell, J., Åkesson, A., Coppock, J., van den Hoogen, F., Herrick, A., Mayes, M. D., Veale, D., Haas, J., Ledbetter, S., Korn, J. H., Black, C. M., & Seibold, J. R. (2007). Recombinant human anti-transforming growth factor β1 antibody therapy in systemic sclerosis: A multicenter, randomized, placebo-controlled phase I/II trial of CAT-192. *Arthritis and Rheumatism*, 56(1), 323–333.

Derynck, R., Lindquist, P. B., Lee, A., Wen, D., Tamm, J., Graycar, J. L., Rhee, L., Mason, A. J., Miller', D. A., Coffey', R. J., Moses', H. L. & Chen, E. Y. (1988). A New Type of Transforming Growth Factor-β, TGF-β3. *The EMBO Journal*, 7(12), 3737-3743.

Desai, V. D., Hsia, H. C. & Schwarzbauer, J. E. (2014). Reversible Modulation of Myofibroblast Differentiation in Adipose-Derived Mesenchymal Stem Cells. *PLoS ONE*, 9(1), 1-12.

Desmouliere, A., Geinoz, A., Gabbiani, F. & Gabbiani, G. (1993). Transforming Growth Factor-Ill Induces u-Smooth Muscle Actin Expression in Granulation Tissue Myofibroblasts and in Quiescent and Growing Cultured Fibroblasts. *The Journal of Cell Biology*, 122(1), 103–111.

Desmoulire, A., Redard, M., Darby, I., & Gabbiani, G. (1995). Apoptosis Mediates the Decrease in Cellularity during the Transition between Granulation Tissue and Scar. *American journal of Pathology*, 146(1), 56-60.

Distler, J. H. W., Jüngel, A., Pileckyte, M., Zwerina, J., Michel, B. A., Gay, R. E., Kowal-Bielecka, O., Matucci-Cerinic, M., Schett, G., Marti, H. H., Gay, S. & Distler, O. (2007). Hypoxia-Induced Increase in the Production of Extracellular Matrix Proteins in Systemic Sclerosis. *Arthritis and Rheumatism*, 56(12), 4203–4215.

Djonov, V. G., Kurz, H. & Burri, P. H. (2002). Optimality in the Developing Vascular System: Branching Remodeling by Means of Intussusception as an Efficient Adaptation Mechanism. *Developmental Dynamics*, 224(4), 391–402.

Domergue, S., Bony, C., Maumus, M., Toupet, K., Frouin, E., Rigau, V., Vozenin, M. C., Magalon, G., Jorgensen, C. & Noël, D. (2016). Comparison between Stromal Vascular Fraction and Adipose Mesenchymal Stem Cells in Remodeling Hypertrophic Scars. *PLoS ONE*, 11(5), 1-16.

Dominici, M., le Blanc, K., Mueller, I., Slaper-Cortenbach, I., Marini, F. C., Krause, D. S., Deans, R. J., Keating, A., Prockop, D. J., & Horwitz, E. M. (2006). Minimal criteria for defining multipotent mesenchymal stromal cells. The International Society for Cellular Therapy position statement. *Cytotherapy*, 8(4), 315–317.

Donaldson, D. J., Smith, G. N. & Kang, A. H. (1982). Epidermal Cell Migration on Collagen and Collagen-Derived Peptides. *Journal of Cell Science*, 57, 15–23.

Dondossola, E., Holzapfel, B. M., Alexander, S., Filippini, S., Hutmacher, D. W. & Friedl, P. (2017). Examination of the Foreign Body Response to Biomaterials by Nonlinear Intravital Microscopy. *Nature Biomedical Engineering*, 1(1), 1-20.

Dong, Z., Fu, R., Liu, L. & Lu, F. (2013). Stromal Vascular Fraction (Svf) Cells Enhance Long-Term Survival of Autologous Fat Grafting through the Facilitation of M2 Macrophages. *Cell Biology International*, 37(8), 855–859.

van Dongen, J. A., Boxtel, J. v, Uguten, M., Brouwer, L. A., Vermeulen, K. M., Melenhorst, W. B., Niessen, F. B., Harmsen, M. C., Stevens, H. P. & van der Lei, B. (2021). Tissue Stromal Vascular Fraction Improves Early Scar Healing: A Prospective Randomized Multicenter Clinical Trial. *Aesthetic Surgery Journal*.

van Dongen, J. A., Getova, V., Brouwer, L. A., Liguori, G. R., Sharma, P. K., Stevens, H. P., van der Lei, B. & Harmsen, M. C. (2019). Adipose Tissue-Derived Extracellular Matrix Hydrogels as a Release Platform for Secreted Paracrine Factors. *Journal of Tissue Engineering and Regenerative Medicine*, 13(6), 973–985.

van Dongen, J. A., Gostelie, O. F. E., Vonk, L. A., de Bruijn, J. J., van der Lei, B. B., Harmsen, M. C., Stevens, H. P., de Bruijn, M., Hieronymus, P., Stevens, K. & Rotterdam, K. P. (2019). Fractionation of Adipose Tissue Procedure with a Disposable One-Hole Fractionator. *Aesthetic Surgery Journal*, 40(4), 1-8.

van Dongen, J. A., Stevens, H. P., Parvizi, M., van der Lei, B., & Harmsen, M. C. (2016). The fractionation of adipose tissue procedure to obtain stromal vascular fractions for regenerative purposes. *Wound Repair and Regeneration*, 24(6), 994–1003.

Dorsch, W., Schneider, E., Bayer, T., Breu, W. & Wagner, H. (1990). Anti-Inflammatory Effects of Onions: Inhibition of Chemotaxis of Human Polymorphonuclear Leukocytes by Thiosulfinates and Cepaenes. *International Archives of Allergy and Immunology*, 92(1), 39–42.

Doyle, C. & Strominger, J. L. (1987). Interaction between CD4 and Class II MHC Molecules Mediates Cell Adhesion. *Nature*, 330, 256–259.

Driskell, R. R., Lichtenberger, B. M., Hoste, E., Kretzschmar, K., Simons, B. D., Charalambous, M., Ferron, S. R., Herault, Y., Pavlovic, G., Ferguson-Smith, A. C. & Watt, F. M. (2013). Distinct Fibroblast Lineages Determine Dermal Architecture in Skin Development and Repair. *Nature*, 504(7479), 277–281.

Ehrlich, H. P., Desmouliere, A., Diegelmann, R. F., Cohen, T. 1 K., Compton, C. C., Garner, W. L., Kapanci, Y. & Gabbianit, G. (1994). Morphological and Immunochemical Differences Between Keloid and Hypertrophic Scar. *American Journal of Pathology*, 145(1), 105-113.

Ejaz, A., Epperly, M. W., Hou, W., Greenberger, J. S. & Rubin, J. P. (2019). Adipose-Derived Stem Cell Therapy Ameliorates Ionizing Irradiation Fibrosis via Hepatocyte Growth Factor-Mediated Transforming Growth Factor-β Downregulation and Recruitment of Bone Marrow Cells. *Stem Cells*, 37(6), 791–802.

El Agha, E., Moiseenko, A., Kheirollahi, V., de Langhe, S., Crnkovic, S., Kwapiszewska, G., Kosanovic, D., Schwind, F., Schermuly, R. T., Henneke, I., MacKenzie, B. A., Quantius, J., Herold, S., Ntokou, A., Ahlbrecht, K., Morty, R. E., Günther, A., Seeger, W., & Bellusci, S. (2017). Two-Way Conversion between Lipogenic and Myogenic Fibroblastic Phenotypes Marks the Progression and Resolution of Lung Fibrosis. *Cell Stem Cell*, 20(2), 261-273.

Engels, P. E., Tremp, M., Kingham, P. J., di Summa, P. G., Largo, R. D., Schaefer, D. J., & Kalbermatten, D. F. (2013). Harvest site influences the growth properties of adipose derived stem cells. *Cytotechnology*, 65(3), 437–445.

Engleman, E. G., Benike, C. J., Carl, F. & Evans, R. L. (1981). Activation of Human T Lymphocyte Subsets: Helper and Suppressor/ Cytotoxic T Cells Recognize and Respond to Distinct Histocompatibility Antigens. *The Journal of Immunology*, 127(5), 2124–2129.

Enoch, S. & Price, P. E. (2004). Cellular, Molecular and Biochemical Differences in the Pathophysiology of Healing between Acute Wounds, Chronic Wounds and Wounds in the Aged. *World Wide Wounds*, 1–16.

Eto, H., Suga, H., Matsumoto, D., Inoue, K., Aoi, N., Kato, H., Araki, J., & Yoshimura, K. (2009). Characterization of structure and cellular components of aspirated and excised adipose tissue. *Plastic and Reconstructive Surgery*, 124(4), 1087–1097.

Estes, B. T., Wu, A. W., Storms, R. W. & Guilak, F. (2006). Extended Passaging, but Not Aldehyde Dehydrogenase Activity, Increases the Chondrogenic Potential of Human Adipose-Derived Adult Stem Cells. *Journal of Cellular Physiology*, 209(3), 987–995.

Evans, R. A., Tian, Y. C., Steadman, R. & Phillips, A. O. (2003). TGF-1-Mediated Fibroblast-Myofibroblast Terminal Differentiation-the Role of SMAD Proteins. *Experimental Cell Research*, 282, 90–100.

Fain, J. N., Madan, A. K., Hiler, M. L., Cheema, P. & Bahouth, S. W. (2004). Comparison of the Release of Adipokines by Adipose Tissue, Adipose Tissue Matrix, and Adipocytes from Visceral and Subcutaneous Abdominal Adipose Tissues of Obese Humans. *Endocrinology*, 145(5), 2273–2282.

Fang, F., Liu, L., Yang, Y., Tamaki, Z., Wei, J., Marangoni, R. G., Bhattacharyya, S., Summer, R. S., Ye, B., & Varga, J. (2012). The adipokine adiponectin has potent anti-fibrotic effects mediated via adenosine monophosphate-activated protein kinase: Novel target for fibrosis therapy. *Arthritis Research and Therapy*, 14(5), 1-13.

Fadel, L., Viana, B. R., Feitosa, M. L. T., Ercolin, A. C. M., Roballo, K. C. S., Casals, J. B., Pieri Naira, C. G., Meirelles, F. V., Martins, D. dos S., Miglino, M. A., & Ambrosio, C. E. (2011). Protocols for obtainment and isolation of two mesenchymal stem cell sources in sheep. *Models, Biological*, 26(4), 267–273.

Ferguson, M. W. J. & O'Kane, S. (2004). Scar-Free Healing: From Embryonic Mechanism to Adult Therapeutic Intervention. *Philosophical Transactions of the Royal Society B: Biological Sciences*, 359, 839–850.

Florin, L., Alter, H., Gröne, H. J., Szabowski, A., Schütz, G. & Angel, P. (2004). Cre Recombinase-Mediated Gene Targeting of Mesenchymal Cells. *Genesis*, 38(3), 139–144.

Fodor, P. B. & Paulseth, S. G. (2016). Adipose Derived Stromal Cell (ADSC) Injections for Pain Management of Osteoarthritis in the Human Knee Joint. *Aesthetic Surgery Journal*, 36(2), 229–236.

Folkman, J., Klagsbrun, M., Sasse, J., Wadzinski, M., Ingber, D. & Vlodavsky, I. (1988). A Heparin-Binding Angiogenic Protein-Basic Fibroblast Growth Factor Is Stored Within Basement Membrane. *American Journal of Pathology*, 130(2), 393-400.

Fortier, S. M., Penke, L. R., King, D., Pham, T. X., Ligresti, G., & Peters-Golden, M. (2021). Myofibroblast dedifferentiation proceeds via distinct transcriptomic and phenotypic transitions. *JCI Insight*, 6(6), 1-18.

Fonsatti, E., & Maio, M. (2004). Highlights on endoglin (CD105): from basic findings towards clinical applications in human cancer. *Journal of Translational Medicine*, 2(18), 1-7.

Francis, M. P., Sachs, P. C., Elmore, L. W., & Holt, S. E. (2010). Brief Report Isolating adipose-derived mesenchymal stem cells from lipoaspirate blood and saline fraction. *Organogenesis*, 11(1), 11–14.

Frantz, C., Stewart, K. M. & Weaver, V. M. (2010). The Extracellular Matrix at a Glance. *Journal of Cell Science*, 123(24), 4195–4200.

lo Furno, D., Tamburino, S., Mannino, G., Gili, E., Lombardo, G., Tarico, M. S., Vancheri, C., Giuffrida, R., & Perrotta, R. E. (2017). Nanofat 2.0: Experimental evidence for a fat grafting rich in mesenchymal stem cells. *Physiological Research*, 66(4), 663–671.

Fuster, J. J., Ouchi, N., Gokce, N. & Walsh, K. (2016). Obesity-Induced Changes in Adipose Tissue Microenvironment and Their Impact on Cardiovascular Disease. *Circulation Research*, 118(11), 1786–1807.

Gabbiani, G. & Ryan, G. B. (1971). Presence of Modified Fibroblasts in Granulation Tissue and Their Possible Role in Wound Contraction. *Experimentia*, 27(5), 549–550.

Gal, S., Ramirez, J. I. & Maguina, P. (2017). Autologous Fat Grafting Does Not Improve Burn Scar Appearance: A Prospective, Randomized, Double-Blinded, Placebo-Controlled, Pilot Study. *Burns*, 43(3), 486–489.

Gao, X., Salomon, C., & Freeman, D. J. (2017). Extracellular vesicles from adipose tissue-A potential role in obesity and type 2 diabetes? *Frontiers in Endocrinology*, 8, 1-8.

Garrison, G., Huang, S. K., Okunishi, K., Scott, J. P., Penke, L. R. K., Scruggs, A. M., & Peters-Golden, M. (2013). Reversal of myofibroblast differentiation by prostaglandin E2. *American Journal of Respiratory Cell and Molecular Biology*, 48(5), 550–558.

Gentile, P., de Angelis, B., Pasin, M., Cervelli, G., Curcio, C. B., Floris, M., di Pasquali, C., Bocchini, I., Balzani, A., Nicoli, F., Insalaco, C., Tati, E., Lucarini, L., Palla, L., Pascali, M., de Logu, P., di Segni, C., Bottini, D. J. & Cervelli, V. (2014). Adipose-Derived Stromal Vascular Fraction Cells and Platelet-Rich Plasma. *Journal of Craniofacial Surgery*, 25(1), 267–272.

Gentile, P., Scioli, M. G., Bielli, A., Orlandi, A. & Cervelli, V. (2017). Comparing Different Nanofat Procedures on Scars: Role of the Stromal Vascular Fraction and Its Clinical Implications. *Regenerative Medicine*, 12(8), 939–952.

Gerhardt, H., Golding, M., Fruttiger, M., Ruhrberg, C., Lundkvist, A., Abramsson, A., Jeltsch, M., Mitchell, C., Alitalo, K., Shima, D. & Betsholtz, C. (2003). VEGF Guides Angiogenic Sprouting Utilizing Endothelial Tip Cell Filopodia. *Journal of Cell Biology*, 161(6), 1163–1177.

Gimble, J. M., & Guilak, F. (2003). Adipose-derived adult stem cells: Isolation, characterization, and differentiation potential. *Cytotherapy*, 5(5), 362–369.

Gineyts, E., Cloos, P. A. C., Borel, O., Grimaud, L., Delmas, P. D. & Garnero, P. (2000). Racemization and Isomerization of Type I Collagen C-Telopeptides in Human Bone and Soft Tissues: Assessment of Tissue Turnover. *Biochemical Journal*, 345, 481-485.

Goodarzi, F., & Zendehboudi, S. (2019). A Comprehensive Review on Emulsions and Emulsion Stability in Chemical and Energy Industries. *Canadian Journal of Chemical Engineering*, 97(1), 281–309.

Gordon, M. K. & Hahn, R. A. (2010). Collagens. *Cell and Tissue Research*, 339(1), 247–257.

Gotch, F., Gallimore, A. & Mcmichael, A. (1996). Mini Review Cytotoxic T Cells-Protection from Disease Progression-Protection from Infection. *Immunology Letters*, 51, 125-128.

Grasys, J., Kim, B. S. & Pallua, N. (2016). Content of Soluble Factors and Characteristics of Stromal Vascular Fraction Cells in Lipoaspirates from Different Subcutaneous Adipose Tissue Depots. *Aesthetic Surgery Journal*, 36(7), 831–841.

Grinnell, F. (2000). Fibroblast-Collagen Matrix Contraction: Growth-Factor Signalling and Mechanical Loading. *Cell Biology*, 10, 362-365.

Gronthos, S., Franklin, D. M., Leddy, H. A., Robey, P. G., Storms, R. W., & Gimble, J. M. (2001). Surface Protein Characterization of Human Adipose Tissue-Derived Stromal Cells. *Journal of Cellular* Physiology, 189, 54-63.

Grotendorst, G. R. & Duncan, M. R. (2005). Individual Domains of Connective Tissue Growth Factor Regulate Fibroblast Proliferation and Myofibroblast Differentiation. *The FASEB Journal*, 19(7), 729–738.

Guerra, A., Belinha, J., Mangir, N., MacNeil, S. & Natal Jorge, R. (2021). Sprouting Angiogenesis: A Numerical Approach with Experimental Validation. *Annals of Biomedical Engineering*, 49(2), 871–884.

Guerrero-Juarez, C. F., Dedhia, P. H., Jin, S., Ruiz-Vega, R., Ma, D., Liu, Y., Yamaga, K., Shestova, O., Gay, D. L., Yang, Z., Kessenbrock, K., Nie, Q., Pear, W. S., Cotsarelis, G. & Plikus, M. v. (2019). Single-Cell Analysis Reveals Fibroblast Heterogeneity and Myeloid-Derived Adipocyte Progenitors in Murine Skin Wounds. *Nature Communications*, 10(1), 1-17.

Guo, J., Nguyen, A., Banyard, D. A., Fadavi, D., Toranto, J. D., Wirth, G. A., Paydar, K. Z., Evans, G. R. D. & Widgerow, A. D. (2016). Stromal Vascular Fraction: A Regenerative Reality? Part 2: Mechanisms of Regenerative Action. *Journal of Plastic, Reconstructive and Aesthetic Surgery*, 69(2), 180–188.

Hamburg-Shields, E., Dinuoscio, G. J., Mullin, N. K., Lafayatis, R. & Atit, R. P. (2015). Sustained β-Catenin Activity in Dermal Fibroblasts Promotes Fibrosis by up-Regulating Expression of Extracellular Matrix Protein-Coding Genes. *Journal of Pathology*, 235(5), 686–697.

Han, H. S., Lee, H., You, D. G., Nguyen, V. Q., Song, D. G., Oh, B. H., Shin, S., Choi, J. S., Kim, J. D., Pan, C. H., Jo, D. G., Cho, Y. W., Choi, K. Y., & Park, J. H. (2020). Human adipose stem cell-derived extracellular nanovesicles for treatment of chronic liver fibrosis. *Journal of Controlled Release*, 320, 328–336.

Han, J., Koh, Y. J., Moon, H. R., Ryoo, H. G., Cho, C.-H., Kim, I. & Koh, G. Y. (2010). Adipose Tissue Is an Extramedullary Reservoir for Functional Hematopoietic Stem and Progenitor Cells. *Hematopoiesis and Stem Cells*, 115(5), 957–964.

Hanson, S. E., Kapur, S. K., Garvey, P. B., Hernandez, M., Clemens, M. W., Hwang, R. F., Dryden, M. J. & Butler, C. E. (2020). Oncologic Safety and Surveillance of Autologous Fat Grafting Following Breast Conservation Therapy. *Plastic and Reconstructive Surgery*, 146(2), 215–225.

Har-Shai, Y., Brown, W., Labbé, D., Dompmartin, A., Goldine, I., Gil, T., Mettanes, I. & Pallua, N. (2008). Intralesional Cryosurgery for the Treatment of Hypertrophic Scars and Keloids Following Aesthetic Surgery: The Results of a Prospective Observational Study. *The International Journal of Lower Extremity Wounds*, 7(3), 169–175.

Hashemibeni, B., Dehghani, L., Sadeghi, F., Esfandiari, E., Gorbani, M., Akhavan, A., Tahani, S. T., Bahramian, H. & Goharian, V. (2016). Bone Repair with Differentiated Osteoblasts from Adipose-Derived Stem Cells in Hydroxyapatite/Tricalcium Phosphate in Vivo. *International Journal of Preventive Medicine*, 7(62), 1-6.

Hassnain Waqas, S. F., Noble, A., Hoang, A. C., Ampem, G., Popp, M., Strauß, S., Guille, M. & Röszer, T. (2017). Adipose Tissue Macrophages Develop from Bone Marrow–Independent Progenitors in Xenopus Laevis and Mouse. *Journal of Leukocyte Biology*, 102(3), 845–855.

Heaton, G. M., Wagenvoord, R. J., Kemp, A. Jr. & Nicholls, D. G. (1978). Brown-Adipose-Tissue Mitochondria: Photoaffinity Labelling of the Regulatory Site of Energy Dissipation. *Journal of Biochemistry*, 82, 515–521.

Hecker, L., Jagirdar, R., Jin, T. & Thannickal, V. J. (2011). Reversible Differentiation of Myofibroblasts by MyoD. *Experimental Cell Research*, 317(13), 1914–1921.

Heldin, C. H. & Moustakas, A. (2016). Signaling Receptors for TGF-β Family Members. *Cold Spring Harbor Perspectives in Biology*, 8(8), 1-33.

Heo, J. S., Choi, Y., Kim, H. S. & Kim, H. O. (2016). Comparison of Molecular Profiles of Human Mesenchymal Stem Cells Derived from Bone Marrow, Umbilical Cord Blood, Placenta and Adipose Tissue. *International Journal of Molecular Medicine*, 37(1), 115–125.

von Heimburg, D., Hemmrich, K., Haydarlioglu, S., Staiger, H., & Pallua, N. (2004). Comparison of Viable Cell Yield from Excised versus Aspirated Adipose Tissue. *Cells Tissues Organs*, 178(2), 87–92.

Herly, M., Ørholt, M., Glovinski, P. v., Pipper, C. B., Broholm, H., Poulsgaard, L., Fugleholm, K., Thomsen, C. & Drzewiecki, K. T. (2017). Quantifying Long-Term Retention of Excised Fat Grafts: A Longitudinal, Retrospective Cohort Study of 108 Patients Followed for up to 8.4 Years. *Plastic and Reconstructive Surgery*, 139(5), 1223–1232.

Hinz, B. (2007). Formation and Function of the Myofibroblast during Tissue Repair. *Journal of Investigative Dermatology*, 127(3), 526–537.

Hinz, B. (2015). Myofibroblasts. *Experimental Eye Research*, 142, 56–70.

Hinz, B., Celetta, G., Tomasek, J. J., Gabbiani, G. & Chaponnier, C. (2001). Alpha-Smooth Muscle Actin Expression Upregulates Fibroblast Contractile Activity. *Molecular Biology of the Cell*, 12, 2730-2741.

Hoerst, K., van den Broek, L., Sachse, C., Klein, O., von Fritschen, U., Gibbs, S., & Hedtrich, S. (2019). Regenerative potential of adipocytes in hypertrophic scars is mediated by myofibroblast reprogramming. *Journal of Molecular Medicine*, 97(6), 761–775.

Hoogewerf, C. J., van Baar, M. E., Middelkoop, E. & van Loey, N. E. (2014). Impact of Facial Burns: Relationship between Depressive Symptoms, Self-Esteem and Scar Severity. *General Hospital Psychiatry*, 36(3), 271–276.

Hotamisligil, G. S., Shargill, N. S. & Spiegelman, B. M. (1993). Adipose Expression of Tumor Necrosis Factor-Alpha: Direct Role in Obesity-Linked Insulin Resistance. *Science*, 259(5091), 87–91.

Hou, C.-C., Wang, W., Huang, X. R., Fu, P., Chen, T.-H., Sheikh-Hamad, D. & Lan, H. Y. (2005). Ultrasound-Microbubble-Mediated Gene Transfer of Inducible SMAD7 Blocks Transforming Growth Factor-Signaling and Fibrosis in Rat Remnant Kidney. *Cell Cycle Molecules*, 166(3), 761-771.

Hu, J., Chen, Y., Huang, Y. & Su, Y. (2020). Human Umbilical Cord Mesenchymal Stem Cell-Derived Exosomes Suppress Dermal Fibroblasts-Myofibroblats Transition via Inhibiting the TGF-β1/SMAD 2/3 Signaling Pathway. *Experimental and Molecular Pathology*, 115, 1-9.

Hu, X., Cifarelli, V., Sun, S., Kuda, O., Abumrad, N. A., & Su, X. (2016). Major role of adipocyte prostaglandin E2 in lipolysis-induced macrophage recruitment. *Journal of Lipid Research*, 57(4), 663–673.

Huang, S. H., Wu, S. H., Lee, S. S., Chang, K. P., Chai, C. Y., Yeh, J. L., Lin, S. D., Kwan, A. L., David Wang, H. M. & Lai, C. S. (2015). Fat Grafting in Burn Scar Alleviates Neuropathic Pain via Anti-Inflammation Effect in Scar and Spinal Cord. *PLOS ONE*, 10(9), 1-15.

Huang, S. J., Fu, R. H., Shyu, W. C., Liu, S. P., Jong, G. P., Chiu, Y. W., Wu, H. S., Tsou, Y. A., Cheng, C. W., & Lin, S. Z. (2013). Adipose-derived stem cells: Isolation, characterization, and differentiation potential. *Cell Transplantation*, 22(4), 701-709.

Humphrey, J. D., Dufresne, E. R. & Schwartz, M. A. (2014). Mechanotransduction and Extracellular Matrix Homeostasis. *Nature Reviews Molecular Cell Biology*, 15(12), 802–812.

Humphries, J. D., Byron, A. & Humphries, M. J. (2006). Integrin Ligands at a Glance. *Journal of Cell Science*, 119(19), 3901–3903.

Hurd, J. L., Facile, T. R., Weiss, J., Hayes, Matthew, Hayes, Meredith, Furia, J. P., Maffulli, N., Winnier, G. E., Alt, C., Schmitz, C., Alt, E. U. & Lundeen, M. (2020). Safety and Efficacy of Treating Symptomatic, Partial-Thickness Rotator Cuff Tears with Fresh, Uncultured, Unmodified, Autologous Adipose-Derived Regenerative Cells (UA-ADRCs) Isolated at the Point of Care: A Prospective, Randomized, Controlled First-in-Human Pilot Study. *Journal of Orthopaedic Surgery and Research*, 15(1), 1-18.

Hynes, R. O. & Naba, A. (2012). Overview of the Matrisome-An Inventory of Extracellular Matrix Constituents and Functions. *Cold Spring Harbor Perspectives in Biology*, 4(1), 1-16.

Illouz, Y.G. (1983). Body Contouring by Lipolysis: A 5 Year Experience with over 300 Cases. *Plastic & Reconstructive Surgery*, 72(5), 591-597.

Imamura, T., Takase, M., Nishihara, A., Oeda, E., Hanai, J., Kawabata, M. & Miyazono, K. (1997). SMAD6 Inhibits Signalling by the TGFB Superfamily. *Nature*, 389, 622–626.

Ishimine, H., Yamakawa, N., Sasao, M., Tadokoro, M., Kami, D., Komazaki, S., Tokuhara, M., Takada, H., Ito, Y., Kuno, S., Yoshimura, K., Umezawa, A., Ohgushi, H., Asashima, M. & Kurisaki, A. (2013). N-Cadherin Is a Prospective Cell Surface Marker of Human Mesenchymal Stem Cells That Have High Ability for Cardiomyocyte Differentiation. *Biochemical and Biophysical Research Communications*, 438(4), 753–759.

Ito, I., Hanyu, A., Wayama, M., Goto, N., Katsuno, Y., Kawasaki, S., Nakajima, Y., Kajiro, M., Komatsu, Y., Fujimura, A., Hirota, R., Murayama, A., Kimura, K., Imamura, T. & Yanagisawa, J. (2010). Estrogen Inhibits Transforming Growth Factor β Signaling by Promoting SMAD2/3 Degradation. *Journal of Biological Chemistry*, 285(19), 14747–14755.

Izadpanah, R., Trygg, C., Patel, B., Kriedt, C., Dufour, J., Gimble, J. M. & Bunnell, B. A. (2006). Biologic Properties of Mesenchymal Stem Cells Derived from Bone Marrow and Adipose Tissue. *Journal of Cellular Biochemistry*, 99(5), 1285–1297.

Jackson, B. A. & Shelton, A. J. (1999). Pilot Study Evaluating Topical Onion Extract as Treatment for Postsurgical Scars. *Dermatologic Surgery*, 25, 267-269.

Jaspers, M. E. H., Brouwer, K. M., van Trier, A. J. M., Groot, M. L., Middelkoop, E., & van Zuijlen, P. P. M. (2017). Effectiveness of Autologous Fat Grafting in Adherent Scars: Results Obtained by a Comprehensive Scar Evaluation Protocol. *Plastic and Reconstructive Surgery*, 139(1), 212–219.

Jauffret, J. L., Champsaur, P., Robaglia-Schlupp, A., Andrac-Meyer, L. & Magalon, G. (2001). Arguments in Favor of Adipocyte Grafts with the S.R. Coleman Technique. *Annales de Chirurgie Plastique et Esthétique*, 46, 31–38.

Jenkins, R. H., Thomas, G. J., Williams, J. D. & Steadman, R. (2004). Myofibroblastic Differentiation Leads to Hyaluronan Accumulation through Reduced Hyaluronan Turnover. *Journal of Biological Chemistry*, 279(40), 41453–41460.

Joannes, A., Brayer, S., Besnard, V., Marchal-Sommé, J., Jaillet, M., Mordant, P., Mal, H., Borie, R., Crestani, B. & Mailleux, A. A. (2016). FGF9 and FGF18 in Idiopathic Pulmonary Fibrosis Promote Survival and Migration and Inhibit Myofibroblast Differentiation of Human Lung Fibroblasts in Vitro. *American Journal of Physiology Lung Cellular and Molecular Physiology*, 310, 615–629.

Johnston, E. F. & Gillis, T. E. (2017). Transforming Growth Factor Beta-1 (TGF-B1) Stimulates Collagen Synthesis in Cultured Rainbow Trout Cardiac Fibroblasts. *Journal of Experimental Biology*, 220(14), 2645–2653.

Jones, I. A., Wilson, M., Togashi, R., Han, B., Mircheff, A. K. & Thomas Vangsness, C. (2018). A Randomized, Controlled Study to Evaluate the Efficacy of Intra-Articular, Autologous Adipose Tissue Injections for the Treatment of Mild-to-Moderate Knee Osteoarthritis Compared to Hyaluronic Acid: A Study Protocol. *BMC Musculoskeletal Disorders*, 19(1), 1-11.

Juhl, A. A., Karlsson, P. & Damsgaard, T. E. (2016). Fat Grafting for Alleviating Persistent Pain after Breast Cancer Treatment: A Randomized Controlled Trial. *Journal of Plastic, Reconstructive & Aesthetic Surgery*, 69(9), 1192–1202.

Karacaoglu, E., Kizilkaya, E., Cermik, H. & Zienowicz, R. (2005). The Role of Recipient Sites in Fat Graft Survival. *Annals of Plastic Surgery*, 55(1), 63–68.

Kato, K., Logsdon, N. J., Shin, Y. J., Palumbo, S., Knox, A., Irish, J. D., Rounseville, S. P., Rummel, S. R., Mohamed, M., Ahmad, K., Trinh, J. M., Kurundkar, D., Knox, K. S., Thannickal, V. J., & Hecker, L. (2020). Impaired myofibroblast dedifferentiation contributes to nonresolving fibrosis in aging. *American Journal of Respiratory Cell and Molecular Biology*, 62(5), 633–644.

Katz, A. J., Tholpady, A., Tholpady, S. S., Shang, H. & Ogle, R. C. (2005). Cell Surface and Transcriptional Characterization of Human Adipose-Derived Adherent Stromal (HADAS) Cells. *Stem Cells*, 23(3), 412–423.

Kelly, P. A. (2004). Medical and Surgical Therapies for Keloids. *Dermatologic Therapy*, 17, 212–218.

Kemaloğlu, C. A. (2016). Nanofat grafting under a split-thickness skin graft for problematic wound management. *SpringerPlus*, *5(*1), 1–4.

Kershaw, E. E. & Flier, J. S. (2004). Adipose Tissue as an Endocrine Organ. *Journal of Clinical Endocrinology and Metabolism*, 89(6), 2548-2556.

Khouri, R. K., Eisenmann-Klien, M., Cardoso, E., Cooley, B. C., Kacher, D., Gombos, E. & Baker, T. J. (2012). Brava and Autologous Fat Transfer Is a Safe and Effective Breast Augmentation Alternative: Results of a 6-Year, 81-Patient, Prospective Multicenter Study. *Plastic & Reconstructive Surgery*, 129, 1173–1187.

Kim, J. H., Sung, J. Y., Kim, Y. H., Lee, Y. S., Chang, H. S., Park, C. S. & Roh, M. R. (2012). Risk Factors for Hypertrophic Surgical Scar Development after Thyroidectomy. *Wound Repair and Regeneration*, 20(3), 304–310.

Klinger, M., Caviggioli, F., Klinger, F. M., Giannasi, S., Bandi, V., Banzatti, B., Forcellini, D., Maione, L., Catania, B., & Vinci, V. (2013). Autologous Fat Graft in Scar Treatment. *Journal of Craniofacial Surgery*, 24(5), 1610–1615.

Klinger, M., Marazzi, M., Vigo, D., & Torre, M. (2008). Fat injection for cases of severe burn outcomes: A new perspective of scar remodeling and reduction. *Aesthetic Plastic Surgery*, 32(3), 465–469.

Knipper, J. A., Willenborg, S., Brinckmann, J., Bloch, W., Maaß, T., Wagener, R., Krieg, T., Sutherland, T., Munitz, A., Rothenberg, M. E., Niehoff, A., Richardson, R., Hammerschmidt, M., Allen, J. E. & Eming, S. A. (2015). Interleukin-4 Receptor α Signaling in Myeloid Cells Controls Collagen Fibril Assembly in Skin Repair. *Immunity*, 43(4), 803–816.

Knuutinen, A., Kokkonen, N., Risteli, J., Vahakangas, K., Kallioinen, M., Salo, T., Sorsa, T. & Oikarinen, A. (2002). Cutaneous Biology Smoking Affects Collagen Synthesis and Extracellular Matrix Turnover in Human Skin. *British Journal of Dermatology*, 146, 588–594.

Kondo, K., Obitsu, S., Ohta, S., Matsunami, K., Otsuka, H., & Teshima, R. (2010). Poly(ADP-ribose) polymerase (PARP)-1-independent apoptosis-inducing factor (AIF) release and cell death are induced by eleostearic acid and blocked by α-tocopherol and MEK inhibition. *Journal of Biological Chemistry*, 285(17), 13079–13091.

Ko, J. H., Kim, P. S., Zhao, Y., Hong, S. J. & Mustoe, T. A. (2012). HMG-CoA Reductase Inhibitors (Statins) Reduce Hypertrophic Scar Formation in Rabbit Ear Wounding Model. *Plastic and Reconstructive Surgery*, 129(2), 252–261.

Koh, Y. J., Koh, B. I., Kim, H., Joo, H. J., Jin, H. K., Jeon, J., Choi, C., Lee, D. H., Chung, J. H., Cho, C. H., Park, W. S., Ryu, J. K., Suh, J. K. & Koh, G. Y. (2011). Stromal Vascular Fraction from Adipose Tissue Forms Profound Vascular Network

through the Dynamic Reassembly of Blood Endothelial Cells. *Arteriosclerosis, Thrombosis, and Vascular Biology*, 31(5), 1141–1150.

Kølle, S. F. T., Fischer-Nielsen, A., Mathiasen, A. B., Elberg, J. J., Oliveri, R. S., Glovinski, P. v., Kastrup, J., Kirchhoff, M., Rasmussen, B. S., Talman, M. L. M., Thomsen, C., Dickmeiss, E. & Drzewiecki, K. T. (2013). Enrichment of Autologous Fat Grafts with Ex-Vivo Expanded Adipose Tissue-Derived Stem Cells for Graft Survival: A Randomised Placebo-Controlled Trial. *The Lancet*, 382(9898), 1113–1120.

Koo, H. Y., El-Baz, L. M. F., House, S. L., Cilvik, S. N., Dorry, S. J., Shoukry, N. M., Salem, M. L., Hafez, H. S., Dulin, N. O., Ornitz, D. M., & Guzy, R. D. (2018). Fibroblast growth factor 2 decreases bleomycin-induced pulmonary fibrosis and inhibits fibroblast collagen production and myofibroblast differentiation. *Journal of Pathology*, 246(1), 54–66.

Kotani, T., Masutani, R., Suzuka, T., Oda, K., Makino, S. & Ii, M. (2017). Anti-Inflammatory and Anti-Fibrotic Effects of Intravenous Adipose-Derived Stem Cell Transplantation in a Mouse Model of Bleomycin-Induced Interstitial Pneumonia. *Scientific Reports*, 7(1), 1-10.

Krastev, T. K., Beugels, J., Hommes, J., Piatkowski, A., Mathijssen, I. & van der Hulst, R. (2018). Efficacy and Safety of Autologous Fat Transfer in Facial Reconstructive Surgery. *JAMA Facial Plastic Surgery*, 20(5), 351–360.

Kruger, M. J., Conradie, M. M., Conradie, M. & van de Vyver, M. (2018). ADSC-Conditioned Media Elicit an Ex Vivo Anti-Inflammatory Macrophage Response. *Journal of Molecular Endocrinology*, 61(4), 173–184.

Kü, P., Gueler, F., Rong, S., Mengel, M., Tossidou, I., Peters, I., Haller, H. & Schiffer, M. (2007). Leptin Is a Coactivator of TGF-β in Unilateral Ureteral Obstructive Kidney Disease. *American Journal of Physiology-Renal Physiology*, 293, 1355–1362.

Kumai, Y., Kobler, J. B., Park, H., Galindo, M., Herrera, V. L. M., & Zeitels, S. M. (2010). Modulation of vocal fold scar fibroblasts by adipose-derived stem/stromal cells. *Laryngoscope*, 120(2), 330–337.

Kuo, Y. R., Jeng, S. F., Wang, F. S., Chen, T. H., Huang, H. C., Chang, P. R. & Yang, K. D. (2004). Flashlamp Pulsed Dye Laser (PDL) Suppression of Keloid Proliferation Through Down-Regulation of TGF-B1 Expression and Extracellular Matrix Expression. *Lasers in Surgery and Medicine*, 34(2), 104–108.

Lagares, D., Ghassemi-Kakroodi, P., Tremblay, C., Santos, A., Probst, C, K., Franklin, A., Santos, D, M., Grasberger, P., Ahluwalia, N., Montesi, S, B., Shea, B, S., Black, K, E., Knipe, R., Blati, M., Baron, M., Wu, B., Fahmi, H., Gandhi, R., Pardo, A., Selman, M., Wu, J., Pelletier, J, P., Martel-Pelletier, J., Tager, A, M., & Kapoor, M. (2017). ADAM10-Mediated Ephrin-B2 Shedding Promotes Myofibroblast Activation and Organ Fibrosis. *Nature Medicine*, 23(12), 1405-1415.

Lago, F., Dieguez, C., Gómez-Reino, J. & Gualillo, O. (2007). The Emerging Role of Adipokines as Mediators of Inflammation and Immune Responses. *Cytokine and Growth Factor Reviews*, 18(3–4), 313–325.

Lateef, Z., Stuart, G., Jones, N., Mercer, A., Fleming, S. & Wise, L. (2019). The Cutaneous Inflammatory Response to Thermal Burn Injury in a Murine Model. *International Journal of Molecular Sciences*, 20(3), 1-17.

Leclère, F. M. & Mordon, S. R. (2010). Twenty-Five Years of Active Laser Prevention of Scars: What Have We Learned? *Journal of Cosmetic and Laser Therapy*, 12(5), 227–234.

Lee, J. W., Park, S. H., Lee, S. J., Kim, S. H., Suh, I. S. & Jeong, H. S. (2018). Clinical Impact of Highly Condensed Stromal Vascular Fraction Injection in Surgical Management of Depressed and Contracted Scars. *Aesthetic Plastic Surgery*, 42(6), 1689–1698.

Lee, M. J., Wu, Y. & Fried, S. K. (2013). Adipose Tissue Heterogeneity: Implication of Depot Differences in Adipose Tissue for Obesity Complications. *Molecular Aspects of Medicine*, 34(1), 1–11.

Lee, S. H., Lee, E. J., Lee, S. Y., Kim, J. H., Shim, J. J., Shin, C., In, K. H., Kang, K. H., Uhm, C. S., Kim, H. K., Yang, K. S., Park, S., Kim, H. S., Kim, Y. M. & Yoo, T. J. (2014). The Effect of Adipose Stem Cell Therapy on Pulmonary Fibrosis Induced by Repetitive Intratracheal Bleomycin in Mice. *Experimental Lung Research*, 40(3), 117–125.

Lee, T. J., Jeong, W. S., Eom, J. S. & Kim, E. K. (2013). Adjuvant Chemotherapy Reduces the Incidence of Abdominal Hypertrophic Scarring Following Immediate TRAM Breast Reconstruction. *Breast Cancer Research and Treatment*, 137(3), 767–771.

Lee, Y. I., Kim, S. M., Kim, J., Kim, J., Song, S. Y., Lee, W. J. & Lee, J. H. (2020). Tissue-Remodelling M2 Macrophages Recruits Matrix Metallo-Proteinase-9 for Cryotherapy-Induced Fibrotic Resolution during Keloid Treatment. *Acta Dermato-Venereologica*, 100(17), 1–8.

Leicht, M., Briest, W., Holzl, A. & Zimmer, H.-G. (2001). Serum Depletion Induces Cell Loss of Rat Cardiac Fibroblasts and Increased Expression of Extracellular Matrix Proteins in Surviving Cells. *Cardiovascular Research*, 52, 429-437.

Lenzi, L. G. S., Santos, J. B. G., Raduan Neto, J., Fernandes, C. H. & Faloppa, F. (2019). The Patient and Observer Scar Assessment Scale: Translation for Portuguese Language, Cultural Adaptation, and Validation. *International Wound Journal*, 16(6), 1513–1520.

Leventhal, D., Furr, M., & Reiter, D. (2006). Treatment of keloids and hypertrophic scars: A meta-analysis and review of the literature. In *Archives of Facial Plastic Surgery*, 8(6), 362-368.

Li, D., Zhang, J., Liu, Z., Gong, Y. & Zheng, Z. (2021). Human Umbilical Cord Mesenchymal Stem Cell-Derived Exosomal MiR-27b Attenuates Subretinal Fibrosis via Suppressing Epithelial–Mesenchymal Transition by Targeting HOXC6. *Stem Cell Research and Therapy*, 12(1), 1-17.

Li, J. H., Zhu, H. J., Huang, X. R., Lai, K. N., Johnson, R. J. & Lan, H. Y. (2002). SMAD7 Inhibits Fibrotic Effect of TGF-β on Renal Tubular Epithelial Cells by Blocking SMAD2 Activation. *Journal of the American Society of Nephrology*, 13(6), 1464–1472.

Li, Y., Zhang, W., Gao, J., Liu, J., Wang, H., Li, J., Yang, X., He, T., Guan, H., Zheng, Z., Han, S., Dong, M., Han, J., Shi, J. & Hu, D. (2016). Adipose Tissue-Derived Stem Cells Suppress Hypertrophic Scar Fibrosis via the P38/MAPK Signaling Pathway. *Stem Cell Research and Therapy*, 7(1), 1-16.

Liechty, K. W., Adzick, N. S. & Crombleholme, T. M. (2000). Diminished Interleukin 6 (IL-6) Production during Scarless Human Fetal Wound Repair. *Cytokine*, 12(6), 671–676.

Liguori, T. T. A., Liguori, G. R., Moreira, L. F. P. & Harmsen, M. C. (2018). Fibroblast Growth Factor-2, but Not the Adipose Tissue-Derived Stromal Cells Secretome, Inhibits TGF-β1-Induced Differentiation of Human Cardiac Fibroblasts into Myofibroblasts. *Scientific Reports*, 8(1). 1-10.

Lin, C., McGough, R., Aswad, B., Block, J. A. & Terek, R. (2004). Hypoxia Induces HIF-1α and VEGF Expression in Chondrosarcoma Cells and Chondrocytes. *Journal of Orthopaedic Research*, 22(6), 1175–1181.

Lin, F., Ren, X. D., Pan, Z., MacRi, L., Zong, W. X., Tonnesen, M. G., Rafailovich, M., Bar-Sagi, D. & Clark, R. A. F. (2011). Fibronectin Growth Factor-Binding Domains Are Required for Fibroblast Survival. *Journal of Investigative Dermatology*, 131(1), 84–98.

Linares, H. A., Kischer, C. W., Dobrkovsky, M. & Larson, D. L. (1972). The Histiotypic Organization of the Hypertrophic Scar in Humans. *The Journal of investigative dermatology*, 59(4), 323–331.

Lindegren, A., Schultz, I., Sinha, I., Cheung, L., Khan, A. A., Tekle, M., Wickman, M. & Halle, M. (2019). Autologous Fat Transplantation Alters Gene Expression Patterns Related to Inflammation and Hypoxia in the Irradiated Human Breast. *British Journal of Surgery*, 106(5), 563–573.

Linge, C., Richardson, J., Vigor, C., Clayton, E., Hardas, B. & Rolfe, K. J. (2005). Hypertrophic Scar Cells Fail to Undergo a Form of Apoptosis Specific to Contractile Collagen - The Role of Tissue Transglutaminase. *Journal of Investigative Dermatology*, 125(1), 72–82.

Livak, K. J., & Schmittgen, T. D. (2001). Analysis of relative gene expression data using real-time quantitative PCR and the 2-ΔΔCT method. *Methods*, 25(4), 402–408.

Lonardi, R., Leone, N., Gennai, S., Trevisi Borsari, G., Covic, T. & Silingardi, R. (2019). Autologous Micro-Fragmented Adipose Tissue for the Treatment of Diabetic Foot Minor Amputations: A Randomized Controlled Single-Center Clinical Trial (MiFrAADiF). *Stem Cell Research and Therapy*, 10(1), 1-9.

Lyons, R. M., Keski-Oja, J. & Moses, H. L. (1988). Proteolytic Activation of Latent Transforming Growth Factor-13 from Fibroblast-Conditioned Medium. *The Journal of Cell Biology*, 106, 1659–1665.

Ma, F., Li, Y., Jia, L., Han, Y., Cheng, J., Li, H., Qi, Y. & Du, J. (2012). Macrophage-Stimulated Cardiac Fibroblast Production of IL-6 Is Essential for TGF β/SMAD Activation and Cardiac Fibrosis Induced by Angiotensin II. *PLoS ONE*, 7(5). 1-9.

Ma, J., Yan, X., Lin, Y. & Tan, Q. (2020). Hepatocyte Growth Factor Secreted from Human Adipose-Derived Stem Cells Inhibits Fibrosis in Hypertrophic Scar Fibroblasts. *Current Molecular Medicine*, 20(7), 558–571.

MacDonald, B. T. & He, X. (2012). Frizzled and LRp5/6 Receptors for Wnt/β-Catenin Signaling. *Cold Spring Harbor Perspectives in Biology*, 4(12), 1-23.

Maeda, K., Okubo, K., Shimomura, I., Funahashi, T., Matsuzawa, Y. & Matsubara, K. (1996). CDNA Cloning and Expression of a Novel Adipose Specific Collagen-like Factor, ApM1 (Adipose Most Abundant Gene Transcript 1). *Biochemical and Biophysical Research Communications*, 221, 286–289.

Maione, L., Memeo, A., Pedretti, L., Verdoni, F., Lisa, A., Bandi, V., Giannasi, S., Vinci, V., Mambretti, A., & Klinger, M. (2014). Autologous fat graft as treatment of post short stature surgical correction scars. *Injury*, 45(6), 126–132.

Makogonenko, E., Tsurupa, G., Ingham, K. & Medved, L. (2002). Interaction of Fibrin (Ogen) with Fibronectin: Further Characterization and Localization of the Fibronectin-Binding Site. *Biochemistry*, 41(25), 7907–7913.

Maltseva, O., Folger, P., Zekaria, D., Petridou, S., & Masur, S. K. (2001). Fibroblast Growth Factor Reversal of the Corneal Myofibroblast Phenotype. *Investigative Ophthalmology & Visual Science*, 42(11), 2490–2495.

Malik, P., Gaba, S., Ahuja, C., Sharma, Ratti, Sharma, Ramesh & Khandelwal, N. (2019). Role of Fat Graft Alone versus Enriched Fat Graft with Stromal Vascular Filtrate in Painful Amputation Stump. *Indian Journal of Orthopaedics*, 53(3), 452–458.

Mannino, G., Gennuso, F., Giurdanella, G., Conti, F., Drago, F., Salomone, S., Furno, D. lo, Bucolo, C. & Giuffrida, R. (2020). Pericyte-like Differentiation of Human Adipose-Derived Mesenchymal Stem Cells: An in Vitro Study. *World Journal of Stem Cells*, 12(10), 1152–1170.

Mariggio, M A, Cassano, A., Vinella, A., Vincenti, A., Fumarulo, R., lo Muzio, L., Maioran0, E., Ribatto, D., Favia, G. & Mariggio, Maria A. (2009). Enhancement of Fibroblast Proliferation, Collagen Biosynthesis and Production of Growth Factors as a Result of Combining Sodium Hyaluronate and Amino Acids. *International Journal of Immunopathology and Pharmacology,* 22(2), 485–492.

Martinez-Santibañez, G., Cho, K. W. & Lumeng, C. N. (2014). Imaging White Adipose Tissue with Confocal Microscopy. *Methods in Enzymology*, 537, 17-30.

Marturano, J. E., Arena, J. D., Schiller, Z. A., Georgakoudi, I. & Kuo, C. K. (2013). Characterization of Mechanical and Biochemical Properties of Developing Embryonic Tendon. *Proceedings of the National Academy of Sciences of the United States of America*, 110(16), 6370–6375.

Mashiko, T., Wu, S. H., Feng, J., Kanayama, K., Kinoshita, K., Sunaga, A., Narushima, M., & Yoshimura, K. (2017). Mechanical Micronization of Lipoaspirates: Squeeze and Emulsification Techniques. *Plastic and Reconstructive Surgery*, 139(1), 79–90.

Masurtt, S. K., Dewalt, H. S., Dinht, T. T., Erenburgt, I. & Petridout, S. (1996). Myofibroblasts Differentiate from Fibroblasts When Plated at Low Density (Transforming Growth Factor Fp/Cornea/Integrins/Fibroblasts/Smooth Muscle α-Actin). *Proceedings of the National Academy of Sciences of the United States of America.* 93, 4219-4223.

Matsumoto, D., Sato, K., Gonda, K., Takaki, Y., Shigeura, T., Sato, T., Aiba-Kojima, E., Iizuka, F., Inoue, K., Suga, H., & Yoshimura, K. (2006). Cell-Assisted Lipotransfer: Supportive Use of Human Adipose-Derived Cells for Soft Tissue Augmentation with Lipoinjection. *Tissue Engineering*, 12(12), 3375-3383.

Mattey, D. L., Dawes, P. T., Nixon, N. B. & Slater, H. (1997). Transforming Growth Factor 1 and Interleukin 4 Induced Smooth Muscle Actin Expression and Myofibroblast-like Differentiation in Human Synovial Fibroblasts in Vitro: Modulation by Basic Fibroblast Growth Factor. *Annals of the Rheumatic Diseases*. 56, 426-431.

Maung, A. A., Fujimi, S., Miller, M. L., MacConmara, M. P., Mannick, J. A. & Lederer, J. A. (2005). Enhanced TLR4 Reactivity Following Injury Is Mediated by Increased P38 Activation. *Journal of Leukocyte Biology*, 78(2), 565–573.

McCubrey, J. A., Steelman, L. S., Chappell, W. H., Abrams, S. L., Wong, E. W. T., Chang, F., Lehmann, B., Terrian, D. M., Milella, M., Tafuri, A., Stivala, F., Libra, M., Basecke, J., Evangelisti, C., Martelli, A. M., & Franklin, R. A. (2007). Roles of the Raf/MEK/ERK pathway in cell growth, malignant transformation and drug resistance. *Biochimica et Biophysica Acta - Molecular Cell Research*, 1773(8), 1263–1284.

McGowan, S. E. (2019). The lipofibroblast: More than a lipid-storage depot. *American Journal of Physiology - Lung Cellular and Molecular Physiology*, 316(5), 869–871.

McIntosh, K., Zvonic, S., Garrett, S., Mitchell, J. B., Floyd, Z. E., Hammill, L., Kloster, A., di Halvorsen, Y., Ting, J. P., Storms, R. W., Goh, B., Kilroy, G., Wu, X. & Gimble, J. M. (2006). The Immunogenicity of Human Adipose-Derived Cells: Temporal Changes In Vitro. *Stem Cells*, 24(5), 1246–1253.

McKee, S. (2011) *Renovo stock demolished by Justiva trial failure.* Available at http://www.pharmatimes.com/news/renovo_stock_demolished_by_jusi=tiva_trial_failure_979597 (Accessed: 10 July 2020)

Mehlem, A., Hagberg, C. E., Muhl, L., Eriksson, U., & Falkevall, A. (2013). Imaging of neutral lipids by oil red O for analyzing the metabolic status in health and disease. *Nature Protocols*, 8(6), 1149–1154.

Melling, G. E., Flannery, S. E., Abidin, S. A., Clemmens, H., Prajapati, P., Hinsley, E. E., Hunt, S., Catto, J. W. F., Coletta, R. della, Mellone, M., Thomas, G. J., Parkinson, E. K., Prime, S. S., Paterson, I. C., Buttle, D. J., & Lambert, D. W. (2018). A miRNA-145/TGF-β1 negative feedback loop regulates the cancer-associated fibroblast phenotype. *Carcinogenesis*, 39(6), 798–807.

Meng, X. M., Huang, X. R., Xiao, J., Chung, A. C. K., Qin, W., Chen, H. Y. & Lan, H. Y. (2012). Disruption of SMAD4 Impairs TGF-β/SMAD3 and SMAD7 Transcriptional Regulation during Renal Inflammation and Fibrosis in Vivo and in Vitro. *Kidney International*, 81(3), 266–279.

Meran, S., Martin, J., Luo, D. D., Steadman, R. & Phillips, A. (2013). Interleukin-1β Induces Hyaluronan and CD44-Dependent Cell Protrusions That Facilitate Fibroblast-Monocyte Binding. *American Journal of Pathology*, 182(6), 2223–2240.

Meyer, M. & Mcgrouther, D. A. (1991). A Study Relating Wound Tension to Scar Morphology in the Pre-Sternal Scar Using Langers Technique. *British Journal of Plastic Surgery*, 44, 291–291.

Michalik, M., Pierzchalska, M., Włodarczyk, A., Wójcik, K. A., Czy, J., Sanak, M. & Madeja, Z. (2011). Transition of Asthmatic Bronchial Fibroblasts to Myofibroblasts Is Inhibited by Cell-Cell Contacts. *Respiratory Medicine*, 105(10), 1467–1475.

Midgley, A. C., Rogers, M., Hallett, M. B., Clayton, A., Bowen, T., Phillips, A. O. & Steadman, R. (2013). Transforming Growth Factor-β1 (TGF-β1)-Stimulated Fibroblast to Myofibroblast Differentiation Is Mediated by Hyaluronan (HA)-Facilitated Epidermal Growth Factor Receptor (EGFR) and CD44 Co-Localization in Lipid Rafts. *Journal of Biological Chemistry*, 288(21), 14824–14838.

Mildmay-White, A., & Khan, W. (2017). Cell Surface Markers on Adipose-Derived Stem Cells: A Systematic Review. *Current Stem Cell Research & Therapy*, 12(6), 484-492.

Miller, M., Cho, J. Y., Mcelwain, K., Mcelwain, S., Shim, J. Y., Manni, M., Baek, J. S. & Broide, D. H. (2006). Corticosteroids Prevent Myofibroblast Accumulation and Airway Remodeling in Mice Corticosteroids Prevent Myofibroblast Accumula-Tion and Airway Remodeling in Mice. *American Journal of Physiology Lung Cellular and Molecular Physiology,* 290, 162–169.

Mitchell, J. B., McIntosh, K., Zvonic, S., Garrett, S., Floyd, Z. E., Kloster, A., di Halvorsen, Y., Storms, R. W., Goh, B., Kilroy, G., Wu, X., & Gimble, J. M. (2006). Immunophenotype of Human Adipose-Derived Cells: Temporal Changes in Stromal-Associated and Stem Cell–Associated Markers. *Stem Cells*, 24(2), 376–385.

Miyazono, K., Olofsson, A., Colosetti, P. & Heldin, C.-H. (1991). A Role of the Latent TGF-3 1-Binding Protein in the Assembly and Secretion of TGF-β1. *The EMBO Journal*, 10(5), 1091-1101.

Mojallal, A., Lequeux, C., Shipkov, C., Breton, P., Foyatier, J. L., Braye, F. & Damour, O. (2009). Improvement of Skin Quality after Fat Grafting: Clinical Observation and an Animal Study. *Plastic and Reconstructive Surgery*, 124(3), 765–774.

Moodley, Y. P., Scaffidi, A. K., Misso, N. L., Keerthisingam, C., Mcanulty, R. J., Laurent, G. J., Mutsaers, S. E., Thompson, P. J. & Knight, D. A. (2003). Fibroblasts Isolated from Normal Lungs and Those with Idiopathic Pulmonary Fibrosis Differ in Interleukin-6/Gp130-Mediated Cell Signaling and Proliferation. *American Journal of Pathology*, 163(1), 345–354.

Moon, K. M., Park, Y. H., Lee, J. S., Chae, Y. B., Kim, M. M., Kim, D. S., Kim, B. W., Nam, S. W. & Lee, J. H. (2012). The Effect of Secretory Factors of Adipose-Derived Stem Cells on Human Keratinocytes. *International Journal of Molecular Sciences*, 13(1), 1239–1257.

Morikawa, M., Derynck, R. & Miyazono, K. (2016). TGF- β and the TGF-β Family: Context-Dependent Roles in Cell and Tissue Physiology. *Cold Spring Harbor Perspectives in Biology*, 8(5), 1-26.

Mork, C., van Deurs, B. & Petersen, O. W. (1990). Regulation of Vimentin Expression in Cultured Human Mammary Epithelial Cells. *Differentiation*, 43(2), 146–156.

Morris, M. E., Beare, J. E., Reed, R. M., Dale, J. R., LeBlanc, A. J., Kaufman, C. L., Zheng, H., Ng, C. K., Williams, S. K. & Hoying, J. B. (2015). Systemically Delivered Adipose Stromal Vascular Fraction Cells Disseminate to Peripheral Artery Walls and Reduce Vasomotor Tone Through a CD11b+ Cell-Dependent Mechanism. *Stem Cells Translational Medicine*, 4(4), 369–380.

Mou, S., Zhou, M., Li, Y., Wang, J., Yuan, Q., Xiao, P., Sun, J. & Wang, Z. (2019). Extracellular Vesicles from Human Adipose-Derived Stem Cells for the Improvement of Angiogenesis and Fat-Grafting Application. *Plastic and Reconstructive Surgery*, 144(4), 869–880.

Murray, L. A., Argentieri, R. L., Farrell, F. X., Bracht, M., Sheng, H., Whitaker, B., Beck, H., Tsui, P., Cochlin, K., Evanoff, H. L., Hogaboam, C. M. & Das, A. M. (2008). Hyper-Responsiveness of IPF/UIP Fibroblasts: Interplay between TGFβ1, IL-13 and CCL2. *International Journal of Biochemistry and Cell Biology*, 40(10), 2174–2182.

Mustoe, T. A., Cooter, R. D., Gold, M. H., Richard Hobbs, F. D., Ramelet, A.-A., Shakespeare, P. G., Stella, M., Téot, L., Wood, F. M. & Ziegler, U. E. (2002). International Clinical Recommendations on Scar Management. *Plastic and Reconstructive Surgery*, 110(2), 560–571.

Mydlo, J. H., Kral, J. G., & Macchia, R. J. (1998). Preliminary results comparing the recovery of basic fibroblast growth factor (FGF-2) in adipose tissue and benign and malignant renal tissue. *The Journal of Urology*, 159, 2159–2163.

Nakano, A., Harada, T., Morikawa, S., & Kato, Y. (1990). Expression of Leukocyte Common Antigen (CD45) on Various Human Leukemia/Lymphoma Cell Lines. *Pathology International*, 40(2), 107–115.

Narayanan, A. S., Page, R. C. & Swanson, J. (1989). Collagen Synthesis by Human Fibroblasts Regulation by Transforming Growth Factor-Fl in the Presence of Other Inflammatory Mediators. *Journal of Biochemistry*, 260, 463-469.

Nedelec, B., Shankowsky, H., Scott, P. G., Ghahary, A. & Tredget, E. E. (2001). Myofibroblasts and Apoptosis in Human Hypertrophic Scars: The Effect of Interferon-A2b. *Surgery*, 130(5), 798–808.

Niessen, F. B., Schalkwijk, J., Vos, H. & Timens, W. (2004). Hypertrophic Scar Formation Is Associated with an Increased Number of Epidermal Langerhans Cells. *Journal of Pathology*, 202(1), 121–129.

Ning, H., Lin, G., Lue, T. F. & Lin, C. S. (2006). Neuron-like Differentiation of Adipose Tissue-Derived Stromal Cells and Vascular Smooth Muscle Cells. *Differentiation*, 74(9–10), 510–518.

Niringiyumukiza, J. D., Cai, H., & Xiang, W. (2018). Prostaglandin E2 involvement in mammalian female fertility: Ovulation, fertilization, embryo development and early implantation. *Reproductive Biology and Endocrinology*, 16(1), 1-10.

Nowak, K. C., McCormack, M. & Koch, R. J. (2000). The Effect of Superpulsed Carbon Dioxide Laser Energy on Keloid and Normal Dermal Fibroblast Secretion of Growth Factors: A Serum-Free Study. *Plastic & Reconstructive Surgery*, 105(6), 2039–2048.

O'Beirne, S. L., Walsh, S. M., Fabre, A., Reviriego, C., Worrell, J. C., Counihan, I. P., Lumsden, R. v., Cramton-Barnes, J., Belperio, J. A., Donnelly, S. C., Boylan, D., Marchal-Sommé, J., Kane, R. & Keane, M. P. (2015). CXCL9 Regulates TGF-β1–Induced Epithelial to Mesenchymal Transition in Human Alveolar Epithelial Cells. *The Journal of Immunology*, 195(6), 2788–2796.

Ohashi, K., Parker, J. L., Ouchi, N., Higuchi, A., Vita, J. A., Gokce, N., Pedersen, A. A., Kalthoff, C., Tullin, S., Sams, A., Summer, R. & Walsh, K. (2010). Adiponectin Promotes Macrophage Polarization toward an Anti-Inflammatory Phenotype. *Journal of Biological Chemistry*, 285(9), 6153–6160.

Olive, P. L., Vikse, C. & Trotter, M. J. (1992). Measurement of Oxygen Diffusion Distance in Tumor Cubes Using a Fluorescent Hypoxia Probe. *International Journal of Radiation Oncology*, 22(3), 397–402.

Olzmann, J. A. & Carvalho, P. (2019). Dynamics and Functions of Lipid Droplets. *Nature Reviews Molecular Cell Biology*, 20(3), 137–155.

Osinga, R., Menzi, N. R., Tchang, L. A. H., Caviezel, D., Kalbermatten, D. F., Martin, I., Schaefer, D. J., Scherberich, A., & Largo, R. D. (2015). Effects of Intersyringe Processing on Adipose Tissue and Its Cellular Components: Implications in Autologous Fat Grafting. *Plastic and Reconstructive Surgery*, 135(6), 1618–1628.

Pachón-Peña, G., Yu, G., Tucker, A., Wu, X., Vendrell, J., Bunnell, B. A., & Gimble, J. M. (2011). Stromal stem cells from adipose tissue and bone marrow of age-matched female donors display distinct immunophenotypic profiles. *Journal of Cellular Physiology*, 226(3), 843–851.

Padoin, A. V., Braga-Silva, J., Martins, P., Rezende, K., Rezende, A. R. D. R., Grechi, B., Gehlen, D., & MacHado, D. C. (2008). Sources of processed lipoaspirate cells: Influence of donor site on cell concentration. *Plastic and Reconstructive Surgery*, 122(2), 614–618.

Pallua, N., Baroncini, A., Alharbi, Z. & Stromps, J. P. (2014a). Improvement of Facial Scar Appearance and Microcirculation by Autologous Lipofilling. *Journal of Plastic, Reconstructive and Aesthetic Surgery*, 67(8), 1033–1037.

Pallua, N., Serin, M. & Wolter, T. P. (2014b). Characterisation of Angiogenetic Growth Factor Production in Adipose Tissue-Derived Mesenchymal Cells. *Journal of Plastic Surgery and Hand Surgery*, 48(6), 412–416.

Parlee, S. D., Lentz, S. I., Mori, H. & MacDougald, O. A. (2014). Quantifying Size and Number of Adipocytes in Adipose Tissue, in: *Methods in Enzymology*, 537, 93–122.

Pauling, Linus. & Corey, R. B. (1951). The Structure of Fibrous Proteins of the Collagen Gelatin Group. *Proceedings of the National Academy of Sciences*, 37, 272–281.

Pérez, P., Page, A., Bravo, A., Río, M., Giménez-Conti, I., Budunova, I., Slaga, T. J. & Jorcano, J. L. (2001). Altered Skin Development and Impaired Proliferative and Inflammatory Responses in Transgenic Mice Overexpressing the Glucocorticoid Receptor. *The FASEB Journal*, 15(11), 2030–2032.

Petridou, S., Maltseva, O., Spanakis, S. & Kazahn Masur, S. (1999). TGF-Receptor Expression and SMAD2 Localization Are Cell Density Dependent in Fibroblasts. *Investigate Ophthalmology & Visual Science*, 41, 89–95.

Pierantozzi, E., Badin, M., Vezzani, B., Curina, C., Randazzo, D., Petraglia, F., Rossi, D. & Sorrentino, V. (2015). Human Pericytes Isolated from Adipose Tissue Have Better Differentiation Abilities than Their Mesenchymal Stem Cell Counterparts. *Cell and Tissue Research*, 361(3), 769–778.

Pilch, P. F., Meshulam, T., Ding, S. & Liu, L. (2011). Caveolae and Lipid Trafficking in Adipocytes. *Journal of Clinical Lipidology*, 6(1), 49-58.

Plikus, M. V., Guerrero-Juarez, C, F., Ito, M., Li, Y, R., Dedhia, P, H., Zheng, Y., Shao, M., Gay, D, L., Ramos, R., His, T, C., Oh, J, W., Wang, X., Ramirez, A., Konopelski, S, E., Elzein, A., Wang, A., Supapannachart, R, J., Lee, H, L., Lim, C, H., Nace, A., Guo, A., Treffeisen, E., Andl, T., Ramirez, R, N., Murad, R., Offermanns, S., Metzger, D., Chambon, P., Widgerow, A, D., Tuan, T, L., Mortazavi, A., Rana, K, G., Hamilton, B, A., Millar, S, E., Seale, P., Pear, W, S., Lazar, M, A., & Cotsarleis, G., (2017). Regeneration of Fat Cells from Myofibroblasts during Wound Healing. *Science*, 355(6326), 748–752.

Pöschl, E., Schlötzer-Schrehardt, U., Brachvogel, B., Saito, K., Ninomiya, Y. & Mayer, U. (2004). Collagen IV Is Essential for Basement Membrane Stability but Dispensable for Initiation of Its Assembly during Early Development. *Development*, 131(7), 1619–1628.

Poulos, E., Taylor, C. & Solish, N. (2003). Effectiveness of Dermasanding (Manual Dermabrasion) on the Appearance of Surgical Scars: A Prospective, Randomized, Blinded Study. *Journal of the American Academy of Dermatology*, 48(6), 897–900.

PRP First. (2021). *Microlyzer Microfat et Nanofat*. Available at https://www.prpfirst.com/en/our-prp-products-online/26-42-microlyser-microfat-et-nanofat.html#/28-microfat_et_nanofat-2400_microns (Accessed: 21 February 2022).

Putra, A., Alif, I., Hamra, N., Santosa, O., Kustiyah, A. R., Muhar, A. M. & Lukman, K. (2020). Msc-Released Tgf-β Regulate α-Sma Expression of Myofibroblast during Wound Healing. *Journal of Stem Cells and Regenerative Medicine*, 16(2), 73–79.

Qiu, H., Jiang, Y., Chen, C., Wu, K., & Wang, H. (2021). The Effect of Different Diameters of Fat Converters on Adipose Tissue and Its Cellular Components: Selection for Preparation of Nanofat. *Aesthetic Surgery Journal*, 41(11), 1734–1744.

Quatresooz, P., Hermanns, J. F., Paquet, P. & Piérard, G. E. (2006). Mechanobiology and Force Transduction in Scars Developed in Darker Skin Types. *Skin Research and Technology*, 12, 279–282.

Rageh, M. A., El-Khalawany, M. & Ibrahim, S. M. A. (2021). Autologous Nanofat Injection in Treatment of Scars: A Clinico-Histopathological Study. *Journal of Cosmetic Dermatology*, 20(10), 3198–3204.

Rahman, S., Patel, Y., Murray, J., Patel, K. v., Sumathipala, R., Sobel, M. & Wijelath, E. S. (2005). Novel Hepatocyte Growth Factor (HGF) Binding Domains on Fibronectin and Vitronectin Coordinate a Distinct and Amplified Met-Integrin Induced Signalling Pathway in Endothelial Cells. *BMC Cell Biology*, 6, 1-17.

Rakocevic, J., Orlic, D., Mitrovic-Ajtic, O., Tomasevic, M., Dobric, M., Zlatic, N., Milasinovic, D., Stankovic, G., Ostojić, M., & Labudovic-Borovic, M. (2017). Endothelial cell markers from clinician's perspective. *Experimental and Molecular Pathology*, 102(2), 303-313.

Ramos, C., Becerril, C., Montaño, M., García-De-Alba, C., Ramírez, R., Checa, M., Pardo, A. & Selman, M. (2010). FGF-1 Reverts Epithelial-Mesenchymal Transition Induced by TGF-β1 through MAPK/ERK Kinase Pathway. *Journal of Physiology Lung and Cellular Molecular Physiology*, 299, 222–231.

Ramos, C., Montaño, M., Becerril, C., Cisneros-Lira, J., Barrera, L., Ruíz, V., Pardo, A., Selman, M. & Cis-neros-Lira, J. (2006). Acidic Fibroblast Growth Factor Decreases α-Smooth Muscle Actin Expression and Induces Apoptosis in Human Normal Lung Fibroblasts. *American Journal of Physiology Lung Cellular and Molecular Physiology*, 291, 871–879.

Raposio, E., Caruana, G., Bonomini, S. & Libondi, G. (2014). A Novel and Effective Strategy for the Isolation of Adipose-Derived Stem Cells: Minimally Manipulated Adipose-Derived Stem Cells for More Rapid and Safe Stem Cell Therapy. *Plastic and Reconstructive Surgery*, 133(6), 1406–1409.

Rathinasabapathy, A., Bruce, E., Espejo, A., Horowitz, A., Sudhan, D. R., Nair, A., Guzzo, D., Francis, J., Raizada, M. K., Shenoy, V. & Katovich, M. J. (2016). Therapeutic Potential of Adipose Stem Cell-Derived Conditioned Medium against Pulmonary Hypertension and Lung Fibrosis. *British Journal of Pharmacology*, 173, 2859–2879.

Rawlins, J. M., Lam, W. L., Karoo, R. O., Naylor, I. L. & Sharpe, D. T. (2006). Quantifying Collagen Type in Mature Burn Scars: A Novel Approach Using Histology and Digital Image Analysis. *Journal of Burn Care & Research*, 27(1), 60–65.

Rehman, J., Traktuev, D., Li, J., Merfeld-Clauss, S., Temm-Grove, C. J., Bovenkerk, J. E., Pell, C. L., Johnstone, B. H., Considine, R. v., & March, K. L. (2004). Secretion of Angiogenic and Antiapoptotic Factors by Human Adipose Stromal Cells. *Circulation*, 109(10), 1292–1298.

Renò, F., Grazianetti, P., Stella, M., Magliacani, G., Pezzuto, C. & Cannas, M. (2002). Release and Activation of Matrix Metalloproteinase-9 During In Vitro Mechanical Compression in Hypertrophic Scars. *Dermatologic Surgery*, 138, 475-478.

Rigamonti, A., Brennand, K., Lau, F. & Cowan, C. A. (2011). Rapid Cellular Turnover in Adipose Tissue. *PLoS ONE*, 6(3), 1-9.

Rigotti, G., Marchi, A., Galiè, M., Baroni, G., Benati, D., Krampera, M., Pasini, A. & Sbarbati, A. (2007). Clinical Treatment of Radiotherapy Tissue Damage by Lipoaspirate Transplant: A Healing Process Mediated by Adipose-Derived Adult Stem Cells. *Plastic and Reconstructive Surgery*, 119(5), 1409–1422.

Ritter, A., Friemel, A., Fornoff, F., Adjan, M., Solbach, C., Yuan, J. & Louwen, F. (2015). Characterization of Adipose-Derived Stem Cells from Subcutaneous and Visceral Adipose Tissues and Their Function in Breast Cancer Cells. *Oncotarget*, 6(33), 34475–34493.

Rodbell, M. (1964). Metabolism of Isolated Fat Cells I. Effects of Hormones on Glucose Metabolism and Lipolysis. *Journal of Biological Chemistry*, 239(2), 375–380.

Rodeheffer, M. S., Birsoy, K. & Friedman, J. M. (2008). Identification of White Adipocyte Progenitor Cells In Vivo. *Cell*, 135(2), 240–249.

Rollings, C. M., Sinclair, L. v., Brady, H. J. M., Cantrell, D. A. & Ross, S. H. (2018). Interleukin-2 Shapes the Cytotoxic T Cell Proteome and Immune Environment–Sensing Programs. *Science Signaling*, 11(526), 1-34.

Romagnani, S. (1999). Th1/Th2 Cells. *Inflammatory Bowel Diseases*, 5(4), 285–294.

Rosales, C. & Uribe-Querol, E. (2017). Phagocytosis: A Fundamental Process in Immunity. *BioMed Research International*, 2017, 1-18.

Rousseau, D. (2000). Fat crystals and emulsion stability - a review. *Food Research International*, 33, 3–14.

Routledge, J. A., Burns, M. P., Swindell, R., Khoo, V. S., West, C. M. L. & Davidson, S. E. (2003). Evaluation of the LENT-SOMA Scales for the Prospective Assessment of Treatment Morbidity in Cervical Carcinoma. *International Journal of Radiation Oncology-Biology-Physics*, 56(2), 502–510.

Roxburgh, J., Metcalfe, A. D., & Martin, Y. H. (2016). The effect of medium selection on adipose-derived stem cell expansion and differentiation: implications for application in regenerative medicine. *Cytotechnology*, 68(4), 957–967.

Roy, S., Hochberg, F. H., & Jones, P. S. (2018). Extracellular vesicles: the growth as diagnostics and therapeutics; a survey. In *Journal of Extracellular Vesicles*, 7(1), 1-11.

Ruhrberg, C., Gerhardt, H., Golding, M., Watson, R., Ioannidou, S., Fujisawa, H., Betsholtz, C. & Shima, D. T. (2002). Spatially Restricted Patterning Cues Provided by Heparin-Binding VEGF-A Control Blood Vessel Branching Morphogenesis. *Genes and Development*, 16(20), 2684–2698.

Salans, L. B., Cushman, S. W. & Weismann, R. E. (1973). Adipose Cell Size and Number in Nonobese and Obese Patients. *The Journal of Clinical Investigation*, 52, 929–941.

Salgado, R. M., Alcántara, L., Mendoza-Rodríguez, C. A., Cerbón, M., Hidalgo-González, C., Mercadillo, P., Moreno, L. M., Álvarez-Jiménez, R. & Krötzsch, E. (2012). Post-Burn Hypertrophic Scars Are Characterized by High Levels of IL-1β MRNA and Protein and TNF-α Type i Receptors. *Burns*, 38(5), 668–676.

Sardesai, M. G. & Moore, C. C. (2007). Quantitative and Qualitative Dermal Change with Microfat Grafting of Facial Scars. *Otolaryngology - Head and Neck Surgery*, 137(6), 868–872.

Sato, F., Wachi, H., Ishida, M., Nonaka, R., Onoue, S., Urban, Z., Starcher, B. C. & Seyama, Y. (2007). Distinct Steps of Cross-Linking, Self-Association, and Maturation of Tropoelastin Are Necessary for Elastic Fiber Formation. *Journal of Molecular Biology*, 369(3), 841–851.

Scherer, P. E., Williams, S., Fogliano, M., Baldini, G. & Lodish, H. F. (1995). A Novel Serum Protein Similar to C1q, Produced Exclusively in Adipocytes. *Journal of Biological Chemistry*, 270(45), 26746–26749.

Schindelin, J., Arganda-Carreras, I., Frise, E., Kaynig, V., Longair, M., Pietzsch, T., Preibisch, S., Rueden, C., Saalfeld, S., Schmid, B., Tinevez, J. Y., White, D. J., Hartenstein, V., Eliceiri, K., Tomancak, P., & Cardona, A. (2012). Fiji: An open-source platform for biological-image analysis. *Nature Methods*, 9(7), 676–682.

Schmidt, B. A. & Horsley, V. (2013). Intradermal Adipocytes Mediate Fibroblast Recruitment during Skin Wound Healing. *Development (Cambridge)*, 140(7), 1517–1527.

Schwartz, M. A. (2010). Integrins and Extracellular Matrix in Mechanotransduction. *Cold Spring Harbor perspectives in biology*, 2(12).

Scott, C. L., Zheng, F., de Baetselier, P., Martens, L., Saeys, Y., de Prijck, S., Lippens, S., Abels, C., Schoonooghe, S., Raes, G., Devoogdt, N., Lambrecht, B. N., Beschin, A. & Guilliams, M. (2016). Bone Marrow-Derived Monocytes Give Rise to Self-Renewing and Fully Differentiated Kupffer Cells. *Nature Communications*, 7, 1-10.

Seale, P., Bjork, B., Yang, W., Kajimura, S., Chin, S., Kuang, S., Scimè, A., Devarakonda, S., Conroe, H. M., Erdjument-Bromage, H., Tempst, P., Rudnicki, M. A., Beier, D. R. & Spiegelman, B. M. (2008). PRDM16 Controls a Brown Fat/Skeletal Muscle Switch. *Nature*, 454(7207), 961–967.

Sephel, G. C. & Davidson, J. M. (1986). Elastin Production in Human Skin Fibroblast Cultures and Its Decline with Age. *Journal of Investigative Dermatology*, 86(3), 279–285.

Serini, G., Bochaton-Piallat, M.-L., Ropraz, P., Geinoz, A., Borsi, L., Zardi, L. & Gabbiani, G. (1998). The Fibronectin Domain ED-A Is Crucial for Myofibroblastic Phenotype Induction by Transforming Growth Factor-1. *The Journal of Cell Biology*, 142(3), 873-881.

Sesé, B., Sanmartín, J. M., Ortega, B., & Llull, R. (2020). Human Stromal Cell Aggregates Concentrate Adipose Tissue Constitutive Cell Population by in Vitro DNA Quantification Analysis. *Plastic and Reconstructive Surgery*, 146(6), 1285–1293.

Sesé, B., Sanmartín, J. M., Ortega, B., Matas-Palau, A., & Llull, R. (2019). Nanofat Cell Aggregates: A Nearly Constitutive Stromal Cell Inoculum for Regenerative Site-Specific Therapies. *Plastic and Reconstructive Surgery*, 144(5), 1079–1088.

Sieber, P., Schäfer, A., Lieberherr, R., le Goff, F., Stritt, M., Welford, R. W. D., Gatfield, J., Peter, O., Nayler, O., & Lüthi, U. (2018). Novel high–throughput myofibroblast assays identify agonists with therapeutic potential in pulmonary fibrosis that act via EP 2 and EP 4 receptors. *PLoS ONE*, 13(11), 1-27.

Shabalina, I. G., Petrovic, N., deJong, J. M. A., Kalinovich, A. v., Cannon, B. & Nedergaard, J. (2013). UCP1 in Brite/Beige Adipose Tissue Mitochondria Is Functionally Thermogenic. *Cell Reports*, 5(5), 1196–1203.

Shah, M., Foreman, D. M. & Ferguson, M. W. (1995). Neutralisation of TGFβ and B2 or Exogenous Addition of TGFβ 3 to Cutaneous Rat Wounds Reduces Scarring. *Journal of Cell Science*, 108, 985–1002.

Shams, S., Mohsin, S., Nasir, G. A., Khan, M. & Khan, S. N. (2015). Mesenchymal Stem Cells Pretreated with HGF and FGF4 Can Reduce Liver Fibrosis in Mice. *Stem Cells International*, 2015, 1-12.

Shen, X., Li, Q. & Zhang, H. (2016). Massive Cerebral Infarction Following Facial Fat Injection. *Aesthetic Plastic Surgery*, 40(5), 801–805.

Shephard, P., Martin, G., Smola-Hess, S., Brunner, G., Krieg, T. & Smola, H. (2004). Myofibroblast Differentiation Is Induced in Keratinocyte-Fibroblast Co-Cultures and Is Antagonistically Regulated by Endogenous Transforming Growth Factor-and Interleukin-1. *American Journal of Pathology*, 164(6), 2055-2066.

Sherman, L. S., Condé-Green, A., Naaldijk, Y., Lee, E. S., & Rameshwar, P. (2019). An enzyme-free method for isolation and expansion of human adipose-derived mesenchymal stem cells. *Journal of Visualized Experiments*, 154, 1-5.

Shockley, W. W. (2011). Scar Revision Techniques: Z-Plasty, W-Plasty, and Geometric Broken Line Closure. *Facial Plastic Surgery Clinics of North America*, 19(3), 455–463.

Shook, B. A., Wasko, R. R., Mano, O., Rutenberg-Schoenberg, M., Rudolph, M. C., Zirak, B., Rivera-Gonzalez, G. C., López-Giráldez, F., Zarini, S., Rezza, A., Clark, D. A., Rendl, M., Rosenblum, M. D., Gerstein, M. B. & Horsley, V. (2020).

Dermal Adipocyte Lipolysis and Myofibroblast Conversion Are Required for Efficient Skin Repair. *Cell Stem Cell*, 26(6), 880-895.

Shi, J., Lu, P., Shen, W., He, R., Yang, M. W., Fang, Y., Sun, Y. W., Niu, N., & Xue, J. (2019). CD90 highly expressed population harbors a stemness signature and creates an immunosuppressive niche in pancreatic cancer. *Cancer Letters*, 453, 158–169.

Shweiki, D., Itin, A., Soffer, D. & Keshet, E. (1992). Vascular Endothelial Growth Factor Induced by Hypoxia-Initiated Angiogenesis. *Nature*, 359, 843–945.

Simiczyjew, A., Dratkiewicz, E., van Troys, M., Ampe, C., Styczeń, I. & Nowak, D. (2018). Combination of Egfr Inhibitor Lapatinib and Met Inhibitor Foretinib Inhibits Migration of Triple Negative Breast Cancer Cell Lines. *Cancers*, 10(9), 1-17.

Sims, D. E. (1986). The Perciyte - A Review. *Tissue & Cell*, 18(2), 153-174.

Singer, A. J. (2022). Healing Mechanisms in Cutaneous Wounds: Tipping the Balance. *Tissue Engineering Part B: Reviews*, 1-17.

Singer, A. J. & Mcclain, S. A. (2002). Persistent Wound Infection Delays Epidermal Maturation and Increases Scarring in Thermal Burns. *Wound Repair and Regeneration*, 10(6), 372–377.

Slukvin, I. I. & Kumar, A. (2018). The Mesenchymoangioblast, Mesodermal Precursor for Mesenchymal and Endothelial Cells. *Cellular and Molecular Life Sciences*, 75(19), 3507–3520.

Smith, C. J., Smith, J. C. & Finn, M. C. (1987). The Possible Role of Mast Cells (Allergy) in the Production of Keloid and Hypertrophic Scarring. *Journal of Burn Care & Rehabilitation*, 8(2), 126–131.

So, K., McGrouther, Duncan, A., Bush, James, A., Durani, P., Taylor, L., Skotny, G., Mason, T., Metcalfe, A., O'Kane, S. & Ferguson, Mark, W, J. (2011). Avotermin for Scar Improvement Following Scar Revision Surgery: A Randomized, Double-Blind, Within-Patient, Placebo-Controlled, Phase II Clinical Trial. *Plastic and Reconstructive Surgery*, 128, 163–172.

Sohn, S. H., Kim, B., Sul, H. J., Kim, H, S., Zang, D. Y. (2020). Foretinib inhibits cancer stemness and gastric cancer cell proliferation by decreasing CD44 and c-MET signaling. *OncoTargets and Therapy,* 13, 1027-1035.

Sonbol, H. (2018). Extracellular Matrix Remodeling in Human Disease. *Journal of Microscopy and Ultrastructure*, 6(3), 123-128.

Sørensen, L. T. (2012). Wound Healing and Infection in Surgery: The Pathophysiological Impact of Smoking, Smoking Cessation, and Nicotine Replacement Therapy: A Systematic Review. *Annals of Surgery*, 255(6), 1069–1079.

Souza-Fernandes, A. B., Pelosi, P. & Rocco, P. R. M. (2006). Bench-to-Bedside Review: The Role of Glycosaminoglycans in Respiratory Disease. *Critical Care*, 10(6), 1-16.

Speight, P., Nakano, H., Kelley, T. J., Hinz, B. & Kapus, A. (2013). Differential Topical Susceptibility to TGFβ in Intact and Injured Regions of the Epithelium: Key Role in Myofibroblast Transition. *Molecular Biology of the Cell*, 24(21), 3326–3336.

Spiekman, M., Przybyt, E., Plantinga, J. A., Gibbs, S., van der Lei, B. & Harmsen, M. C. (2014). Adipose Tissue-Derived Stromal Cells Inhibit TGF-β1-Induced Differentiation of Human Dermal Fibroblasts and Keloid Scar-Derived Fibroblasts in a Paracrine Fashion. *Plastic and Reconstructive Surgery*, 134(4), 699–712.

Steen, V. D., Oddis, C. v, Conte, C. G., Janoski, J., Casterline, G. Z., Medsger, T. A. & Ziegler Casterline, G. (1997). Incidence of Systemic Sclerosis in Allegheny County, Pennsylvania. *Arthritis & Rheumatism,* 40(3), 441-445.

Steinman, R. M. & Witmer, M. D. (1978). Lymphoid Dendritic Cells Are Potent Stimulators of the Primary Mixed Leukocyte Reaction in Mice. *Proceedings of the National Academy of Sciences of the United States of America*, 75(10), 5132–5136.

Steppan, C. M., Bailey, S. T., Bhat, S., Brown, E. J., Banerjee, R. R., Wright, C. M., Patel, H. R., Ahima, R. S. & Lazar, M. A. (2001). The Hormone Resistin Links Obesity to Diabetes. *Nature*, 409, 307-312.

Sugihara, K., Sasaki, S., Uemura, A., Kidoaki, S. & Miura, T. (2020). Mechanisms of Endothelial Cell Coverage by Pericytes: Computational Modelling of Cell Wrapping and in Vitro Experiments. *Journal of the Royal Society Interface*, 17(162), 1-13.

Sultan, S. M., Barr, J. S., Butala, P., Davidson, E. H., Weinstein, A. L., Knobel, D., Saadeh, P. B., Warren, S. M., Coleman, S. R. & Hazen, A. (2012). Fat Grafting Accelerates Revascularisation and Decreases Fibrosis Following Thermal Injury. *Journal of Plastic, Reconstructive & Aesthetic Surgery*, 65(2), 219–227.

Sumpio, B. E., Riley, J. T. & Dardik, A. (2002). Molecules in Focus Cells in Focus: Endothelial Cell. *The International Journal of Biochemistry & Cell Biology*. 34, 1508-1512.

Sun, Q., Guo, S., Wang, C.-C., Sun, X., Wang, D., Xu, N., Jin, S.-F. & Li, K.-Z. (2015). Cross-Talk between TGF-β/SMAD Pathway and Wnt/β-Catenin Pathway in Pathological Scar Formation. *International Journal of Clinical & Experimental Pathology*, 8(6), 7631-7639.

Sun, X., & Kaufman, P. D. (2018). Ki-67: more than a proliferation marker. *Chromosoma*, 127(2), 175-186.

Tandara, A. A. & Mustoe, T. A. (2011). MMP- and TIMP-Secretion by Human Cutaneous Keratinocytes and Fibroblasts - Impact of Coculture and Hydration. *Journal of Plastic, Reconstructive and Aesthetic Surgery*, 64(1), 108–116.

Tarbit, E., Singh, I., Peart, J. N. & Rose'Meyer, R. B. (2019). Biomarkers for the Identification of Cardiac Fibroblast and Myofibroblast Cells. *Heart Failure Reviews*, 24, 1-15.

Tashiro, J., Elliot, S. J., Gerth, D. J., Xia, X., Pereira-Simon, S., Choi, R., Catanuto, P., Shahzeidi, S., Toonkel, R. L., Shah, R. H., el Salem, F. & Glassberg, M. K. (2015). Therapeutic Benefits of Young, but Not Old, Adipose-Derived Mesenchymal Stem Cells in a Chronic Mouse Model of Bleomycin-Induced Pulmonary Fibrosis. *Translational Research*, 166(6), 554–567.

Tonnard, P., Verpaele, A. & Carvas, M. (2020). Fat Grafting for Facial Rejuvenation with Nanofat Grafts. *Clinics in Plastic Surgery*, 47(1), 53–62.

Tonnard, P., Verpaele, A., Peeters, G., Hamdi, M., Cornelissen, M. & Declercq, H. (2013). Nanofat Grafting: Basic Research and Clinical Applications. *Plastic and Reconstructive Surgery*, 132(4), 1017–1026.

Torio-Padron, N., Paul, D., von Elverfeldt, D., Stark, G. B. & Huotari, A. M. (2011). Resorption Rate Assessment of Adipose Tissue-Engineered Constructs by Intravital Magnetic Resonance Imaging. *Journal of Plastic, Reconstructive and Aesthetic Surgery*, 64(1), 117–122.

Torre-Villalvazo, I., Bunt, A. E., Alemán, G., Marquez-Mota, C. C., Diaz-Villaseñor, A., Noriega, L. G., Estrada, I., Figueroa-Juárez, E., Tovar-Palacio, C., Rodriguez-López, L. A., López-Romero, P., Torres, N., & Tovar, A. R. (2018). Adiponectin synthesis and secretion by subcutaneous adipose tissue is impaired during obesity by endoplasmic reticulum stress. *Journal of Cellular Biochemistry*, 119(7), 5970–5984.

Traktuev, D. O., Merfeld-Clauss, S., Li, J., Kolonin, M., Arap, W., Pasqualini, R., Johnstone, B. H. & March, K. L. (2008). A Population of Multipotent CD34-Positive Adipose Stromal Cells Share Pericyte and Mesenchymal Surface Markers, Reside in a Periendothelial Location, and Stabilize Endothelial Networks. *Circulation Research*, 102(1), 77–85.

Tsai, C. C., Wu, S. B., Kau, H. C. & Wei, Y. H. (2018). Essential Role of Connective Tissue Growth Factor (CTGF) in Transforming Growth Factor-B1 (TGF-B1)-Induced Myofibroblast Transdifferentiation from Graves' Orbital Fibroblasts. *Scientific Reports*, 8(7276), 1-10.

Tuan, T. L., & Nichter, L. S. (1998). The molecular basis of keloid and hypertrophic scar formation. *Molecular Medicine Today*, 19–24.

TULIP Aesthetics. (2022) *TULIP NANOFAT KIT™ (GEN 2)*. Available at https://tulipaesthetics.com/collections/single-use-nanofat-kit/products/dnts-5p?variant=33566693916803 (Accessed: 21 February 2022).

Ţuţuianu, R., Maria Roşca, A., Florea, G., Prună, V., Mădălina Iacomi, D., Andreea Rădulescu, L., Paul Neagu, T., Lascăr, I., & Domnica Titorencu, I. (2019). Heterogeneity of human fibroblasts isolated from hypertrophic scar. *Romanian Journal of Morphology and Embryology,* 60(3), 793–802.

U.S. Department of Health and Human Services, Food and Drug Administration, Center for Biologics Evaluation and Research, Center for Devices and Radiological Health, & Office of Combination Products. (2020). *Regulatory Considerations for Human Cells, Tissues, and Cellular and Tissue-Based Products: Minimal Manipulation and Homologous Use Guidance for Industry and Food and Drug Administration Staff*. Available at: https://www.fda.gov/regulatory-information/search-fda-guidance-documents/regulatory-considerations-human-cells-tissues-and-cellular-and-tissue-based-products-minimal (Accessed: 13 March 2022).

Uysal, C. A., Tobita, M., Hyakusoku, H. & Mizuno, H. (2014). The Effect of Bone-Marrow-Derived Stem Cells and Adipose-Derived Stem Cells on Wound Contraction and Epithelization. *Advances in Wound Care*, 3(6), 405–413.

Uyulmaz, S., Sanchez Macedo, N., Rezaeian, F., Giovanoli, P. & Lindenblatt, N. (2018). Nanofat Grafting for Scar Treatment and Skin Quality Improvement. *Aesthetic Surgery Journal*, 38(4), 421–428.

Varghese, J., Griffin, M., Mosahebi, A., & Butler, P. (2017). Systematic review of patient factors affecting adipose stem cell viability and function: implications for regenerative therapy. *Stem cell research & therapy*, 8(45), 1-15.

Verhaegen, P. D. H. M., van Zuijlen, P. P. M., Pennings, N. M., van Marle, J., Niessen, F. B., van der Horst, C. M. A. M. & Middelkoop, E. (2009). Differences in Collagen Architecture between Keloid, Hypertrophic Scar, Normotrophic Scar, and Normal Skin: An Objective Histopathological Analysis. *Wound Repair and Regeneration*, 17(5), 649–656.

Vezzani, B., Shaw, I., Lesme, H., Yong, L., Khan, N., Tremolada, C. & Péault, B. (2018). Higher Pericyte Content and Secretory Activity of Microfragmented Human Adipose Tissue Compared to Enzymatically Derived Stromal Vascular Fraction. *Stem Cells Translational Medicine*, 7(12), 876–886.

Viallard, J. F., Pellegrin, J. L., Ranchin, V., Schaeverbeke, T., Dehais, J., Longy-Boursier, M., Ragnaud, J. M., Leng, B. & Moreau, J. F. (1999). Th1 (IL-2, Interferon-Gamma (IFN-g)) and Th2 (IL-10, IL-4) Cytokine Production by Peripheral Blood Mononuclear Cells (PBMC) from Patients with Systemic Lupus Erythematosus (SLE). *Clinical and Experimental Immunology*, 115, 189–195.

Villena, J. A., Cousin, B., Pénicaud, L. & Casteilla, L. (2001). Adipose Tissues Display Differential Phagocytic and Microbicidal Activities Depending on Their Localization. *International Journal of Obesity*, 25, 1275–1280.

Wagenseil, J. E. & Mecham, R. P. (2007). New Insights into Elastic Fiber Assembly. *Birth Defects Research Part C - Embryo Today: Reviews*, 81(4), 229–240.

Walker, M., Godin, M., & Pelling, A. E. (2020). Mechanical stretch sustains myofibroblast phenotype and function in microtissues through latent TGF-β1 activation. *Integrative Biology*, 12(8), 199–210.

Walocko, F. M., Eber, A. E., Kirsner, R. S., Badiavas, E. & Nouri, K. (2018). Systematic Review of the Therapeutic Roles of Adipose Tissue in Dermatology. *Journal of the American Academy of Dermatology*, 79(5), 935–944.

Wang, J., Liao, Y., Xia, J., Wang, Z., Mo, X., Feng, J., He, Y., Chen, X., Li, Y., Lu, F., & Cai, J. (2019). Mechanical micronization of lipoaspirates for the treatment of hypertrophic scars. *Stem Cell Research and Therapy*, 10(1), 1-10.

Wasmuth, H. E., Lammert, F., Zaldivar, M. M., Weiskirchen, R., Hellerbrand, C., Scholten, D., Berres, M. L., Zimmermann, H., Streetz, K. L., Tacke, F., Hillebrandt, S., Schmitz, P., Keppeler, H., Berg, T., Dahl, E., Gassler, N., Friedman, S. L. & Trautwein, C. (2009). Antifibrotic Effects of CXCL9 and Its Receptor CXCR3 in Livers of Mice and Humans. *Gastroenterology*, 137(1), 309-319.

Weisberg, S. P., McCann, D., Desai, M., Rosenbaum, M., Leibel, R. L. & Ferrante, A. W. (2003). Obesity Is Associated with Macrophage Accumulation in Adipose Tissue. *Journal of Clinical Investigation*, 112(12), 1796–1808.

Wetzels, S., Bijnen, M., Wijnands, E., Biessen, E. A. L., Schalkwijk, C. G. & Wouters, K. (2018). Characterization of Immune Cells in Human Adipose Tissue by Using Flow Cytometry. *Journal of Visualized Experiments*, 133, 1-10.

Whitby, D. J., & Ferguson, M. W. J. (1991). The Extracellular Matrix of Lip Wounds in Fetal, Neonatal and Adult Mice. *Development*, 112, 651–668.

Wijelath, E. S., Rahman, S., Namekata, M., Murray, J., Nishimura, T., Mostafavi-Pour, Z., Patel, Y., Suda, Y., Humphries, M. J. & Sobel, M. (2006). Heparin-II Domain of Fibronectin Is a Vascular Endothelial Growth Factor-Binding Domain: Enhancement of VEGF Biological Activity by a Singular Growth Factor/Matrix Protein Synergism. *Circulation Research*, 99(8), 853–860.

Wipff, P. J., Rifkin, D. B., Meister, J. J. & Hinz, B. (2007). Myofibroblast Contraction Activates Latent TGF-B1 from the Extracellular Matrix. *Journal of Cell Biology*, 179(6), 1311–1323.

Witherel, C. E., Abebayehu, D., Barker, T. H. & Spiller, K. L. (2019). Macrophage and Fibroblast Interactions in Biomaterial-Mediated Fibrosis. *Advanced Healthcare Materials*, 8(4), 1-35.

Whitby, D. J. & Ferguson, M. W. J. (1991). Immunohistochemical Localization of Growth Factors in Fetal Wound Healing. *Developmental Biology*, 147, 207-215.

Wilson, M. S., Madala, S. K., Ramalingam, T. R., Gochuico, B. R., Rosas, I. O., Cheever, A. W. & Wynn, T. A. (2010). Bleomycin and IL-1β-Mediated Pulmonary Fibrosis Is IL-17A Dependent. *Journal of Experimental Medicine*, 207(3), 535–552.

Wu, H., Ghosh, S., Perrard, X. D., Feng, L., Garcia, G. E., Perrard, J. L., Sweeney, J. F., Peterson, L. E., Chan, L., Smith, C. W. & Ballantyne, C. M. (2007). T-Cell Accumulation and Regulated on Activation, Normal T Cell Expressed and Secreted Upregulation in Adipose Tissue in Obesity. *Circulation*, 115(8), 1029–1038.

Wu, J., Boström, P., Sparks, L. M., Ye, L., Choi, J. H., Giang, A. H., Khandekar, M., Virtanen, K. A., Nuutila, P., Schaart, G., Huang, K., Tu, H., van Marken Lichtenbelt, W. D., Hoeks, J., Enerbäck, S., Schrauwen, P. & Spiegelman, B. M. (2012). Beige Adipocytes Are a Distinct Type of Thermogenic Fat Cell in Mouse and Human. *Cell*, 150(2), 366–376.

Wu, S. H., Liao, Y. T., Hsueh, K. K., Huang, H. K., Chen, T. M., Chiang, E. R., Hsu, S. H., Tseng, T. C. & Wang, J. P. (2021). Adipose-Derived Mesenchymal Stem Cells from a Hypoxic Culture Improve Neuronal Differentiation and Nerve Repair. *Frontiers in Cell and Developmental Biology*, 9, 1-10.

Xing, D., Liu, L., Marti, G. P., Zhang, X., Reinblatt, M., Milner, S. M. & Harmon, J. W. (2011). Hypoxia and Hypoxia-Inducible Factor in the Burn Wound. *Wound Repair and Regeneration*, 19(2), 205–213.

Yang, E., van Nimwegen, E., Zavolan, M., Rajewsky, N., Schroeder, M., Magnasco, M. & Darnell, J. E. (2003). Decay Rates of Human MRNAs: Correlation with Functional Characteristics and Sequence Attributes. *Genome Research*, 13(8), 1863–1872.

Yang, J., Dai, C. & Liu, Y. (2003). Hepatocyte Growth Factor Suppresses Renal Interstitial Myofibroblast Activation and Intercepts SMAD Signal Transduction. *American Journal of Pathology*, 163(2), 621–632.

Yang, J., Dai, C. & Liu, Y. (2005). A Novel Mechanism by Which Hepatocyte Growth Factor Blocks Tubular Epithelial to Mesenchymal Transition. *Journal of the American Society of Nephrology*, 16(1), 68–78.

Yang, J., Murphy, T. L., Ouyang, W. & Murphy, K. M. (1999). Induction of Interferon-γ Production in Th1 CD4+ T Cells: Evidence for Two Distinct Pathways for Promoter Activation. *European Journal of Immunology*, 29(2), 548–555.

Yang, Z., Jin, S., He, Y., Zhang, X., Han, X. & Li, F. (2021). Comparison of Microfat, Nanofat, and Extracellular Matrix/Stromal Vascular Fraction Gel for Skin Rejuvenation: Basic Research and Clinical Applications. *Aesthetic Surgery Journal*, 41(11), 1557–1570.

Yao, L., Liu, C. J., Luo, Q., Gong, M., Chen, J., Wang, L. J., Huang, Y., Jiang, X., Xu, F., Li, T. Y. & Shu, C. (2013). Protection against Hyperoxia-Induced Lung Fibrosis by KGF-Induced MSCs Mobilization in Neonatal Rats. *Pediatric Transplantation*, 17(7), 676–682.

Yao, Y., Dong, Z., Liao, Y., Zhang, P., Ma, J., Gao, J., & Lu, F. (2017). Adipose Extracellular Matrix/Stromal Vascular Fraction Gel: A Novel Adipose Tissue-Derived Injectable for Stem Cell Therapy. *Plastic and Reconstructive Surgery*, 139(4), 867–879.

Yi, Y., Hu, W., Lv, W., Zhao, C., Xiong, M., Wu, M., Zhang, Q. & Wu, Y. (2021). FTY720 Improves the Survival of Autologous Fat Grafting by Modulating Macrophages Toward M2 Polarization Via STAT3 Pathway. *Cell Transplantation*, 30, 1-10.

Yoshimura, K., Sato, K., Aoi, N., Kurita, M., Hirohi, T., & Harii, K. (2008). Cell-assisted lipotransfer for cosmetic breast augmentation: Supportive use of adipose-derived stem/stromal cells. *Aesthetic Plastic Surgery*, 32(1), 48–55.

Yoshimura, K., Shigeura, T., Matsumoto, D., Sato, T., Takaki, Y., Aiba-Kojima, E., Sato, K., Inoue, K., Nagase, T., Koshima, I. & Gonda, K. (2006). Characterization of Freshly Isolated and Cultured Cells Derived from the Fatty and Fluid Portions of Liposuction Aspirates. *Journal of Cellular Physiology*, 208(1), 64–76.

Yu, Q., Cai, Y., Huang, H., Wang, Z., Xu, P., Wang, X., Zhang, L., Zhang, W., & Li, W. (2018). Co-Transplantation of Nanofat Enhances Neovascularization and Fat Graft Survival in Nude Mice. *Aesthetic Surgery Journal*, 38(6), 667–675.

Zalewski, A., Shi, Y. & Johnson, A. G. (2002). Diverse Origin of Intimal Cells: Smooth Muscle Cells, Myofibroblasts, Fibroblasts, and Beyond? *Circulation Research*, 91(8), 652–655.

Zhang, H. Y., Gharaee-Kermani, M. & Phan, S. H. (1997). Regulation of Lung Fibroblast Alpha-Smooth. *The Journal of Immunology*, 158, 1392–1399.

Zhang, J., Deng, Z., Jin, L., Yang, C., Liu, J., Song, H., Han, W. & Si, Y. (2017). Spleen-Derived Anti-Inflammatory Cytokine IL-10 Stimulated by Adipose Tissue-Derived Stem Cells Protects Against Type 2 Diabetes. *Stem Cells and Development*, 26(24), 1749–1758.

Zhang, Y., Lee, T. C., Guillemin, B., Yu, M. C. & Rom, W. N. (1993). Pulmonary Fibrosis or after Asbestos Exposure. Expression in Macrophages from Idiopathic Factor-Alpha Release and Messenger RNA Enhanced IL-1 Beta and Tumor Necrosis. *The Journal of Immunology*. 150(9), 4188-4196.

Zhang, Y., Proenca, R., Maffei, M., Barone, M., Leopold, L. & Friedman, J. M. (1994). Positional Cloning of the Mouse Obese Gene and Its Human Homologue. *Nature*, 372, 425–432.

Zhang, Z., Finnerty, C. C., He, J., & Herndon, D. N. (2012). SMAD ubiquitination regulatory factor 2 expression is enhanced in hypertrophic scar fibroblasts from burned children. *Burns*, 38(2), 236–246.

Zhao, H., Shang, Q., Pan, Z., Bai, Y., Li, Z., Zhang, H., Zhang, Q., Guo, C., Zhang, L. & Wang, Q. (2018). Exosomes from Adipose-Derived Stem Cells Attenuate Adipose Inflammation and Obesity through Polarizing M2 Macrophages and Beiging in White Adipose Tissue. *Diabetes*, 67(2), 235–247.

Zhong, C., Chrzanowska-Wodnicka, M., Brown, J., Shaub, A., Belkin, A. M., Burridge, K., Checovich, J., Peters, D. M., Albrecht, R. M. & Mosher, D. F. (1998). Rho-Mediated Contractility Exposes a Cryptic Site in Fibronectin and Induces Fibronectin Matrix Assembly. *The Journal of Cell Biology*, 141(2), 539-551.

Zhou, B. R., Zhang, T., bin Jameel, A. A., Xu, Yang, Xu, Yan, Guo, S. L., Wang, Y., Permatasari, F. & Luo, D. (2016). The Efficacy of Conditioned Media of Adipose-Derived Stem Cells Combined with Ablative Carbon Dioxide Fractional Resurfacing for Atrophic Acne Scars and Skin Rejuvenation. *Journal of Cosmetic and Laser Therapy*, 18(3), 138–148.

Zhou, B., Li, F., Chen, H., & Song, J. (2005). The modulation of apoptosis by cyclic AMP involves Akt and epidermal growth factor receptor. *International Journal of Biochemistry and Cell Biology*, *37*(7), 1483–1495.

Zhou, Z. Q., Chen, Y., Chai, M., Tao, R., Lei, Y. H., Jia, Y. Q., Shu, J., Ren, J., Li, G., Wei, W. X., Han, Yu di & Han, Yan. (2019). Adipose Extracellular Matrix Promotes Skin Wound Healing by Inducing the Differentiation of Adipose-Derived Stem Cells into Fibroblasts. *International Journal of Molecular Medicine*, 43(2), 890–900.

Zhu, M., Xue, J., Lu, S., Yuan, Y., Liao, Y., Qiu, J., Liu, C. & Liao, Q. (2018). Anti-inflammatory Effect of Stromal Vascular Fraction Cells in Fat Transplantation. *Experimental and Therapeutic Medicine*, 17, 1435-1439.

Zillhardt, M., Park, S., Romero, I., Sawada, K., Montag, A., Krausz, T., Yamada, S., Peter, M., Lengyel, E. (2011). Foretinib (GSK1363089), an orally available multikinase inhibitor of c-Met and VEGFR-2, blocks proliferation, induces anoikis, and impairs ovarian cancer metastasis. *Clinical Cancer Research*, 17(12), 4042-4051.

van Zuijlen, P. P. M., Ruurda, J. J. B., van Veen, H. A., van Marle, J., van Trier, A. J. M., Groenevelt, F., Kreis, R. W. & Middelkoop, E. (2003). Collagen Morphology in Human Skin and Scar Tissue: No Adaptations in Response to Mechanical Loading at Joints. *Burns*, 29(5), 423–431.

Zuk, P. A., Zhu, M., Ashjian, P., de Ugarte, D. A., Huang, J. I., Mizuno, H., Alfonso, Z. C., Fraser, J. K., Benhaim, P., & Hedrick, M. H. (2002). Human adipose tissue is a source of multipotent stem cells. *Molecular Biology of the Cell*, 13(12), 4279–4295.

Zuk, P. A., Zhu, M., Mizuno, H., Huang, J., Futrell, J. W., Katz, A. J., Benhaim, P., Lorenz, H. P., & Hedrick, M. H. (2001). Multilineage Cells from Human Adipose Tissue: Implications for Cell-Based Therapies. *Tissue Engineering*, 7(2), 211-228.